TWISTED AMIDES: CHARACTERIZATION OF THEIR ELECTRONIC STRUCTURE AND ANALYSIS OF THEIR ACCELERATED HYDROLYSIS

J. I. Mujika Gorostidi

Doctoral Dissertation

Supervisor: X. Lopez Pestaña

December 2005

TESIAREN ZUZENDARIAREN BAIMENA TESIA AURKEZTEKO

Xabier Lopez Pestaña jaunak **Twisted Amides: characterization of their electronic structure and analysis of their accelerated hydrolysis** izenburua duen doktorego-tesiaren zuzendari naizenak, tesia aurkezteko baimena ematen dut, defendatua izateko baldintzak betetzen dituelako. **Jon Iñaki Mujika Gorostidi** doktoregai jaunak egin du aipaturiko tesia, **Polimeroen Zientzia eta Teknologia** sailean.

, -(e)ko (a)ren a

TESIAREN ZUZENDARIA

Izpta.: Xabier Lopez Pestaña

7. DOKUMENTUA

TUTOREAREN BERRESPENA

Xabier Lopez Pestaña jaunak, **Twisted Amides: characterization of their electronic structure and analysis of their accelerated hydrolysis** izenburua duen doktorego-tesiaren tutore naizenak, tesia aurkezteko sailak eman duen baimena berresten dut. **Jon Iñaki Mujika Gorostidi** doktoregai jaunak egin du aipaturiko tesia, **Polimeroen Zientzia eta Teknologia** sailean.

, -(e)ko (a)ren a

TESIAREN ZUZENDARIA

Izpta.: Xabier Lopez Pestaña

8. DOKUMENTUA

SAILAREN ADOSTASUNA

Polimeroen Zientzia eta Teknologia Saileko Kontseiluak, -(e)ko bileran, **Twisted Amides: characterization of their electronic structure and analysis of their accelerated hydrolysis** izenburua duen doktorego-tesia aurkeztearen alde dagoela adierazi du. **Xabier Lopez Pestaña** jaunaren zuzendaritzapean egin den tesi hori **Jon Iñaki Mujika Gorostidi** jaunak aurkeztu du sail honetan.

, -(e)ko (a)ren a

O.E. SAILEKO ZUZENDARIA SAILEKO IDAZKARIA

Izpta.: Pedro A. Santamaria Izpta.: Jose I. Eguiazabal

9. DOKUMENTUA

DOKTORE GRADUKO AKTA
DOKTORE TESIAREN DEFENTSAKO AKTA

DOKTOREGAIA : **Jon Iñaki Mujika Gorostidi**
TESIAREN IZENA : **Twisted Amides: characterization of their electronic structure and analysis of their accelerated hydrolysis**
UPV/EHUko Doktorego Batzordeak epaimahaia izendatu zuen goian adierazitako doktore tesia epaitzeko. Epaimahai hori behean aipatzen den egunean bildu da, eta doktoregaiak defentsa burututa, eta aurkeztu zaizkion eragozpen edota proposamenei erantzuna eman ondoren, epaimahaiak, ,
honako kalifikazio hau eman dio:

, -(e)ko (a)ren a

Epaimahaiko burua, Idazkaria,

Izpta.: Izpta.:

1. epaimahaikidea 2. epaimahaikidea 3. epaimahaikidea

Izpta.: Izpta.: Izpta.:

Doktoregaia,

Izpta.: **Jon Iñaki Mujika Gorostidi**

Eskerrak denori!

Beno, ba iritsi da eskerrak eman eta errepaso txiki bat egiteko ordua. Dena orain dela 5 urte hasi zen, Txonik tesia egiten hasteko aukera zegoela esan zidanean. Lehen momentu horiek ez ziren oso errazak izan. Zenbat aldiz pentsatu nuen "a ze munduan sartu naizen!!". Gogoratzen naiz nola Txoni hasi zitzaidan explikatzen ordenagailu-cluster-en antolaketa, bi motatakoak zaudela, bat sqab00 (non ote dago traste hori??) eta bestea squa00 (Orpheusen "aita"), nola bidali kalkuloak, ... zer zen guzti hori! Gero, oraindik zailagoa egiteko, hasi ta lehenengo astean ESPA ospatu zen Donostian, ta han azaldu nintzen ni, metodo bat edo base bat zer zen ez nekiela. Ez nuen tutik ere ulertu! Baina, beno, orain konturatzen naiz 5 urte hauetan zerbait ikasi detela, behintzat badakit metodo bat edo base bat zer den bereizten eta. Baina, noski, garrantzitsuena ez da hori izan, baizik mundu hontan sartzeak jendea ezagutzeko eman didan aukera, ta espero jende gehiago ere ezagutzeko aukera ematea.

Eskerrak emateko garaian Xabirekin hasiko naiz, bera izan baita tesi honen zuzendaria, eta tesi hau bion arteko lanaren fruitua izan baita. Dakidan ia guztia berari zor diot, eta erraza izan da berarekin lan egitea, beti egon baita laguntzeko prest eta berak dakien guzti hori (ez dela gutxi) erakusteko prest. Eskerrik asko Xabi!

Jesus, zuri ere eskerrik asko, zure taldean sartzeko eman zenidan aukeragatik, ta behar izan ezkero hor egon zarelako beti laguntzeko prest. Hori bai, denbora hontan zehar astelehenero errealaren egoerari buruz azalpenak eskatu dizkidazu, ta orokorrean ez dira urte errezak izan alde hortatik, baina hori gogorrena izatea seinale ona da, ez? Eskerrik asko Jesus!

Txoniri ere esker mordo bat eman nahi dizkiot, nola ez. Lehen esan bezela, berak eman zidan kimilka kuantikoaren lehenengo berri, ta batez ere lehenengo hasiera haietan gauza asko erakutsi zizkidan. Gainera, tartean ere 3 urtez batera bizi ta gero, zer gehiago esan dezaket berak ez dakienik? Eskerrik asko!!

Txemari, zuri ere esker mila. Zergatik? Nahiz ta pelota partiduetan nirekin beti galdu, ba hurrengo astean ere nirekin jolasteko prest zinelako!! Ta, noski, ez horregatik bakarrik, ordenagailuen mundu zail hortan, ta beste gauza askotan ere emandako laguntza guztiagatik ere eskerrak eman nahi dizkizut!

Ni hasi nintzenean Iñaki ere hemen zegoen. Gure bideak antzekoak izan direla esan daiteke, ez? Batera hasi, gutxi gora behera batera bukatu, batera joan ginen Valentziara... ba zuri ere eskerrak denbora guzti hontan behar zenean laguntzeagatik!

Konturatuko zineten bezela, orain arte denak mutilak aipatu ditut. Ze sartu nintzenean denak ziren gizonezkoak! Zorionez Jesus hortaz konturatu zen ta neurriak hartu zituen: hurrengo hiru fitxajeak neskak izan ziren eta: Eider, Eli ta gero Elena.

Eider izan zen lehenengoa taldera etortzen (nahiz ta teorian beste departamentu batekoak izan), ta bera izan zen Charmm-eko penak kontatzeko izan nuen lehenengo laguntza. Ta begira zenbat ikasi dezun orain! Gainera, denbora batez Estrasburgon egon ginen batera, ta hori ere esperientzia polita izan zen. Eskerrik asko Eider!

Gero Eli etorri zen, aluminioen mundu arraro hortan murgildu zaiguna, ta beraz zientifikoki tratu zuzenik izan ez arren, hortxe egon zara beti, ta eskerrik asko, batez ere egin dizkizudan sabotaia guztiak eta gero ez akatzeagatik!

Beranduago Elena etorri zen, hau ere Charmm-eko mundu berezi hortan murgildu dena, ta beno, beste gauza askotan ere bai. Ea Charmm-eko zenbat kasu berezi eta arraroak aurkitzen dituzun etorkizunean! Eskerrik asko Elena, ta espero zuri ere sabotaia gehiagorik ez egitea!

Azkenik, azkeneko fitxajeak: Julen, Mario eta Jiang. Uste det ondo egongo zaretela talde honetan. Ta nola ez, Mariari ere eskerrak, moltes gràcies, tesi hau burutzen estimatzekoa den laguntza emateagatik!

Beno, ba aurkeztu dizkizuet urte hauetan nire ondoan egon diren jendea. Ez nuke nire familiaz ahaztu nahi, nahiz ta oso ondo ez dakiten zer den egiten aritu naizena, beti babestu nautelako. Eskerrik asko zuei ere.

Bukatzeko, lan hau nire lagun bati eskeini nahi nioke, Iker Ruiz-i, bera joan zenean hasi bainintzen doktoradutza egiten, ta tesi hau berarentzako omenaldi txiki bat izatea nahiko nuke.

Contents

Sarrera Orokorra

Amida lotura

Prozesu biologiko askotan proteinek zeregin garrantzitsua dute, eta gorputzeko organu, ehun eta zelulen egitura, funtzio eta erregulazioan beharrezkoak dira. Proteinek funtzio desberdin asko burutzen dituzte, hala nola katalisi entzimatikoa, garraio eta metatzea (hemoglobina proteinak oxigenoa garraiatzen du), mugimendu koordinatuak, euskarri mekanikoa (giharren osagarri nagusia proteinak dira) edo inmune babesa (antigorputzak proteina oso espezifikoak dira). Beraz, argi dago proteinen azterketa ikertzaileentzako gai garrantzitsua izan dela.

Kimikoki, proteinak oinarrizko egitura unitatea (aminoazidoa) duten molekula handiak dira. Aminoazido bat amino talde bat, talde karboxiliko bat eta bi talde hauen artean dagoen eta alboko kate bat duen karbono batez (α karbonoa deritzaiona) osatua dago. α karbonoari lotuta dagoen alboko taldearen arabera hogei aminoazido mota desberdin ezagutzen dira. Aminoazido desbedinak 1. irudian azaltzen den modura konbinatuz eraikitzen dira: aminoazido baten talde karboxilikoa hurrengo aminoazidoaren amino taldearekin elkartzen da **lotura peptidiko** bat sortuz eta ondorioz ur molekula bat galduaz. Modu hortara aminoazido asko elkartu ondoren proteina bat osatzen da.

Lotura peptidikoaren ezaugarri garrantzitsu bat baldintza fisiologikoetan duen egonkortasun kimikoa da, hau da, lotura peptidikoaren hidrolisi ez entzimatikoa oso prozesu geldoa da. Adibidez, (fenil-lazetil)glizil molekularen bizitza erdia 243 urtetakoa da eta glizil-D-valine-rena 267 urtetakoa pH 7 denean.[1] Baina, zein da azalpen fisiko-kimikoa egonkortasun handi honentzat?

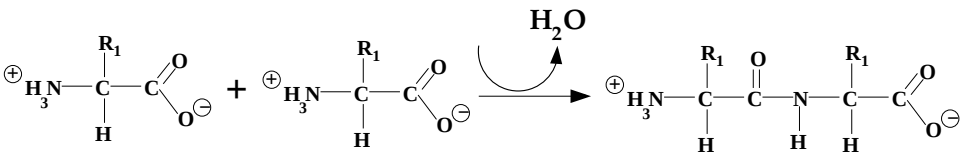

Irudia 1: Lotura peptidiko baten eraketa.

Amida loturaren ezaugarriak

Lotura peptidikoaren egonkortasuna hobeto ulertzeko asmoz eta proteinen tamaina handia dela eta, amida molekulak erabili izan dira lotura peptidikoen eredu bezela.[2,3] Amidak, $-CONH_2$ taldea duten konposatu organikoak dira. Beraz, amida lotura kimikoki lotura peptidikoaren analogoa da. Formamidaren ikerketa esperimental eta teorikoek amida loturaren ezaugarri garrantzitsuenak zehaztu dituzte:

- Nitrogeno atomoari lotuta dagoen taldeen koplanaritatea.[4–6] Hau da, nitrogeno atomoak amino taldeetan konformazio piramidala erakusten duen bitartean, atomo honek konformazio planarrra erakusten du amidatan.
- C-N lotura distantzia amino molekula batean baina dexente motzagoa da, eta C-O karbonilo loturaren distantzia aldehido batean baino zertxobait luzeagoa.[4,7,8]
- Molekulak C-N loturarekiko biratzen denean energi-langa handia (15-20 kcal/mol) erakusten du.[9–11]
- C-N loturaren luzatzea eta C-O loturaren murriztea amida loturekiko biratzen denean.[12–14]
- C-O frekuentzi murritza karbonilo talde bakun batekin konparatuz.[15,16]
- Nitrogenoaren basikotasun murritza amina baten nitrogenoarekin konparatuz.[17]
- Egongortasun kinetikoa eraso nukleofiliko edo hidrolisiarekiko. Adibidez, azetil-glizil-glizinaren bitzitza erdia 500 urtetakoa da pH=6.8 eta 25 °C-tan.[18,19]

Amida loturaren egonkortasunaren jatorria: erresonantzi eredua

Amida loturaren ezaugarri berezi hauen azalpen klasikoa **Erresonantzi Eredua**-ren bitartez ematen da.[20–23] Erresonantzia Pauling-ek deskribatu zuen lehenengoz[20] balentzi-lotura motako egitura elektroniko bakun batez bere propietateak azaldu ezin ziren substantzientzat, baina balentzi teoriaren eskema klasikoaren barruan egokitu daitezkenak bi egitura edo gehiago kontutan hartu ezkero. Amiden kasuan, molekula honen ezaugarriak 2. irudiko I eta II egiturak nahastuz azaldu daitezke. I erresonantzi egituran N atomoak sp^3 hibridazioa dauka eta ondorioz konformazio piramidala, C-N loturak izaera bakuna duelarik. Bestalde, II erresonantzi egituran N atomoak sp^2 hibridazioa daukanez C-N loturak izaera bikoitz partziala dauka,

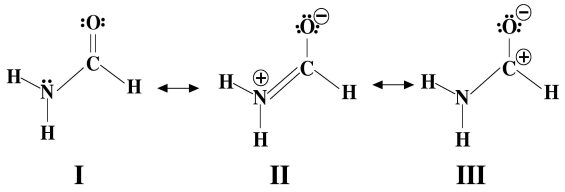

Irudia 2: Erresonantzi ereduaren Lewis egiturazko hiru kontribuzio nagusiak.

eta honek azaltzen du amiden berezko planaritasuna eta honek dakarren egonkortasuna.

Orbital Molekular teoriaren barruan, amidetan ematen den erresonantzia dagokien π orbitalen izaera deslokalizatua aztertuz ondoriozta daiteke (ikus 3. irudia). Nitrogenoaren 2p orbitala eta karbonilo taldearen π^* orbitalaren arteko partaidetzak, N-C-O egituran zehar π orbitalaren deslokalizaio zabala dakar. π_1 HOMO-2 orbitalari dagokion energia baxua ikusiz, neurri batean egonkortasun efektua ondorioztatu daiteke. Hala ere, orbital molekularren berezko natura deslokalizatua dela eta zaila da modu hontan egindako egitura elektronikoaren deskripzioaren bitartez erresonantzi efektuaren neurketa zehatz bat egitea.

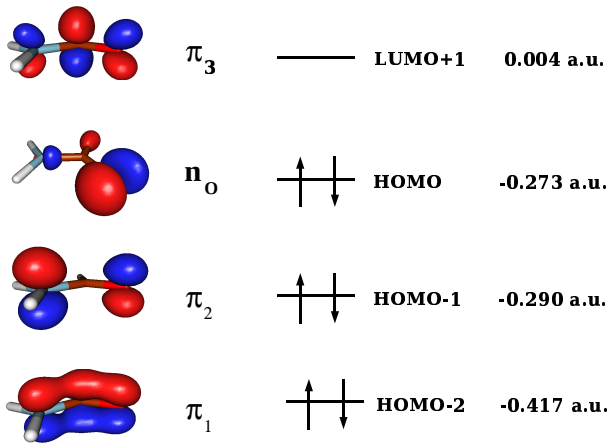

Irudia 3: Formamida molekularen zenbait orbital molekular. B3LYP/6-31+G(d) teoria mailan kalkulatutako beraien orbital-energia erakusten da, unitate atomikotan.

Amida erresonantziaren deskripzio kuantitatiboago bat egiteko "Natural Bond Orbital" (NBO) analisia erabil daiteke, zeina Weinhold *et al.*-ek[24,25] garatutako teknika den uhin funtzio poliatomikoetan hibridazio eta kobalentzi efektuak aztertzeko. NBO-ak, molekulen egitura elektronikoa

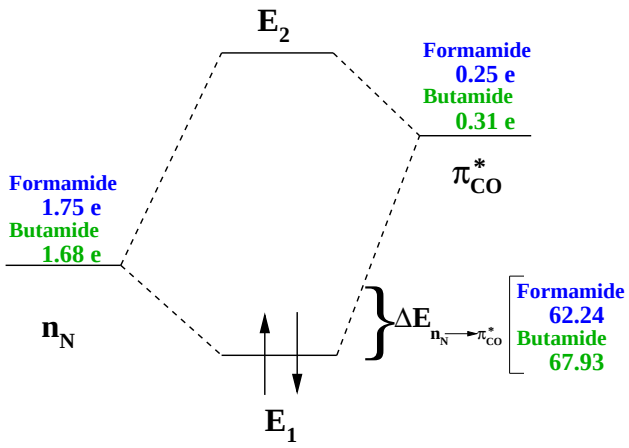

Irudia 4: Nitrogenoaren konpartitu gabeko bikotea (n_N) eta karboniloaren antiloturazko π orbitalaren (π^*_{CO}) arteko elkarrekintza. Formamida eta butamidarentzat B3LYP/6-31+G(d) teoria mailan elkarrekintza horren ondorioz ematen den energiaren jeitsiera erakusten da kcal/mol-etan.

lotura lokalizatu eta konpartitu gabeko elektroi bikoteen bitartez osatzen ditu. Hala ere, NBO-rantzko transformazio orokorrak Lewisen egitura formalean okupatu gabe dauden orbitalak sortzen ditu, eta hauek efetu "ez-kobalenteak" deskribatzeko erabil daitezke. Hauen artean, garrantzitsuenak σ^* eta π^* antiloturak dira. Antiloturek erabili gabeko balentzi-geruzen gaitasuna adierazten dute, lotura kobalentearen eraketaren baitan formalki saturatu gabe dauden atomo-balentzia eremuen zatiak kontuan hartuz. Hartree-Fock teoriaren barruan, antilotura hauen okupazio txiki batek Lewis egitura idealetik hurrentzea suposatzen du; ondorioz, ez-kobalentzi zuzenketa txiki batzuk kontuan eduki behar dira lotura kobalente lokalizatuen irudian. Normalean zuzenketa hauek oso txikiak direnez (energi totalaren % 1 baino gutxiago) ondorengo ekuazioan azaltzen den bigarren ordeneko perturbazio espresioaren bidez hurbildu daiteke:

$$\Delta E^{(2)}_{\sigma\rightarrow\sigma^*} = -2\frac{<\sigma|\hat{F}|\sigma^*>^2}{\sigma^* - \sigma} \quad (1)$$

non $\hat{F}$ Fock operadorea den, σ Lewis orbital bat den eta σ^* ez-Lewis orbital bat. Amiden kasuan, mota hontako egonkortze-elkarrekintzarik garrantzitsuena $n_N \rightarrow \pi^*_{CO}$ deslokalizazio edo erresonantziari dagokio (4. irudian eskematikoki azaltzen da). Elkarrekintza honek 62.24 eta 67.93 kcal/mol suposatzen du formamida eta butamidaren kasuan hurrenez-hurren. Beraz, NBO teoria erabiliz amidaren egonkoratsunaren jatorria erresonantzi efektuan dagoela zehaztu daiteke, bereziki, $n_N \rightarrow \pi^*_{CO}$ elektroi-deslokalizazioa.

Azkenik, "Natural Resonance Theory" (NRT)[14,26] erabili izan da erresonantzi egitura desberdinen pisua zehazteko. Bertan ikusi denez, 2. irudiko I eta II egiturek erresonantzi hibrido guztien % 90 suposatzen dute, eta hauen artean II Lewis egiturak gutxi gora behera erresonantzi hibrido guztien %30-a suposatzen du.

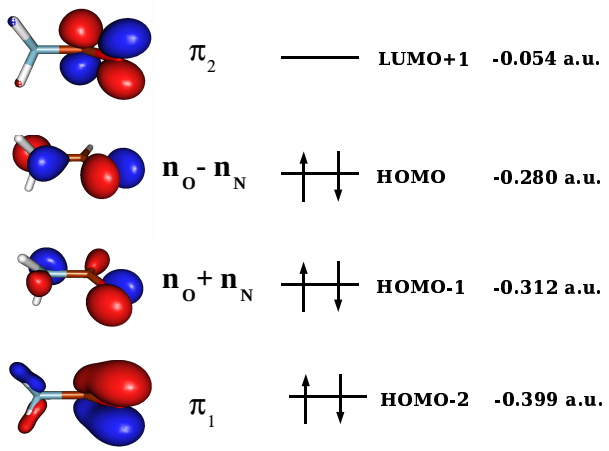

Irudia 5: Formamida molekularen biraketa anti trantsisio egoeraren zenbait orbital molekular. B3LYP/6-31+G(d) teoria mailan kalkulatutako beraien orbital-energia erakusten da, unitate atomikotan.

Bihurdura-katalisia

$n_N \rightarrow \pi^*_{CO}$ deslokalizazio optimo bat eman dadin amida taldearen planaritatea ezinbestekoa da. Ikerketa esperimental[27–31] eta teorikoen[32–36] ondorioz amidek biraketa-langa altu bat dutela zehaztu da, 15-20 kcal/mol ingurukoa. Gainera, langa hauek amiden erresonantzi-egonkoartasunaren neurri bezela erabili izan dira. Kontuan izan transitio egoeran (ikusi 5. irudia) n_N orbitala π^*_{C-O} orbitalaren planu nodalean kokatzen dela, $n_N \rightarrow \pi^*_{CO}$ deslokalizazioa eragotziz. Hau NBO analisiak konfirmatzen du, non $n_N \rightarrow \pi^*_{CO}$ elkarrekintza ez den antzematen; orbital molekularren analisian ere (ikus 5. irudia) elkarrekintza horrek ez duela existitzen antzeman daiteke, n_N eta π_{C-O}/π^*_{C-O} orbitalak ortogonalak direla argi ikusten baita. $n_N \rightarrow \pi^*_{CO}$ elkarrekintza puskatzearen ondorioz, nitrogen atomoak sp^3 hibridazioa hartzen du, dagokion konfigurazio piramidalarekin. Lewis egituren terminotan, I erresonantzi-egitura nahikoa da egitura elektronikoaren ezaugarri garrantzitsuenak deskribatzeko. Laburbilduz, asko biratutako amida egitura hauetan, $n_N \rightarrow \pi^*_{CO}$ erresonantzia puskatua dagoelako du egitura planarrak baino energia altuagoa.

Hidrolisiarekiko amida lotura aktibatzeko hipotesi batek goian azaldutako propietatea aprobetxatu nahi du eta aldez aurretik bihurritutako egitura duen amida bilatu, non ez dagoen $n_N \rightarrow \pi^*_{CO}$ erresonantziarik. Amida loturaren bihurriketa modu desberdinetan lortu daiteke, bai behartutako egitura baten bitartez, edota baita entzima baten eraginez substratoak bihurritako konformazio bat hartu dezan behartuz ere. Mota hontako "egoera egonkorraren desegonkortzea", "Protein Splicing" deritzaion prozesu batean ematen den katalisi mekanismo bezela proposatu da.[37–40] Hau ere trantsisio egoeren antzekotasuna deritzaion diseinuaren oinarria izan daiteke, zeina antigorputz katalitikoak garatzeko "haptens" bezela erabiltzen diren, erreaktiboan egoera egonkorraren desegonkortasuna eragiten duten lotura peptidikoaren apurketa katalizatzeko asmoz.[41–43] Bestalde, bihurriketaren bitartez entzimak lotura peptidikoaren apurketa katalisatzen duen zenbait kasu ezagutzen dira, proline cis-trans isomerasak adibidez.[44–46] Ondorioz, peptidoetan eman daitekeen amida loturen deformazio ez-planarra interes handia sortu du.[47]

Bihurritutako amidak

Amidaren bihurriketak bere egitura eta energi-propietateetan ze eragin duen aztertzeak berez garrantzia izateaz gain, bihurdura-katalisiak eragin dezakeen abiadura azkartzea ulertzeko asmoz ezinbestekoa da amida mota hauen ikerketa. X-izpien data[48] eta formamidaren biraketa landaren ikerketa konputazionalek[12,13,49–52] argi ta garbi usten dute C-N lotura biratzerakoan lotura hori ahultzen dela. Zoritxarrez, bihurritutako amida ez planarrei buruzko data kinetiko zehatz gutxi dago eskuragarri. Blackburn *et al.*-en lan batean,[53,54] egitura zikliko baten bitartez amida lotura bihurritua duen amida molekula baten (benzoquinuclidin-2-one) hidrolisi alkalinoa, bihurritu gabeko antzeko amida baten hidrolisiarekin konparatzen da, lehengoaren kasuan erreakzioa 10^7 azkarragoa izanik; honek aktibazio-langa 10 kcal/moltan jeistea suposatzen du. Esperimentu honekin bat dator Brown *et al.*-ek aurkitutako azelerazioa distorsionatutako amidentzat.[2,55] Gainera, dirudienez azkartze-maila pH egoeraren funtzioan dago, hidrolisi alkalinoan 7 magnitu-ordenekoa den bitartean hidrolisi azidoan 11 magnitude-ordenekoa baita. Beranduago, Kirby *et al.*-ek[56–58] bihurdura handiko amida-lotura duen 1-aza-2-adamantanone molekulak uretan (partzialki egoera azidoan) jasaten duen hidrolisi azkarraz berri eman zuten, zeinak hidrolisi abiaduraren oraindik abiadura handiagoa adierazi dezakeen. Bihurdua handiko amida honen kristal-egiturak 1.475 Å-ko amida lotura eta 1.196 Å-ko karbonilo lotura erakusten du; balio hauek formamidaren biratze trantsizio-egoeran neurtako balioetatik oso gertu daude, amida hontan $n_N \rightarrow \pi^*_{CO}$ deslokalizaziorik ez dagoela pentsa daitekeelarik.

Lan honen helburua

Bihurritutako amidaren eta bere antza duen amida planarraren hidrolisi erreakzioaren arteko berdintasun eta desberdintasunak aztertu gabeko gai bat da oraindik, eta lan asko dago egiteko beraien erreakzio-bideen karakterizazio eta trantsizio-egoeren aurkikuntzan. Lan hau helburu horren ekarpen bat da kimika kuantikoak eskeintzen dituen tresnak aprobetxatuz. Amiden hidrolisiaren konputazio-azterketak batez ere formamida bezelako amida planarrei zuzendu dira,[59–75] bihurritutako amidei buruz literaturan ikerketa gutxi aurkitu daitezkeen bitartean.[55,76–78] Beraz, tesi honen helburua amiden propietateetan eta erreaktibitatean bihurritzeak dituen eraginak sakonkiago deskribatzea da. Tesi hau bi zatitan banatua dago:

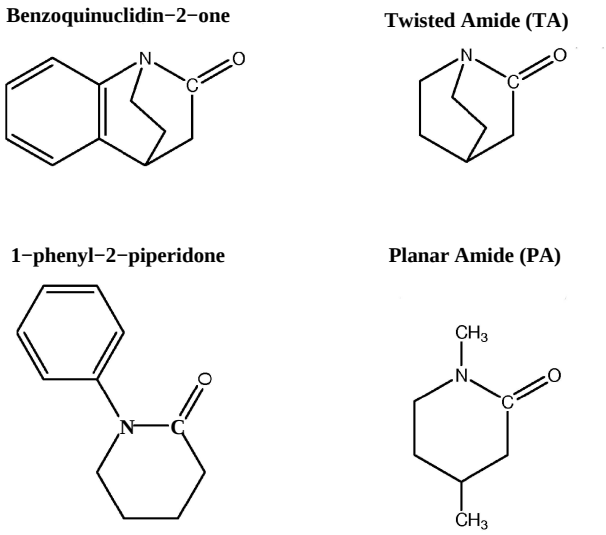

Irudia 6: Ezkerraldean, Blackburn *et al.*-ek[54] erabilitako amida erreaktiboa C-N bihurritzearen ondorioz ematen den hidrolisiaren abiadura-azkartzea ikertzeko. Eskubialdean, molekula experimental horien gure eredu teorikoak: goian bihurritutako amida (Twisted Amide, **TA**), eta behen amida planarra (Planar Amide, (**PA**).

- I zatia: Bihurritutako amiden funtsezko propietateen azterketa. Lehenengo kapituluan amida-erresonantzia maila karakterizatu eta arrazonatzen da, hortarako Atomoak Molekulan ("Atoms in Molecules", AIM) deritzaion teorian oinarritutako deslokalizazio indizeak erabiliz. Ikerketa hauen helburua, bihurriketaren ondorioz galdutako $n_N \rightarrow \pi^*_{CO}$ erresonantzia maila kuantitatiboki neurtzeaz gain, erresonantzia karakterizatzeko indize kuantiko egoki bat definitzea da. Bigarren kapituluan zenbait bihurritutako amiden pK_a balioak karakterizatzen

dira. Balio hauek garrantzitsuak dira pH-ren funtzion erreakzio-bide jakin batzuk aurkitzeko. Hala ere, bihurritutako amiden hidrolisi azkarra dela eta arazoak daude esperimentalki balio horiek ebaluatzeko.

- II zatia: bihurritutako amida prototipo baten hidrolisi alkalinoa (hirugarren kapitulua), neutroa (laugarren kapitulua) eta azidoen (bostgarren kapitulua) erreakzioak karakterizatuko ditugu. Erabilitako bihurritutako amida (6. irudiko **TA**) Blackburn-ek erabilitakoaren antzekoa da. Egitura honek duen kaxa egitura dela eta nitrogeno atomoak konformazio piramidala har dezan behartzen da. Erreakzio mota bakoitzarentzat zenbait mekanismo proposatzen dira: i) kontzertatua vs. pausoka, ii) ur molekula baten laguntzarekin edo gabe, eta iii) gas fasean vs. soluzioan. Gainera, bihurriketaren ondorioz ematen den abiadura-azkartzea zalantzarik gabe neurtzeko, antzeko amida planar baten (6. irudiko **PA**) hidrolisi erreakzioa ere aztertzen da kasu guztietan.

I zatiko (batez ere pK_a-ren ebaluazioa) eta II zatiko erreaktibotasun emaitzetan oinarriturik, pH-ren funtzioan erreakzio konplexu honen irudi orokor bat egiteko gai izango gara, bihurritutako amida eta amida planarraren hidrolisiaren arteko berdintasun eta desberdintasunak azpimarratuz. Emaitzak ez dira teoriaren ikuspuntutik interesgarriak bakarrik; erreakzio mota hontan amida loturaren biraketak duen eragina argitzen ere lagundu dezake, eta katalisia eman aurretik amidaren bihurriketa eskatzen den katalisi biokimikoak hobeto ulertzen ere lagundu dezake.

Bukatzeko, lan honen antolaketa kronologikoari buruz azalpen bat egin beharra dago. Lan honen kapitulu bakoitza argitarapen independente baten gaia izan da. Hala ere, publikazio hauen orden kronologikoa eta tesi hontako kapitulu desberdinen ordena ez datoz bat. Lehenengo argitarapena argitaratzen hirugarren kapituluko hidrolisi alkalinoa izan zen,[79] ondoren zenbait bihurritutako amiden pK_a-en ebaluazioa,[80] gero hidrolisi neutroa (laugarren kapitulua),[81] eta azkenik, bidali diren azken bi lanak hidrolisi azidoa (bostgarren kapitulua)[82] eta deslokalizazio indizeen karakterizazioa amidetan (lehenengo kapitulua)[83] izan dira. Kapitulu desberdinen arteko errepikotasunak kentzen ahalegindu gara, baina kapitulu bakoitzaren kohorentzia eta kapitulu eta argitarapenen arteko koherentzia galdu gabe.

Hurrengo atalean tesi hontan zehar erabili diren zenbait metodo kuantiko-mekanikoen deskripzio labur bat aurkezten da. Tesi honen helburuetatik kanpo dago metodo hauen deskripzio zehatz eta sakon bat. Interesatuek lan espezifikoagoak aurki ditzakete hortarako.[84]

Kimika kuantikoa

Joan den mendearen hasieran garaturiko teoria kuantikoak[85–88] zeharo aldatu zuen mundu mikroskopikoaren inguruan fisikariek zuten ikuspuntua. Teoria hau baino lehenago garaturiko teoria guztiek ezin zuten atomoen egonkortasuna azaldu. Bohr-ek atomo sinpleenaren egonkortasuna elektroiak nukleoaren inguruan orbita egonkorretan bueltaka ibiltzen direla esanez azaldu zuen. Elektroi batek orbita batetik bestera mugitzeko energi kuantu bat askatu edo absorbatu egin behar du. Beste hitzetan esanda, energia kuantizaturik dago, ez da jarraia. Teoria kuantikoan hau teoriaren ondorioa da, ez da aldez aurretik finkaturiko gauza. Hasiera batean teoria fisikarien munduan garatu zen, baina berehala kimikan izan zitzazkeen aplikazioak behatu ziren, kimika kuantikoa sortuz. Urteen poderioz kimika kuantikoa kimikarientzako arrunt erabilgarria bihurtu da, molekulen propietateak kalkulatu, ulertu eta iragartzeko.

Printzipioz sistema bati buruzko informazio guztia bere uhin funtzioak ematen digu. Uhin funtzioa zein den jakiteko Schrödinger-en ekuazioa askatu "besterik"ez dugu egin behar:

$$\widehat{H}\Psi = E\Psi \tag{2}$$

$\widehat{H}$ hamiltondarrak nukleo eta elektroien energia kinetikoa, elektroi-elektroi, elektroi-nukleo eta nukleo-nukleo elkarrekintzak kontuan hartzen ditu. Born-Oppenheimer[89] hurbilketa kontuan hartuta, elektroien eta nukleoen higidura banatzen dira, eta hortaz $\widehat{H}$-an nukleoen koordenatuak parametro konstanteak dira. Zoritxarrez, ekuazio hau elektroi bat baino ez duten sistemen kasuan bakarrik askatu daiteke, hidrogeno atomoa, adibidez. Hau dela eta metodo hurbilduak garatu behar izan dira:

1. Uhin-funtzioan oinarritzen diren metodoak: bariazionalak (konfigurazioen elkarrekintza) edo gorputz-anitzezko perturbazio teoria.

2. Dentsitate-funtzionalaren teoria (DFT).

Ez da atal honen helburua metodo hauen guztien deskribapen osoa egitea. Beraz, interesaturik dauden irakurleak gai hauek lantzen dituzten literaturara zuzentzen ditugu. Ikusi adibidez:[90–94]

Uhin-funtzioan oinarrituriko metodoak izan ziren lehenengoak garatzen. Urte askotan zehar erabilienak izan diren bi metodoak Balentzi Lotura (BL) metodoa eta Molekula-Orbitalen (MO) metodoa izan dira. BL metodoa 1927. urtean Heitler eta London-ek formulatu zuten.[95] MO metodoa beranduago garatu zen, Hund,[96] Mulliken[97] eta beste batzuen eskutik. Metodo hau erabiliena bilakatu zen bere botere kuantitatiboaren ondorioz. MO-k

orbital ortogonalak erabiltzen ditu, kalkulua anitz errazten delarik. Ez ordea VB metodoak, orbital ez-ortogonalak erabiltzearen ondorioz kalkulua luzeagoa eta korapilotsuagoa, hortaz garestiagoa, delarik.

Hastapenetan garatu zen lehendabizietako molekula-orbital metodoa Hartree Fock (HF) metodoa[98,99] izan zen. Bertan uhin-funtzioa elektroi-bakarreko orbitalen antisimetrizaturiko biderkadura da. Elektroiak nukleoaren eta beste elektroien eraginez sorturiko batezbesteko eremuaren eraginpean higitzen direla suposatzen da. Metodo honen arazorik handiena da kontrako spina duten elektroien arteko korrelazioa kontuan hartzen ez duela. Korrelazio mota hau kontuan hartzeko hainbat bide dago. Møller-Plesset[100] teoria (MPn, n perturbazio-ordena izanik) bezalako perturbazio-metodoetan elektroi korrelazioa HF arazoaren perturbazioa bezala kontsideratzen da. Konfigurazioen Elkarrekintza[101,102] metodoan uhin-funtzioa konfigurazio desberdinen konbinazio lineala bezala adierazten da, elektroi-anitzezko uhin-funtzio zehatzaren emaitza bariazional hobeagoa lortzeko asmoz. Beste metodo sofistikatuagoak egon badaude, Coupled Cluster (CC),[103–105] Erreferentzia Anitzezko Konfigurazioen Elkarrekintza edo Espazio Eraginkor Osoa metodoak,[106,107] oinarrizko egoera zein egoera eszitatuen propietate elektronikoak aztertzeko tresna arras erabilgarriak direlarik.

Tesi honetan aurkezten dugun lanaren gehiena dentsitate-funtzionalean oinarrituriko metodoak erabilita burutu da. Ondorengo azpiatalean metodo hauek sakonago deskribatuko ditugu.

Dentsitate-Funtzionalaren Teoria

Dentsitate-Funtzionalaren Teoriaren formalismoak N elektroiren uhin funtzioa eta dagokion Schrödinger-en ekuazioaren ordez askoz ere sinpleagoa den $\rho(\vec{r})$ elektroi-dentsitatea jartzen du. Hau hiru aldagai espazialen funtzioa da. Egoera elektronikoa, energia eta edozein sistemaren propietate elektroniko guztiak $\rho(\vec{r})$ honen funtzioan deskritu daitezke.[92,93]

Hohenberg eta Kohn-ek[108] degeneratua ez den oinarrizko egoera duen sistema baten propietate elektronikoak $\rho(\vec{r})$ elektroi-dentsitateak determinatzen dituela demostratu zuten. Hortaz, E_0 oinarrizko egoeraren energia $\rho(\vec{r})$-ren funtzionala da. Orokortuz, oinarrizko egoeraren elektroi-dentsitatea jakinez gero, oinarrizko egoeraren propietate elektroniko guztiak kalkulatzea posible da, behin funtzional-dependentziak finkatu ondoren. Energi funtzionala aurkitzeko energiaren bariazio-printzipio bat finkatu zuten, uhin funtzioaren bariazio-printzipioaren antzerakoa. Horrela, $E[\rho]$ funtzionalaren forma zehatza jakinik oinarrizko egoeraren dentsitatea bilatu dezakegu (uhin-funtzioaren kasuaren antzera). Tamalez, funtzioanalaren forma esaktoa ezezaguna denez, Kohn eta Sham-ek[109] funtzional honen hurbilketa ez-zuzen bat garatu zuten, Kohn-Sham metodoa, alegia. Ondorioz DFT kalkulu zehatzak

egiteko tresna erabilgarria bihurtu zen. Haiek N elektroiz osaturiko eta ρ oinarrizko egoeraren elektroi-dentsitate duen molekula baten E_0 oinarrizko egoeraren energia elektronikoa ondorengoa dela erakutsi zuten:

$$E_0 = -\frac{1}{2}\sum_{i=1}^{N} < \psi_i(1)|\nabla_1^2|\psi_i(1) > + \tag{3}$$

$$+ \int \upsilon(r)\rho(1)d\vec{r}_1 + \frac{1}{2}\int\int \frac{\rho(1)\rho(2)}{r_{12}} d\vec{r}_1 d\vec{r}_2 + E_{xc}[\rho]$$

$\upsilon(r) = -\sum_\alpha \frac{Z_\alpha}{r_{1\alpha}}$ nukleoen eraginez dagoen kanpo-potentziala da, ψ_i Kohn-Sham orbitalak dira, eta $E_{xc}[\rho]$ truke-korrelazio energia da.

Kohn-Sham prozeduran oinarrizko egoeraren ρ esaktoa Kohn-Sham orbitaletatik lortu daiteke,

$$\rho = \sum_{i=1}^{N} |\psi_i|^2 \tag{4}$$

eta Kohn-Sham orbitalak,

$$\hat{F}_{KS}(1)\psi_i(1) = \varepsilon_i\psi_i(1) \tag{5}$$

elektroi bakarreko ekuazioak ebatziz lortzen dira, $\hat{F}_{KS}$ Kohn-Sham operadorea

$$\hat{F}_{KS} = -\frac{1}{2}\nabla_1^2 + \upsilon(1) + \sum_{j=1}^{n} \hat{J}_j(1) + V_{xc}(1) \tag{6}$$

delarik. $\hat{J}$ Coulomb operadorea da, eta V_{xc} truke-korrelazio potentziala. $\hat{F}_{KS}$ HF ekuazioetan agertzen den Fock operadorea bezalakoa da, gauza batean izan ezik. Truke operadorearen ordez, truke eta korrelazioa kontuan hartzen dituen V_{xc} jartzen da.

Ekuazio hauek iteratiboki ebazten dira. Hasierako dentsitate batetik hasita $\hat{F}_{KS}$ eraikitzen da, eta 4. ekuazio-taldea ebazten da. Emaitza $\hat{F}_{KS}$ berri bat eratzeko erabiltzen da. Prozedura hau konbergentzia lortu arte errepikatzen da.

Kohn-Sahm orbitalen esanahi fisikoa eztabaidan dago oraindik. Autore batzuen arabera ez dute inolako esanahirik, bakarrik ρ zehatzaren kalkuluan erabilgarriak dira. Era berean, Kohn-Sham orbitalen energiak molekula-orbitalen energiekin ez lirateke nahastu behar. Beste batzuk, ordea, HOMO-ren Kohn-Sham energia ionizazio potentzialaren negatiboa dela kontuan harturik,[110,111] eta honetaz gain Kohn-Sham ekuazioak, HF kasuaren antzera, partikula askeen eredua gogora ekartzen duela kontuan harturik, Kohn-Sham orbitalei HF orbital kanonikoek duten antzeko esanahi fisikoa egokitzen diete.

Azken aldiko argitalpenetan DFT-aren bidez lorturiko molekula-orbitalak eta estandar MO-LCAO metodoen bidez lorturikoak arras antzekoak direla ikusi da. Hortaz, molekulei buruzko informazio erabilgarri asko beraien MO-ak aztertuz lortu izan da, hauek DFT-aren bidez lortuak izan arren.[110,112]

Dena dela, beste arazo bat dago: $E_{xc}[\rho]$ truke-korrelazio funtzionala eta beraz $v_{xc}[\rho;\overrightarrow{r}]$ truke-korrelazio potentziala elektroi-gas uniformearen kasurako baino ez da ezagutzen. Zorionez, funtzional hurbilduak garatu dira. Hurbilketa sinple bat dentsitate lokalaren hurbilketa (DLH) da. Honen ideia $\rho(\overrightarrow{r})$ dentsitate lokala duen bolumen elementu bakoitza elektroi-gas homogeneoa bezala kontsideratzea da. Ikuspuntu honetatik hurbilketa hau dentsitatea espazioan zehar mantso aldatu ezkero zehatza izango da. $E_{xc}[(\rho)]$ ondorengo espresioak ematen du:

$$E_{xc}^{LDA}[(\rho)] = \int \rho(\vec{r})\varepsilon_{xc}(\rho)d\vec{r} \tag{7}$$

$\varepsilon_{xc}(\rho)$ ρ elektroi-dentsitate duen elektroi-gas homogeneoaren truke plus korrelazio energia elektroi bakoitzeko da. $\varepsilon_{xc}(\rho)$-rentzako espresio zehatz bat Vosko, Wilk eta Nusair-ek[113] aurkitu zuten. Espresio hau aplikatuta dentsitate lokalaren hurbilketa (DLH) edo spin dentsitate lokalaren hurbilketa (SDLH)[114] lortzen dira. Azken honen kasuan spin desberdina duten elektroientzako orbital eta ρ^{α} eta ρ^{β} dentsitate desberdinak erabiltzen dira. Noski, molekulen kasuan hauek benetako funtzionalaren hurbilketak besterik ez dira, ρ homogeneoa ez delako. Hurbilketa dentsitate-gradientearen araberako espansio bat eginez hobetu daiteke. Metodo hauek generalizaturiko gradientearen hurbilketa (GGA) dira, eta molekulen azterketan garrantzi handia dute, elektroi-dentsitatea homogeneoa dela ezin baita kontsideratu.

DFT metodoek sistema kimiko gehienetan emaitza bikainak ematen dituztela demostratu da,[115] CPU intentsiboak diren elektroi-korrelazio metodoekin konparagarriak izanik. Hala ere, askotan loturen disoziazio energiak gainestimatzen dituzte.[116] HF eta DFT-ren arteko hibridoak disoziazio energiaren zehaztasuna handitzen dute, Johnson-ek *et al.* erakutsi bezala.[117] Becke 3 hibridoa[118] Lee-Yang-Parr (B3LYP)[108,119,120] korrelazio funtzionalarekin konbinatuta, erabilienetako bat bihurtu da, ondorengo forma duelarik:

$$(1-a_0)E_x^{LSDA} + a_0E_x^{HF} + a_xE_x^{B88} + a_cE_c^{LYP} + (1-a_c)E_c^{VWN} \tag{8}$$

Parametroen baloreak a_0=0.20, a_x=0.72 eta a_c=0.81 dira, hurrenez hurren. Funtzional honi Becke-ren 3 parametrodun funtzionala esaten zaio, B3LYP.

DFT kalkuluek E_{xc} zehatza erabiltzen ez dutenez, ez dira, zehazki mintzatuz, ab-initio kalkuluak. Dena dela, datu esperimentalak doitzeko parametrorik erabiltzen ez dutenez, espiritualki ab-initio kalkuluetatik erdienpirikoetatik baino gertuago daude. Metodo hauen abantaila handienetako bat HF metodoaren koste konputazional antzekoa izanik elektroi-korrelazioa

kontuan hartzen dutela da. Dena dela, korrelazio efektu hauek ezin dira zehazki sailkatu, hastapenetik ez-korrelaturiko emaitzarekin nahasturik baitaude. Honetaz gain, sofistikazio gehiago aplikatuz, kalkuluak hobetzeko bide sistematikorik ez dago, eta honen ondorioz emaitzak diren bezala onartu behar dira. Arazo hauek izan arren, DFT-k sistema kimiko batzuen oinarrizko egoeraren propietateentzako emaitza onak eman ditu, MP2-rekin alderagarria den kalitatearekin[121] batzuetan, eta hobeagoa beste kasu batzuetan. Koste konputazional baxua dela eta, sistema handien kasurako DFT aukeratzen den metodoa da, elektroi-korrelazioa MP edo CI metodoen bidez kontsideratzea oso garestia baita.

Oinarri-taldeak

Uhin-funtzioan zein dentsitate-funtzionalean oinarrituriko metodoek uhin-funtzioa espanditzeko funtzio-talde bat beharrezkoa dute. Funtzio-talde hauei oinarri-taldeak deritze. Oinarri-talde egokiaren aukeraketa oso garrantzitsua da kalkuluaren arrakastarako. Dena dela, oinarri-taldearen zehaztasuna eta bere tamaina kontuan hartu behar ditugu, oinarriaren tamaina handitzean kalkuluaren kostea garestiago egiten baita. Kimika kuantikoan egiten diren kalkuluetan gehien erabiltzen diren funtzioak Kontraituriko Funtzio Gaussiarrak (KFG) dira. Hauek funtzio Gaussiarren (hasierakoak) konbinazio linealez (kontrakzioak) osaturik daude.

$$\varphi_\mu^{CGF}(|\vec{r}-\vec{R}_A|) = \sum_{p=1}^{L} d_{p\mu} g(\alpha_{p\mu}, |\vec{r}-\vec{R}_P|) \tag{9}$$

$\alpha_{p\mu}$ aintzindarien berretzaileak eta $d_{p\mu}$ kontrakzioen koefizienteak elementu desberdinentzako optimizatzen dira.

Potentzial-Energi Gainazalean zehar mugitzen

Born-Oppenheimer hurbilketak Potentzial-Energi Gainazal (PEG)-aren kontzepturantz zuzentzen gaitu. Nukleoak bata bestearekiko mugitzean potentzial energia nola aldatzen den deskribatzen duen funtzionala da PEG-a. Molekula osoaren errotazio eta translazioren sei askatasun graduak kenduta, molekula ez-linearren kasuan 3N-6 askatasun gradu egongo dira. Beraz, PEG-a 3N-6 dimentsiodun hipergainazal ba da, non guk minimo eta "ahulki puntua"-ak (saddle-point) aurkitu nahi ditugun.

Minimo eta ahulki puntuak

Maila kuantikoan PEG osoaren karakterizazioa molekula txikiekin bakarrik egin daiteke, baina PEG-aren zenbait puntu konkretu lortu ezkero informazio asko eskuratu daiteke molekulari eta bere konportamenduari buruz. Molekularen isomero egonkorrak adierazten dituztenez, funtsezko puntuak dira PEG-an dauden minimo lokalak. Beraiek molekularen egitura

eta inertzi momentua zehazten dituzte, zeinetatik errotazio-espektroa lortu daitekeen. Minimo lokalaren inguruko PEG multi-dimentsionalaren kurbaturak, pareten maldak, molekularen bibrazio-propietateak determinatzen ditu, modu normalak eta bibrazio-frekuentzia harmonikoak barne.

PEG-eko beste funtsezko puntu bat bi bailara edo minimo konektatzen dituen energia baxueneko ahulki puntua da. Ahulki puntua, bi minimo hauek konektatzen dituen energi baxueneko bide osoko punturik altuena da. Askatasun gradu batekiko maximoa den bitartean gainontzeko askatasun graduekiko minimoa izatearen propietatea dauka. Ahulki puntuaren esanahia da "botila-lepo" dinamikoaren hurbilketa dela, itzulerarik gabeko puntua izanik minimo lokal baten ingurutik beste minimo lokal baterako transformazioan. Erreakzio probabilitateak (edo abiadurak) ahulki puntu honen energiaren altuerarekiko menpekotasun handia dauka.

Bai minimoa eta baita ahulki puntua ere puntu egonkorrak dira PEG-ean; energiaren deribatua geometri-koordenatu bakoitzarekiko, eta beraz indarra, atomo bakoitzean zero da; ondorioz, i guztientzat,

$$\frac{dE(q_1, q_2, ..., q_m)}{dq_i} = 0 \tag{10}$$

Minimo eta ahulki puntuak kokatzen

Puntu egonkorrak aurkitzeko garaian, barne-koordenatuen sistemak definitzen du lehenengo pausoa. Parametroak elkar-erlazionatuak (parekatuak) ez dauden koordenatu sistema bat aukeratzeko esfortzuak egin dira. Parekatzea ezin denean ekiditu, analitikoki kalkulatutako Hessiar bat izango da abiapuntua. Bestalde, pare-koordenatuen ordez beste aukera batzuk aurkeztu dira (koordenatu kartesiarrak eta koordenatu erredundanteak).

PEG batean puntu egonkorrak kokatzeko metodo desberdinak daude, "optimizazio metodoak".[122–124] Kimika konputazionalean esfortzu handia egin da ebaluatu beharreko funtzio kopurua murrizten kalkulu denbora azkartzeko asmoz. Gaur egun ia ab-initio metodo guztietan lehenengo deribatuak eskuragarri direnez, hurrengo diskuzioa metodo horietan oinarrituko da.

Metodorik eraginkorrenari metriko aldakorra edo quasi-Newton metodoa deritzaio. Metodo honek bigarren deribatuaren matrizearen hurbilketa bat behar du, zeina optimizazioan zehar informazio berriarekin eguneratzen doan. Metodo arruntenek ekuazio desberdinak dituzte bigarren deribatuaren matrizea (Hessiar matrizea deritzaio) eguneratzeko. PEG-a, 3N koordenatu kartesiar edo 3N-6 barne-koordenatuekiko (3N-5 molekula linearrentzat) funtzioa puntu arbitrario batean espanditu daiteke, non desplazaturiko $\vec{x}$ puntu bateko energia Taylor seriek ematen duen,

$$E(\vec{x}) = E_0 + \sum_i \frac{\partial E}{\partial x_i} x_i + \frac{1}{2} \sum_{i,j} \frac{\partial^2 E}{\partial x_i \partial x_j} x_i x_j + ... \tag{11}$$

Seriea termino kuadratikoa eta gero mozten bada, bektore notazioan horrela geratzen da seriea:

$$E(\vec{x}) = E_0 + g_o^\dagger x + \frac{1}{2} x^\dagger F_0 x \tag{12}$$

non,

$$g_i = \frac{\partial E}{\partial x_i}|_0 \tag{13}$$

$$F_{i,j} = \frac{\partial^2 E}{\partial x_i \partial x_j}|_0 \tag{14}$$

$E(\vec{x})$- ren deribatua hartuz,

$$\frac{\partial E}{\partial x} = g_0 + F_0 x \tag{15}$$

Puntu egonkor batean $\frac{\partial E}{\partial x} = 0$ eta $x = -F_0^{-1} g_0$ edo $x = -H_0 g_0$ dira, non H_0 Hessiar matrizearen inbertsoa (F_0^{-1})-ren hurbilketa bat den. Hurrengo pausoetan H_0 eguneratu egiten da eguneratze-formula baten bitartez H_0 berri bat lortzeko.

Eguneratze eskema desberdinak proposatu dira. Arrakastatsuenak BFGS eta DFP (David-Fletcher-Powell) eguneratze-formulak dira. Lehenengo eguneratze formulak sendoagoa dirudi.[125,126] Bilatzen ari den puntu egonkorraren natura Hessiarrak ongi isladatzen badu metodoak oso ondo funtzionatzen du.

Mota konkretu bateko puntu egonkor bat aurkitzeko (esaterako, indar-konstanteen matrizean eigenbalio negatibo kopuru jakin bat dituen puntua), Newton-Raphson metodoa Hessiar hurbilduak eigenbalio negatiko kopuru zuzena dituen zonaldean hasi behar da. Beraz, metodoa ezingo litzateke minimo batean hasi eta ahulki puntoruntz igo. Hala ere, metodoa eraldatua izan da eigenbalio negatiboen kopuru zuzena aurkitu ezin den kasutan ere bilaketak funtziona dezan (Eigenvalue Following).[127–129] Aldaketaren funtsa λ aldatze-parametroa erabiltzea da; parametro honen balioaren arabera $x_i = -g_i(h_i - \lambda)$ positiboa edo negatibo izango da. Beraz, Hessiarra positiboa den kasuan ahulki puntu bat aurkitu nahi bada, λ-ren aukeraketa egoki batekin x_i modu bakoitzean zehar beherantz joango da x_i batean ezik, non goruntz joango den. Metodo honen aldaketa gehiagorekin, minimotik kanpo edozein metodorekin "gainazalean ibili" daiteke.

Puntu egonkorren karakterizazioa

Puntu egonkor bat aurkitu eta gero bere izaera aztertu behar da bibrazio-frekuentzien kalkuloen bitartez.[130] Puntu egonkorra minimoa izango da frekuentzi guztiak errealak badira. Frekuentzi imajinario bat baldin badago puntu egonkor hori ahulki puntu bat izango da eta trantsizio bektoreak distortzioaren zentzua emango du, direkzio batean erreaktiboruntz eta produkturuntz bestean. Kontuan eduki behar da frekuentzi imajinarioen kopurua (eta beraz puntu egonkorraren izaera), frekuentzia horiek kalkulatutako teoria mailan bakarrik direla onargarriak. Maila altuago batean egindako kalkuloek emaitza desberdina eman dezakete. Adibidez, ahulki puntu batean oinarri handiago batekin eta elektroi-korrelazioa kontutan hartuz egindako kalkuluoek teoria maila baxuago batekin konparatuz energi-landa desberdina ematen badute, orduan gainazala kualitatiboki desberdina izango da maila altuago hortan. Egoera hau ematen denean, puntu egonkor guztiak teoria maila altuagoan berkalkulatzea komeni da.

Kopuru termodinamikoak

Bibrazioen analisia, puntu egonkorren izaera karakterizatzeaz gain, zenbait kopuru termodinamiko ebaluatzeko ere erabili daitezke. Erlazio termodinamiko eta energi-osagai nagusiak horrela sailka daitezke:

$$G = H - T \cdot S \tag{16}$$

$$H = U + R \cdot T \tag{17}$$

$$U = E_0 + E_{vib} + E_{rot} + E_{trans} \tag{18}$$

$$E_0 = (E_{elec} + E_{NN}) + E_{ZPV} = E + E_{ZPV} \tag{19}$$

non G, U, H, S eta T Gibbs aske-energia, barne-energia, entalpia, entropia eta tenperatura diren hurrenez-hurren, R gas konstante unibertsala eta E_{elec}, E_{NN}, E_{ZPV}, E_{vib}, E_{rot} eta E_{trans} energia elektronikoa, nukleo-nukleo aldarapen energia, zero-puntu bibrazio energia, bibrazio-energiaren zuzenketa termikoa, errotazio energiaren eta translazio energiaren osagaiak diren hurrenez-hurren. Entalpiaren espresioak (17 ekuazioa) partikula mol batentzat gas idealen legea bereganatzen du. Barne-energia eta entropia kalkulatzeko garaian multzo kanonkioaren barruan osziladore harmoniko, errotore zurruna, kaxa barruko gas/partikula idealaren ereduaren barruan bibrazio, errotazio eta translazio kontribuzioak separagarrietatatik mekanika estadistiko estandarretik lortzen dira.[131] Egoera estandarrean $T = 298$ K eta 1 atm-ko presioa ($V = R \cdot T/P$) dira. Goian aipatutako kopuru guztiek, E_0, E_{elec}, E_{NN} eta E_{ZPV} izan ezik tenperaturarekiko menpekotasuna dute.

Kalkuloak soluzioan

Disolbatzailearen eragina nabarmena izan daiteke, batez ere dielektriko handiko disolbentea baldin bada (ura adibidez) eta erreakzioan tartean espezie kargatuak baldin badaude, eragin hori geometrian eta energian antzematen delarik.[132,133] Uraz inguraturiko prozesu kimikoen simulazio teorikoa ez da erraza, eta ondorioz mota hontako kalkuluentzat metodo teoriko desberdinak eskuragarri daude.[134–136] Tesi hontan metodo jarraiak erabili izan dira disolbentearen efektuak kontutan hartzeko, eta konkretuki Modelu Jarrai Polarizagarria ("Polarizable Continuum Model", PCM).[137–139] Metodo hontan solutua molekula-itxura duen kabitate batean sartzen da. Kabitate hau inguru dielektriko jarrai batez inguratua dago, bere polarizazioa kabitatearen gainazalean banatutako karga-puntu batzuen bitartez erreproduzitzen delarik. Disoluzio aske energia, ΔG_{sol}, honela definitzen da:

$$\Delta G_{sol} = G_{aq} - G_{gas} \tag{20}$$

non G_{gas} eta G_{sol} molekularen energia askeak diren gas fasean eta disoluzioan hurrenez-hurren. Zehazkiago, hurbilketa hontan disoluzio energia honako hau izango da:

$$\Delta G_{sol} = \left(E\left[\Psi_{sol}\right] + E_{sol}\left[\rho_{sol}\right]\right) - E\left[\Psi_{gas}\right] \tag{21}$$

non $E\left[\Psi_{gas}\right]$ $E\left[\Psi_{sol}\right]$ gas fasean (Ψ_{gas}) eta soluzioan (Ψ_{sol}) optimizitaruko uhin funtzioen Kohn-Sham-en determinante bakunak argumentu bezela hartzen dituzten Kohn-Sham-en energi-funtzionalak diren. $E_{sol}\left[\rho_{sol}\right]$-k, berriz, argumentu bezela $\rho_{sol}(\mathbf{r})$ disolbatzailean polarizaturiko elektroi-dentsitatea (zeina Ψ_{sol}-tik deribatzen den) argumentu bezela hartzen duen solbatazio-energia da. $E\left[\Psi\right]$ Kohn-Sham energi-funtzionala honela definitzen da:

$$\begin{aligned} E\left[\Psi\right] &= T_S\left[\Psi\right] + J\left[\rho\right] + E_{XC}\left[\Psi\right] + \int \rho(\mathbf{r}) v_0(\mathbf{r})\, d^3r + E_{NN} \\ &= E_{elec}\left[\Psi\right] + E_{NN} \end{aligned} \tag{22}$$

non $T_S\left[\Psi\right]$ elkarrekintzarik gabeko energi-funtzional kinetikoa den, $J\left[\rho\right]$ energi elektrostatiko klasikoa, $E_{XC}\left[\Psi\right]$ trukatze-korrelazio energia eta E_{NN} nukleo-nukleo errepultsio energia diren. 22 ekuazioko funtzionala parametrikoki nukleoen koordenatuen funtzioan dago eta Born-Oppenheimer hurbilketaren barruan $v_0(\mathbf{r})$ nukleo-potentzial externo batean zehar aldatzen da.

PCM modeloan $E_{sol}\left[\rho_{sol}\right]$ solbatazio-energi funtzionala honela idatz daiteke:

$$\begin{aligned} E_{sol}\left[\rho\right] &= \frac{1}{2}\left(\int \rho(\mathbf{r}) \cdot v_{RF}(\mathbf{r})\, d^3r - \sum_{\alpha} Z_\alpha \cdot v_{RF}(\mathbf{R}_\alpha)\right) \\ &+ G_{disp-repul} + G_{cav} \end{aligned} \tag{23}$$

non $v_{RF}(\mathbf{r})$ disolbatzailearen erreakzio-kanpo potentziala den, eta Z_α, $\mathbf{R}_\alpha$ posizioan kokatua dagoen α atomoaren nukleo-karga den. 23 ekuazioaren 1/2 faktorea modelo dielektrikoaren izaera linealari zor zaio, eta $G_{dis-repul}$ eta G_{cav} dispertsio-errepultsio eta kabitazio kontribuzioak errepresentatzen dute.[140]

Kabitazio terminoa eskalatutako partikulen teoriatik lortutako espresio bat erabiliz konputatzen da.[141] Dispertsio-errepultsio terminoa Floris *et al.*[142]-ek deskribatutako prozesu baten bidez kalkulatzen da, non disolbatzailea ailegatu daitekeen gainazala definitzen den UAHF erradioa gehi 1.385 Å-ko disolbatzaile proba erradio bezela eraikitzen den.

$v_{RF}(\mathbf{r})$ disolbatzaile erreakzio-kanpo potentziala, dielektriko bezela bat duen kabitate baten bidez osatzen da, zeina ϵ konstante dielektrikoa duen isotropi lineal polarizagarri jarrai batez inguratua dagoen (ikus[140] eta[143] erreferentziak). Erreakzio-kanpo potentziala muga-elementuen metodoa erabiliz numerikoki ebazten da.[134,138,139,144] Metodoak ez du esplizitoki kontutan hartzen bolumenaren "polarizazioa".[145] Hala ere, GAUSSIAN98-n ezarrita dagoen PCM-ak Gauss-en legea erabiliz kargen polarizazioa normalizaten du,[146] zeina inplizituki bolumenaren polarizioaren ezaugarri garrantzitsuenak eskuratzeko ahalegin bat den. Bi modelo hauetako parametroak solbatazio aske-energi esperimentalak erreproduzitzeko egokitu dira (ondorioz, neurri batean orden handiagoko efektuak kontutan hartzen dituzte).

PCM bariazio desberdinak daude kabitatea definitzeko moduaren arabera. Hiru garrantzitsuenak hauek dira:

- PCM estandarra: kabitatea esfera atomiko desberdinen gainezartzea bezela definitzen da. Solutua sartzen den kabitatea, solutuaren atomo edo atomo taldeetan zentraturiko esferak elkartuz osatzen da; ondoren kabitatea tesserae deritzaien zati txikitan zatitzen da, bertan polarizazio-kargan ezartzen direlarik. PCM estandarraren kalkuluetan pentakisdodekahedro baten 60 triangeluak esferetan proiektatuz sortzen dira: era bat kabitatearen barruan dauden tessaraeak ez dira kontutan hartzen, eta beste esfera batez moztutakoak kurbaturiko poligono egoki batez ordezkatzen dira.

- IPCM: Kabitatea gas faseko isodentsitate gainazal baten arabera definitzen da, zeina konstante mantentzen den SCF prozeduran.

- SCIPCM: kabitatea isodentsitate gainzala baten bitartez definitzen da, zeina SCF prozeduran eguneratzen den. Hau da, kabitatea SCRF bariazio-prozesuaren barruan optimizatzen da.

Chapter 1

General Introduction

1.1 Amide Bond

Proteins play a crucial role in most biological processes, and they are required for the structure, function and regulation of the body's cells, tissues and organs. They mediate a wide range of functions, such as enzymatic catalysis, transport and storage (the hemoglobin protein transports oxygen), coordinated motions, mechanical support (the major component of muscle are proteins) or immune protection (antibodies are highly specific proteins). Hence, it is obvious that the study of proteins has been an important issue for researches.

Chemically, proteins are large molecules with basic structural units, the amino acids. An amino acid consists of an amino group, a carboxyl group, a carbon atom between these two groups (called α carbon) and a side chain. There are twenty different amino acid type depending on the side chain bound to the α carbon. Proteins are built combining several amino acids in the way depicted in Figure 1.1: a carboxyl group of an amino acid joins to the amino group of the next amino acid creating the so-called **peptide bond** with the accompanying removal of a molecule of water. After the joining of many amino acid units the protein is built.

An important characteristic of the peptide bond is its chemical stability at physiological conditions, which means that the non-enzymatic peptide bond hydrolysis is a very slow process. For instance, the half-life for (pheny-

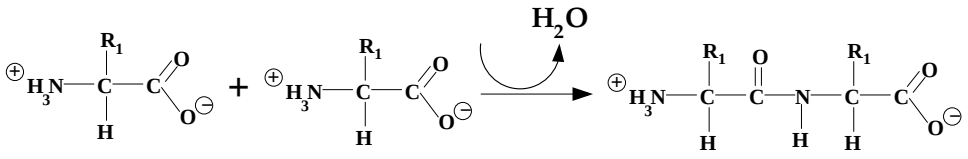

Figure 1.1: Formation of a peptide bond.

lacetyl)glycyl bond hydrolysis is 243 years and 267 years for glycyl-D-valine bond hydrolysis at pH 7.[1] But, which is the physical-chemical explanation for this high stability?

1.1.1 Characteristics of the amide bond

In order to improve our understanding of the peptide bond stability and due to the large size of proteins, amide molecules have been used as a model for peptide bonds.[2,3] Amides are organic compounds containing the group $-CO.NH_2$. The amide linkage is therefore chemically analogous to that of a peptide bond. Both experimental and theoretical studies of formamide determined the main characteristic of the amide bond, summarized below:

- Coplanarity of the group attached to the nitrogen atom.[4–6] That is, while the nitrogen atom shows a pyramidalized conformation in an amine group, this atom adopts a planar conformation in the amide bond.
- The C-N bond distance is significantly shorter than in an amine molecule and the carbonyl C-O distance slightly larger than in an aldehyde.[4,7,8]
- Substantial energetic barrier (about 15-20 kcal/mol) when the molecule rotates around the C-N bond.[9–11]
- Elongation of the C-N bond and shortening of the C-O when rotates around the amide bond.[12–14]
- Reduced C-O stretching frequency comparing with a single carbonyl group.[15,16]
- Reduced nitrogen basicity with respect to an amine nitrogen.[17]
- Kinetic stability toward nucleophilic attack or hydrolysis. For example, the half- life for the hydrolysis of acetyl-glycil-glycine is 500 years at pH 6.8 and 25 °C.[18,19]

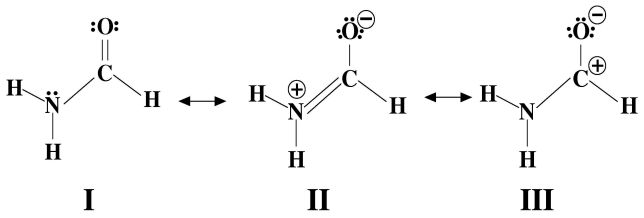

Figure 1.2: The three main Lewis structure contributions to the Resonance Model.

1.1.2 Origin of the amide bond stability: Resonance model

The classical explanation for the specific characteristic of the amide bond has been given in terms of the **Resonance Model**.[20–23] Resonance was first described by Pauling[20] for substances whose properties cannot be accounted for by means of a single Lewis structure of the valence-bond type, but which can be fitted into the scheme of classical valence theory by the consideration of resonance among two or more such structures. In the case of amides, the characteristic of this molecule can be explained by the mixture of resonant structures I and II depicted in Figure 1.2. In resonant structure I, nitrogen atom adopts a sp^3 hybridisation with a pyramidal configuration, and therefore, C-N bond has a single-bond character. Resonant structure II, however, leads to a sp^2 hybridisation of the nitrogen and a partial double bond character for the C-N bond, which explains the characteristical planarity of amides and their inherent stability.

In the framework of Molecular Orbital theory, resonance in amides can be inferred by the delocalized nature of the corresponding π orbitals (see Figure 1.3). The strong involvement of the nitrogen $2p$ orbital in conjugation with the π^* orbital of the carbonyl group leads to π orbitals highly delocalized over the entire N-C-O skeleton. The high stabilizant effect of this delocalization can be inferred at certain extent from the low orbital energy associated to the π_1 HOMO-2 orbital. However, it is difficult from the present electronic structure description to make an unambiguous measure of the resonance effect, due to the intrinsic delocalized nature of molecular orbitals.

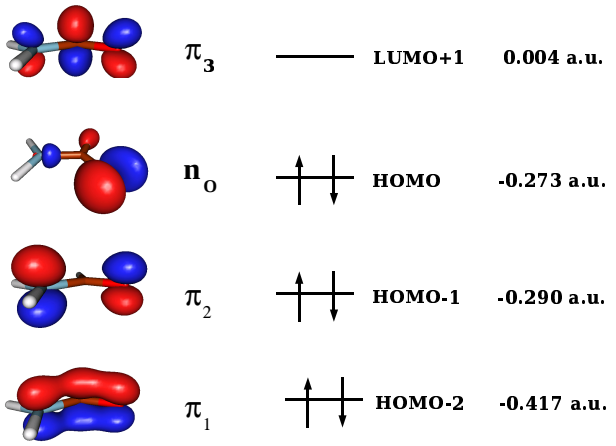

Figure 1.3: Selected Molecular Orbitals for the formamide molecule. Orbital energy in atomic units are also illustrated calculated at the B3LYP/6-31+G(d) level of theory.

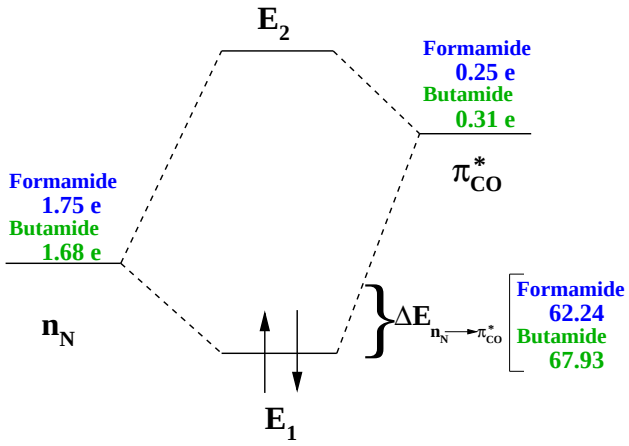

Figure 1.4: Interaction between the nitrogen lone pair and the carbonyl antibonding π orbital. The resultant energy lowering for the formamide and butamide are shown in kcal/mol calculated at the B3LYP/6-31+g(d) level of theory.

For a more quantitative description of amide resonance, Natural Bond Orbital (NBO) analysis can be used. Developed by Weinhold *et al.*[24,25] as a technique for studying hybridisation and covalency effects in polyatomic wave functions, NBOs were conceived as a "chemist's basis set" that would correspond closely to the picture of localized bonds and lone pairs as basic units of molecular electronic structure. However, the general transformations to NBOs also leads to orbitals that are unoccupied in the formal Lewis structure and that may thus be used to describe non-covalency effects. In particular, the most important of those are the antibonding σ^* and π^*. The antibonds represent unused valence-shell capacity, spanning portions of the atomic valence space that are formally unsaturated by covalent bond formation. Small occupancies of these antibonds correspond, in Hartree-Fock theory, to departures from the idealized Lewis picture and thus to small noncovalent corrections to the picture of localized covalent bonds. The corrections are usually so small (typically less than 1% of the total energy) as to be well approximated by simple second-order perturbative expressions of the type,

$$\Delta E^{(2)}_{\sigma\rightarrow\sigma^*} = -2\frac{<\sigma|\hat{F}|\sigma^*>^2}{\sigma^* - \sigma} \tag{1.1}$$

where $\hat{F}$ is the Fock operator, σ is a Lewis orbital and σ^* a non-Lewis orbital. In the case of amides, the highest of these stabilizant interactions correspond to a $n_N \rightarrow \pi^*_{CO}$ delocalization or resonance, represented schematically in Figure 1.4. The interaction energy is found to be 62.24 and 67.93 kcal/mol for the formamide and butamide, respectively. Therefore, using NBO theory

one can assess that the origin of the amide stability is a resonance effect, more specifically, described as a $n_N \rightarrow \pi^*_{CO}$ electron delocalization.

Finally, Natural Resonance Theory (NRT)[14,26] has also been used to give an specific weight for the different candidate resonant structures. It has been observed that resonant structures I and II of Figure 1.2 account for about 90 % of the resonance hybrid, and more specifically, Lewis structure II accounts for roughly the 30 % of the total resonance hybrid.

1.1.3 Torsional Catalysis

A necessary condition for an optimum $n_N \rightarrow \pi^*_{CO}$ electron delocalization is the planarity of the amide group. In fact, amides show high rotational barriers, between 15-20 kcal/mol according to many experimental[27–31] and theoretical[32–36] studies. Furthermore, these barriers have been often used as a measure of resonance stabilization in amides. Notice that at the transition state (see Figure 1.5), n_N lies in the nodal plane of the π^*_{CO} orbital, preventing any $n_N \rightarrow \pi^*_{CO}$ delocalization. This is confirmed by NBO analysis which show no $n_N \rightarrow \pi^*_{CO}$ interaction, and from the analysis of the molecular orbitals (Figure 1.5), which clearly shows the orthogonality between n_N and π_{C-O}/π^*_{C-O} orbitals. As a consequence of the breakdown of the $n_N \rightarrow \pi^*_{CO}$ interaction, nitrogen adopts a sp^3 hybridisation with a pyramidal configuration. In terms of Lewis structure, only resonant structure I is needed to describe the main features of the electronic structure. In summary, the $n_N \rightarrow \pi^*_{CO}$ type resonance is broken at this highly torsionated amide structures, and hence, their high energies with respect to planar structures.

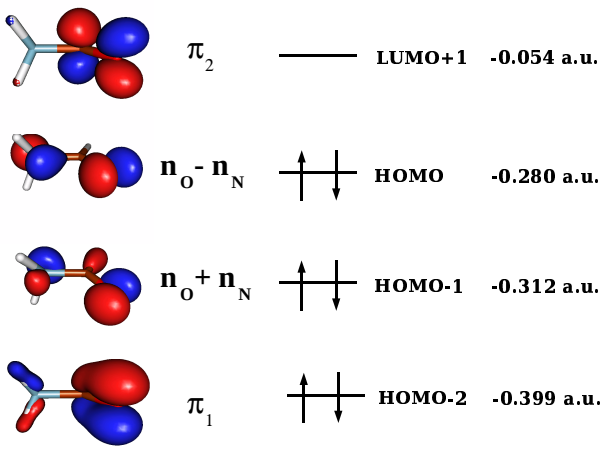

Figure 1.5: Selected Molecular Orbitals for the rotational transition state of the formamide molecule. Orbital energies in atomic units are also illustrated calculated at the B3LYP/6-31+G(d) level of theory.

A venerable hypotheses for amide bond activation towards hydrolysis tries to take advantage of the above-mentioned property, and seek for a preorganized amide twisted structure, in which there is no $n_N \rightarrow \pi^*_{CO}$ resonance. The twist of the amide bond can be induced by specific geometrical constraints in the reactants or by enzyme action on a preferential twisted conformation of the substrate. In this latter case, the enzyme would reduce the barrier of the reaction by destabilization of the amide reactant. This type of "ground-state destabilization" has been suggested to be part of the mechanism of catalysis in the case of protein splicing.[37–40] This is as well also the basis for the design of transition state analogues which are then used as haptens to develop catalytic antibodies[41–43] that are able to catalyze peptide bond cleavage by inducing "ground-state destabilization" of the reactant. On the other hand, several cases where the enzyme catalyzes the peptide bond cleavage by twisting mechanism are known, as for example the proline cis-trans isomerases.[44–46] In fact, non-planar deformations of amide bonds in peptides have been the focus of considerable interest.[47]

1.1.4 Twisted amides

The specific study of how the twist of amides affects its structural and energetical properties is, apart from being an interest topic by itself, crucial for a full understanding of the possibilities for rate acceleration of torsional catalysis. X-Ray data[48] and computational studies[12,13,49–52] on the rotational barrier of formamide and its derivatives have clearly supported the idea of C-N bond weakening upon C-N bond twist. Unfortunately, few accurate kinetic data on hydrolysis of non-planar twisted amides are available. In a seminal work by Blackburn *et al.*, it was reported that the alkaline hydrolysis of benzoquinuclidin-2-one, a strained cyclic amide with a significantly twisted amide bond, was 10^7 times faster than its strainless counterpart.[53,54] This corresponds to a decrease in the reaction activation energy by about 10 kcal/mol. In agreement with these experiments, Brown *et al.* also reported[2,55] significant accelerations for the hydrolysis of distorted amides. Quite interestingly the degree of acceleration seems to depend on the pH conditions, ranging from 7 orders of magnitude for the alkaline hydrolysis to 11 orders of magnitude for acid-catalyzed hydrolysis. More recently, Kirby *et al.*[56–58] also reported the rapid hydrolysis in water (under slight acidic conditions) of a highly twisted amide bond in 1-aza-2-adamantanone, suggesting an even higher acceleration of the hydrolysis rate. The crystal structure of this highly twisted amide shows an amide bond and carbonyl bond length of 1.475 and 1.196 Å respectively, values that are close to the ones of the rotational transition state of formamide, suggesting an absence of the $n_N \rightarrow \pi^*_{CO}$ delocalization.

1.1.5 Scope of this work

A full understanding of the similarities and differences between the reaction of twisted amides with respect to their planar analogues is still missing, and much work is needed in terms of characterization of specific reaction pathways and determination of transition states. The present thesis is a contribution to this goal using the tools provided by quantum chemistry. Computational studies[59–75] on the hydrolysis of amides have been mainly focused on the reaction of undistorted planar amides such as formamide, although few studies may be found in the literature concerning twisted amides.[55,76–78] The aim of the present thesis is to provide a deeper description of the effect that the twist has on various fundamental properties of amides and in their reactivity. The thesis's work is divided in two parts:

- Part I: Fundamental properties of twisted amides are studied. Chapter 1 is devoted to the characterization and rationalization of amide resonance strength in terms of delocalization indexes based on the Atoms in Molecule theory. The aim of these studies is to measure quantitatively the degree of loss of $n_N \rightarrow \pi^*_{CO}$ resonance upon twisting and define a proper quantum index to characterize this resonance. In Chapter 2, we characterize the pK_a values of several twisted amides. These quantities are important to uncover specific reaction pathways as a function of pH. However, there are sometimes problems to evaluate these quantities experimentally, due to the rapid hydrolysis of twisted amides.

- Part II: We will characterize the reactivity of a prototype twisted amide towards alkaline hydrolysis (Chapter 3), neutral hydrolysis (Chapter 4) and acid hydrolysis (Chapter 5). A prototype twisted amide is used for this purpose (**TA** in Figure 1.6) analogous to the one early considered by Blackburn.[54] In this structure, nitrogen is constrained to adopt a pyramidal conformation by a cage structure. For each reaction type, several possible mechanism or regimes are considered, i) concerted versus stepwise, ii) water assisted versus non-assisted and iii) gas phase versus solvent phase. In addition, to unequivocally determine the rate-acceleration associated to the twisting, the hydrolysis reaction for a planar amide analogue is also studied for every case (**PA** structure in Figure 1.6).

Based on the results of Part I, specially the pKa evaluations, and Part II on the reactivity, we will be in situation to draw a general picture for this complex reaction as a function of pH, remarking differences and similarities between hydrolysis reactions of twisted and planar amides. The results are not only interesting from a theoretical point of view, but they can shed light into the effect of amide bond torsion on this important type of reactions,

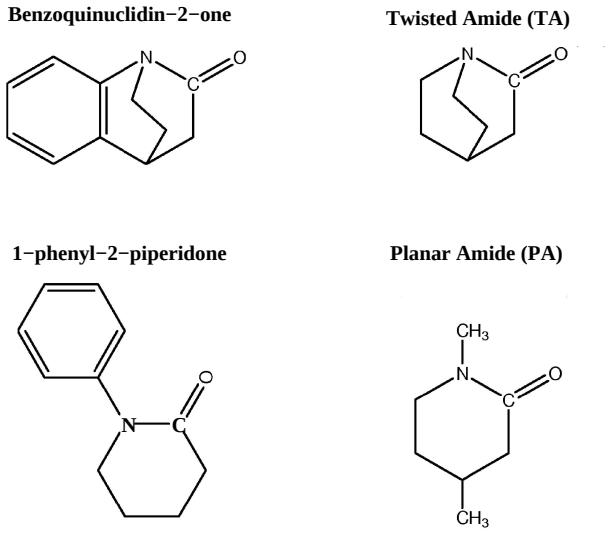

Figure 1.6: On the left-hand side, amide reactants used by Blackburn *et al.*[54] to study the rate acceleration for the hydrolysis of amides caused by the C-N bond twist. On the right-hand side, our theoretical models for the compounds studied experimentally: at the top of the picture the Twisted Amide (**TA**), and at the bottom the Planar Amide (**PA**)

and lead to a better understanding of biochemical catalysis in which the torsion of the amide is required previous to its catalysis.

A final note should be made on the chronological order of the present work. The work presented in each of the chapters has actually been the subject of an independent publication. However, the chronological order of these publications is not coincident with the order of the chapters followed in the thesis. Chapter 3 on the alkaline hydrolysis of twisted amides was the first publication,[79] then followed by the evaluation of the pKa for several twisted amides (Chapter 2),[80] the neutral hydrolysis of twisted amides (Chapter 4),[81] and finally, the two latest submitted publications correspond to the acidic hydrolysis (Chapter 5)[82] and the characterization of delocalization indexes in amides (Chapter 1).[83] We have tried to remove redundancies among chapters but without compromising the self-consistency of each of the chapters and the coherency between the chapter and the corresponding publication.

In the next subsection a brief description of the quantum mechanical methods used in the present thesis is presented. It is beyond of the scope of this thesis to give a detailed and deep explanation of quantum mechanical methods. Interested readers are referred to other more specific works.[84]

1.2 Quantum chemistry

The theory of quantum mechanics, developed in the twenties of the last century,[85–88] changed the viewpoint of scientists over the microscopic world. Before it, all attempts that tried to explain the stability of atoms failed. Bohr explained the stability of the simplest atom, hydrogen, by fixing that electrons were stable in the stationary orbits around the nucleus. An electron needs a quantum of energy in order to move from one of the stationary orbits to another. In other words, the energy is quantized, and not continuous. In quantum mechanics this statement arises from the theory. At the beginning the theory was mainly the playground of physicists, but it soon found applications in chemistry, creating what is called quantum chemistry. Over the years quantum chemistry has produced very important tools for chemists in order to calculate, understand and predict molecular properties.

In principle, all the amenable information of a system, a molecule, for instance, may be obtained from its wave function. In order to know it, we 'only' have to solve the Schrödinger equation (here in its time independent form):

$$\widehat{H}\Psi = E\Psi \tag{1.2}$$

where the Hamiltonian $\widehat{H}$ contains the kinetic energy terms of the electrons and the nuclei, the interactions between the nuclei, the electrons, and the nuclei-electrons. Within the Born-Oppenheimer[89] approximation the motion of the nuclei are separated from that of the electrons, and therefore the coordinates of the nuclei become fixed parameters in $\widehat{H}$. Unfortunately, equation (1) can only be solved for one electron systems, i.e. the hydrogen atom. Therefore approximate methods have been developed:

1. Wave-function based methods: variational (configuration interaction, direct expansion of Ψ in some suitable basis), and many-body perturbation theory.

2. Density functional theory (DFT).

It is beyond the scope of this section to develop a full description of these methods, so refer the interested reader to the literature devoted to these topics. See for example:[90–94]

Wave-function based methods were the earliest developed ones. Two of these methods have been widely used throughout the years, the Valence Bond (VB) method and the Molecular Orbital (MO) method. The VB method was formulated in 1927 by Heitler and London.[95] The MO method was developed a bit later in by Hund,[96] Mulliken[97] and others. This theory became the most popular due to its quantitative power, which come from

the use of orthogonal orbitals, in opposition to the VB theory which plays with non-orthogonal orbitals.

One of the first developed molecular orbital method was the Hartree-Fock method,[98,99] where the wave function is an antisymmetrized product of one-electron orbitals. The electrons are treated as moving in a mean field due to the nucleus and the remaining electrons. The main drawback of this method is that correlation of electrons with opposite spins is neglected. There are different ways in which this correlation can be taken into account. One of them are the perturbational methods such as Møller-Plesset[100] theory (denoted as MPn, where n is the order of the perturbation). In these methods the electron correlation is treated as a perturbation of the HF problem. In the Configuration-Interaction (CI) method[101,102] the wave function is expressed as a linear combination of configurations to provide a better variational solution to the exact many-electron wave function. There are other more sophisticated methods such as Coupled Cluster,[103–105] Multi-Reference Configuration Interaction (MR-CI) or Complete-Active-Space (CAS) methods,[106,107] which are very useful tools to study electronic properties of both ground and excited states.

Mainly all the work presented in this thesis has been carried out within the density-functional framework. In the following subsection these methods are described in more detail.

1.2.1 Density Functional methods

The Density Functional Theory formalism replaces the N-electron wave function and the associated Schrödinger equation by a much simpler electron density $\rho(\vec{r})$ which is a function of the three spatial variables. Then, the electronic state, the energy and all the electronic properties of a system can be described in terms of this $\rho(\vec{r})$.[92,93]

Hohenberg and Kohn[108] proved that the electronic properties of a system with a non-degenerate ground state are uniquely determined by the electron density $\rho(\vec{r})$. Hence, the ground-state energy E_0 is a functional of $\rho(\vec{r})$, and therefore, if we know the ground-state electron density it is possible to calculate all the ground-state electronic properties from ρ once we have been able to set all the appropriate functional dependencies. In order to find these functionals, they also established an energy variational principle for the energy functional, analogous to the variational principle for wave functions. Thus, knowing the exact form of the $E[\rho]$ functional, we can search for the ground state density (as it is the case for the wave function). However, since the exact form of the functional is unknown, Kohn and Sham[109] developed an indirect approach to this functional, the Kohn-Sham method, and DFT turned into a practical tool for rigorous calculations. They showed that the exact ground-state purely electronic energy E_0 of an N-electron molecule with ground-state electron probability density ρ is given by

$$E_0 = -\frac{1}{2}\sum_{i=1}^{N} < \psi_i(1)|\nabla_1^2|\psi_i(1) > + \tag{1.3}$$

$$+ \int \upsilon(r)\rho(1)d\vec{r}_1 + \frac{1}{2}\int\int \frac{\rho(1)\rho(2)}{r_{12}} d\vec{r}_1 d\vec{r}_2 + E_{xc}[\rho]$$

where $\upsilon(r) = -\sum_\alpha \frac{Z_\alpha}{r_{1\alpha}}$ is the external potential due to the nuclei, ψ_i are the Kohn-Sham orbitals, and the $E_{xc}[\rho]$ is the exchange-correlation energy.

In the Kohn-Sham procedure, the exact ground state ρ can be found from the Kohn-Sham orbitals according to,

$$\rho = \sum_{i=1}^{N} |\psi_i|^2 \tag{1.4}$$

and the Kohn-Sham orbitals are found by solving the one-electron equations:

$$\hat{F}_{KS}(1)\psi_i(1) = \varepsilon_i\psi_i(1) \tag{1.5}$$

being the Kohn-Sham operator $\hat{F}_{KS}$,

$$\hat{F}_{KS} = -\frac{1}{2}\nabla_1^2 + \upsilon(1) + \sum_{j=1}^{n} \hat{J}_j(1) + V_{xc}(1) \tag{1.6}$$

where $\hat{J}$ is the Coulomb operator, and V_{xc} is called the exchange-correlation potential. $\hat{F}_{KS}$ is like the Fock operator in HF equations, except that the exchange operators are replaced by V_{xc}, which handles the effects of both the exchange and electron correlation.

These equations are iteratively solved. Starting from a guess density, $\hat{F}_{KS}$ is build and the set of equations 1.4 solved. The solution then is transfered to $\hat{F}_{KS}$, in order to build a new $\hat{F}_{KS}$. This process is repeated until convergence is achieved.

The physical significance of the Kohn-Sham orbitals is still under debate. Some authors claim that they do not have any significance other than in allowing the exact ρ to be calculated from equation 1.3. Likewise, the Kohn-Sham orbital energies should not be confused with molecular orbital energies. However, others based on the fact that the exact Kohn-Sham orbital energy for the HOMO is just the negative of ionization potential,[110,111] and due to the fact that the set of Kohn-Sham equations remind us, as in the HF case, the independent particle model, they associate to the Kohn-Sham orbitals a similar physical significance and legitimacy than to the HF

canonical orbitals. In recent publications it is shown the results obtained from molecular orbitals obtained from DFT are quite similar to the molecular orbitals from standard MO-LCAO methods, and that one can extract a lot of useful information about molecular systems from analysis of their MOs even if the density functional methods are used.[110,112]

However, there is one more problem: the exchange-correlation functional $E_{xc}[\rho]$ and hence the exchange-correlation potential $v_{xc}[\rho;\overrightarrow{r}]$ is not known except for the case of the uniform electron gas. Fortunately, approximate functionals have been developed. One simple approximation is the so called local density approximation (LDA). The idea is to consider each volume element with local density $\rho(\overrightarrow{r})$ to be a homogeneous electron gas. From this point of view the approximation would be expected to be accurate if the density varies slowly in space. Then, $E_{xc}[(\rho)]$ is given by:

$$E_{xc}^{LDA}[(\rho)] = \int \rho(\vec{r})\varepsilon_{xc}(\rho)d\vec{r} \tag{1.7}$$

where $\varepsilon_{xc}(\rho)$ is the exchange plus correlation energy per electron in a homogeneous electron gas with electron density ρ. An accurate expression for $\varepsilon_{xc}(\rho)$ was found by Vosko, Wilk and Nusair.[113] Application of this expression leads to the local density approximation (LDA), or local spin density approximation (LSDA),[114] if one uses different orbitals and densities ρ^{α} and ρ^{β} for electrons with different spins. Of course, in the case of molecules these are only approximations to the true functionals, since ρ is far from being homogeneous. One might hope to improve the approximation by introducing an expansion in terms of gradients of the density. These methods are called generalized gradient approximations (GGA), and are of great importance in the study of molecules, where the electron density can not be considered as homogeneous.

Density functional methods have proved to give excellent results in most chemical systems,[115] with results comparable to those given by CPU intensive electron-correlation methods. However they frequently overestimate bond dissociation energies.[116] The hybrids of HF and DFT theories increment the accuracy of the dissociation energy as was validated by Johnson *et al.*.[117] The hybrid[118] Becke 3 combined with the correlation functional Lee-Yang-Parr (B3LYP)[108,119,120] has become one of the most popular one, having the following form:

$$(1-a_0)E_x^{LSDA} + a_0E_x^{HF} + a_xE_x^{B88} + a_cE_c^{LYP} + (1-a_c)E_c^{VWN} \tag{1.8}$$

being the values of the parameters a_0=0.20, a_x=0.72 and a_c=0.81. This functional is known as the Becke's 3 parameter functional, B3LYP.

Since density-functional calculations do not use the exact E_{xc} they are not, strictly speaking, ab-initio calculations. However, they do not use pa-

rameters fitted to experimental data, hence they lie closer in spirit to ab-initio calculations than to semiempirical ones. One of the main advantages of these methods is that with a similar computational cost to HF methods, they include some kind of electron correlation, being the major drawback that the correlation effects cannot be sorted out precisely. They are already mixed from the beginning with the uncorrelated solution. Besides, there is not any systematic way to improve the calculations by applying more and more sophistication, so the results must be accepted as they stand. In spite of these facts, DFT have been found to yield good results for ground state properties of various chemical systems, with a quality comparable to MP2 results,[121] or even better in some cases. Due to their relative low computational cost, DFT is the method of choice for large systems, for which the inclusion of electron correlation by MP or CI methods is prohibitive.

1.2.2 Basis Sets

In both wave function based methods and density functional theory a set of functions to span the wave function are needed. These sets of function are the so called basis sets. The choice of an appropriate basis set is an essential requirement for the success of the calculation. However, we have to balance the precision of the basis set and its size, since increasing the size of the basis set the calculation cost becomes more expensive. The Contracted Gaussian Functions (CGF) are the most used in quantum chemistry calculations. They consist of linear combinations (contractions) of Gaussian functions (primitives),

$$\varphi_{\mu}^{CGF}(|\vec{r}-\vec{R}_A|) = \sum_{p=1}^{L} d_{p\mu} g(\alpha_{p\mu}, |\vec{r}-\vec{R}_P|) \tag{1.9}$$

where the exponent of the primitives $\alpha_{p\mu}$ and the contraction coefficients $\mathrm{d}_{p\mu}$ are optimized for the different elements.

1.2.3 Moving Through the Potential Energy Surface

The Born-Oppenheimer approximation leads to the concept of a *potential energy surface* (PES). The PES is the function that describes how the potential energy changes as the nuclei move relative to one another. Discarding six degrees of freedom for overall rotation and translation of the molecules leaves, for a nonlinear molecule, 3N-6 *internal* degrees of freedom. Thus, the PES is a 3N-6 dimensional hypersurface, where we search for minima and saddle points.

Minima and Saddle Points

Clearly mapping out the full PES at a quantum level of theory is tractable only for small molecules, but a great deal about a molecule and its behavior can be learned from knowledge of a few selected points of the PES. Local minima on the PES are fundamental points since they represent stable isomers of a molecule. They determine the molecular structure and the moments of inertia by which the rotational spectra can be estimated. The curvature of the many-dimensional PES about the local minima, the steepness of the walls, determines the vibrational properties of the molecule including the normal modes and harmonic vibrational frequencies.

Another fundamental point on the PES is the lowest-energy *saddle point* connecting two local valleys or minima. The saddle point is the highest point on a lowest total energy pathway connecting these minima. It has the property that it is a maximum with respect to one degree of freedom and is a minimum with respect to all other degrees of freedom. The significance of the saddle point is that it is an approximate dynamic bottleneck, a point of no return, for a transformation from the vicinity of one local minimum or valley to another. The probability (or rate) of reaction is very strongly influenced by the height in energy of this saddle point.

Both the minima and the saddle points are *stationary points* on the PES; the derivative of the energy with respect to each of the geometry coordinates, and thus the force on each of the atoms is zero; for all i,

$$\frac{dE(q_1, q_2, ..., q_m)}{dq_i} = 0 \tag{1.10}$$

Locating Minima and Saddle Points

The initial step in locating a stationary point is defined by the internal coordinate system. Effort should be made to choose a coordinate system where the parameters are not interdependent (coupled). In situations where the coupling cannot easily or conveniently be avoided, one should start the optimization with an analytically calculated Hessian. On the other hand, alternatives to internal coordinates have been suggested to have some advantages (i.e, Cartesian coordinates and redundant coordinates).
There are various methods to locate stationary points on a PES, *optimization methods*.[122–124] In computational quantum chemistry great effort is given to reduce the number of function evaluations since that part of the calculation is time consuming. Since first derivatives are now available for almost all ab-initio methods, the discussion will focus on methods where first derivatives are available.

The most efficient methods, called variable metric or quasi-Newton methods, require an approximate matrix of second derivatives that can be updated with new information during the course of the optimization. Some of the more common methods have different equations for updating the second derivative matrix (also called the Hessian matrix).
The PES, a function of 3N cartesian coordinates or 3N-6 internal coordinates (3N-5 for linear molecules) can be expanded about an arbitrary point such that the energy at a displaced point $\vec{x}$ is given by the Taylor series,

$$E(\vec{x}) = E_0 + \sum_i \frac{\partial E}{\partial x_i} x_i + \frac{1}{2} \sum_{i,j} \frac{\partial^2 E}{\partial x_i \partial x_j} x_i x_j + ... \tag{1.11}$$

If the series is truncated after the quadric term, in vector notation, the series become,

$$E(\vec{x}) = E_0 + g_o^\dagger x + \frac{1}{2} x^\dagger F_0 x \tag{1.12}$$

where,

$$g_i = \frac{\partial E}{\partial x_i}|_0 \tag{1.13}$$

$$F_{i,j} = \frac{\partial^2 E}{\partial x_i \partial x_j}|_0 \tag{1.14}$$

Taking the derivative of $E(\vec{x})$,

$$\frac{\partial E}{\partial x} = g_0 + F_0 x \tag{1.15}$$

At a stationary point $\frac{\partial E}{\partial x} = 0$ and $x = -F_0^{-1} g_0$ or $x = -H_0 g_0$ where H_0 is the approximate inverse Hessian matrix F_0^{-1}. In subsequent steps H_0 is updated by an updating formula to yield a new H_0.

Various updating schemes have been proposed. The most successful are the BFGS updating formula and the DFP (David-Fletcher-Powell) updating formula. The former update formula appears to be more robust.[125,126] The methods work very well if the Hessian correctly reflects the nature of the stationary point being sought.

To find a stationary point of a particular type (i.e., with a particular number of negative eigenvalues of the force constant matrix), the Newton-Raphson method must start in a region where the approximate Hessian has the correct number of negative eigenvalues. Thus, the method would not be able to start from a minimum and walk up toward the saddle point. However, the method has been modified to allow searching even when the correct number of negative eigenvalues is not found (Eigenvalue Following.[127–129]) The essence of the modification is to use a shift parameter λ, which has

a value such that the step $x_i = -g_i(h_i - \lambda)$ will be positive or negative depending on the value of λ. Thus, if searching for a saddle point with a positive definite Hessian, the search direction, with an appropriate choice of λ, can be made to go downhill along each mode x_i except one, which is searched uphill. With further modification, the method can "surface walk" out of the minimum along any chosen method.

Characterization of Stationary Points

Once the stationary point is found, its nature should be tested by calculating vibrational frequencies.[130] The stationary point is a minimum if all frequencies are real. If there is one imaginary frequency, the stationary point is a saddle point and the transition vector will give the sense of the distortion toward the reactants in one direction an toward products in the other. It must be remembered that the number of imaginary frequencies (and therefore the nature of the stationary point) is valid only at the level of theory used to calculate the frequencies. Calculations at higher levels of theory may present a different picture. For example, if a calculation on a saddle point with a larger basis set and including electron correlation gives a substantially different energy barrier than the lower level of theory, then the surface may be qualitatively different at higher level.

1.2.4 Thermodynamic quantities

Apart from characterizing the nature of the stationary points, vibrational analysis can also be used for the evaluation of several thermodynamic quantities. The breakdown of the key thermodynamics relations and energy components is summarized below:

$$G = H - T \cdot S \tag{1.16}$$

$$H = U + R \cdot T \tag{1.17}$$

$$U = E_0 + E_{vib} + E_{rot} + E_{trans} \tag{1.18}$$

$$E_0 = (E_{elec} + E_{NN}) + E_{ZPV} = E + E_{ZPV} \tag{1.19}$$

where G, U, H, S and T are the Gibbs free energy, internal energy, enthalpy, entropy and temperature, respectively, R is the universal gas constant, and E_{elec}, E_{NN}, E_{ZPV}, E_{vib}, E_{rot} and E_{trans} are the electronic energy, nuclear-nuclear repulsion energy, zero-point vibrational energy, thermal vibrational energy correction, rotational and translational energy components, respectively. The expression for the enthalpy (Eq. 1.17) assumes the ideal gas law for a mole of particles. The internal energy and entropy are derived from standard statistical mechanical expressions for separable vibrational, rotational and translational contributions within the harmonic oscillator, rigid rotor, ideal gas/particle-in-a-box models in the canonical ensemble.[131] The

standard state is for a mole of particles at $T = 298$ K and 1 atm pressure ($V = R \cdot T/P$). All quantities above except E_0, E_{elec}, E_{NN} and E_{ZPV} have explicit temperature dependence.

1.2.5 Solvation Calculations

Bulk solvent effects can have a substantial effect on geometries and energies, specially when high-dielectric solvents, such as aqueous medium, are considered and charged species are involved in the reaction.[132,133] Theoretical simulation of chemical processes in aqueous solution is not without difficulty and a variety of theoretical methods are available for this type of calculations.[134–136] In the present thesis, continuum methods have been employed to evaluate bulk solvent effects. In particular, the Polarizable Continuum Model[137–139] has been used. In this method, the solute is embedded in a cavity of molecular shape surrounded by a continuous dielectric medium, whose polarization is reproduced by point charges distributed on the cavity surface. The solvation free energy, ΔG_{sol}, is defined as

$$\Delta G_{sol} = G_{aq} - G_{gas} \tag{1.20}$$

where G_{gas} and G_{sol} are the molecular free energies in the gas phase and in solution, respectively. More precisely, within this approximation, the solvation energy is given by

$$\Delta G_{sol} = \left(E\left[\Psi_{sol}\right] + E_{sol}\left[\rho_{sol}\right]\right) - E\left[\Psi_{gas}\right] \tag{1.21}$$

where $E\left[\Psi_{gas}\right]$ and $E\left[\Psi_{sol}\right]$ are the the Kohn-Sham energy functionals that take as arguments the Kohn-Sham single-determinant wave function optimized in the gas phase (Ψ_{gas}) and in solution (Ψ_{sol}), and $E_{sol}\left[\rho_{sol}\right]$ is the solvation energy that takes as argument the polarized electron density in solution $\rho_{sol}(\mathbf{r})$ (which can be derived from Ψ_{sol}). The Kohn-Sham energy functional $E\left[\Psi\right]$ is given by

$$\begin{aligned} E\left[\Psi\right] &= T_S\left[\Psi\right] + J\left[\rho\right] + E_{XC}\left[\Psi\right] + \int \rho(\mathbf{r}) v_0(\mathbf{r})\, d^3r + E_{NN} \\ &= E_{elec}\left[\Psi\right] + E_{NN} \end{aligned} \tag{1.22}$$

where $T_S\left[\Psi\right]$ is the non-interacting kinetic energy functional, $J\left[\rho\right]$ is the classical electrostatic energy, $E_{XC}\left[\Psi\right]$ is the exchange-correlation energy and E_{NN} is the nuclear-nuclear repulsion energy. The functional in Eq. 1.22 depends parametrically on the nuclear coordinates and charges under the classical Born-Oppenheimer approximation through the external nuclear potential $v_0(\mathbf{r})$.

In the PCM model, the solvation energy functional $E_{sol}\left[\rho_{sol}\right]$ can be written

$$E_{sol}\left[\rho\right] = \frac{1}{2}\left(\int \rho(\mathbf{r}) \cdot v_{RF}(\mathbf{r})\, d^3r - \sum_{\alpha} Z_\alpha \cdot v_{RF}(\mathbf{R}_\alpha)\right)$$

(1.23) $$+ \quad G_{disp-repul} + G_{cav}$$

where $v_{RF}(\mathbf{r})$ is the solvent reaction-field potential, Z_α is the nuclear charge of atom α located at position $\mathbf{R}_\alpha$. The factor of 1/2 in Eq. 1.23 results from the linear-response nature of the dielectric models, and the $G_{dis-repul}$ and G_{cav} represent the dispersion-repulsion and cavitation contributions, respectively.[140]

The cavitation term is computed using an expression obtained from scaled particle theory.[141] The dispersion-repulsion term is calculated according to the prescription described by Floris *et al.*[142] with a solvent accessible surface that is constructed from the UAHF radii plus a solvent probe radius of 1.385 Å.

The solvent reaction field potential $v_{RF}(\mathbf{r})$ is generated (see references[140] and[143] for details) by considering a cavity of unit dielectric surrounded by a linear isotropic polarizable continuum of dielectric constant ϵ. The reaction field potential is solved numerically[134,138,139,144] using a boundary element method. The method do not account explicitly for the effect of "volume polarization" (referred to also as "outlying charge" or "charge penetration" effects).[145] However, PCM as implemented in GAUSSIAN98 normalize the polarization charge in accord with Gauss' law,[146] which is an implicit attempt to capture the main features of the volume polarization term. The parameters in both models have also been adjusted to reproduce experimental solvation free energies (and hence, to some extent, take into account higher order effects implicitly).

There are different variants of PCM depending on the definition of the cavity. The main three variants are:

- Standard PCM: the cavity is defined as the overlap of different atomic spheres. The cavity where the solute is embedded is formed by the envelope of spheres centered on solute atoms or atomic groups; the cavity is then subdivided into small domains (call tesserae) where the polarization charges are placed. In Standard PCM calculations the tesserae are drawn by projecting on each sphere the 60 triangular faces of an inscribed pentakisdodecahedroan: the tesserae completely buried inside the cavity are discarded, and those cut by other spheres are replaced by suitable curved polygons.

- IPCM: Cavity is defined according to an isodensity surface in gas-phase and it is kept constant in the SCF procedure.

- SCIPCM: Cavity is defined according to an isodensity surface that is self-consistently updated in the SCF procedure. That is, the cavity is optimized within the SCRF variational process.

Part I

Characterization of Twisted Amides

Chapter 2

Resonance in amides. Characterization by electron-delocalization indexes.

Abstract

Delocalization indexes based on magnitudes derived from electron pair-densities are demonstrated to be useful indicators of electron resonance in amides. These indexes, based on the integration of the two-electron density matrix over the atomic basins defined through the zero-flux condition, are calculated for a series of amides at the B3LYP/6-31+G* level of theory. These quantities, which can be viewed as a measure of the electron sharing between atoms, behave in concordance with the traditional resonance model, even though they are integrated in Bader's atomic basins. Thus, the use of these quantities overcomes contradictory results from analysis of atomic charges, yet keeps the theoretical appeal of using non-arbitrary atomic partitions and unambiguously defined functions such as densities and pair-densities. Moreover, for a large data set consisting of 24 amides plus their corresponding rotational transition states, a linear relation is found between the rotational barrier for the amide and the delocalization index between nitrogen and oxygen, indicating that this parameter can be used as an ideal physical-chemical indicator of the electron resonance in amides.

2.1 Introduction

As it has been explained in the Introduction, the amide bond shows peculiar geometrical and energetic features, as the planarity of the nitrogen atom, shorter C-N bond distances than in amines and larger C-O distances than in aldehydes,[4–6] and a characteristic stability towards nucleophilic attack.[18,19]

Traditionally, resonance theory and molecular orbital theory[20–23] have been used for the explanation of these properties, which states that there is a resonance between the nitrogen lone pair (n_N) and the carbonyl π orbital (π_{CO}), which leads to a sp^2 hybridisation of the nitrogen. In terms of standard resonance theory, the description of the electronic structure is accomplished through the introduction of two resonant structures (I and II in Figure 1.2), with structure II leading to a partial double bond character of the C-N bond, and therefore, its planarity and stability.

Attempts have been made to quantify the resonance effect using different theoretical methods: Natural Population Analysis and Natural Resonance Theory[14] supported the traditional resonance model, showing that strong $n_N \rightarrow \pi^*_{C-O}$ type resonance lead to a significant stabilization of the electronic structure in amides. Besides, analysis of the Mulliken atomic charges[147] as a function of C-N bond rotation also gives trends that are in agreement with the resonance model, predicting a transfer of electronic charge from nitrogen to oxygen as the C-N bond rotates. In addition, valence bond theory[148,149] has also lead to results in accordance with the resonance model. However, the use of orbital and partitioning schemes such as Mulliken are not fully unambiguous criteria as to ascertain the nature of the electronic structure of molecules. Furthermore, an analysis based on localized orbitals could be far from adequate to describe electronic effects based on the delocalization of electron density among various nuclei.

Correspondingly, efforts have been made to use the electron density and its topological analysis, reliant on a non-arbitrarily modified physical observable, to characterize the nature of the electronic structure in amides.[12,13,49–51,150] However, analysis of the corresponding atomic charges, based on the integration of the electron density in the atomic volumes defined in the context of the Atoms In Molecules (AIM) theory,[151] led to a contradictory picture with respect to the resonance model and experimental estimates of electron density changes upon C-N rotation based on ^{13}C, ^{15}N, and ^{17}O NMR chemical shifts[152] and N1s and O1s core ionization energies.[153] Thus, a qualitatively different electronic charge transfer is predicted: a transfer of electronic charge from nitrogen to carbon, but small changes within the oxygen atom. It has been argued[52] that the differences between the two analyses can be reconciled if one takes into account the high polarity of the C=O bond, remarking the importance of resonant structure III (Figure 1.2).[51] Nevertheless, the controversy on the use of Bader's atomic charges and their interpretation is not new,[154–156] and some authors[147] have

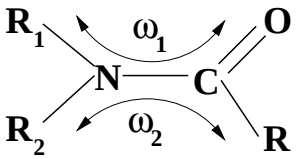

Figure 2.1: The two dihedral angles (ω_1 and ω_2) used for determining the torsional angle τ. The ω_1 angle was constrained along the butamide rotation.

even claimed that Bader's atomic charges is not suitable for this kind of analysis.

In summary, questions remain as to relate the resonance in amides to a well founded physical-chemical quantity which overcomes the limitations of the use of molecular orbitals and complement the useful analysis provided by orbital based theories. In this vein, the present chapter applies recently developed localization and delocalization indexes[157,158] to characterize the electron resonance in amides. These type of indexes has been successfully used to get insight on the electronic structure of various molecules. They are based on the topological analysis of a well defined unambiguous quantum object: the two electron density matrix, which resembles the simultaneous probability density of finding two electrons at two points in space. Indexes derived form the two-particle density matrix are integrated over atoms following Bader's criteria to define atoms within molecules. Hence, these quantities are well defined physical objects integrated over atoms defined in a non-arbitrary way. It is through the analysis of these pair densities that the Lewis model of electronic structure finds physical expression.

The chapter is divided in two parts: first we present a detailed analysis of butamide and the change of the main delocalization indexes as a function of C-N bond rotation. The results for butamide will be used to set up the conceptual basis for the interpretation of resonance theory in terms of delocalization indexes. In the second part of the chapter, the analysis is extended to cover a dataset of 24 amides with different degrees of torsion about the C-N bond.

2.2 Methodology

All the geometrical optimizations were carried out in gas-phase using the Gaussian 98 suite of programs[159] at the B3LYP/6-31+G(d) level of theory. The use of the B3LYP functional[118,120,160,161] is motivated by its success in the evaluation of reliable reaction enthalphies for the hydrolysis of amides.[66,79,81] The rotation of the butamide was carried out constraining the C_1-N-C-O dihedral angle (ω_1 of Figure 2.1). The τ torsional angle characterizes the mean twisting angle around the C-N bond[48,162] and ranges from 0^o (planar amide group) to 90^o (when the two planes defined by the

O-C-R and $R_1 - N - R_2$ atoms are perpendicular; see Figure 2.1) .

$$\tau = \frac{\omega_1 + \omega_2}{2} \tag{2.1}$$

Moreover, as the rotational free energy of several amides is related to τ and to several delocalization indices, the structures of both the reactants and the rotational transition states were characterized at the B3LYP/6-31+G(d) level of theory. The enthalpic and entropic corrections were determined with frequency calculations at the same level.[130] These frequencies were also used to verify the nature of the stationary points encountered along the potential energy surfaces. Thus, reactants showed real frequencies for all the normal modes of vibration, whereas rotational transition states showed one imaginary frequency along the normal mode that connects the appropriate minima. The frequency calculations were also used to allow for an evaluation of thermodynamic quantities such as the zero-point vibrational energy, and thermal vibrational contributions to the enthalpy, entropy and Gibbs free energy.

Insight on the electronic structures of molecules can be gained by using the localization index,

$$\lambda_A = -\int_A \int_A \left(2\Gamma(\mathbf{r_1}, \mathbf{r_2}) - \rho(\mathbf{r_1})\rho(\mathbf{r_2})\right) d\mathbf{r_1} d\mathbf{r_2} \tag{2.2}$$

and the delocalization index,

$$\delta_{AB} = -2\int_A \int_B \left(2\Gamma(\mathbf{r_1}, \mathbf{r_2}) - \rho(\mathbf{r_1})\rho(\mathbf{r_2})\right) d\mathbf{r_1} d\mathbf{r_2} \tag{2.3}$$

where $\rho(\mathbf{r})$ and $\Gamma(\mathbf{r_1}, \mathbf{r_2})$ are the one- and two-electron densities, respectively. The delocalization index is formally equivalent to integration of the exchange-correlation density ($\rho_{xc}(\overline{\mathbf{r}}_\mathbf{1}, \overline{\mathbf{r}}_\mathbf{2})$) over the basins of atoms A and B (defined from the zero-flux gradient condition applied to the one-electron density, $\rho(\mathbf{r})$):

$$\delta_{AB} = -2\int_A \int_B \rho_{xc}(\overline{\mathbf{r}}_\mathbf{1}, \overline{\mathbf{r}}_\mathbf{2})\, d\overline{\mathbf{r}}_\mathbf{1} d\overline{\mathbf{r}}_\mathbf{2} \tag{2.4}$$

The integrations are carried out through one or two atomic basins, as defined from the condition of zero-flux gradient in $\rho(\mathbf{r})$. Thus, the localization and delocalization indexes are defined in the framework of the Bader's theory of Atoms in Molecule (AIM).[151] They were calculated with the AIMPAC suite of programs[163] at the B3LYP/6-31+G(d) geometries optimized.

The electron pair density, in conjunction with the definition of an atom in a molecule, enables one to determine the average number of electron pairs that are localized to each atom and that are formed between any given pair of atoms. Localization and delocalization indexes that determine intra- and

inter-atomic distribution of electron pairs enables one to compare the pairing predicted by theory with that of a Lewis structure. The agreement is best at Hartree-Fock level, where the Fermi hole is the sole source of correlation between electrons. The introduction of the remaining Coulomb correlation, disrupts the sharing of electron pairs between the atoms and reduce the number of shared pairs.

The λ and δ indices are obtained only from first- and second-order densities, which are physical observables. In principle, there is no need to resort to any particular model, such as MO theory for these calculations. Therefore, provided that ρ and Γ are available, this analysis could be performed at any level of theory. At present, practice provides second-order densities only for the HF and CISD approximations. In addition, practical quantum calculations are performed in the framework of Molecular Orbital theory. In this case, these indexes can be efficiently calculated through the evaluation of the overlap integrals within the corresponding basins. Thus, the delocalization index for a pair of atoms at HF level of theory would be calculated using the following expression,

$$\delta_{AB} = 4 \sum_{i,j}^{N/2} S_{ij}(A) S_{ij}(B) \tag{2.5}$$

The summations run over all the occupied orbitals. $S_{ij}(A)$ is the overlap of the orbitals i and j within the basin of atom A.

In the framework of Khon-Sham (KS) Density Functional Theory (DFT), $\lambda(A)$ and δ_{AB} cannot be calculated exactly because the electron-pair density has to be approximated by an unknown exchange-correlation functional.[164] As a practical workaround, one can derive a HF-like electron-pair density from the KS orbitals and calculate approximate localization and delocalization indices at the DFT level using Eq. 2.5. Since there is not yet a practical way to obtain molecular electron-pair densities in DFT methods, this is the only feasible approach at the moment for the calculation of approximate delocalization indices at DFT level. In fact, although Coulomb correlation effects are included to some extent in the one-electron density, they are not properly taken into account in the two-electron density calculated using the HF ansatz. Therefore, the delocalization indexes obtained using this approximation are generally closer to the HF values than to the correlated ones (e.g. Configuration Interaction). However, it has been shown that delocalization indices evaluated within DFT provide useful chemical insight and constitute a suitable tool for the electronic characterization of molecules in different systems, including those with delocalized electrons in aromatic molecules.[158,164,165]

Units: In all the tables and figures of this chapter and throughout the text, atomic units are used for the delocalization indexes, relative energies are given in kcal/mol, the distances in Å and the angles in degrees.

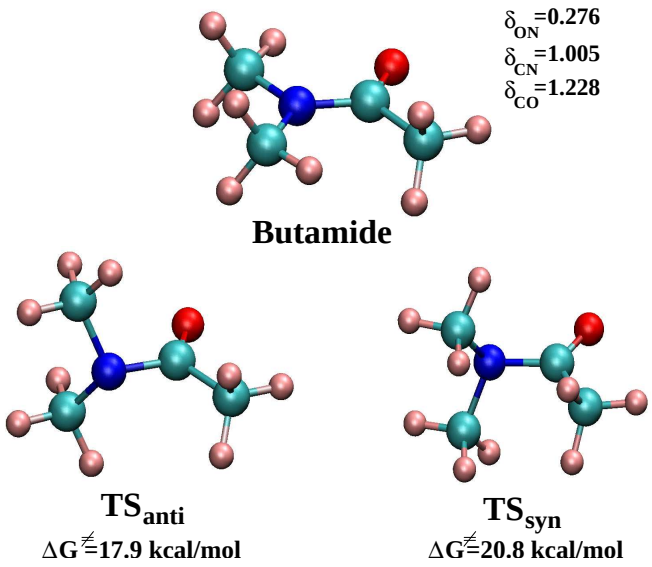

Figure 2.2: The butamide reactant and its rotational transition states TS_{anti} and TS_{syn} which depend on the orientation of n_N with respect to the O atom. Structures characterized at the B3LYP/6-31+G(d) level of theory.

2.3 Results and Discussion

2.3.1 Delocalization indexes in butamide: a case study

We first study butamide (Figure 2.2) as our prototype. The values for the delocalization indexes δ_{CN} and δ_{CO} in butamide are 1.005 and 1.228, respectively. As explained in the Methodology section, delocalization indexes at correlated levels of theory tend to give lower values than one would expect from an interpretation of these indexes as the shared electron density in a Lewis model. In order to have some reference values to interpret these indexes as shared electron pairs, we also studied a variety of reference molecules (see Figure 2.3) at the same level of theory. $(CH_3)_3C-N(CH_3)_2$ is taken as a prototype C-N single bond ($\delta_{CN} = 0.915$), $(CH_3)_2C=NCH_3$ as a typical C=N double bond ($\delta_{CN} = 1.551$), and $CH_3C \equiv NCH_3$ as a triple C≡N bond ($\delta_{CN} = 2.321$). Regarding reference indexes for C-O bonds, we consider $(CH_3)_3C-OCH_3$ ($\delta_{CO} = 0.834$) for a single bond, and $(CH_3)_2C=O$ for a double bond ($\delta_{CO} = 1.399$). These indexes are complemented with the values for partial bond orders, such as the one in triazine (C-N bond order of 1.5 and $\delta_{CN} = 1.219$) and the one in methyl acetate (C-O bond order of 1.5 and $\delta_{CO} = 1.110$). Notice again that the values for delocalization indexes are significantly lower than the nominal electron pair shared from the Lewis model, as corresponds to the use of correlated level of theory. Based on these reference values, we can asses that the C-N

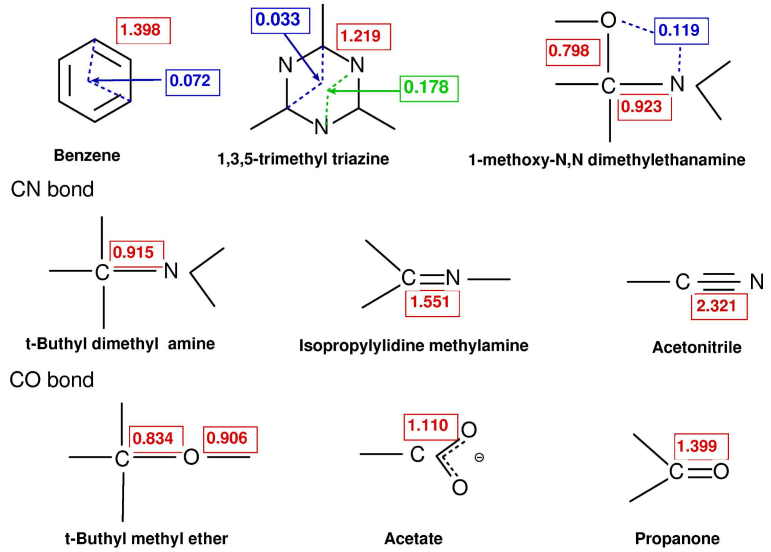

Figure 2.3: Reference values for delocalization indexes calculated at the B3LYP/6-31+G(d) level of theory.

bond in butamide with $\delta_{CN} = 1.005$, shows a partial double bond character. Assuming a linear relationship between bond order and δ_{CN} values, an estimation of a bond order of 1.17 is obtained for this bond. Concomitantly, we observe that the C-O bond has partially lost its double bond character, with a $\delta_{CO} = 1.228$. Assuming again a linear relationship between bond order and δ_{CO}, a bond order of 1.7 is obtained for C-O bond in butamide. This is in agreement with the classical resonance model and with the relevance of resonant structures I and II in the description of the electronic structure of amides.

The delocalization indexes are based on the analysis of the second order electron density function and provide electron populations that are delocalized between two atoms independent of whether they are directly bound or not. Therefore, we can also measure the delocalization index between nitrogen and oxygen, δ_{ON}. A very high value for this index is observed, 0.276, even though these two atoms are not directly bound. For instance, in triazine a lower value for the delocalization between non-bonded nitrogen atoms is obtained (0.178). A lower value is also obtained for δ_{ON}, 0.119, in $CH_3O - CH_2 - N(CH_3)_2$. In the latter, there is no π system in which to delocalize the nitrogen lone pair and, correspondingly, the values of δ_{CO} (0.798) and δ_{CN} (0.923) suggest single bonds in both cases. The δ_{ON} delocalization index therefore reveals a high electronic delocalization between nitrogen and oxygen coming from the high aromaticity along the N-C-O skeleton, and this could be a good indicator for resonance in amides.

Table 2.1: Main parameters along butamide rotation. The ω_1 dihedral angle was constrained in order to obtain intermediate points along the rotation. The τ twist angle, ΔE relative electronic energy and, δ_{ON}, δ_{CN} and δ_{CO} delocalization indices at the corresponding points are presented. The ellipticity (ϵ) and electron density (ρ) for the CN and CO bonds calculated at the corresponding bond critical points are also included.

ω_1	τ	ΔE	δ_{ON}	δ_{CN}	δ_{CO}	ϵ_{CN}	ϵ_{C-O}	ρ_{C-N}	ρ_{C-O}
0.0	0.0	0.0	0.276	1.005	1.228	0.159	0.090	0.314	0.399
8.8	2.6	0.0	0.275	1.004	1.230	0.157	0.090	0.314	0.399
18.9	7.6	0.2	0.273	1.005	1.242	0.151	0.091	0.315	0.399
28.5	13.3	0.8	0.269	1.003	1.245	0.143	0.092	0.315	0.400
37.8	19.5	1.9	0.264	1.001	1.255	0.136	0.092	0.314	0.400
47.0	26.1	3.4	0.256	0.998	1.266	0.129	0.091	0.313	0.401
56.0	33.1	5.4	0.247	0.991	1.279	0.121	0.090	0.310	0.402
66.2	41.3	7.8	0.236	0.981	1.292	0.112	0.088	0.307	0.403
77.3	50.3	10.1	0.222	0.963	1.309	0.100	0.088	0.302	0.405
86.6	58.8	12.4	0.208	0.945	1.324	0.087	0.087	0.297	0.406
96.0	67.9	14.4	0.196	0.925	1.338	0.074	0.085	0.292	0.407
106.4	78.1	15.9	0.187	0.909	1.348	0.063	0.084	0.288	0.408
118.1	90.0	16.4	0.184	0.901	1.351	0.060	0.084	0.287	0.409

Delocalization indexes and rotation around the C-N bond

Next, we investigate how the delocalization indexes are influenced by C-N bond rotation. Thus, the C-N-C-O dihedral angle was constrained at different values and the delocalization indexes were evaluated. Also shown in Table 2.1 are the ρ electron density and the ellipticity values at the C-N and C-O bond critical points, the τ torsion angle and the relative energy with respect to the planar butamide (ΔE). In Figure 2.4, the percentage of change in δ_{CO}, δ_{CN} and δ_{ON} delocalization indexes as functions of the torsion angle are depicted.

Rotation around the C-N bond can lead to two possible transition states, TS_{anti} and TS_{syn} with *anti* or *syn* orientation between oxygen and nitrogen lone pairs (see Figure 2.2). The free energy barriers associated with these two transition states are 20.8 kcal/mol for TS_{syn} and 17.9 kcal/mol for TS_{anti}. Thus, TS_{anti} is the preferred transition state for rotation, and our chose of dihedral angle for the constrained optimizations leads from the planar butamide to TS_{anti}. In both transition states, nitrogen adopts a sp^3 hybridisation and therefore, a pyramidal conformation (Figure 2.2) with concomitant lengthening of the peptide bond and shortening of the carbonyl bond. Rotational barriers in amides have been extensively studied in the literature.[32–36] The high barriers are attributed to the stabilization caused by the $n_N \rightarrow \pi^*_{CO}$ delocalization, and are therefore a measure of amide bond stability. Wiberg *et al.* estimated[166] both theoretically and experimentally

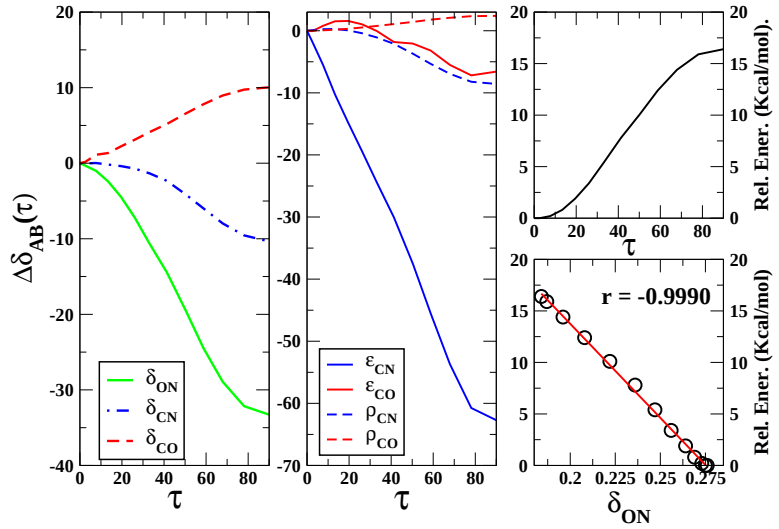

Figure 2.4: Rotation of butamide around the C-N bond. On the left hand side, the percentage change for δ_{ON}, δ_{CO} and δ_{CN} indexes with respect to the values in planar butamide as defined in Eq. 2.6 are displayed. In the center diagram, the percentage change in the C-N and C-O bonds ellipticity and ρ electron density at the bond critical points are shown. To the right, the relative electronic energy with respect to the τ torsional angle, and the δ_{ON} index are shown.

the rotational free energy barrier in N,N dimethyl acetamide, and obtained a barrier of 15.3 $\pm$ 0.1 kcal/mol experimentally (with respect to the anti TS) using NMR selective inversion-recovery experiments in several solvents. They also calculated the barrier using quantum methods (at the G2(MP2) level of theory), giving a value of 15.64 kcal/mol for the anti TS and 18.13 kcal/mol for syn TS in good agreement with experiments and with our own results.

Variations of δ_{CN}, δ_{CO} and δ_{ON} delocalization indices as functions of the C-N bond rotation are shown in Table 2.1. In Figure 2.4, the percentage change in localization indexes ($\Delta\delta_{AB}(\tau)$) with respect to the values at the planar amide are depicted, namely,

$$\Delta\delta_{AB}(\tau) = \frac{\delta_{AB}(\tau) - \delta_{AB}(\tau = 0.0)}{\delta_{AB}(\tau = 0.0)} \times 100 \tag{2.6}$$

The value of δ_{CO} increases from 1.228 in butamide to 1.351 at TS_{anti}, whereas δ_{CN} decreases from 1.005 in butamide to 0.901 in TS_{anti}. At the transition state, the values of δ_{CN} and δ_{CO} are indicative of the presence of a C-N single bond and a C-O double bond, in agreement with the resonance model, which would predict a loss in the contribution of resonant structure II upon rotation. The δ_{ON} index, shown in Figure 2.4, is extremely sensitive

to C-N bond rotation. It goes from 0.276 in planar butamide to 0.184 in TS_{anti}. This value still shows some degree of delocalization between nitrogen and oxygen, although the analysis of δ_{CN} and δ_{CO} prevents from associating this delocalization to a π-type delocalized interaction.

The changes in electron delocalization indexes are also reflected t a certain extent by the change in properties at the bond critical points. The density at the C-N bond critical point lowers (from 0.314 to 0.287) and the one at the C-O bond slightly increases (0.399 to 0.409). However, the analysis of the values of the ellipticities (which measures the anisotropy of the curvature of the electron density)[167] at these critical points leads to contradictory results for the C-O bond. The value of ϵ_{CN} shows a dramatic decrease of 70% in accordance with a loss in C-N double bond character. However, ϵ_{CO} also shows a decrease of ca 5%, which is in disagreement with a reinforcement of the π character of the bond. This result pinpoints the limitations of the use of analyse based on the properties of just one point in space. Delocalization indexes are integrated in volumes of well-defined boundaries and are, in this sense, taking into account the whole atomic volume.

Table 2.2: Electron population (N_A) and localization indices (λ_A) along the rotation of the butamide towards the anti TS.

τ	N_A			λ_A		
	C	N	O	C	N	O
0.0	4.543	8.180	9.217	2.866	6.364	8.299
2.6	4.546	8.176	9.217	2.867	6.380	8.299
7.6	4.561	8.164	9.214	2.874	6.348	8.295
13.3	4.567	8.147	9.211	2.878	6.335	8.292
19.5	4.581	8.127	9.207	2.886	6.318	8.287
26.1	4.596	8.105	9.203	2.895	6.300	8.281
33.1	4.611	8.081	9.199	2.904	6.282	8.276
41.3	4.627	8.059	9.195	2.914	6.266	8.272
50.3	4.643	8.036	9.190	2.926	6.255	8.266
58.8	4.657	8.018	9.184	2.937	6.247	8.260
67.9	4.666	8.006	9.181	2.945	6.245	8.257
78.1	4.673	8.001	9.178	2.953	6.246	8.253
90.0	4.671	8.007	9.177	2.953	6.254	8.253

Analysis of the localization indexes and atomic charges lead to similar results as those described by Wiberg *et al.*,[12,13] namely an increase in electronic charge on carbon and a decrease on nitrogen. The electronic charge associated with the oxygen decreases upon rotation but to a much lesser degree. This behavior, which is somewhat contrary to the one predicted by the

traditional resonance model, has generated an interesting theoretical discussion on the origin of amide stabilization. The interpretation associated with Bader's atomic charges is still a matter of controversy. In addition, several experimental estimates of trends of atomic charges upon rotation suggest that Bader's atomic charges give the wrong trend. For instance, Yamada[152] characterized by X-ray diffraction the structure of 3-acyl-1,3-thiazolidine-2-thione derivatives and related their τ torsional angle to the ^{13}C, ^{15}N, and ^{17}O NMR chemical shifts. The results showed that as the twist angle increases the $\Delta\delta^{13}C$ and $\Delta\delta^{17}O$ increase while the $\Delta\delta^{15}N$ decreases. These $\Delta\delta$ chemical shifts are directly related with the charge densities around each atom. Therefore, the increment of the twist of the amide bond leads to a decrease in the electron density of the C and O atoms and an increase in that of the N atom, in agreement with what the resonance model would predict. Greenberg *et al.*[153] reached similar conclusions based on the analysis of the N1s and O1s core ionization energies for a group of planar and distorted amides and lactams using X-ray photoelectron spectroscopy. On the other hand, when the analysis of the electron density in these compounds is done in terms of electron pair densities integrated in the corresponding atomic basins rather than in terms of atomic charge densities, the discrepancies with the resonance model disappear.

In summary, the trend of the delocalization indexes supports the traditional resonance model, in that a decrease in the electron sharing between carbon and nitrogen and an increase between carbon and oxygen is observed with C-N bond rotation. Moreover, there is a high electron delocalization between nitrogen and oxygen, only possible if there is a substantial electronic resonance along the N-C-O skeleton. In this sense, rotation around the C-N bond leads to a substantial decrease in δ_{ON}. In addition, when the values of this index versus the relative energies of the structures with different degree of twisted amide bond are plotted (Figure 2.4, right-bottom diagram), there is a clear correlation (r=-0.9990) between decrease in δ_{ON} and energetic destabilization of the structure. Its physical interpretation is consistent with the classical resonance model, and furthermore a well defined physical quantity, in principle not subjected to the typical shortcomings of the use of molecular orbitals. Thus, it seems that δ_{ON} is an ideal physical-chemical property to measure the degree of electronic delocalization along the N-C-O skeleton in amides. To investigate this hypotheses, a more general analysis is required with a sufficiently large amide dataset. This is the subject of the next section.

2.3.2 Delocalization indexes in an amide dataset

A series of 24 amides with varying degree of twist were investigated (Figure 2.5). Amides were classified in three different families depending on the functional group attached to the carbonyl carbon (R position in Figure 2.5):

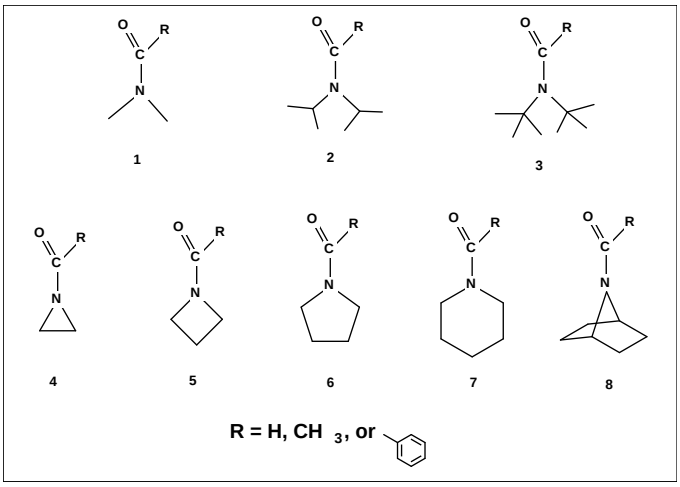

Figure 2.5: Amide dataset studied at the B3LYP/6-31+G(d) level of theory. Three different families were characterized depending on the group attached to the carbonyl group (R = H, Methyl or Phenyl). Notice that compounds 1-3 are aliphatic while 4-8 are cyclic amides where the degree of N pyramidalization and therefore the τ twist angle changes. The TS_{anti} were also characterized at the same level of theory in order to determine the corresponding rotational free energy barrier.

Table 2.3: Rotational free energies (ΔG_{rot}), main geometrical parameters, O-N, C-N and C-O delocalization indices and the ellipticity and electron density values at C-N and C-O bonds for compounds 1-8 and their rotational TSs, where R=H.

Molecule	ΔG_{rot}	**Geom. par.**			**Delocal. ind.**			**Ellipticity**		ρ	
		τ	r_{C-N}	r_{C-O}	δ_{O-N}	δ_{C-N}	δ_{C-O}	ϵ_{C-N}	ϵ_{C-O}	ρ_{C-N}	ρ_{C-O}
1	22.2	0.0	1.364	1.224	0.288	1.026	1.269	0.151	0.086	0.320	0.403
TS_1		90.0	1.440	1.209	0.190	0.929	1.410	0.063	0.086	0.295	0.411
2	19.9	0.2	1.368	1.226	0.280	1.046	1.265	0.163	0.081	0.321	0.401
TS_2		89.5	1.428	1.213	0.192	0.934	1.396	0.073	0.095	0.298	0.408
3	13.9	7.5	1.374	1.230	0.272	1.052	1.259	0.156	0.081	0.317	0.397
TS_3		89.2	1.435	1.212	0.185	0.931	1.375	0.080	0.091	0.296	0.408
4	6.3	11.1	1.384	1.216	0.266	0.982	1.327	0.070	0.100	0.313	0.408
TS_4		90.0	1.426	1.212	0.203	0.962	1.374	0.007	0.073	0.300	0.409
5	20.0	0.0	1.349	1.227	0.300	1.023	1.265	0.135	0.091	0.328	0.401
TS_5		90.0	1.432	1.211	0.193	0.947	1.401	0.042	0.080	0.298	0.409
6	21.8	0.2	1.353	1.227	0.295	1.027	1.263	0.146	0.092	0.326	0.400
TS_6		90.0	1.435	1.211	0.190	0.936	1.404	0.049	0.084	0.297	0.410
7	23.4	0.1	1.358	1.227	0.291	1.033	1.261	0.154	0.090	0.324	0.401
TS_7		90.0	1.433	1.210	0.190	0.934	1.403	0.059	0.087	0.298	0.410
8	19.0	3.1	1.356	1.226	0.292	1.021	1.271	0.128	0.092	0.322	0.402
TS_8		90.0	1.430	1.213	0.189	0.949	1.397	0.041	0.085	0.298	0.408

Table 2.4: Rotational free energies (ΔG_{rot}), main geometrical parameters, O-N, C-N and C-O delocalization indices and the ellipticity and electron density values at C-N and C-O bonds for compounds 1-8 and their rotational TSs, where R=Methyl.

Molecule	ΔG_{rot}	**Geom. par.**			**Delocal. ind.**			**Ellipticity**		ρ	
		τ	r_{C-N}	r_{C-O}	δ_{O-N}	δ_{C-N}	δ_{C-O}	ϵ_{C-N}	ϵ_{C-O}	ρ_{C-N}	ρ_{C-O}
1	17.9	0.0	1.375	1.231	0.276	1.005	1.228	0.160	0.090	0.314	0.399
TS_1		90.0	1.456	1.214	0.182	0.897	1.347	0.060	0.084	0.287	0.409
2	14.2	2.9	1.381	1.234	0.268	1.031	1.225	0.175	0.086	0.314	0.397
TS_2		86.2	1.445	1.217	0.185	0.908	1.339	0.067	0.095	0.289	0.406
3	3.4	43.7	1.400	1.228	0.246	1.000	1.251	0.153	0.102	0.307	0.399
TS_3		88.1	1.453	1.217	0.179	0.905	1.324	0.073	0.090	0.287	0.406
4	5.2	17.9	1.398	1.221	0.250	0.954	1.284	0.071	0.096	0.307	0.405
TS_4		90.0	1.442	1.216	0.193	0.925	1.319	0.003	0.071	0.291	0.407
5	17.9	1.5	1.359	1.232	0.287	0.991	1.224	0.133	0.091	0.324	0.398
TS_5		90.0	1.447	1.216	0.185	0.913	1.338	0.043	0.077	0.290	0.407
6	18.2	0.8	1.364	1.233	0.282	1.001	1.221	0.148	0.094	0.321	0.397
TS_6		90.0	1.450	1.215	0.182	0.904	1.342	0.048	0.082	0.289	0.408
7	17.8	2.4	1.371	1.233	0.278	1.013	1.222	0.161	0.091	0.318	0.397
TS_7		90.0	1.449	1.215	0.182	0.902	1.342	0.056	0.085	0.290	0.408
8	16.0	5.3	1.370	1.231	0.277	0.993	1.234	0.128	0.093	0.317	0.399
TS_8		90.0	1.444	1.217	0.181	0.915	1.337	0.042	0.084	0.290	0.406

an hydrogen, methyl or a phenyl group. To provoke different torsions on the amide bond, different substituents are attached to the nitrogen. In compound **1** we introduced two methyl groups, in **2** two isopropyl group and in **3** two tert-butyls. In addition, the nitrogen was embedded in a ring whose size and, hence, the level of amide bond twist was varied from compounds **4** to **8**. To facilitate the identification of these amides a number code is employed (illustrated in Figure 2.5) with a subscript defining the substituent at the carbon position (R): H, methyl (Met) or phenyl (Phe). Tables 2.3, 2.4 and 2.5 show the values of the various delocalization indexes at the reactant and TS_{anti} transition states, along with the corresponding rotational free energy barriers, and relevant geometrical parameters.

Geometries. The different substituents have a large effect on the degree of amide bond torsion. For instance, dimethylformamide (1_H) is completely planar (τ=0.0), but as more bulky substituents are added at the nitrogen position, the planarity is broken, and compound 3_H shows a τ of 7.5^o. Substitution at the R position also leads to sizeable differences in the degree of amide bond torsion, specially when phenyl groups are introduced. For example, while compounds 1_H and 1_{Met} are planar, compound 1_{Phe} is significantly twisted, τ being 13.9^o. In general, we observe that the planarity of the compounds decrease as we go from R=H to R=Met, and from R=Met to R=Phe, the average τ angle over the 8 compounds being 2.8^o for R=H, 9.3^o for R=Met and 18.4^o for R=Phe. With respect to substitution at nitro-

Table 2.5: Rotational free energies (ΔG_{rot}), main geometrical parameters, O-N, C-N and C-O delocalization indices and the ellipticity and electron density values at C-N and C-O bonds for compounds 1-8 and their rotational TSs, where R=Phenyl.

Molecule	ΔG_{rot}	**Geom. par.**			**Delocal. ind.**			**Ellipticity**		ρ	
		τ	r_{C-N}	r_{C-O}	δ_{O-N}	δ_{C-N}	δ_{C-O}	ϵ_{C-N}	ϵ_{C-O}	ρ_{C-N}	ρ_{C-O}
1	12.7	13.9	1.376	1.233	0.274	1.007	1.225	0.163	0.093	0.315	0.397
TS_1		90.0	1.452	1.220	0.179	0.901	1.317	0.059	0.080	0.289	0.404
2	11.3	16.0	1.378	1.236	0.270	1.032	1.226	0.176	0.092	0.316	0.395
TS_2		84.4	1.440	1.223	0.182	0.913	1.307	0.068	0.090	0.292	0.401
3		49.5	1.407	1.230	0.232	0.991	1.251	0.145	0.103	0.305	0.397
TS_3											
4	4.1	21.4	1.402	1.224	0.239	0.950	1.268	0.070	0.089	0.306	0.403
TS_4		90.0	1.439	1.222	0.190	0.926	1.292	0.003	0.067	0.292	0.403
5	13.6	10.0	1.368	1.234	0.277	0.997	1.221	0.136	0.088	0.321	0.397
TS_5		90.0	1.444	1.222	0.181	0.917	1.309	0.042	0.073	0.292	0.402
6	13.8	8.1	1.367	1.236	0.279	1.009	1.214	0.159	0.094	0.320	0.396
TS_6		90.0	1.446	1.221	0.179	0.907	1.312	0.047	0.078	0.290	0.403
7	14.0	11.4	1.371	1.235	0.276	1.017	1.217	0.170	0.094	0.319	0.396
TS_7		89.8	1.445	1.221	0.179	0.905	1.312	0.056	0.080	0.292	0.403
8	12.8	16.5	1.376	1.233	0.267	0.996	1.231	0.128	0.090	0.317	0.397
TS_8		90.0	1.439	1.223	0.178	0.918	1.307	0.042	0.080	0.293	0.401

gen, the highest degree of twist is obtained for compounds **3**, with a bulky tert-butyl substituents, and **4**, which show the smallest ring structure and therefore a very constrained environment around nitrogen. As we add less bulky substituents (compounds **1** or **2**), or the size of the ring is increased (compounds **5**, **6** or **7**), the amides are more planar. Similar effects introduced by bulky substituents[168] and with differing ring-size[169] have been reported in the literature.

Rotational Transition States. Rotational transition states for each of the 24 amides of the series were also characterized, except in the case of 3_{Phe} for which all the attempts to trap the transition state failed. All transition states display torsional τ angles close to 90.0^o. The trends in C-N and C-O bond distances are the same for all systems, in that torsion around the C-N bond leads to an elongation of the C-N bond and a reduction of the C-O one. Rotational free energy barriers show large variations, from 3.4 kcal/mol for 3_{Met} to 23.4 kcal/mol for 7_H. These variations reveal substantial differences in the stability of the amides, and has its formal origin in the differences in electron resonance caused by the specific degree of torsion induced in each amide. The relationship between geometrical parameters and the amide bond stability is well established. For instance, Brown *et al.*[55] showed a relationship between the distortion of the amide bond and

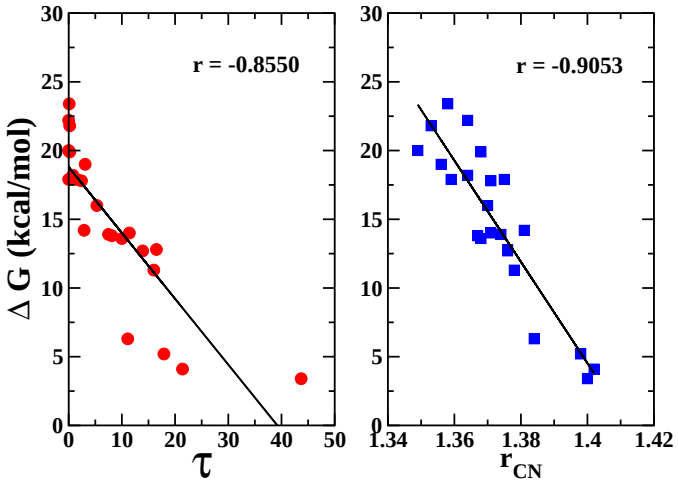

Figure 2.6: Representation of the rotational energy of different twisted amides with respect to the torsional angle (left-hand side) and the C-N bond length (right-hand side). The correlation coefficients among the points of each graphic are shown.

the rate of hydrolysis in both acid and base. In general, the more twisted the amide bond the lower the rotational barrier and, therefore, weaker C-N bond. In Figure 2.6, we plot the values of the free energy barriers versus the degree of amide bond twist (τ angle) of the amide reactant. There is an inverse relation between these two properties with a correlation coefficient of -0.855. On the other hand, Brown and coworkers related the amide carbonyl stretching frequencies with the rotational barrier for a set of anilides and toluamides.[170] Moreover, they correlated the rotational barrier with the C-N amide bond distance indicating short amide bond distances yielded higher rotational barriers. Plotting our calculated barriers vs the C-N bond distances (Figure 2.6), we also find a linear inverse relation (r=-0.905).

Delocalization indexes The comparison of the data for each amide with its transition state is consistent with the predictions of the resonance model: a lowering of the electron sharing between carbon and nitrogen and an increase in the electron sharing between carbon and oxygen, or in other words, *i) a lowering of δ_{C-N} towards values typical of C-N single bonds, and ii) an increase in δ_{C-O} to values closer to those of C-O double bonds.*

Changes in δ_{ON} are also consistent with these electronic changes, and *at any of the transition states the values for δ_{ON} are significantly lower than the one of the amide reactant.* However, the specific values for δ_{ON} vary significantly among the various compounds. From 0.300 of 4_H to 0.232 of 3_{Phe}. In general compounds with R=H have the largest values for δ_{ON}, with an average δ_{ON} of 0.286 calculated among the 8 amide reactants, then there is R=Met with average δ_{ON} of 0.271, and finally, the lowest values

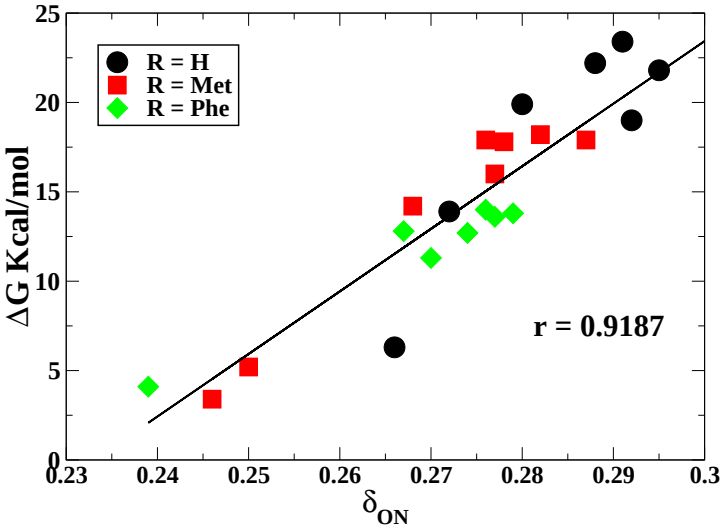

Figure 2.7: Rotational free energy versus δ_{ON} delocalization index for the amide dataset.

are found for the R=Phe series, with an average of 0.264. This indicates a substantial π electron withdrawing effect by the phenyl group. In addition, there is a direct correlation between degree of N-O delocalization and rotational barrier. Thus, in Figure 2.7, we plot the values of δ_{ON} versus the rotational barriers. A linear correlation is obtained (r=0.9187), indicating the direct relation between high electron delocalization between nitrogen and oxygen basins and stability of amide bond as characterized by values of the rotational barriers. The advantage of using δ_{ON} for this type of correlations is that this parameter is sensible not only to geometrical changes in amides but also to electronic effects induced by the different substituents that could not be directly inferred from changes in the degree of planarity of the amide. For example, both 1_H and 1_{Met} are planar (τ is 0.0), but the rotational barrier is 22.2 kcal/mol for the former and 17.9 kcal/mol for the latter, indicating that the electron delocalization and its induced stabilization should be stronger in 1_H. An analysis of δ_{ON} effectively reproduce a change in the degree of electron delocalization in these two amides, and 1_H shows higher value for the delocalization index (0.288, compared with δ_{ON} 1_{Met} = 0.276).

Attempts to correlate rotational barriers and parameters derived from electronic structure calculations are not new. For instance, Otani et al.[169] found a good correlation between the experimental rotational free energy barrier in solution of a series of N-benzoyl-7-azabicyclo[2,2,1]heptanes with respect to the delocalization indexes derived from differences in the relative ratio of the coefficients for the n_N orbital and the π^*_{CO} orbital between the

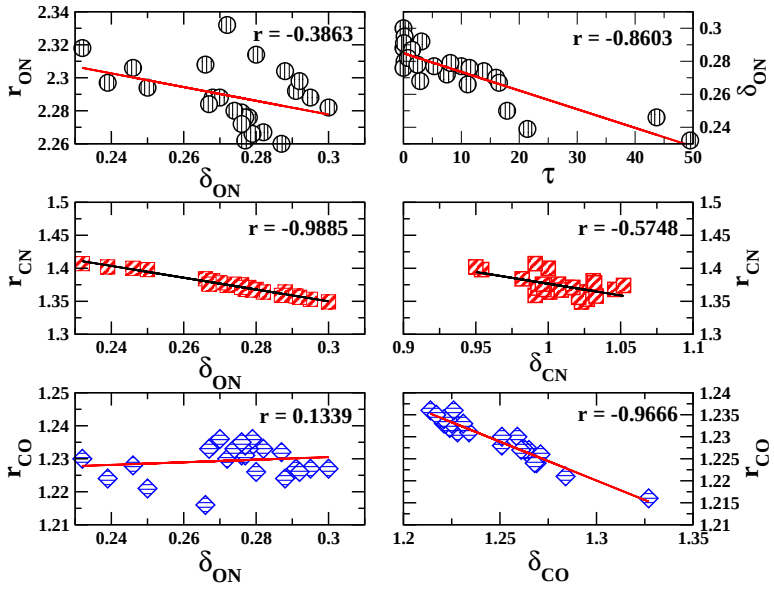

Figure 2.8: Relation between delocalization indexes and geometrical parameters in amides.

transition state and the ground state configuration. However, the use of indexes such as δ_{ON} to characterize electron delocalization has the appeal of being a well defined quantum mechanical quantity, being in principle less dependent on the choice of molecular orbitals, and not relying upon an arbitrary partitioning of the electron density.

2.3.3 Relation between delocalization indexes and geometrical parameters

The relation between delocalization indexes and selected inter-atomic distances (r_{ON}, r_{CN} and r_{CO}) was also investigated. For the relaxed amide structures, the following trends are found (see Figure 2.8): *i) there is a linear relationship between δ_{ON} and r_{CN}, but the correlation of δ_{ON} with r_{CO} and r_{ON} is less clear. ii) r_{CO} correlates well with δ_{CO} and iii) poor correlation between δ_{CN} and r_{CN}.*

At the transition states (see Figure 2.9), there are changes in these trends: *i) no clear correlation between δ_{ON} and any of the r_{ON}, r_{CN} or r_{CO} distances ii) clear inverse relations between δ_{CO} and r_{CO}, and between δ_{CN} and r_{CN}.*

These results suggest that in amides the r_{CN} bond distance is most sensitive to the degree of delocalization between nitrogen and oxygen, and differences in this distance can efficiently monitor changes in resonance along the N-C-O skeleton. This result supports the use of the r_{CN} geometrical

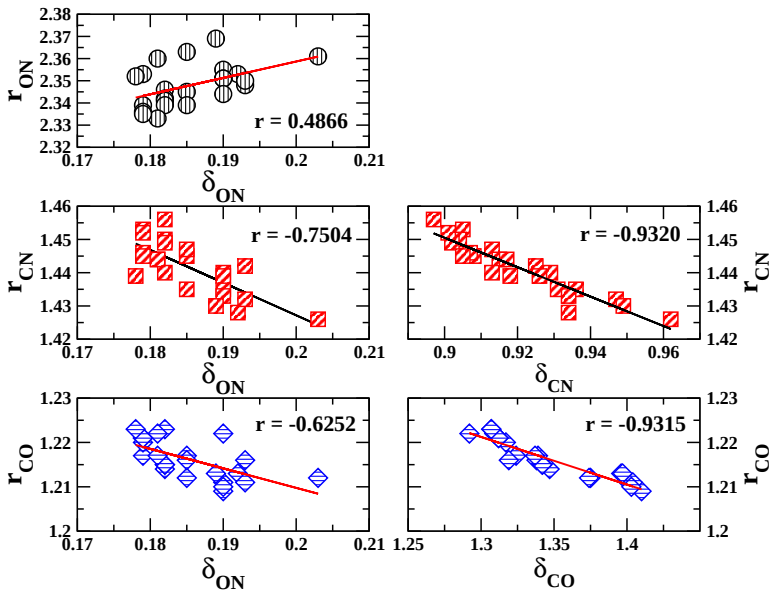

Figure 2.9: Relation between delocalization indexes and geometrical parameters at the transition states.

parameter to provide a quantitative estimate of the degree of electron resonance in amides as suggested by Brown *et al.*.[170] Furthermore, Laidig and Cameron[150] pointed out that the predominant change upon pyramidalization of N is the weakening of the C-N interaction. On the contrary, we find that C-O bond distances are quite insensitive to the degree of δ_{NO} delocalization, which could explain why there is little change in this distance upon C-N bond rotation. Interestingly, at the transition state structures, in which the possibility of π-type resonance is disrupted, both C-N and C-O bonds are linearly correlated to their own inter-atomic delocalization indexes (δ_{CN} and δ_{CO}, respectively).

Regarding the torsional angle, τ, the best correlation is obtained to the delocalization index δ_{ON}. However, this is significantly poorer than the one obtained between δ_{ON} and r_{CN} and therefore, it seems that τ is a less efficient geometrical parameter for the characterization of electron resonance.

2.4 Conclusions

Electron resonance is an important concept to rationalize the special geometrical and energetic features of amides. However, there is no unique way to measure the degree of electron resonance or delocalization in a given chemical structure. In the present chapter, we have shown how electron resonance in amides can be characterized in terms of quantities derived from the two-

electron density matrix and integration over atomic basins derived from the zero-flux surface condition. The physical interpretation of pair densities as simultaneous probability densities of finding electrons at two points in space allows for a direct connection of these quantities with chemical concepts such as resonance or aromaticity. In particular, we have demonstrated that the delocalization index between nitrogen and oxygen (δ_{ON}) is a reliable tool to analyze the electron delocalization through the N-C-O skeleton in amides. Our results suggest a linear relationship between this delocalization index and the rigidity of the amide bond, inferred through the values of its rotational barriers. The proposed index to characterize resonance in amides is superior to other correlations based on geometrical parameters such as the torsional angle τ. In addition, the use of this index gives a picture for the electron resonance in amides very close to the traditional resonance model, and could overcome the discrepancies found between these models and previous applications of Bader's type analysis.

Chapter 3

Theoretical evaluation of pK_a for Twisted Amides

Abstract

We present an ab-initio study of the pK_a of a series of twisted amides in aqueous solution. The shift of the pK_a with respect to the known value for trimethyl amine (TMA) is used in the evaluation. Calculations were made with DFT using the B3PW91 functional. Aqueous solvent effect is introduced by use of the Polarizable Continuum Model (PCM). The protocol is tested on a series of tertiary amines and twisted amides and a good agreement with the available experimental data is found. Finally, mechanistic implications of the change in basicity of the nitrogen as a function of the twist of the amide bond for the activation of C-N bond hydrolysis are discussed.

3.1 Introduction

In the previous chapter, the resonance model for the explanation of amide bond stability was validated using δ_{AB} delocalization indexes. We found that the high rotational free energy barriers in amides were related with the degree of electron delocalization in amides shown by the δ_{ON} index. Now, we start determining the consequences that the twist of the amide bond has on other properties of the amide molecule.

Structural distortion of the amide unit from the lowest energy planar configuration has been shown to alter not only the reactivity involving nucleophilic attack/hydrolysis[2,53–57] but also to induce important changes in the basicity of the amide group.[2,17,55,77] Planar amides have very low pK_a values (for instance, the pK_a of formamide is 0.12[171]) with a preference for the O-protonated tautomer.[172] However, higher pK_a's have been found for twisted amides. Moreover, the nature of the protonation in twisted amides is different from that of their undistorted counterparts. An accurate knowledge of the pK_a of twisted amides is thus of importance for an understanding of the differential reactivity of distorted versus undistorted compounds. Unfortunately, experimental determination of these pK_a's is not always feasible; e.g., Kirby *et al.*[56,57] were not able to determine the pK_a of compound **1** (see Figure 3.1) due to its fast hydrolysis in water. In other cases, the pK_a has been inferred indirectly from the hydrolytic profile as a function of the pH.[55] Consequently, quantum-mechanical calculations are needed to complement and confirm the available experimental data. Gas-phase acidity/basicity can be calculated quite accurately provided that extended basis sets are used and electron correlation effects are taken into account. In this regard, Density Functional Theory (DFT) is a good compromise between efficiency and accuracy. However, the gas phase results must be corrected for the effect of aqueous solvation, which is large for ionic systems. Solvation effects can be introduced by a variety of approaches.[136] Computationally, the most efficient is the use of dielectric continuum models.[134,135] These models properly account for long-range bulk solvent effects,[173] although they fail to include short-range effects, such as hydrogen bonding, which can be important for determining accurate pK_a values.[173] One possibility is to consider a few water molecules explicitly in the first solvation shell,[174,175] and to then treat the rest of the solvent by a continuum model. A useful alternative[176] is to calculate the pK_a's with respect to a closely related compound for which the experimental pK_a is known. The calculation of the pK_a is thus reduced to the evaluation of a change in the free energy for a balanced chemical reaction which conserves the number of charged species. This leads to a cancellation of errors when evaluating the solvation contribution to the pK_a. It also avoids the need to introduce the solvation free energy of the proton, which is still somewhat uncertain.[173] We use this latter approach in the present study to evaluate the pK_a's of a series of distorted amides (com-

pounds **1**, **2a-c**) and **3a-b** (presented in Figure 3.1) relative to the known pK_a of trimethyl amine (TMA); we first determine the most stable protonated tautomer and then, using the energy for that tautomer, we estimate the pK_a for the molecule.

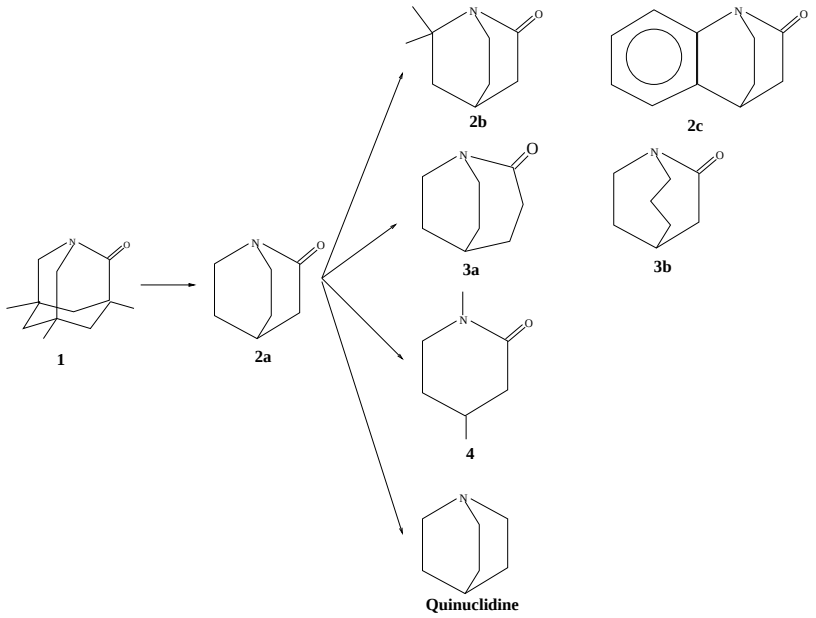

Figure 3.1: Scheme showing the twisted amides considered in this chapter. Compound **1** have been synthesized by Kirby *et al.*,[56,57] compound **2a** is a simplified version of compound **1**, which we will used as a model of twisted amide in the hydrolysis reactions. Compounds **2b** and **2c** are derivatives of **2a** which conserve the degree of twist of the amide bond. Compounds **3a** and **3b** are generated from elongations of the aliphatic chain in the cage of **2a** and leads to a partial release of the twist of the amide bond. Compound **4** is the δ-lactam planar analogue of **2a**, and finally quinuclidine is a tertiary amine structurally related to **2a**.

3.2 Methodology

3.2.1 Ab-initio Calculations

All the structures were optimized in the gas phase at B3PW91/6-31+G(d,p) level of theory[118,120,160,161,177,178] using GAUSSIAN98.[159] To confirm that the optimized structures were minima on the potential energy surfaces, frequency calculations were done at B3PW91/6-31+G(d,p) level. The frequencies were then used to evaluate the zero-point vibrational energy (ZPVE) and the thermal (T=298 K) vibrational corrections to the enthalpy and Gibbs free energy[130] in the harmonic oscillator approximation. These calculations were also made with GAUSSIAN98.[159] To calculate the entropy, the different contributions to the partition function were evaluated using the

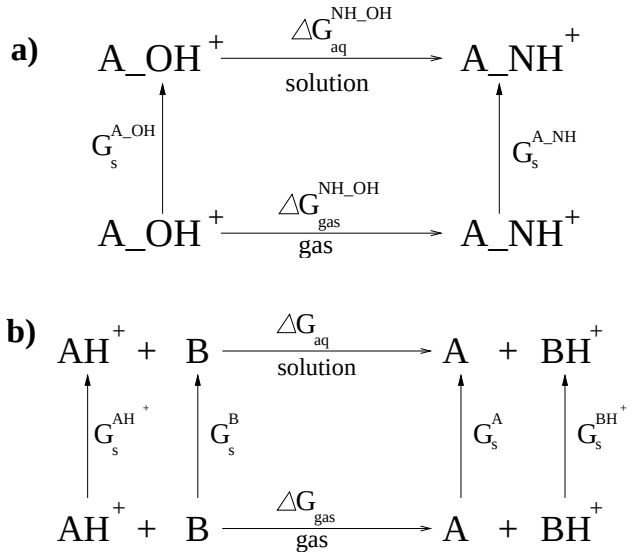

Figure 3.2: Scheme showing the thermodynamic cycles used to evaluate the free energy difference in solution between N- and O- protonated tautomers in amides (top diagram), and the relative proton affinity with respect to trimethyl amine (bottom diagram, compound B refers to trimethyl amine).

standard expressions for an ideal gas in the canonical ensemble and the harmonic oscillator and rigid rotor approximation.[179] The electronic energy was refined by single-point energy calculations with a higher basis set, namely B3PW91/6-311++G(3df,2p). The final gas-phase enthalpy and free energy is obtained from the B3PW91/6-311++G(3df,2p) electronic energy and the enthalpic and entropic corrections evaluated at B3PW91/6-31+G(d,p).

Other functionals, such as B3LYP, were also tried for the gas-phase calculations. However, B3LYP showed a slightly poorer agreement with experimental pK_a's (the mean absolute deviation was 0.6 pK_a units) than B3PW91 (mean absolute deviation of 0.4). Therefore, we decided to use the B3PW91 functional, and only those results are presented.

3.2.2 Solvent Contributions

Solvation free energies at the gas phase B3PW91/6-31+G(d,p) geometries were estimated with the Polarizable Continuum Model (PCM)[139,180–182] approach, using the HF/6-31G* wave function for the solute. We used the United Atom Hartree-Fock (UAHF)[139] set of atomic radii to define the cavity. These radii have been optimized with the HF/6-31G* wavefunction to give accurate solvation free energies of a dataset of anionic/cationic and neutral organic and inorganic molecules. To obtain the relative energy of two tautomers in solution, the contributions of solvation are added to the corre-

sponding gas-phase relative energies calculated according to Section 3.2.1. The thermodynamic cycle of Figure 3.2 is employed to evaluate the relative free energies in aqueous solvent (ΔG_{aq}) between the O- and N-protonated tautomers (designed as OH and NH):

$$\Delta G_{aq}^{NH-OH} = \Delta G_{gas}^{NH-OH} - G_s^{A\_OH} + G_s^{A\_NH} \tag{3.1}$$

Here ΔG_{aq}^{NH-OH} is the free energy difference in aqueous solution between the N- and O-protonated tautomers, ΔG_{gas}^{NH-OH} is the relative free energy in the gas-phase and is obtained by the methods described in Section 3.2.1 and G_s^i is the solvation free energy for the ith molecule and is calculated with the HF(PCM)/6-31G* approach.

3.2.3 Evaluation of pK$_a$values

We have estimated the pK$_a$ of twisted amides **1**, **2a-c** and **3a,b** by means of quantum mechanical calculations. Considerable cancellation of errors is expected if, instead of evaluating absolute pK_a, relative pK$_a$'s are evaluated. This requires the choice of a similar reference molecule for which the experimental pK_a is known. Using a thermodynamic cycle with the reference molecule (Figure 3.2b) avoids the need to deal with the proton solvation free energy.[173] Also, it is important that the number of charged species is conserved on both sides of the chemical equation for which the free energy difference is calculated. One can expect that inaccuracies of the continuum models for describing the strong hydrogen bonds of the first solvation shell around ions will cancel approximately providing the charged species have similar first solvation shells. This protocol has been previously used to evaluate pK$_a$'s for phosphoranes,[176] and obtained results that are nearly coincident with experimental estimates and density functional based ab initio molecular dynamics calculations.[183] In the present work, we follow this approximation and use trimethyl amine (TMA) as the reference molecule. This molecule is a tertiary amine, with a pyramidal nitrogen that accepts the proton, as is the case for the twisted amides **1**, **2a-c** and **3a,b**. The experimental pK_a of TMA has been measured[184](pK$_a$ = 9.8), and there is a single protonation site. In addition, very good agreement with the experiments is obtained for the solvation free energies of charged and neutral amines using the PCM model with the UAHF set of radii.[139] For instance, the experimental solvation free energy of trimethyl amine is -3.2 kcal/mol and it is -59 kcal/mol for the protonated species. These values are well reproduced with the HF(PCM)/6-31G* method,[139] which gives -2.8 and -58.9 kcal/mol, respectively. Therefore our choice of reference system and method is justified.

We evaluated the free energy change corresponding to the reaction:

$$AmideNH^+ + (CH_3)_3N \overset{\Delta G}{\leftrightarrow} AmideN + (CH_3)_3NH^+ \tag{3.2}$$

where ΔG for the reaction is evaluated according to the methods described in Section 3.2.1 and 3.2.2, and the thermodynamic cycle of Figure 3.2b; i.e., ΔG_{aq} is given by:

$$\Delta G_{aq} = \Delta G_{gas} - G_s^{AH^+} - G_s^B + G_s^{BH^+} + G_s^A \tag{3.3}$$

where A and B are the amide of interest and $(CH_3)_3N$, respectively. The gas-phase free energy is evaluated according to the methods described in Section 3.2.1, and G_s^i, the solvation free energy of compound i, it is estimated with the PCM model, as described in Section 3.2.2. The pK$_a$ of the amide group being studied (i.e. **1**, **2a-c**, **3a,b**) is determined from the calculated ΔG_{aq} values for the above equilibria and the experimental pK$_a$ of TMA, according to:

$$pK_a = \frac{\Delta G_{aq}}{ln10\, RT} + pK_a^{\mathrm{TMA}}(Exp) \tag{3.4}$$

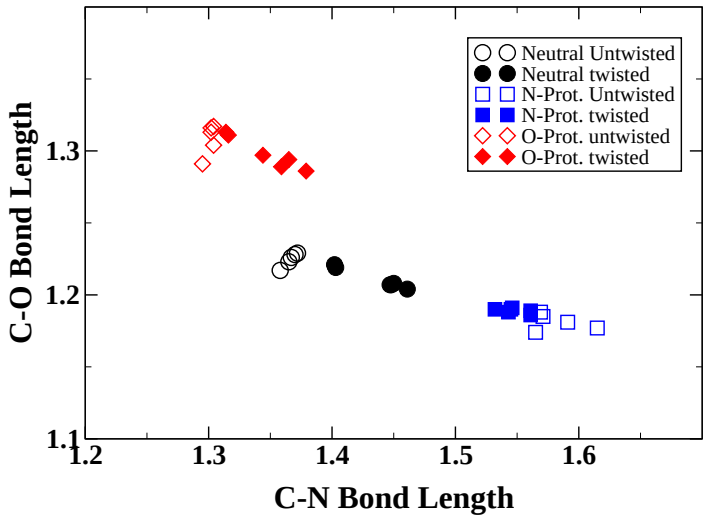

Figure 3.3: C-N versus C-O bond lengths in Å, for twisted and untwisted amides in the neutral (circles), and the two protonated states: N-protonated (squares) and O-protonated (diamonds). The bond lengths are in Å and are calculated using the B3PW91/6-31+G(d) level of theory.

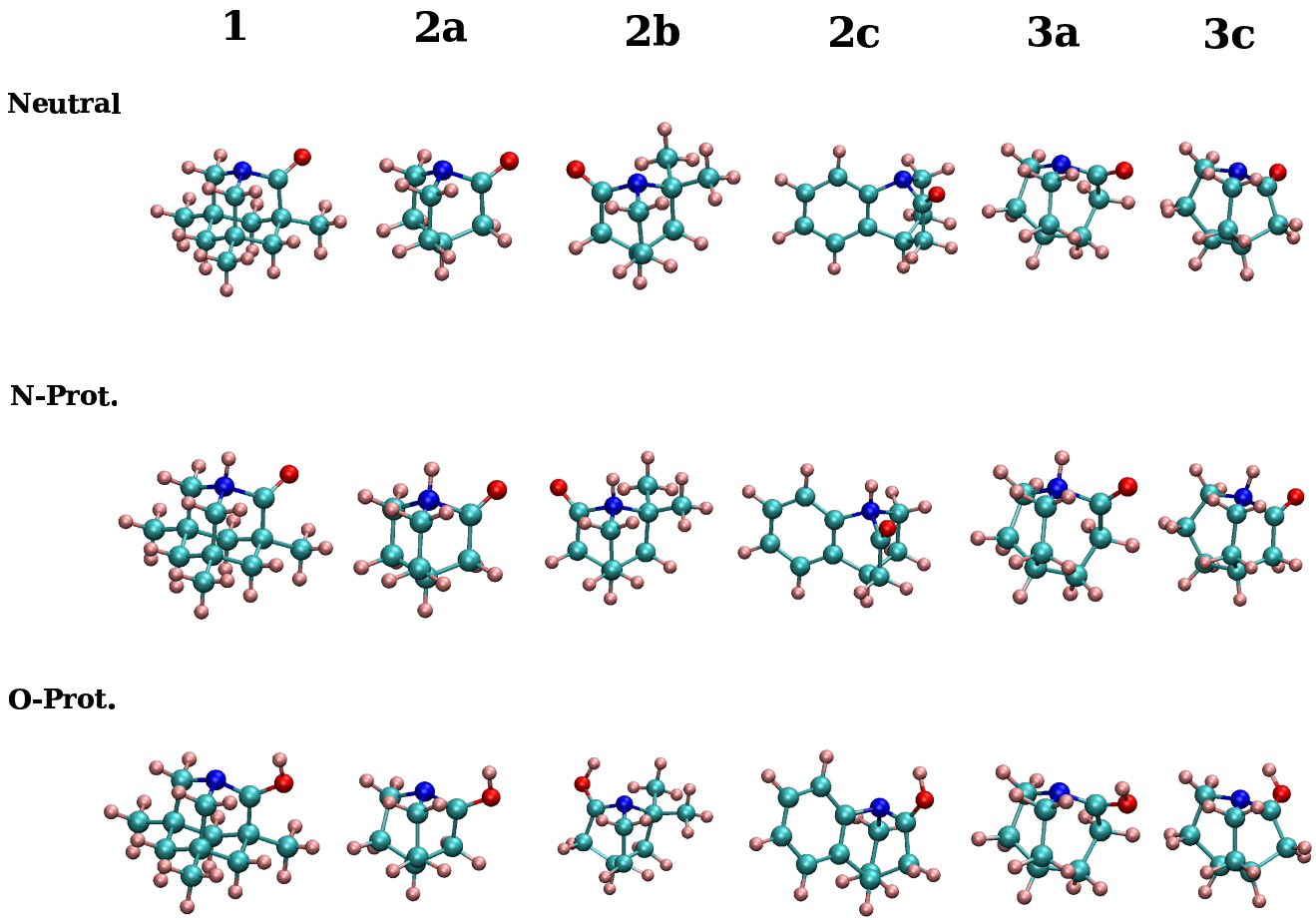

Figure 3.4: B3PW91/6-31+G(d) structures for the twisted amides in three protonation states: Neutral, N-protonated and O-protonated

Table 3.1: B3PW91/6-31+G* geometrical parameters for the undistorted planar and twisted amides for the three different protonation states: neutral, N-protonated and O-protonated. Distances are in Å and angles in degrees.

Undistorted Amides										**Twisted Amides**									
	Bond Distances				Angles			Improper Dh.			Bond Distances				Angles			Improper Dh.	
Molecule	C_1N	C_1O	OH	NH	τ	χ_C	χ_N	N	C_1	Molecule	C_1N	C_1O	OH	NH	τ	χ_C	χ_N	N	C_1
formamide	1.358	1.217	-	-	0.0	0.0	0.0	180.0	180.0	**1**	1.450	1.208	-	-	89.7	0.2	60.0	119.4	179.8
N-prot.	1.565	1.174	-	1.030	30.1	0.0	60.2	121.7	180.0	N-prot.	1.546	1.191	-	1.026	90.0	0.0	56.7	122.4	180.0
O-prot.	1.295	1.291	0.975	-	0.0	0.0	0.0	180.0	180.0	O-prot.	1.365	1.294	0.981	-	67.3	14.7	59.7	117.3	165.1
acetamide	1.365	1.223	-	-	0.0	0.0	0.0	180.0	180.0	**2a**	1.447	1.207	-	-	89.8	0.1	62.1	117.1	177.9
N-prot.	1.615	1.177	-	1.027	44.6	0.0	62.1	119.9	180.0	N-prot.	1.543	1.188	-	1.026	90.0	0.0	58.0	120.9	180.0
O-prot.	1.304	1.304	0.974	-	0.0	0.0	0.0	180.0	180.0	O-prot.	1.359	1.289	0.982	-	61.8	13.6	63.7	113.3	166.4
propamide	1.367	1.226	-	-	1.3	0.9	8.9	171.9	179.1	**2b**	1.448	1.207	-	-	88.5	1.9	59.7	118.6	178.1
N-prot.	1.591	1.181	-	1.027	15.8	0.4	56.0	123.1	179.5	N-prot.	1.532	1.190	-	1.026	89.7	1.5	55.6	122.3	178.5
O-prot.	1.302	1.313	0.973	-	0.0	0.0	0.0	180.0	180.0	O-prot.	1.344	1.297	0.977	-	62.0	13.4	60.3	116.9	165.6
butamide	1.372	1.229	-	-	0.0	0.0	0.0	180.0	180.0	**2c**	1.461	1.204	-	-	86.2	1.6	64.7	114.5	178.4
N-prot.	1.571	1.185	-	1.025	30.9	0.0	61.8	119.1	180.0	N-prot.	1.561	1.186	-	1.025	88.2	0.5	60.0	118.0	179.5
O-prot.	1.304	1.317	0.972	-	2.0	0.5	1.8	178.3	179.4	O-prot.	1.379	1.286	0.983	-	70.1	4.5	65.5	105.4	175.5
4	1.370	1.228	-	-	2.6	1.6	17.2	162.9	178.4	**3a**	1.402	1.221	-	-	36.0	11.5	50.9	129.4	168.4
N-prot.	1.569	1.188	-	1.027	45.8	1.0	51.5	128.0	178.8	N-prot.	1.561	1.189	-	1.026	53.1	0.2	53.2	126.3	179.8
O-prot.	1.302	1.316	0.972	-	1.3	1.0	0.5	179.5	179.0	O-prot.	1.314	1.313	0.973	-	31.0	17.8	44.5	137.0	161.3
										3b	1.403	1.219	-	-	39.9	11.2	46.0	134.4	168.8
										N-prot.	1.545	1.190	-	1.026	70.2	0.3	50.0	128.5	179.6
										O-prot.	1.316	1.311	0.973	-	33.1	16.8	40.4	139.8	163.2

3.3 Structural Results

Several untwisted and twisted amides are considered in this study. Formamide, acetamide, propamide and butamide are used as examples of untwisted amides with different numbers of C-C and C-N bonds. As twisted amides we have chosen the compounds **1**, **2a-c** and **3a-b** in Figure 3.1. Compound **1** has been synthesized by Kirby *et al.*[56,57] and showed a highly accelerated hydrolysis when dissolved in water. Compound **2a** (**TA** of Figure 1.6) is the twisted amide that we are using as a model along this work, which combines a high amide distortion and simplicity. Compounds **2b** and **2c** can be viewed as derivatives of **2a** by double methylation of a carbon vicinal to the nitrogen (**2b**), or by addition of a phenyl ring in the structure (**2c**). For compounds **2b** and **2c** experimental estimates of the pK_a's exist.[55,56] Compounds **3a-b** can also be viewed as derivatives of **2a** corresponding to different elongations of the aliphatic chain determining the cage structure, they are expected to have different twists of the amide group. These compounds along with **2a** have been characterized in the gas phase at the HF/6-31G* level of theory by Greenberg *et al.*;[17,77] they reported intermediate twisting of the amide bond. For each of these amides, we have studied the neutral, N-protonated and O-protonated species. First, we describe the structures with a particular focus on the twisting of the amide bond. Then, we consider the changes in structure that are caused by N- and O-protonation. In Section 3.4, we describe the relative stability of the N- and O-protonated tautomers in the gas phase and in solution, the latter are then used to calculate the pK_a values with equation 3.4.

Selected bond distances and angles optimized at B3PW91/6-31+G* level of theory are shown in Table 3.1 for all the compounds studied (untwisted and twisted amides), while C-N versus C-O bond lengths are shown in Figure 3.3. The out-of-plane deformations and amide bond twisting are described by the angles τ, χ_C and χ_N, following the definitions of some references.[48,162] The angle τ characterizes the mean twisting angle around the C-N bond and ranges from 0^o (planar amide group) to 90^o (when the two planes defined by the O-C_1-C_2 and C_5-N-C_6 atoms are perpendicular); χ_C and χ_N are a measure of the degree of pyramidalization at the C and N atoms, respectively. They range from approximately 0^o (planar sp^2 atoms) to 60^0 (tetrahedral sp^3 atoms). The combination of dihedrals used to define τ, and χ_C and χ_N is as follows. Defining the four torsion angles (ω_1=O-C_1-N-C_5, ω_2=C_2-C_1-N-C_6, ω_3=C_2-C_1-N-C_5, ω_4=O_1-C_1-N-C_6, for the atom numbering definition see Figure 3.5) we can write,

$$\tau = \frac{\omega_1 + \omega_2}{2} \tag{3.5}$$

$$\chi_C = \omega_1 - \omega_3 + \pi(mod2\pi) = -\omega_2 + \omega_4 + \pi(mod2\pi) \tag{3.6}$$

$$\chi_N = \omega_2 - \omega_3 + \pi(mod2\pi) = -\omega_1 + \omega_4 + \pi(mod2\pi) \tag{3.7}$$

The absolute values of these angles with projection on the 0^o-90^o quadrant are shown in Tables 3.1; the improper dihedrals for C and N defined as O-C_1-N-C_2 and C_1-N-C_5-C_6 dihedral angles, respectively, are also reported.

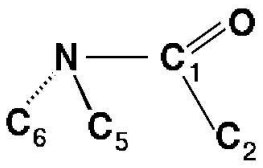

Figure 3.5: Numbering of atoms used for the definition of τ, χ_C and χ_N.

3.3.1 Neutral Amides

The values of τ, χ_C and χ_N are very low for neutral untwisted amides, indicating that both the nitrogen and the carbonyl carbon show a planar configuration. Formamide, acetamide and butanamide show values of τ, χ_C and χ_N of 0.0^o, whereas propanamide show only slight deviations, namely, a value of 1.3^o for τ, 0.9^o for χ_C, and 8.9^o for χ_N. The situation is very different for the twisted amides **1** and **2a-c**. The geometrical constraints imposed by the "cage" structure of these compounds leads to calculated τ values between 85^o and 90^o. The crystallographic structure[56] of **1** has τ of 90.5^o. An intermediate twist is observed for compounds **3a-b**, with values for τ of 36^o(**3a**) and 40^o (**3b**). There is a general agreement with the results of Greenberg *et al.*[77] for these compounds, although the theoretical level used by them is different (they used HF/6-31G*). They reported values of τ of 39.2^o and 44.0^o for **3a** and **3b**, and a value of 90.0^o for **2a**. These twisted structures have planar carbonyl carbon (χ_C is 0^o), but the planarity at nitrogen is lost (e.g., χ_N is 61.8^o for **2a**), in accord with the breakdown of the $n_N \rightarrow \pi^*_{CO}$ resonance. Interestingly, structures **3a** and **3b** show slight deviations from planarity for the carbonyl carbon with χ_C values around 11^o.

As expected, the twist about the C-N bond has a substantial effect on its length. Amides **1** and **2a-c** show the longest C-N bonds among the neutral amides, between 1.450 Å for **1** and 1.461 Å for **2c**. These bond lengths are almost 0.1 Å longer than any of the C-N bonds in the undistorted planar amides (Table 3.1). Correspondingly, the C-O bond lengths shorten, although the differences are not as dramatic; they are on the order of 0.02 Å. For instance, the C-N bond length in **2a** is 1.453 Å and the C-O bond length is 1.209 Å, whereas in butamide the values are 1.372 Å and 1.229 Å, respectively. Amides **3a** and **3b** with intermediate twisting have C-N and C-O bond lengths between those of planar amides and twisted amides; the

C-N bond length for **3a** is 1.408 Å and the C-O bond length is 1.222 Å. The calculated values for the C-N and C-O bond lengths compare well with the available crystallographic data; e.g., in the case of **1** we obtain 1.450 Å and 1.208 Å for the C-N and C-O bond lengths, respectively, while the experimental values are 1.475 Å and 1.196 Å. The present results are also in general agreement with those of Greenberg *et al.*,[77] although we get somewhat longer bond lengths in general, as expected when electron correlation is introduced. Overall, the results indicate that the C-N bond is more sensitive to the twist of the amide group than is the C-O bond. The same trend was observed when analyzing the rotation barrier in formamide and derivatives.[12,13,49–52] This fact has been used to challenge the traditional amide $n_N \rightarrow \pi^*_{CO}$ resonance model.[52] However, the data can be reconciled with the $n_N \rightarrow \pi^*_{CO}$ resonance model if one takes into account the strong polarization of the C=O bond and its ionic bond character.[52] In fact, Glendenning *et al.*[14] have reexamined the role of the resonance interactions in formamide by using the Natural Population Analysis[185] and Natural Resonance Theory (NRT).[186] They found that the NRT representation of planar amides consist primarily of two resonant structures, one with a formal double C=O bond and a single C-N one (contributing by 60-65%) and another resonant structure with a formal C=N double bond and a single C-O one (contributing by 28-30%). This situation corresponds to the traditional $n_N \rightarrow \pi^*_{CO}$ resonance model. The suitability of the resonance model was extensively analyzed in the previous chapter.

3.3.2 Structural effects of N- and O-protonation

The effect of N- and O-protonation on the amide structure for both twisted and untwisted amides is quite important, and follows opposite trends. As shown by Greenberg *et al.*[17,77] O-protonation lengthens the C-O bond and shortens the C-N bond, affecting untwisted and twisted amides in a similar way. If we look at the diagram of Figure 3.3, O-protonated amides are in the top-left corner, where the longest C-O bonds and the shortest C-N ones occur, in agreement with the results of Greenberg *et al.*

On the other hand, N-protonation has the opposite effect, it elongates the C-N bond and shortens the C-O bond, since the proton binds to the unique lone pair of the nitrogen and prevent the $n_N \rightarrow \pi^*_{CO}$ resonance. The τ and χ_N angles reflect this change in resonance, and in the case of planar amides, χ_N goes from values close to 0^o to around 60^o upon N-protonation. There is also a significant elongation of the C-N bond for twisted amides[77] for compounds **2a**, **3a** and **3b**. The C-N bond in N-protonated amides is the most "activated" bond (its length ranges from 1.55 to 1.62 Å); they lay at the right-bottom corner of the diagram in Figure 3.3.

As shown in Figure 3.3, there is an strong anticorrelation between the C-N and C-O bond lengths as a function of twisting in the amide bond.

Table 3.2: N- versus O-protonation. The relative free energy (ΔG_{NH-OH}) of the N-protonated species versus the O-protonated one in kcal/mol in the gas phase and in solution.

Species	Gas Phase	Solution
Untwisted Planar Amides		
formamide	18.8	13.4
acetamide	16.7	13.7
propamide	15.5	11.8
butamide	14.3	12.5
4	16.2	14.0
Twisted Pyramidal Amides		
1	-19.4	-22.0
2a	-19.7	-21.0
2b	-21.4	-21.7
2c	-18.6	-20.0
3a	-4.8	-5.9
3b	-6.0	-7.0
3c	-4.1	-5.7

The longer the C-N bond, the shorter is the C-O bond when strong $n_N \rightarrow \pi^*_{CO}$ resonance exists, as in neutral and O-protonated untwisted amides. However, in N-protonated species, there is no such effect because of the absence of the $n_N \rightarrow \pi^*_{CO}$ resonance after protonation. Finally, protonation has an strong effect on the amide bond structure. Whereas protonation at O tends to strengthen the C-N amide bond, protonation at nitrogen leads to a big activation of the C-N bond. To determine whether O- or N-protonation will be more likely, the relative stability of each of the tautomers should be analyzed. This is done in the following section.

3.4 Free energy Results and pK$_a$ values

3.4.1 Relative stability of N- versus O-protonation in the gas phase and in solution

The relative stabilities of the N- versus O-protonated tautomers are listed in Table 3.2. Values calculated in the gas phase and in solution are shown. For all planar amides the ΔG^{NH-OH}_{aq} defined in Eq. 3.1 is positive indicating that O-protonated tautomers are more stable than N-protonated tautomers. The ΔG^{NH-OH}_{gas} values ranges from 14 to 18 kcal/mol . This preference for O-protonated tautomers confirms earlier ab-initio studies.[187] It appears unlikely that higher levels of theory would change this qualitative behavior. Solvent has only a small effect in the relative affinities for the proton between

Table 3.3: Estimated values of pK_a's for tertiary amines and twisted amides.

molecule	ΔG_{gas}	ΔG_{solv}	pK_a (theor.)	pK_a (exp.)
	Tertiary Amines			
triethylamine	8.3	0.7	10.3	11.0
tripropylamine	10.5	0.8	10.4	10.7
triallylamine	7.7	-2.0	8.3	8.3
dimethylcyclohexylamine	8.2	0.9	10.5	10.7
dimethylbenzylamine	4.8	-1.0	9.0	9.0
diethylbenzylamine	7.1	-1.3	8.8	9.5
Quinuclidine	8.8	2.2	11.4	11.0
	Twisted Amides			
1	6.3	-4.2	6.7	-
2a	2.5	-4.5	6.5	-
2b	5.9	-5.5	5.8	5.3
2c	1.0	-9.4	2.9	3.7
3a	-4.0	-12.2	0.8	-
3b	-3.0	-10.7	1.9	-

nitrogen and oxygen in these systems, i.e., the ΔG_{aq}^{NH-OH} are in the range from 11 to 14 kcal/mol, indicating that the preference for O-tautomers is preserved in solution.

Twisted amides show a preference for N-protonation, as already pointed by Greenberg *et al.*,[77] and there is a correlation between the degree of twist and N-tautomer stabilization. Amides **1** and **2a-c** with near 90^o twist have ΔG^{NH-OH} ranging from -18.6 to -21.4 kcal/mol in the gas phase, and from -20.0 kcal/mol to -22.0 kcal/mol in solution. Again, the solvent has only a small effect on the relative stabilities of the tautomers. Consistently with this, the ΔG^{NH-OH} values for amides **3a** and **3b** are between those for planar amides and **2a-c** amides but they do show a preference for N-protonations; it is -5.9 kcal/mol for **3a** and -7.0 kcal/mol for **3b**.

In summary, O-protonation is favored for planar amides, whereas N-protonation is preferred for the twisted amides **2a-c** and **3a,b**.

3.4.2 pK_a Values

Planar amides show a sufficiently low pK_a that ensure they remain unprotonated at a wide range of pH. However, twisted amides can have very different pK_a values. Based on the hydrolytic profile as a function of pH, Wang *et al.*[55] estimated a value of 3.7 for the pK_a of **2c**. In addition, they gave values of -0.3 and 0.5 for compounds analogous to **3a** and **3b**, but with an additional phenyl ring as in **2c**. Also, Pracejus has measured an apparent pK_a of 5.3 for amide **2b**.[188]

The theoretical pK_a's were obtained for the molecules and the model

systems according to the protocol described in Section 3.2.3. To validate the method, a series of tertiary amines with known experimental pK_a were studied. The theoretical and experimental values are compared in Table 3.3 and Figure 3.6 for this series of amines and for compounds **2b** and **2c**. In the case of tertiary amines, we obtain pK_a values that are within 0.7 units of the experimental mark; the mean absolute error is 0.3 pK_a units. Particularly encouraging is the result obtained for quinuclidine (see Figure 3.1), an amine with an cage structure analogous to that of amides **1** and **2a-c**. For quinuclidine, we obtain a pK_a value of 11.4, in very close agreement with the experimental (pK_a = 11.0) value. Good agreement is also obtained for the twisted amides **2b** and **2c**. The experimental estimates for the pK_a of **2b** and **2c** are 5.3 and 3.7, respectively, which compare well with the calculated 5.8 and 2.9 values. However, it should be noted that these experimental values are only estimates, as described in the Introduction of this chapter. For the rest of twisted amides the values are 6.7 (**1**), 6.5 (**2a**), 0.8 (**3a**) and 1.9 (**3b**).

The calculated values indicate interesting qualitative trends. First, the calculations show a tendency of twisted amides to have higher pK_a's than untwisted amides. The fully distorted amides (τ close to 90^o) **1** and **2a-b** show values between 5.8-6.7, whereas undistorted amides such as formamide show values between 1-3, although one has to take into account the protonation state of reference in untwisted amides is the O-protonated tautomer. Following this trend, amides with intermediate twisting, **3a** and **3b** have lower pK_a values, 0.8 and 2.0 respectively. The values for gas-phase and solution free energy differences for equilibrium Eq. 3.2 can be found in Table 3.3. These free energy differences measure the relative proton affinity of each species with respect to TMA. In the gas phase, the numbers are positive for the fully twisted amides **1** and **2a-c**, and negative for the intermediate twisted amides **3a,b**. After solvent corrections have been included all numbers are negative, indicating the larger proton affinity of TMA in solution with respect to any of these amides. However, in terms of relative proton affinities between twisted and partially twisted amides the results are similar in the gas phase and in solution. In both cases, partially twisted amides show lower proton affinities than fully twisted amides. The origin of this shift in proton affinities can be easily explained in terms of the $n_N \rightarrow \pi^*_{CO}$ resonance model. Amides with a high degree of bond twist do not show the $n_N \rightarrow \pi^*_{CO}$ stabilization effect for the neutral state, and therefore, they have larger proton affinities in the gas phase, and larger pK_a's in solution than partially twisted amides for which there is a certain degree of $n_N \rightarrow \pi^*_{CO}$ resonance.

Another remarkable trend observed is the important effect that a phenyl group has in the calculated pK_a's. In going from **2a** to **2c**, a significant lowering in the pK_a is observed, from 6.5 to 2.9. This effect is confirmed when comparing the results obtained for amides **3a,b** (0.8 and 1.9, respectively)

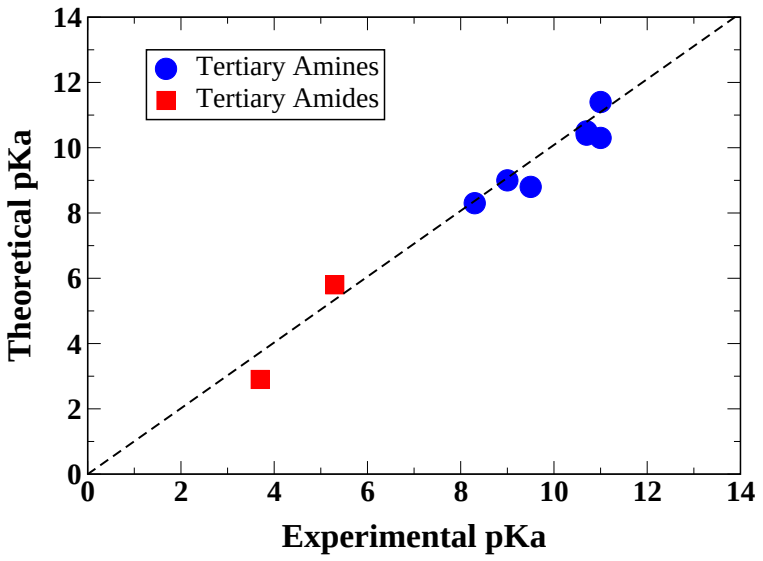

Figure 3.6: Experimental versus theoretical pK_a. Data taken from Table 3.3.

with the estimates inferred by Brown *et al.*[2,55] for analogous compounds but with a phenyl group attached to them. Based on the hydrolytic profile as a function of pH, their estimate of the pK_a for **3a,b-Phe** were -0.3 and 0.6 respectively. Thus, their numbers are lower by 1-1.5 units than the calculated pK_a values of **3a,b**, consistent with the effect expected from phenyl substitution when comparing **2a** and **2c**.

Finally, we compare the results between twisted amides and amines of similar size. For instance, if we compare the pK_a for quinuclidine and amide **2a**, we observe that the pK_a of quinuclidine is between 4.5-5 units larger than that of **2a**. If we compare the free energies for the following equilibrium:

$$\mathbf{2a} - H^+ + Quinu. \overset{\Delta G}{\leftrightarrow} \mathbf{2a} + Quinu. - H^+ \tag{3.8}$$

we obtain values of -6.3 kcal/mol and -6.7 kcal/mol in gas phase and in solution, respectively. This indicates that the lower proton affinity of these twisted amides compared to structurally related amine compounds has only a small solvent effect, and that the carbonyl group is destabilizing the N-position for protonation.

3.5 Concluding Remarks

Density Functional Theory was used in combination with dielectric continuum methods to estimate the pK_a's for a series of twisted amides. To avoid the inherent difficulties in calculating absolute pK_a's, we have employed a protocol based on the calculus of a relative pK_a. Trimethyl amine was taken as the reference molecule and the relative pK_a's for a series of tertiary amines and twisted amides were evaluated. Good agreement was found between theory and experiment for the systems for which experimental data exist. Our calculations confirmed that twisted amides have higher pK_a's in solution than untwisted amides, and that the preferential protonation site is at the nitrogen in twisted amides. In addition, we estimated the pK_a for highly twisted amides for which experimental data are not available, due to their fast hydrolysis which makes experimental measurements very challenging. They showed the highest pK_a values (between 6 and 7) in the series.

The calculations have shown that in neutral or slightly acidic media there is a high probability for twisted amides to be found at their N-protonated state. This is expected to have implications for the hydrolysis mechanism of twisted amide compared to undistorted amides. In fact, Brown *et al.*[2,55] observed that the degree of rate acceleration of twisted amides is pH dependent; i.e., compound **2c** showed an increase in rate by a factor of 10^7 under basic conditions, with respect to untwisted analogues, while the rate acceleration was up to a factor of 10^{11} under acid-catalyzed conditions. This suggests that a different mechanism is involved in the latter. The additional factor leading to extra activation of the C-N bond under acidic media could be the differential protonation of twisted amides with respect to untwisted ones. In the case of undistorted amides, the protonated species are not very likely at a wide range of pH, since these amides have small pK_a values. Moreover, at low pH, when protonated, the O-protonated tautomer is preferred, which strengthens the C-N bond. However, as established by the gas-phase calculations of Greenberg *et al.*[17,77] and by our results in solution, twisted amides have a very different protonation scheme, with preference for the N-protonated tautomer, which leads to a weakening of the C-N bond. This along with the high pK_a values between 5-7 for certain twisted amides (compounds **1**, **2a** and **2b**) can lead to substantial populations of N-protonated amides at only slightly acidic media, with the resulting activated states of the C-N bond. In this regard, recall that **1** has one of the highest pK_a's of the series investigated in the present chapter and as reported by Kirby *et al.*[56,57] hydrolyzes extremely fast. The mechanistic consequences of such protonation would be significant and for a full understanding of the mechanism further theoretical characterization of the resultant transition states and intermediates will be necessary. This will be covered in the Part II of this thesis.

Part II

Hydrolysis Reactions

Introduction

In this second part of the thesis, the hydrolysis reaction will be compared for a model of a highly twisted amide (TA of Figure 3.7) and its undistorted amide analogue (PA of Figure 3.7) along the entire pH range. As described in Part I, amide bond twist causes a breakdown of the $n_N \rightarrow \pi^*_{CO}$ resonance, leading to pyramidalization of the nitrogen and elongation and weakening of the C-N bond. Therefore, amide bond is activated and desestabilized, and it is expected that this will accelerate the otherwise slow hydrolysis reaction of undistorted amide. Our goal is to characterize this acceleration, and in addition, to determine how the breakdown of resonance affects the hydrolysis mechanism itself. There is a number of theoretical studies focusing on the structural properties and gas-phase proton affinities of twisted amides,[17,77] but these contain no characterization of reactivity. In the present study, we do an analysis of the reactivity by comparing the activation barrier for the hydrolysis reaction of the highly twisted amide **TA** with the hydrolysis reaction of the analogous planar amide **PA** (both reactants are presented in Figure 3.7). One of the goals is to determine how much of the calculated rate acceleration is due to an intrinsic electronic effect (i.e., breakdown of the $n_N \rightarrow \pi^*_{CO}$ resonance). Also, how sensitive is this acceleration to the presence of auxiliary water molecules that can catalyze the reactions serving as proton bridges. Finally, how this rate acceleration and reaction mechanism depend on the different pH media (alkaline, neutral and acid) will also be investigated. The study is divided in three chapters. In Chapter 4, the alkaline reaction is studied, i.e., the nucleophile is an hydroxide anion. Chapter 5 comprises our studies on the neutral reaction mechanism in which the attacking nucleophile is a water molecule. Finally, Chapter 6 corresponds to the acid hydrolysis, in which the amide will be protonated previous to the attack of a water molecule. In each case, both concerted and stepwise mechanisms will be considered in the presence and absence of an auxiliary catalytic water molecule. Thus, a big variety of possible mechanism and pathways are considered with the aim of covering the most general possible picture for this reaction.

Next, we briefly introduce the characteristics of both amide reactants and the methodology followed for the calculations.

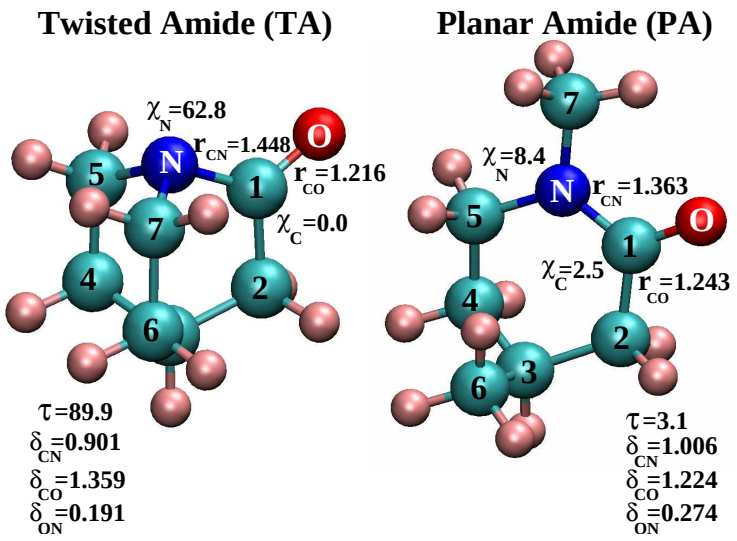

Figure 3.7: The two amide reactants considered for the hydrolysis reactions. On the left-hand side, **TA**, a highly twisted amide. On the right-hand side, **PA** an undistorted amide analogous to **TA**. The structures were optimized in solution with the SCI-PCM method. The main structure parameters and delocalization index are presented.

Geometrical and Electronic Features of the Reactants

The choice of these amide reactants was motivated by their resemblance to the reactants used by Blackburn et al.[54] (for comparison, see Figure 1.6). The TA reactant presents an amide bond with a significant degree of twist, which is enforced by the cage structure of the molecule. As it can be seen in Figure 3.7, the twist measured by the τ angle (the τ, χ_C and χ_N geometrical parameters were defined in the methodology section of Chapter 3) is 89.9^o, that is almost 100% degree of twist. Due to this twist, the carbonyl π_{C_1-O} orbital and the nitrogen's lone pair are orthogonal, and therefore, formally there is no $n_N \rightarrow \pi^*_{CO}$ resonance. The formal partial double bond character of the amide bond is therefore lost, which can be observed in the amide bond lengthening compared to untwisted amide bonds. In particular, the amide bond length in TA is 1.448 Å, almost 0.1 Å longer than the one found in formamide at the same level of theory. As expected, the twist of the amide bond does not affect the carbonyl carbon planarity, χ_C is 0.0^o, but it does affect the configuration of atoms around nitrogen, leading to a pyramidalization around this atom (χ_N is 62.8^o).

The planar amide **PA** (see Figure 3.7) is the planar analogue to the twisted amide **TA**, and it can be viewed as the species resultant from hy-

drogenation of the $C_6 - C_7$ bond of **TA**. This leads to the breaking of the cage structure, which relieves the geometrical constraints that maintained the amide bond in a twisted conformation. The **PA** amide reactant now shows a planar untwisted amide bond with a corresponding low value of τ, 3.1^o, and a nitrogen atom in a quasi-planar conformation ($\chi_N = 8.4^o$). This is the standard situation for an undistorted amide bond with substantial degree of $n_N \rightarrow \pi^*_{CO}$. In fact, the amide bond length is significantly shorter, 1.363 Å, than for the twisted amide reactant, 1.448 Å.

The differences in electronic structure between both amide reactants were confirmed by the calculation of the delocalization indexes (showed in Figure 3.7), based on the topological analysis of the second order electron density, following the methodology of Chapter 2. The δ_{AB} delocalization index is a measure of the amount of electrons shared between two atoms and the δ_{ON} value can be taken as indicative of the degree of electron delocalization in the amide bond and its resonance stabilization. The δ_{ON} value for the planar amide **PA** is 0.274, very similar to the one in butamide, 0.276. Therefore the δ_{ON} index in **PA** suggests that the amide bond in this compound is stabilized by electron resonance to a similar degree as in butamide. However, δ_{ON} in **TA** is much lower, 0.191. This value is in the range of values displayed by rotational transition states (Tables 2.3, 2.4 and 2.5) and indicates that the amide resonance stabilization is lost in this compound. Moreover, **TA** presents a lower δ_{CN} and larger δ_{CO} than **PA**, indicating a more activated amide bond for the hydrolysis reaction, and a stronger carbonyl bond. In summary, the electronic features displayed by these two amides are ideal for the purpose of this work, in the sense that the comparative study of their hydrolysis should lead to a description of the effect of the breaking the $n_N \rightarrow \pi^*_{CO}$ resonance on the reactivity of amides.

Methodology

Ab-initio studies of the alkaline, neutral and acid hydrolysis of **TA** and **PA** were carried out in gas phase and in solution. The protocol followed for gas-phase optimizations was identical in the three media, while the characterization of the potential energy surface in solution differed: in the alkaline hydrolysis reaction the geometries optimized in gas-phase were employed to carry out single-point calculations using two different solvation methods, while in neutral and acidic hydrolysis the different stationary points were optimized in solution by the SCI-PCM method. In the next section, we explain the methodology used for the characterization of all reaction pathways.

Gas-Phase

All structures were optimized at the B3LYP/6-31+G(d) level of theory. The electronic energy was further refined by by single-point calculations

at the B3LYP/6-311++G(d,p) level of theory. The use of the B3LYP functional[118,120,160,161] was motivated by its success in the evaluation of reliable reaction enthalphies for the hydrolysis of neutral amides.[66] However, it should be remarked that in some cases differences are found between B3LYP and other correlated methods such as MP2.[65] To check that the main conclusions of the chapter would not differ by applying another level of theory, single point MP2 calculations were carried out. The results showed similar qualitative trends as the ones specified throughout the chapter.

To determine the nature of each stationary point and calculate enthalpic and entropic corrections,[130] frequency calculations were performed at B3LYP/6-31+G(d) level of theory. Reactant, intermediate and product structures showed real frequencies for all the modes of vibration, whereas transition states showed one imaginary frequency along the desired normal mode. The free energy was obtained as a sum of the B3LYP/6-311++G(d,p) energy and the zero-point vibrational energy (ZPVE), the vibrational correction to the ZPVE at 298 K and the rotational and translational energies at 298 K. The zero-point vibrational energy and the thermal vibrational energy were calculated in the rigid rotor-harmonic oscillator approximation. The rotational and translational energies were treated classically as 1/2RT per degrees of freedom. The calculations were performed using the GAUSSIAN98 program.[159]

Solution-Phase

Alkaline Hydrolysis

Solvation free energies at the gas phase B3LYP/6-31+G* geometries were estimated by two methods. They are Poisson-Boltzmann calculations using the Jaguar program[189] (PB-J), and Polarizable Continuum Method (PCM) using GAUSSIAN98 suite of programs.[159] Both PB-J and PCM are self consistent reaction field (SCRF) methods. In the Poisson-Boltzmann calculations done by Jaguar, the gas phase wavefunction is calculated and from that the electrostatic potential. Then a set of atomic charges that fits this electrostatic potential is calculated and these charges are passed to the Jaguar Poisson-Boltzmann solver, which then determines the reaction field by numerical solution of the Poisson-Boltzmann equations and represents it by a layer of charges at the molecular surface (dielectric continuum boundary). These "solvent" point charges are returned to the SCF program, which performs another quantum mechanical wavefunction calculation, which incorporates the solvent charges. This process is repeated until self consistency is achieved. The Polarizable Continuum Method was previously explained in Section 1.2.5.

For both PB-J and PCM the B3LYP/6-311++G(d,p) level of theory were employed. In the case of the PB-J calculations the default atomic van

der Waals of the Jaguar program were used.[189] In the case of the PCM calculations with GAUSSIAN98 the UAHF (united atom Hartree-Fock) parameterization[139] of the polarizable continuum model was used. All these solvation calculations were done at the gas phase B3LYP/6-31+G* geometries, and we consider that this is the main limitation of this chapter. Preliminary attempts to optimize the transition states in solution using PCM models led to problems in the convergence, which are associated to discontinuities in the solvation potential.[190] However, according to the agreement between our data and experiments for the differential in barriers between the two reactions (see Discussion of the alkaline hydrolysis, Section 4.3), the lack of geometry optimization does not seem to introduce major errors when estimating the rate acceleration of a pyramidal amide with respect to the planar amide. Probably this is an indication that geometry optimization in solution will have a similar effect for both reactions, and they tend to cancel when comparing relative energy barriers.

Neutral and Acidic Hydrolysis

All structures were optimized in solution using the Self-Consistent Isodensity Polarizable Continuum Model (SCI-PCM) method[191,192] at the B3LYP/6-31+G(d) level of theory, and the same level of theory was used for the frequency calculations. The value of the electron density used to describe the cavity's size and shape into which the solute is placed was set to 0.0004 au,[193] and 146 grid points were considered for the surface charges. The different electronic and free energies in solution were calculated following the same protocol than in gas-phase, and therefore the electronic energy was refined by a single-point calculations at the B3LYP/6-311++G(d,p) level of theory (at the geometries optimized with SCI-PCM).

Units: In all the tables and figures of the following chapters and throughout the text the relative energies are given in kcal/mol, the distances in Å and the angles in degrees.

Calculation Support

The SGI/IZO–SGIker UPV/EHU (supported by the National Program for the Promotion of Human Resources within the National Plan of Scientific Research, Development and Innovation – Fondo Social Europeo and MCyT) is gratefully acknowledged for generous allocation of computational resources.

Chapter 4

Alkaline Hydrolysis

Abstract

We present an ab-initio study of the alkaline hydrolysis reaction of planar and pyramidal amides. The aim is to investigate the effect of C-N bond twisting and nitrogen pyramidalization on the rate of alkaline hydrolysis of amides. The transition states, intermediates and products for the two steps of the reaction (hydroxide attack and breaking of the C-N bond) were characterized in the gas-phase using B3LYP density functional quantum mechanical method with the 6-31+G* basis set. The energetics were then refined using the 6-311++G(d,p) basis set. The effect of the solvent was introduced by means of two methods: Poisson-Boltzmann (PB) and Polarizable Continuum Model (PCM) calculations at the gas-phase geometries; both allow for charge relaxation in solution. We found that the transition state corresponding to the second step of the reaction (TS2), breaking of the C-N bond, is the transition state of highest energy in the gas-phase and in solution. However, inclusion of an explicit water molecule significantly decreases the TS2 barrier. The $\Delta\Delta G^{TS2}$ between the twisted and planar species is about 15.0 kcal/mol in solution, favoring the hydrolysis of the former. Our estimation for the value of the $\Delta\Delta G^{TS1}$ for the first step of the reaction, hydroxide addition, ranges between 7.0-9.7 kcal/mol. There are also significant differences between the planar and twisted form in the thermodynamics of the reaction. In solution the hydrolysis of the twisted amide is exothermic by -6.8 kcal/mol, whereas the hydrolysis of the planar amide is highly endothermic, 16.0 kcal/mol. Thus, twisting of the amide bond and nitrogen pyramidalization is found to be an effective way of accelerating the otherwise slow hydrolysis of planar amides. As much as 14.7 kcal/mol of acceleration could be expected if the rate-limiting transition state is the breaking of the C-N bond from the tetrahedral intermediate, and 7.0-9.7 kcal/mol if the rate limiting step is hydroxide attack. The fact that experimental studies have demonstrated a rate enhancement of about 10.0 kcal/mol suggest that the latter step is rate-limiting in alkaline solution.

4.1 Introduction

The alkaline hydrolysis of amides follows the stepwise mechanism,[72,194–196] where the first step of the reaction involves formation of a tetrahedral intermediate and pyramidalization at the amide nitrogen. Thus, distortion of the nitrogen from its planar ground state could accelerate the rate of hydrolysis. Early kinetic work[53,54] showed that pyramidalization of the amide nitrogen by use of benzoquinuclidin-2-one, a twisted amide analogous to our model TA (see Figure 3.7), leads to alkaline hydrolysis that is 10^7 times faster than its strain-less counterpart. This correspond to a decrease in the activation energy of the reaction by about 10.0 kcal/mol. Moreover, Antonczak *et al.*[64] found that the presence of a water dimer can induce substantial pyramidalizations in neutral formamide, with the resultant activation of the amide bond.

The formamide or similar undistorted amides have been used for the study of the alkaline hydrolysis of amides both experimentally[59,194,196–201] and theoretically.[60–63,68–72,74,75,202–204] In this chapter we compare the alkaline hydrolysis of the distorted amide TA with respect to the reaction of PA in order to determine the rate acceleration due to the losing of $n_N \rightarrow \pi^*_{CO}$ resonance at this media. To do so, the amide reacts with the hydroxide ion following the stepwise mechanism where firstly a tetrahedral intermediate is formed while in the second step the cleavage of the amide bond is caused by a proton transfer to the nitrogen. As we have explained in the Methodology section (page 83) the geometry optimization were carried out in gas-phase and the effect of solvent is introduced by use of continuum models. Two different solvent models were employed: Poisson-Boltzmann calculations using the Jaguar program[189] (PB-J), and Polarizable Continuum Method (PCM) calculations using the GAUSSIAN98 suite of programs.[159] Moreover, we also analyze the catalyst effect of an auxiliary water molecule in the second part of the reaction where this water molecule may aid the proton transfer from the oxygen to the nitrogen atom.

4.2 Results

4.2.1 Non-Assisted reaction

Twisted Amide Reactant

Structures. The geometries optimized in gas-phase for the hydrolysis of the twisted amide are shown in Figure 4.1. Structural and energetic data are given in Table 4.1 and 4.2, respectively. Figure 4.1 shows that the reaction goes through an intermediate, so that there are five stationary points: $React_{TA}$, $TS1_{TA}$, INT_{TA}, $TS2_{TA}$, and $PROD_{TA}$. Pyramidalization of the nitrogen and twist of the amide bond is measured by the values of χ_N

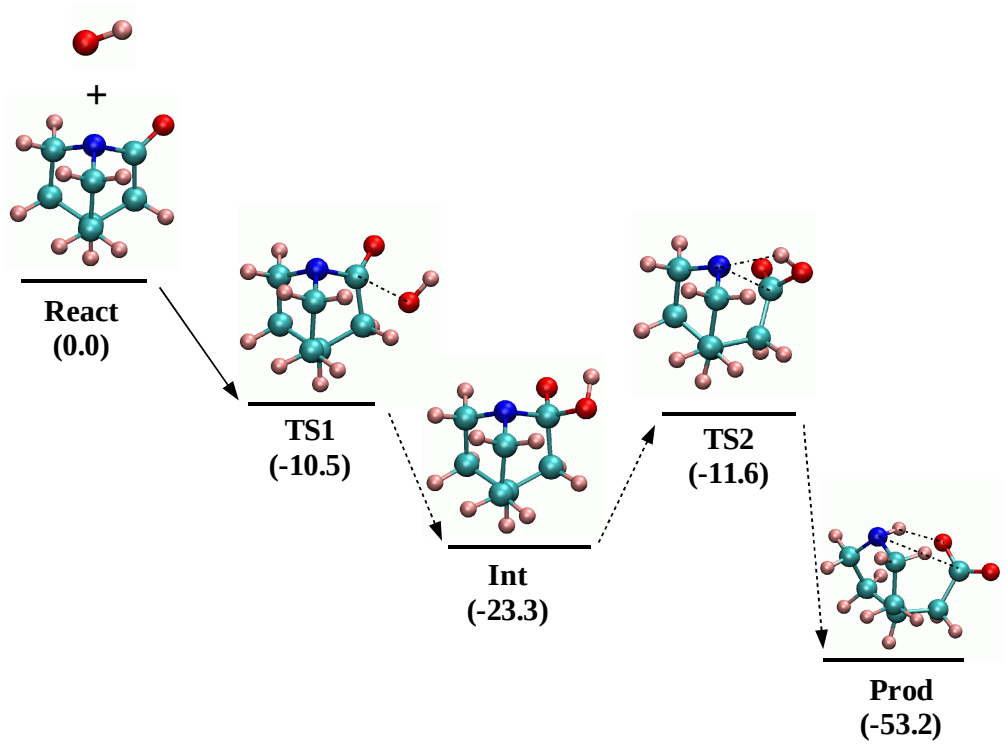

Figure 4.1: B3LYP/6-31+G(d) structures in the hydrolysis of the twisted amide (**TA**). Numbers in parenthesis correspond to ΔG_{gas} values. Energies in kcal/mol relative to the reactants.

Table 4.1: B3LYP/6-31+G* Geometrical parameters for the stationary points of the PES's of the hydrolysis of twisted and planar amides. Distances are in Å and angles in degrees.

	Bond Distances						Angles			Improper Dh.	
Molecule	C_1N	C_1O_1	$C_1O_{nu^-}$	O_1H	$O_{nu^-}H$	NH	τ	χ_C	χ_N	N	C_1
Formamide	1.361	1.219					0.1	0.1	0.1	180.0	180.0
Formamide (TS)	1.439	1.203					90.0	0.1	64.8	115.2	179.9
Twisted amide											
$React_{TA}$	1.453	1.209					89.4	0.1	62.4	117.3	179.8
$TS1_{TA}$	1.466	1.297	2.667	3.300	0.971	3.648	69.5	17.6	61.8	120.1	162.4
INT_{TA}	1.554	1.227	1.493	2.219	0.972	2.764	53.5	52.7	60.0	119.0	127.3
$TS2_{TA}$	2.378	1.226	1.400	2.603	0.994	1.894	41.5	56.1	66.0	115.9	162.8
$PROD_{TA}$	3.375	1.257	1.270	2.008	3.568	1.026	42.4	60.1	70.6	115.9	179.1
Planar amide											
$React_{PA}$	1.375	1.232					3.1	2.9	11.6	169.5	177.2
$TS1_{chair}$	1.408	1.243	2.308	2.601	0.971	3.199	5.9	24.9	44.3	137.2	155.1
$INT1_{chair}$	1.516	1.298	1.548	2.135	0.971	2.973	3.8	52.2	50.7	130.5	127.4
$INT2_{chair}$	1.542	1.310	1.495	2.130	0.972	2.982	0.4	70.4	57.8	122.0	128.9
$INT3_{chair}$	1.570	1.287	1.509	3.083	0.973	2.340	3.3	70.5	60.0	120.4	129.1
$TS2_{chair}$	2.341	1.228	1.393	2.872	0.996	1.883	19.4	66.7	55.6	127.4	156.0
$PROD_{chair}$	3.394	1.255	1.274	1.871	1.871	1.029	32.6	60.3	29.0	127.8	178.7
$TS1_{boat}$	1.419	1.248	2.156	2.547	0.971	3.170	12.2	29.2	41.9	139.3	150.8
INT_{boat}	1.511	1.292	1.553	2.145	0.971	2.985	14.2	52.0	48.0	132.9	128.0

Table 4.2: Ab-Initio Energies and Free Energies in gas phase and solution for the hydrolysis of twisted and planar amides. All quantitaties in kcal/mol. Experimental values[205, 206] for the solvation free energy of OH^- range from -104.0 to -107.5 kcal/mol.

	Gas-Phase		$G_{Solvation}$		Solution-Phase	
Molecule	ΔE	ΔG_{gas}	G_s^{PB-J}	G_s^{PCM}	ΔG_{aq}^{PB-J}	ΔG_{aq}^{PCM}
OH^-			-105.5	-109.8		
Twisted amide						
$React_{TA}$	0.0	0.0	-11.5	-9.8	0.0	0.0
$TS1_{TA}$	-20.8	-10.5	-78.1	-71.6	28.4	37.5
INT_{TA}	-36.2	-23.3	-73.6	-72.6	20.1	23.7
$TS2_{TA}$	-21.8	-11.6	-60.5	-57.0	44.9	51.0
$PROD_{TA}$	-65.5	-53.2	-71.0	-73.2	-7.2	-6.8
Planar amide						
$React_{PA}$	0.0	0.0	-10.9	-8.0	0.0	0.0
$TS1_{chair}$	-16.4	-5.6	-76.1	-67.7	34.7	44.5
$INT1_{chair}$	-19.7	-7.6	-62.3	-69.8	46.5	40.5
$INT2_{chair}$	-19.2	-6.9	-73.4	-79.8	36.1	31.2
$INT3_{chair}$	-15.0	-3.1	-77.7	-74.0	35.6	40.7
$TS2_{chair}$	-4.7	5.1	-58.1	-57.2	63.4	65.7
$PROD_{chair}$	-40.8	-30.7	-66.7	-71.1	19.0	16.0
$TS1_{boat}$	-12.9	-2.3	-76.4	-68.3	37.7	47.2
INT_{boat}	-15.5	-4.1	-67.0	-71.8	45.3	41.9

angle and τ, respectively. Values obtained for these angles in formamide are also included for comparison. In a standard amide bond, such as the one found in formamide, the amidic group is planar, which corresponds to a "non-twist" situation (τ is 0^o) and both carbon and nitrogen show planar sp^2 hybridisation (the corresponding χ angles are 0^o). In the twisted amide reactant we find that the nitrogen is significantly pyramidalized, with χ_N of 62.4^o, and the peptide bond is substantially twisted, the τ angle is 89.4^o. A similar twist has been reported[77] for this compound at the HF/6-31G* level of theory. The planarity of the carbonyl group is kept at values similar to the ones found in formamide (χ_{C_1} is 0.1^o). The values of the bond distances for the peptide bond reflects this twist of the amide bond and the pyramidalization of the nitrogen. The amide (C_1-N) bond length is 1.453 Å, almost 0.1Å longer than in formamide, whereas the the C_1-O distance is 1.209 Å, very close to the 1.219 Å found in formamide. These distances are slightly longer than the bond distances reported by Greenberg *et al.*,[77] namely, they obtained a C_1-N distance of 1.433 Å and a C_1-O one of 1.183 Å. The slight elongation is a consequence of the fact that the present calculations include electron correlation, which tends to elongate bonds. The significant elongation of the C_1-N bond and the relative small shrinking of the C_1-O bond in the twisted amide follow the trend observed when rotating the amide bond in formamide and its derivatives.[12,13,49–52]

Next, we analyze the structures for the TS's, intermediates and products of the hydroxide attack. In terms of the τ and χ angles, there are two aspects of interest. The χ_N angle shows little change upon hydroxide attack; i.e., the pyramidalization at the nitrogen is not affected by the hydroxide attack. By contrast, the χ_{C_1} angle increases from 0.1^o to close to 60^o, indicative of the loss of planarity at the carbonyl carbon as the nucleophilic attack takes place. The change in C_1 hybridisation also causes τ to decrease.

The transition state for the attack of the hydroxide anion ($TS1_{TA}$) is early, with a C_1-O_{nu^-} distance of 2.667 Å, relative to the value (1.493 Å) in the intermediate. The other geometrical parameters are only slightly altered with respect to their values in the amide reactant(see Table 4.1); e.g., the carbonyl bond distance is 1.220 Å and the amide bond is 1.466 Å, both very close to their original values. After hydroxide attack, an intermediate INT_{TA} is formed; it is the so-called "tetrahedral intermediate" of the amide hydrolysis reaction. The C_1-O_{nu^-} distance is 1.493 Å and the amide bond is significantly elongated (1.554 Å) with respect to the reactant. The χ_C angle now is very close to 60^o, namely 52.7^o and it reflects the expected trend of the transition between an sp^2 and sp^3 carbon as the hydroxide attack takes place. The next step of the reaction corresponds to breaking the C_1-N amide bond, which is concerted with proton transfer from the nascent carboxylic acid group to the departing nitrogen. The transition state for this second step is $TS2_{TA}$. At the transition state, the proton is oriented towards the nitrogen, and their separation is only 1.894 Å. The C_1-O_{nu^-} bond distance

has decreased to 1.400 Å, and the amide C_1-N distance has increased to 2.378 Å. Since the peptide bond is being broken, τ loses its meaning, and the χ angles are of limited value for describing the planarity of the C_1 and N atoms. For these structures, it is better to look at the improper dihedrals for these atoms (see Table 4.1). After complete breaking of the amide bond and the transfer of the proton to the nitrogen, the product structure $PROD_{TA}$ is obtained. In this structure the carboxylate is anionic, with a C_1-N distance of 3.375 Å. Carbon has recovered its planarity according to the value of the C_2-C_1-O_1-O_{nu^-} dihedral angle of 179.1^o. The structure is stabilized by an intra-molecular hydrogen bond between the NH proton and one of the carboxylate oxygens. This hydrogen bond slightly enhances the pyramidalization of the nitrogen; the value defined in terms of H-N-C_5-C_6 dihedral angle is 115.9^o.

Energy Profile. The energies (relative to the reactants) of the stationary points described above are in Table 4.2 and in Figure 4.2. In gas-phase all stationary points show a lower energy than the reactants, even when entropic and enthalpic corrections are included. The transition state for the hydroxide attack, $TS1_{TA}$, has a ΔG_{gas} of -10.5 kcal/mol. This negative ΔG_{gas} for the transition state is indicative of the existence of the expected ion-molecule complex for the approach of the hydroxide to the amide. These ion molecule complexes are characteristic of the gas phase reaction but they will not longer be stable species in aqueous medium. To demonstrate this, we have trapped an ion molecule complexes in the potential energy surfaces. The ion molecule complex form a hydrogen bond with an aliphatic C-H bond of the cage. Its ΔG_{gas} is -16.9 kcal/mol. However, after solvation corrections are introduced using the PCM model, its energy is 34.7 kcal/mol, indicating that it will not be a stable species in solution.

The intermediate INT_{TA} formed after the hydroxide attack is very stable; i.e., ΔG_{gas} of -23.3 kcal/mol. The barrier for the breaking of the C_1-N bond in this intermediate, is 11.7 kcal/mol, the $TS2_{TA}$ transition state having a slightly lower ΔG_{gas} than $TS1_{TA}$ transition state. The breaking of the amide bond is concerted with a transfer of a proton to the nitrogen from the carboxyl group (Figure 4.1), and makes the resultant product $PROD_{TA}$ a very stable; ΔG_{gas} is -53.2 kcal/mol. Thus, $PROD_{TA}$ is the global minimum along this potential energy surface and has a lower energy than INT_{TA}. This is a consequence of the fact that the oxygen in INT_{TA} can only form a single bond with C_1 because this carbon is already involved in three other bonds (C_1-O_{nu^-}, C_1-C_2, and C_1-N). However in $PROD_{TA}$, the C_1-N bond is broken, and O forms a double bond with C_1. In addition, since the proton at O_{nu^-} has been transfered to the nitrogen, there is considerable resonance stabilization of the π electrons in the $\pi_{O-C-O_{nu^-}}$ delocalized orbital.

The two methods used to evaluate the solvent free energies, (Poisson-Boltzmann with Jaguar [PB-J] and PCM), give qualitatively similar solvent

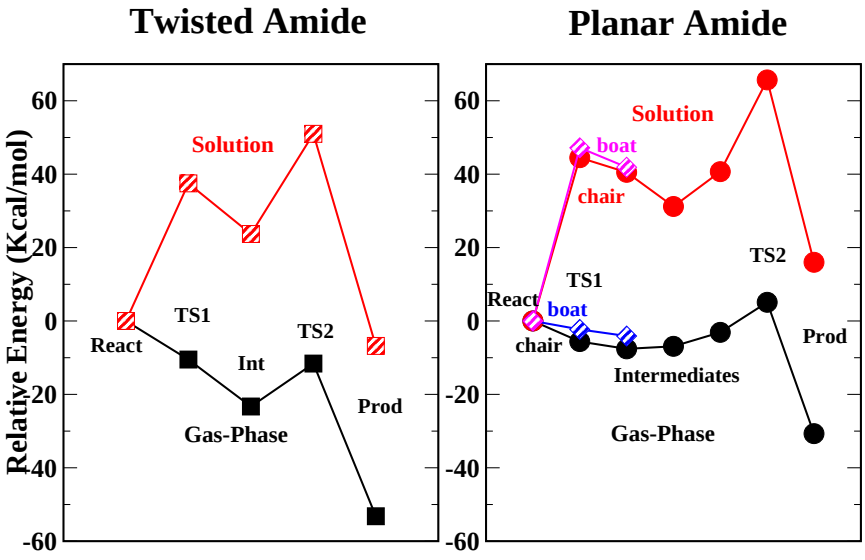

Figure 4.2: Diagram showing the relative energies (kcal/mol) with respect to the reactants for the hydrolysis of **TA** (left-hand side diagram), and for the hydrolysis of **PA** (right-hand side diagram). Both gas-phase profile and solvated profile are shown (estimated using the PCM results of Table 4.2).

effects for the reaction. Solvation favors the separate reactants over the transition states and intermediates, so that the solvent increases the barrier to hydrolysis. This corresponds to what have been reported by Weiner *et al.*[61] for the alkaline hydrolysis of formamide. The better solvation of the hydroxide anion relative to the transition state and intermediates, where the negative charge is delocalized over the entire molecule, is the origin of the enhanced barrier. This result is similar to what has been found in other ion-molecule reactions.[207]

Therefore, almost all the relative free energies with respect to reactants are positive; the sole exception is the product free energy, which is still negative, though much less so than in the gas phase. The largest differences in solvation free energies between PB-J and PCM occur for $TS1_{TA}$, -78.1 kcal/mol for the former and -71.6 kcal/mol for the latter. As a consequence, the barrier obtained with PB-J for the first step of the reaction (hydroxide addition) is lower than the one obtained with PCM, namely, 28.4 kcal/mol versus 37.5 kcal/mol, respectively. This difference arises mainly from the solvation free energy of OH^- (see above). The agreement between PB-J and PCM solvation free energies is better for other stationary points, specially for the INT_{TA} structure. The intermediate is at 20.1/23.7 kcal/mol (PB-J/PCM) with respect to the reactants. Both PB-J and PCM give the lowest solvation free energy for the $TS2_{TA}$ structure, -60.5 kcal/mol (PB-J) and -57.0 kcal/mol (PCM). Because of this, $TS2_{TA}$ is the stationary

point with highest ΔG_{aq}^{PB-J} and ΔG_{aq}^{PCM}, 44.9 kcal/mol and 51.0 kcal/mol, respectively. Finally, the exothermicity of the reaction is maintained with solvation, but to a much lower degree than in the gas-phase. The reaction is now slightly exothermic by -7.2 kcal/mol at PB-J and -6.8 kcal/mol at PCM.

Although the solvation free energies vary significantly, the barrier for hydroxide attack (ΔG_{aq} [$TS1_{TA}$] - ΔG_{aq}[React]) is larger than the barrier for the C-N bond breaking ($\Delta G_{aq}[TS2_{TA}]$-$\Delta G_{aq}[INT_{TA}]$) for all three methods, as shown in Table 4.2. The importance of this in the overall reaction is discussed in Section 4.3.

Planar Amide Reactant

Structures. The B3LYP/6-31+G* optimized structures for the reaction are shown in Figure 4.3 while the geometrical and energetic data are given in Table 4.1 and 4.2, respectively. As can be seen, the potential energy surface for the planar amide reaction is more complicated than for the constrained pyramidal amide. This is due to the greater flexibility of the monocyclic lactam ring, compared with the more rigid bicyclic lactam structure. There are two possible initial transition states, $TS1_{chair}$ and $TS1_{boat}$. These lead, respectively, to *chair* and *boat* intermediates. There are three *chair* ($INT1_{chair}$, $INT2_{chair}$ and $INT3_{chair}$) and one *boat* intermediate (INT_{boat}) that are stable (local minima) species. We also characterized a transition state for the breaking of the C_1-N bond, $TS2_{chair}$, and the final product of the reaction, $PROD_{chair}$. Boat structures beyond INT_{boat} were not considered because of the higher energy of these structures as compared with the *chair* conformers. Flexibility of the monocyclic lactam ring will presumably makes possible other intermediates of similar energy to the ones we have shown. Besides, transition states interconnecting intermediates were not determined. This is justified in the context of the present chapter because our main focus is to compare the energetics of the transition states corresponding to the formation of the tetrahedral intermediate (TS1) and the breakdown of the C-N bond (TS2) for the hydrolysis of a twisted amide and its planar counterpart. The difference of the barriers for these two TS's determines the relative reaction rates for the two reactions.

The planar amide reactant is a six-membered lactam ring. The value of τ, 3.1^o, indicates that there is almost no twist in the peptide bond, and the low value of χ_N, 11.6^o, describes a nearly planar nitrogen atom. Thus, the $n_N \rightarrow \pi^*_{CO}$ resonance is presumably very similar to the one in formamide, and makes this compound a good model system for comparison with the hydrolysis of the pyramidal amide. The deviation from planarity in χ_N arises from a tendency toward a chair conformation to avoid eclipsing of the methylene hydrogens; it contributes to a partial loss of the $n_N \rightarrow \pi^*_{CO}$ resonance. Based on the values of the amide bond distances, we expect this

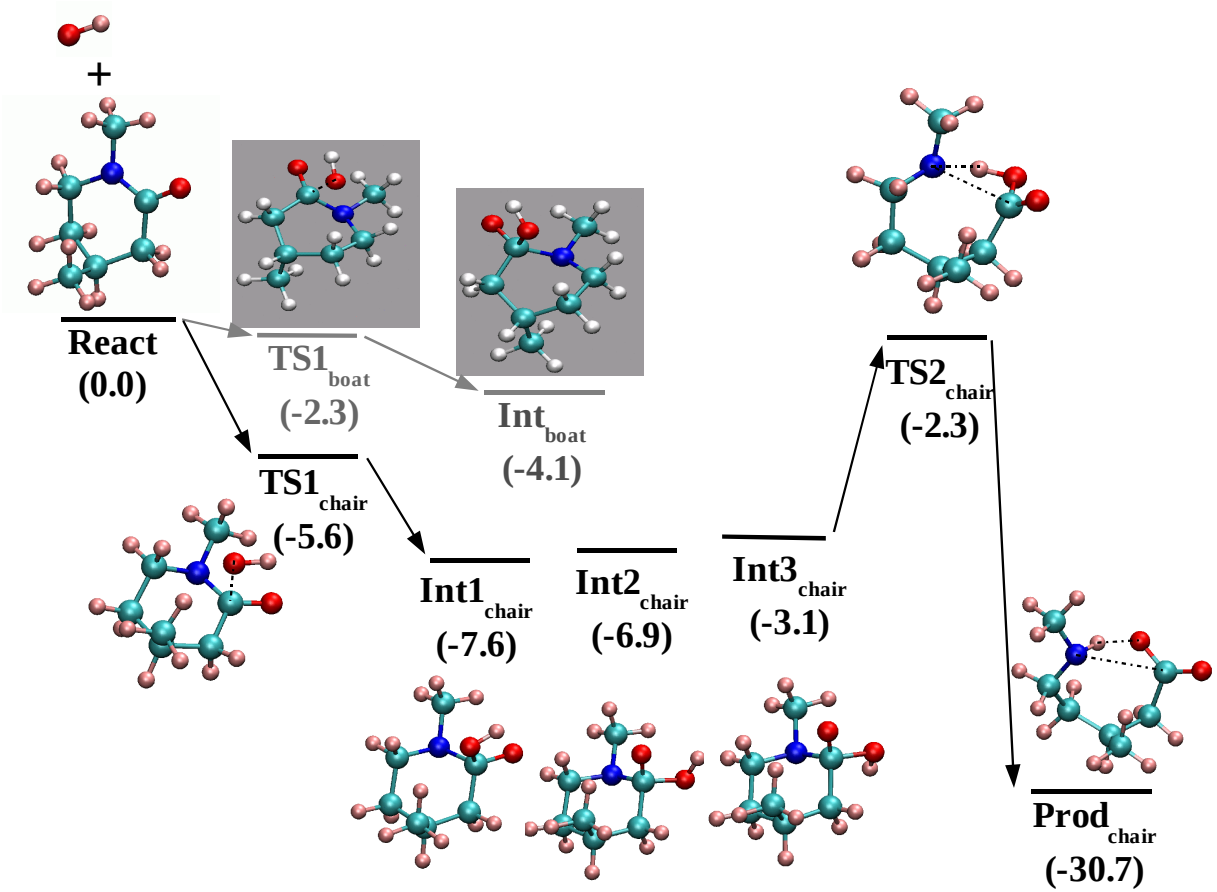

Figure 4.3: B3LYP/6-31+G(d) structures in the hydrolysis of the **PA** planar amide. Numbers in parenthesis correspond to ΔG_{gas} values in kcal/mol relative to the reactants. The pathway in grey refers to the energetically less favorable boat conformation.

loss to be small, since the amide bond distance is only 0.014 Å larger than the one in formamide. As the reaction proceeds and the intermediate is formed, the value of χ_C increases to 60^o, similar to what was calculated in the hydrolysis of the twisted amide. Contrary to the twisted amide case, χ_N changes substantially as the hydroxide approaches; i.e., the nitrogen goes from being almost planar in the reactant to being pyramidal in the intermediates. Consequently χ_N increases from a value of 11.6^o in the reactant to a value of 50-60^o in the intermediates.

The two transition states for the attack of the hydroxide ion on the carbonyl carbon, $TS1_{chair}$ and $TS1_{boat}$, differ as to the side of the ring on which the attack takes place. $TS1_{chair}$ involves the attack of the OH^- on the side of the C_3-methyl group, and $TS1_{boat}$ corresponds to the attack on the opposite side (see Figure 4.3). The large repulsion between the nitrogen lone pair and the incoming hydroxide anion leads to an accentuation of the *chair* conformation of the ring in the former and to the *boat* conformation in the latter. In the constrained system (see Figure 4.1), only the *boat* conformation is possible. Interestingly, the C_1-$O_{nu^-}(H)$ distance in the $TS1_{chair}$ is significantly longer (2.308 Å) than in $TS1_{boat}$ (2.156 Å). In both TS's, the nitrogen has attained a significant degree of pyramidalization, according to both the χ_N angle and the improper dihedral. Thus, χ_N has augmented from 11.6^o in the reactant to 44.3^o in $TS1_{chair}$, and 41.9^o in $TS1_{boat}$, i.e., χ_N has augmented by 30-33^o. If pyramidalization is measured according to the decrease in the C_1-N-C_5-C_6 pseudo-dihedral angle (from 180^o for planar nitrogen to 120^o for pyramidal nitrogen), a similar change of 30^o is observed. Therefore, a substantial decrease in the $n_N \rightarrow \pi^*_{CO}$ resonance in these structures is expected (see Section 4.3).

A *boat* intermediate, INT_{boat}, and three *chair* structures, $INT1_{chair}$ $INT2_{chair}$ and $INT3_{chair}$ are shown in Figure 4.3. All the vibrational frequencies characterized for these stationary points were real (i.e., positive force constants), demonstrating so that they are stable minima of the potential energy surface. There is considerable pyramidalization of the nitrogen in all of the intermediates (see Table 4.1), evidenced by both χ_N and C_1-N-C_5-C_6 pseudo-dihedral angle. The C_1-N amide bond length in the intermediates varies significantly depending on the orientation of the proton of the $> CO_{nu^-}H$ group. For the three *chair* conformations, the shortest C_1-N bond length is obtained for $INT1_{chair}$ (1.516 Å) the structure with the proton on the oxygen furthest from nitrogen. When the proton is transfered to the other oxygen of the carboxyl group ($INT2_{chair}$), the C_1-N distance is elongated to 1.542 Å, and when the proton is oriented towards the nitrogen in $INT3_{chair}$, the distance is 1.570 Å.

For the second step of the reaction, which involves breaking of the amide C_1-N bond, we have only analyzed the *chair* pathway. The reaction from *boat* conformers are expected to lead to a higher-energy transition state, since *boat* conformers were higher in energy for **TS1** and **INT1** (see the sec-

tion on the "Energy profile", below). On the other hand, the *boat* conformer could be converted to the *chair* conformer by an inversion at the nitrogen, not studied in the present work. The transition state, $TS2_{chair}$, for the breaking of the C_1-N amide bond is concerted with O to N proton transfer. The $TS2_{chair}$ transition state connects the $INT3_{chair}$ intermediate with the $PROD_{chair}$ structure. The C_1-N and N-H distances are very similar to those found for $TS2_{TA}$ (see Table 4.1). $PROD_{chair}$ is formed by breaking the C_1-N bond. An intra-molecular hydrogen bond is formed between the H(N) and the carboxyl group, and the geometrical parameters are again similar to the pyramidal case. The shorter O-H(N) hydrogen bond distance (1.871 Å) is possible because of the greater flexibility of this structure, as compared with the $PROD_{TA}$ product.

Energy Profile. In gas-phase, the values of ΔG_{gas} for all the stationary points on the unconstrained amide are larger than the corresponding values for the hydrolysis of the twisted amide (see Table 4.2) . This is due to the energy required for pyramidalization of the nitrogen along the reaction path of the planar system, in contrast to the constrained amide which is already destabilized by the pyramidalization of its nitrogen. This point is considered in more detail in the Discussion section. The reaction is qualitatively similar to the twisted case, in that ion-molecule complexes form as the first step of the reaction in the gas phase, while the transition states for the hydroxide attack and formation of the tetrahedral intermediates are lower in energy than the reactants; i.e., ΔG_{gas} is -2.3 kcal/mol for $TS1_{boat}$ and -5.6 for $TS1_{chair}$. As in the pyramidal case, we have characterized one of the possible ion-molecule complexes which showed a ΔG_{gas} of -14.3 kcal/mol. After solvent corrections are included the ΔG_{aq}^{PCM} is 31.5 kcal/mol, therefore this kind of stationary points in the gas phase are not going to be relevant for the reaction in solution, and we focus in the rest of stationary points throughout the chapter.

The four intermediate structures have free energies between -7.6 and -3.1 kcal/mol, substantially larger than the -22.3 kcal/mol obtained for the intermediate, INT_{TA}, of the pyramidal system. The differences in energy among the four intermediates are related to two factors: the *chair-boat* conformation and the orientation of the carboxylic proton. From the relative energies for $INT1_{chair}$ and INT_{boat}, we estimate a value of 4.0 kcal/mol for the *boat* versus *chair* stabilization. By comparing $INT2_{chair}$ and $INT3_{chair}$, we see that there is also a 4.0 kcal/mol energy penalty for a change of the orientation of the carboxylic proton from a position in which it is oriented towards one of the lone pairs of the other carboxylic ($INT2_{chair}$) oxygen, to one where it is oriented towards the lone pair of the nitrogen ($INT3_{chair}$). However, it is only from the latter (less stable) structure that the proton can be transferred to the nitrogen in $TS2_{chair}$.

The transition state for the breaking of the C_1-N amide bond is at 5.1

kcal/mol with respect to the reactants, and it is the stationary point of highest energy on the potential energy surface. The barrier with respect to $INT3_{chair}$ is 8.0 kcal/mol, almost 4.0 kcal/mol lower than in the pyramidal case. This is attributable to the 4.0 kcal/mol destabilization of $INT3_{chair}$ in orienting the proton towards the nitrogen (see above).

The product structure $PROD_{chair}$ is formed by breaking the C_1-N bond. It is the most stable structure on the potential energy surface, namely, -30.7 kcal/mol relative to the reactants. However, this relative stability is significantly less than that for the product $PROD_{TA}$ (-52.7 kcal/mol). As we discuss in Section 4.3, this difference is due to the destabilization of the pyramidal amide reactant by loss of $n_N \rightarrow \pi^*_{CO}$ resonance.

As in the case of the pyramidal reactant, the introduction of the bulk solvent effects lead to more positive relative free energies. In fact, all species, including the product, are less stable than the reactants. The difference between **TA** and **PA** reactant species originates in the gas phase free energies, rather than in the solvation free energies, which are similar. After adding the solvation free energies to ΔG_{gas} (see Table 4.2), all the species have values of ΔG_{aq} larger than those obtained in the reaction of the pyramidal amide. Again, the solvation corrections differ significantly depending on the method, but this general behavior is independent of the method. For example, in the lowest energy *chair*-pathway, the barrier for hydroxide attack is 6.3/7.0 kcal/mol (PB-J/PCM) higher than in the hydrolysis of the pyramidal amide. If we make the comparison with the *boat* pathway, this difference increases to 9.3/9.7 kcal/mol. These differential barriers between the hydrolysis of **TA** and **PA**, are about 4.0 kcal/mol larger than in the gas-phase. Thus, solvent favors the hydroxide attack on the pyramidal amide with respect to the planar amide by a non-negligible factor.

The two transition states for the hydroxide approach ($TS1_{chair}$ and $TS1_{boat}$) have similar solvation free energies, -76.1/-67.7 and -76.4/-68.3 kcal/mol (PB-J/PCM), respectively. They are somewhat smaller in absolute value than the solvation free energy of $TS1_{TA}$ (-78.6/-71.6 kcal/mol at PB-J/PCM). However, the solvation free energies calculated with PB-J are 8.0-9.0 kcal/mol larger in absolute value than those calculated with PCM. In contrast to $TS1_{chair}$ and $TS1_{boat}$, the intermediates show a wide range of solvation free energies. Except for $INT3_{chair}$, the PB-J solvation free energies are smaller in absolute value than the PCM ones. PB-J and PCM agree in having $INT1_{chair}$ as the intermediate with the lowest solvation free energy. However, the largest solvation free energy in absolute value is obtained for $INT3_{chair}$ with PB-J and for $INT2_{chair}$ with PCM. The smallest solvation free energy in absolute value is found for $TS2_{chair}$ with both PB-J and PCM levels.

The planar intermediates show positive ΔG_{aq} at PB-J and PCM levels of theory. The relative stabilities change somewhat when the solvent contributions are added. For PB-J,

$$INT3_{chair}\ (35.6) \approx INT2_{chair}\ (36.1) > INT_{boat}\ (45.3) > INT1_{chair}\ (46.5)$$

while for PCM,

$$INT2_{chair}\ (31.2) > INT1_{chair}\ (40.5) > INT3_{chair}\ (40.7) > INT_{boat}\ (41.9)$$

where the number in parenthesis correspond to the ΔG_{aq} for each of the isomers in kcal/mol.

Both PB-J and PCM solvent contributions stabilize the $INT2_{chair}$ intermediate with respect to the other intermediates. However, the solvent stabilization of $INT3_{chair}$ observed with PB-J is less clear, since the same is not obtained with PCM. By contrast, there is destabilization of the $INT1_{chair}$ structure. This is the most stable intermediate in the gas-phase, but it is the less stable at PB-J (46.5 kcal/mol) and is at 9.3 kcal/mol larger energy than $INT2_{chair}$ at PCM. The ΔG_{aq}^{PB-J} value for $INT1_{chair}$ is 12.0 kcal/mol larger that the ΔG_{aq}^{PB-J} of $TS1_{chair}$. This indicates that solvent could significantly distort the transition state in solution to geometries closer to $INT1_{chair}$ by reducing the C_1-$O_{nu^-}(H)$ bond length.

The ΔG_{aq} for $TS2_{chair}$ is similar with PB-J (63.4 kcal/mol) and PCM (65.7 kcal/mol). The barrier for the breaking of the amide bond, calculated with respect to $INT3_{chair}$, is 27.8/25.0 kcal/mol (PB-J/PCM), substantially larger than the 8.0 kcal/mol gas-phase barrier. The cause of this barrier enhancement is mainly the small solvation free energy for structure $TS2_{chair}$, relative to that of the intermediate. The barrier is only 3.0 kcal/mol lower than the barrier of the pyramidal complex. $PROD_{chair}$ is significantly destabilized by the solvent and the reaction is now endothermic by 19.0/16.0 kcal/mol at PB-J/PCM levels of theory.

4.2.2 Water assisted breakdown of the Tetrahedral intermediate

The breakdown of the tetrahedral intermediate (INT_{TA} and $INT3_{chair}$ in Figures 4.1 and 4.3, respectively) involves the transition states of largest energy with respect to the reactants, as shown in Figure 4.2. Both $TS2_{TA}$ and $TS2_{chair}$ structures correspond to the cleavage of the C_1-N bond concerted with a proton transfer from the carboxylic acid to nitrogen. The transition states resemble a four-membered ring in which all the bonds that are breaking and forming are part of the ring. In the case of formamide, it has been reported[61,64,72] that an explicit water molecule from the solvent can assist in this proton transfer. This water molecule acts as a proton bridge between one of the carboxylic oxygens and nitrogen, receiving the proton of the oxygen and donating in turn, one of its protons to nitrogen. The resultant transition state has a six-membered ring structure (see Figure 4.4). Explicit water molecules have also been found to have a substantial effect on the one step concerted mechanism for the hydrolysis of neutral

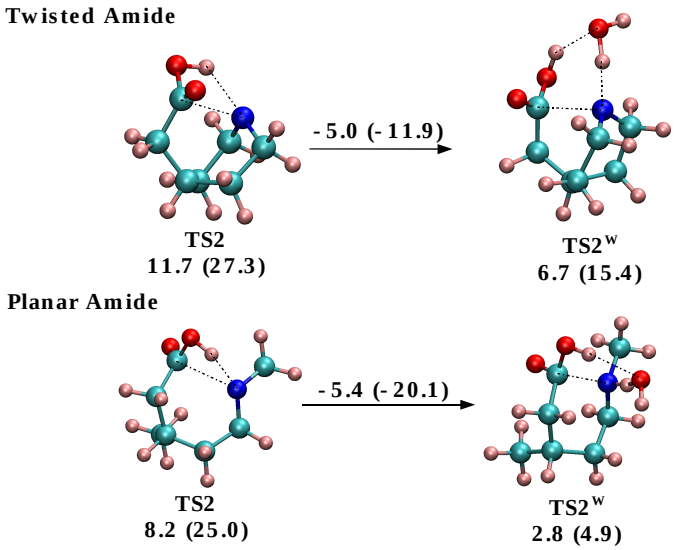

Figure 4.4: The different **TS2** structures characterized for **TA** (above) and **PA** (below). On the left-hand side the non-assisted structures are shown while on the right-hand side the C-N cleavage is assisted by an auxiliary water molecule. The values below the structures correspond to their relative energy in kcal/mol with respect to the intermediate, both in gas-phase and in solution (in brackets) and the values above the arrows show the barrier relaxation due to the catalytic effect of the water molecule in gas-phase and in solution (in brackets).

formamide. Antonczak *et al.*[64] found that the hydrogen bond interaction between a water dimer and formamide led to substantial pyramidalization of the nitrogen in the reagents, because of the high proton donor character of the dimer due to cooperative effects.[208] The resultant hydrolysis was found to be activated with respect to the non assisted mechanism, although it was difficult to isolate the effect of the pyramidalization and the effect of a favorable proton donation, since the nucleophilic attack, the proton transfer and amide bond cleavage were concerted in the mechanism.

To investigate the effect that an specific water-assisted proton transfer would have on the energetics of the species contributing to the reaction, we added a water molecule to the second step of the hydrolysis reaction in order to assist the proton transfer to the N atom. We followed the same methodological protocol than in the non-assisted reaction, although in the new system the nomenclature is more complex because of the auxiliary water molecule. Thus, the O_{nu^-} stands for the oxygen of the hydroxide ion (which has acted as the nucleophile in the first step) while the oxygen of the water molecule is called O_{as}. On the other hand, the proton that initially was bound to O_{nu^-} is called H_t^{nu}. This proton will be transfered to the water molecule which in turn will transfer one of its proton (H_t^{as}) to the N.

Table 4.3: B3LYP/6-31+G* geometrical parameters for the stationary points of the second step (C-N cleavage) assisted by an auxiliary water molecule for both **TA** and **PA** amides. The bond distances are in Å and the improper dihedrals in degrees.

	Bond Distances							Improper Dh.	
Molecule	C_1N	C_1O_1	C_1-O_{nu^-}	O_{nu^-}-H_t^{nu}	O_{as}-H_t^{nu}	O_{as}-H_t^{as}	N-H_t^{as}	N	C_1
Twisted Amide									
Int_{TA}^W	1.564	1.294	1.496	0.972	3.365	1.003	1.834	121.4	127.0
$TS2_{TA}^W$	2.213	1.236	1.388	0.988	1.935	1.073	1.543	116.3	153.6
$Prod_{TA}^W$	3.416	1.262	1.272	1.978	0.983	4.106	1.023	116.4	178.8
Planar Amide									
Int_{PA}^W	1.602	1.282	1.491	0.974	2.706	1.017	1.755	118.9	127.8
$TS2_{PA}^W$	1.838	1.258	1.428	0.987	1.970	1.252	1.268	119.2	137.7
$Prod_{PA}^W$	3.326	1.277	1.258	1.986	0.982	3.785	1.025	127.8	178.8

Structures. Geometrical parameters can be found in Table 4.3, and the water-assisted TS2 transition states for both reactions are depicted in Figure 4.4. Non-assisted TS2 structures are also shown for comparison. Addition of the water molecule does not alter significantly the intermediate structure for the hydrolysis of **TA**, the main difference being a slight lengthening of the C_1-N bond distance by about 0.01 Å. In this stationary point, the assistant water molecule is hydrogen-bonded to the nitrogen (the N-H_{as}^t distance is 1.834 Å). The $TS2_{TA}^W$ transition state corresponds to the cleavage of the C_1-N bond coupled with a transfer of the H_t^{nu} proton from the carboxylic group to the water molecule, which in turn transfers one of its proton (H_t^{as}) to the nitrogen atom. As for the non-assisted reaction, all these changes do not take place simultaneously: while the peptide bond is quite elongated (2.213 Å, 0.1 Å shorter than in the non-assisted $TS2_{TA}$ case), the transfer of the protons are still in an initial stage (the O_{nu^-}-H_t^{nu} and O_{as}-H_t^{as} are 0.988 Å and 1.073 Å respectively). Intrinsic Reaction Coordinate (IRC)[209,210] calculations confirmed that $TS2_{TA}^W$ is the transition state that connects the intermediate with the product, and that the reaction coordinate is very asynchronous, with an elongation of the C_1-N bond first leading to a significant increase in energy and then followed by a proton transfer which relaxes the system energy after passing through the $TS2_{TA}^W$ structure. Finally, the product is formed, which shows analogous structure to the non-assisted product.

We also characterized the water-assisted cleavage of the intermediate for the hydrolysis reaction of **PA**. Geometrical parameters are presented in Table 4.3 and the TS2 geometry is depicted in Figure 4.4. As for **TA**, the intermediate structures is not altered by the addition of the water molecule. However, there is an important changes in the C_1-N distance for TS2, being 2.341 Å in the non-assisted case and 1.838 Å for the water-assisted $TS2_{PA}^W$. There are also significant differences in the degree of proton transfer at TS2:

Table 4.4: Free Energy barrier relaxation for **TS2**, in kcal/mol, due to the inclusion of an explicit water molecule in the calculations (water-assisted mechanism) for the hydrolysis of **TA** and **PA**. Barriers were calculated as the free energy difference between **TS2** and the intermediate **INT** for the non-assisted and water-assisted reactions.

		Non-Assisted	Water Assisted	ΔΔ G
TA	Gas Phase	11.7	6.7	**5.0**
	Solution	27.3	12.4	**14.9**
PA	Gas Phase	8.2	2.8	**5.4**
	Solution	25.0	4.9	**20.1**

in the non-assisted transition state the proton transfers are still in an early stage but in $TS2^W_{PA}$ the H^{as}_t has significantly departed from the assistant water molecule and it is shared by O_{as} (1.252 Å) and nitrogen (1.268 Å) atoms. In a earlier work of Bakowies*et al.*,[72] the MP2/6-31+G* level of theory was employed to characterized the base hydrolysis of the formamide catalyzed by a water molecule. The transition state that they obtained qualitatively has similar characteristics to the ones described here for the planar amide.

Energies. The relative free energies of $TS2^W$ with respect to the intermediate were calculated and results can be found in Table 4.4 compared with those for the non-assisted case. $\Delta\Delta G$ values in Table 4.4 stands for the C-N cleavage acceleration due to the assistant water molecule. The introduction of an explicit solvent water molecule lowers the barriers by a significant amount. The barrier relaxation amounts up to 14.9 kcal/mol for **TA** and 20.1 kcal/mol for **PA**. Therefore, proton transfer in the second step of the reaction is very sensitive to the influence of an assistant water molecule from the solvent facilitating the proton transfer process. If this effect is included in the evaluation of the barriers for the second step of the hydrolysis of **TA** and **PA**, then both steps of the reaction (TS1 and TS2) would show similar barriers. In the case of the non-assisted reaction, the free energy barriers with respect to the separate reactants for the hydrolysis of **TA** were 37.5 kcal/mol for $TS1_{TA}$ and 51.0 kcal/mol for $TS2_{TA}$. In the case of the planar amide, the differences were larger, 44.5 kcal/mol ($TS1_{chair}$) versus 65.7 kcal/mol ($TS2_{chair}$). After the $\Delta\Delta G$ corrections of Table 4.4 are included, the energies for TS2 are reduced to 36.1 kcal/mol ($TS2_{TA}$) and 45.6 kcal/mol ($TS2_{chair}$).

4.3 Discussion

In this section, we compare the differences in free energy between the hydrolysis of the twisted pyramidal and planar amides and we relate the difference in free energy between the two reactions to electronic factors affecting the stability of the amide reactants (Section 4.3.1). Then, we compare our estimates with the experimental evidence[54] of acceleration of hydrolysis of the pyramidal amides (Section 4.3.2). To facilitate the discussion, we show in Table 4.5 the difference in ΔG ($\Delta\Delta G$) between analogue stationary points of the planar and pyramidal potential energy surfaces; e.g., the $\Delta\Delta G$ for TS1 is equal to $\Delta G^{TS1}_{planar} - \Delta G^{TS1}_{pyramidal}$.

4.3.1 Electronic Origin of Transition State Stabilization

The values of $\Delta\Delta G$ are positive for all the stationary points both in gas phase and in solution with the continuum approximation; i.e., the hydrolysis of the twisted amide involves smaller barriers than the hydrolysis of the planar amide. Importantly, the values for $\Delta\Delta G$ found in solution are similar to the ones in the gas phase. This demonstrates that the faster hydrolysis of pyramidal amides results primarily from differential electronic effects present in the gas phase. Among them, the most relevant one, according to Glendening *et al.*,[14] is the absence of the $n_N \rightarrow \pi^*_{CO}$ stabilizing resonance in the twisted amide with a pyramidal conformation of the nitrogen.

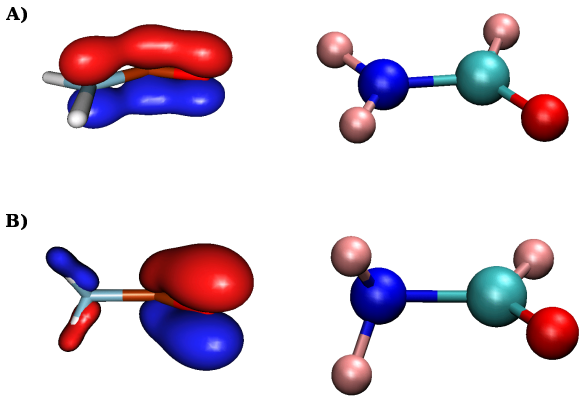

Figure 4.5: Formamide, ground state geometry (A) and transition state geometry (B) corresponding to the rotation along the C-N bond with loss of the $n_N \rightarrow \pi^*_{CO}$ resonance. Notice the planar N conformation in A) , and the pyramidal one in B).

To illustrate this effect, we consider the simplest amide, formamide (Figure 4.5). The ground state of formamide has a planar nitrogen (Figure 4.5A), corresponding to the partial double bond between N and C. Rotation around

the C-N bond leads to a transition state (Figure 4.5B), in which the nitrogen now has a pyramidal conformation and where the resonance between the n_N lone pair and the $\pi^*_{C=O}$ orbital has been broken. As a consequence, longer C-N bond distances and shorter C-O ones are observed in the TS. These changes in bond lengths with rotation of the C-N bond have been extensively analyzed by Wiberg *et al.*.[12,13,49–52] The fact that the C-O bond length changes by an order of magnitude less than the C-N bond elongates has lead[14,49,52,150] to a revision of the amide resonance model. However, a recent natural population analysis by Glendening *et al.*[14] has confirmed the important role of $n_N \rightarrow \pi^*_{CO}$ resonance in characterizing the ground state electron density of planar formamide; they find natural resonant structures which are in agreement with the traditional $n_N \rightarrow \pi^*_{CO}$ resonance model. Therefore, our analysis is based on this type of model.

The rotation around the C-N bond in formamide shows an energy barrier of 20.0 kcal/mol at B3LYP/6-311++G(d,p) level of theory. This barrier is not affected by solvent effects; i.e., when PCM contributions are included a value of 20.6 kcal/mol is obtained. This value for the rotational barrier provided a measure of the stabilization energy of the $n_N \rightarrow \pi^*_{CO}$ resonance since the transition state structure of formamide is very similar to the conformation adopted by the amide bond in the pyramidal reactant. This is nicely shown by an inspection of the values of τ and χ at the TS and the twisted amide reactant (see Table 4.1). The similarity of the value of these angles and the improper dihedrals also leads to the result that the amide bond and C-O bond distances do not change significantly.

We can also estimate the destabilization of the pyramidal reactant arising from the loss of the $n_N \rightarrow \pi^*_{CO}$ resonance by reducing the pyramidal and planar species to their formamide "equivalent". First, we take the conformation of the (C_5, C_6)-N-C_1-$(O_1$-$C_2)$ atoms in the pyramidal amide reactant (see Figure 4.1), substitute C_2, C_5 and C_6 atoms by H and relax the geometries with the constraint that angles and dihedrals be kept the same as in the reactant. We do the same for the planar amide reactant (Figure 4.3), and we calculate the difference in energy between the two formamide structures. The result is 20.1 kcal/mol, a very similar value to the rotational barrier of formamide. These numbers also are very similar to the 23.0 kcal/mol resonance energy loss reported by Greenberg *et al.*,[77] based on differences in heats of formation for isodesmic processes in which amide is compared with its model amine and ketone components.

We now take the conformation of the (C_6, C_5)-N-C_1-(O_1, O_{nu^-}) skeleton of INT_{TA} and $INT1_{chair}$ intermediates (see Figure 4.1 and 4.3), substitute C_2, C_5 and C_6 atoms by H, relax the geometries with frozen angles and dihedrals, and calculate the difference in energy between the two structures. The resulting difference in energy is only 0.6 kcal/mol, suggesting that there is no differential stability arising from the $n_N \rightarrow \pi^*_{CO}$ resonance when the intermediates are formed and the π_{CO} bond is broken.

Table 4.5: Comparing ΔG between the hydrolysis of **TA** and **PA**. $\Delta\Delta G$ values defined as $\Delta G_{planar} - \Delta G_{twisted}$ in the gas-phase and in aqueous solvent using PB-J and PCM methods (See Methods Section). All values in kcal/mol.

Molecule			Solution-Phase	
Planar	Pyramidal	$\Delta\Delta G_{gas}$	$\Delta\Delta G_{aq}^{PB-J}$	$\Delta\Delta G_{aq}^{PCM}$
$TS1_{chair}$	$TS1_{py}$	4.9	6.3	7.0
$TS1_{boat}$	$TS1_{py}$	8.2	9.3	9.7
INT_{chair}	INT_{py}	15.8	26.5	16.8
INT_{boat}	INT_{py}	19.2	25.2	18.2
$TS2_{chair}$	$TS2_{py}$	16.7	18.5	14.7
$PROD_{chair}$	$PROD_{py}$	22.5	26.2	22.8

If we consider the *boat* attack in the planar amide, which takes place on the face corresponding to the attack in the pyramidal amide, and look at the $\Delta\Delta G$ values of Table 4.5, we see that the $\Delta\Delta G$ values in the gas-phase are 8.2 kcal/mol and 19.2 kcal/mol for **TS1** and the intermediate, respectively. This value of 19.2 kcal/mol is very close to the estimate of the stabilizing energy from the $n_N \rightarrow \pi^*_{CO}$ resonance discussed above. Thus, the results are coherent with the conclusion that the pyramidal amide reactant is destabilized relative to the planar amide by about 20.0 kcal/mol, and there is no resonance stabilization in either intermediate. In the **TS1** transition state, a value for $\Delta\Delta G$ of 8.2 kcal/mol is obtained. This suggests that around 40% of the $n_N \rightarrow \pi^*_{CO}$ resonance has been lost in $TS1_{boat}$.

Since the *chair* attack leads to lower $\Delta\Delta G$ values than the *boat* attack, a reaction that passes through *chair* conformation of the ring would be expected for the planar amide. The chair-boat stabilization is around 4.0 kcal/mol for the intermediate, and 3.3 kcal/mol for TS1. The value of $\Delta\Delta G$ is 4.9 kcal/mol for $TS1_{chair}$ and 15.8 kcal/mol for the $INT1_{chair}$ intermediate. For TS2 a value of $\Delta\Delta G$ very similar to the one found for the intermediate, 16.7 kcal/mol, is obtained, and the $\Delta\Delta G$ of the product is augmented to 22.5 kcal/mol. These numbers can be understood from the fact that the $\Delta\Delta G$ values for the intermediates, TS2 and product should reflect the 20.0 kcal/mol destabilization of the pyramidal amide reactant and, in addition, the 4.0 kcal/mol stabilization of chair relative to the boat conformation of the ring.

4.3.2 Comparison with Experiment.

Early kinetic work[54] suggested that a rate acceleration by a factor of 10^7 could be expected from the twist of the peptide bond and pyramidalization of nitrogen in amides under alkaline conditions. This corresponds to a barrier lowering of about 10.0 kcal/mol. Recent work by Kirby *et al.*[56,57]

demonstrates even faster hydrolysis of highly twisted amides, though the conditions (i.e. pH) are different in the two sets of experiments. The observed rate acceleration in experiments is that of the overall rate of the reaction, inclusive of hydroxide attack and breakdown of the tetrahedral intermediate. Depending on the relative free energies of TS1 and TS2, the relevant data to compare with the experimental $\Delta\Delta G^{\neq}$ is $\Delta\Delta G^{TS1}$ (when $\Delta G^{TS1} > \Delta G^{TS2}$) or $\Delta\Delta G^{TS2}$ (if $\Delta G^{TS2} > \Delta G^{TS1}$). As depicted in Table 4.5, $\Delta\Delta G^{TS1}$ is 6.3/7.0 kcal/mol (at PB-J/PCM) when we consider $TS1_{chair}$. This value increases to 9.3/9.7 kcal/mol if we compare $TS1_{boat}$ with $TS1_{TA}$, structures that show an equivalent conformation of the lactam ring. The differential barrier for the second step of the reaction $\Delta\Delta G^{TS2}$ is larger, 18.5/14.7 kcal/mol at PB-J/PCM levels of theory. Based on the data presented in Table 4.2, TS2 is higher than TS1 for the hydrolysis of the planar amide, so that we would expect that the break in the resonance should account for 15.0-19.0 kcal/mol of barrier relaxation. However, we need to consider other aspects.

Analysis of multiple isotope effects[211,212] of the hydrolysis of formamide suggests that breakdown of the anionic intermediate to the reactants or to the products involves TS's of similar energies. The discrepancy between this and our calculated relative energies of TS1 versus TS2 is a consequence of the use of our solvation model in which explicit waters that could assist in the proton transfer of the second step of the reaction are not included. To estimate this effect, we studied the water-assisted reaction were we added an explicit water molecule that assist the unique proton transfer that takes place along the hydrolysis reaction. This has been performed for the formamide as a model for peptide hydrolysis in several other studies.[70,72,74] In our systems, we obtained a barrier relaxation of 14.9 kcal/mol for the **TA** twisted amide and 20.1 kcal/mol for **PA** planar amide. Calculating the free energy barrier with respect to the reactants, in the case of **TA** the barrier for $TS2_{TA}$ is estimated to be 36.1 kcal/mol (i.e., $\Delta G_{TS2_{TA}}$ minus 14.9), a slightly lower barrier than $TS1_{TA}$, which is 37.5 kcal/mol. In the case of the hydrolysis of the planar amide, the corrected barrier for TS2 (ΔG^{TS2}_{chair} minus 20.1) is 45.6 kcal/mol, very similar to $TS1_{chair}$ (44.5 kcal/mol). Additional explicit water molecules will probably decrease this number more, although the effect of a second water molecule is expected to be smaller than the first addition. These results indicate that TS1 and TS2 have similar activation free energies, in agreement with the measured kinetic isotope effects. Applying the corresponding argument to the hydrolysis of the twisted amide that we have studied, suggests that TS1 is the rate limiting transition state for that reaction.

If the hydroxide attack is the rate-limiting step, the experimental $\Delta\Delta G^{\neq}$ should be compared with $\Delta\Delta G^{TS1}$, and the agreement with the kinetic data of Blackburn[54] improves significantly, especially if one compares $TS1_{TA}$ with $TS1_{boat}$, for which $\Delta\Delta G^{TS1}$ would have the value of 9.3/9.7 kcal/mol in

solution and 8.2 kcal/mol in the gas-phase. In summary, based on kinetic isotope effects and the stabilizant effect of explicit water from our calculations, we believe that TS1 and TS2 will have similar energies in the case of the hydrolysis of a planar amide and TS1 will be the rate-limiting step for the hydrolysis of the twisted amide. This leads to very good agreement between the theoretical $\Delta\Delta G^{TS1}$ and the experimental estimates for $\Delta\Delta G^{\neq}$ by Blackburn.[54]

4.4 Concluding Remarks

In this chapter we have studied how the rate acceleration observed in the hydrolysis of twisted amides is related to the loss of the π-resonance. To do so, we have characterized several intermediates, the key transition states, and products of the alkaline hydrolysis of a two closely-related amides, one of which has a twisted amide bond and pyramidalized nitrogen in the reactant, and the other has a normal planar amide bond. Based on the difference in the barriers for the pyramidal and planar systems of the two transition states for the reactions (TS1, corresponding to hydroxide attack, and TS2, corresponding to breakdown of the intermediate), we conclude that a $\Delta\Delta G^{\neq}$ of 15.0-19.0 kcal/mol can be expected if TS2 is the rate-limiting step of the reaction, and 7.0-9.0 kcal/mol if TS1 is the rate-limiting step. From kinetic isotope effects measurement and model studies of the effect of explicit solvent molecules on the mechanism of the hydrolysis of both amides studied we conclude that TS1 and TS2 will have similar energies for the hydrolysis of the planar amide, whereas TS1 will be rate limiting in the case of the hydrolysis of the pyramidal amide. If this is the case, our estimation of the rate acceleration caused by the breakdown of π-resonance in the reactant correspond to a decrease in barrier of 7.0-9.0 kcal/mol, in good agreement with early kinetic estimates of 10.0 kcal/mol by Blackburn *et al.*.[54] The major contribution to the lowering of the barrier arises from the breaking of the π-resonance and the solvent effect is small.

Chapter 5

Neutral Hydrolysis

Abstract

The water-promoted hydrolysis of a highly twisted amide is studied using Density Functional Theory in conjunction with a continuum dielectric method to introduce bulk solvent effects. The aim of these studies is to reveal how the twist of the C-N bond affects the neutral hydrolysis reactions of amides. To do so, both concerted and stepwise mechanisms are studied and the results compared to the ones from the hydrolysis of an undistorted amide used as reference. In addition, the catalysis induced by an additional water molecule is studied. Our results predict important rate accelerations of the neutral hydrolysis of amides when the C-N bond is twisted, the corresponding barrier relaxation being dependent on the specific reaction pathway and transition state involved. In general, the trends observed can be well explained qualitatively by the consequences that the twist of the amide bond has on the electronic features of amide, which can be summarized as i) loss of the $n_N \rightarrow \pi^*_{CO}$ resonance and consequent destabilization of the reactant ii) higher basicity of the amide nitrogen and iii) lower basicity of the carbonyl oxygen. The twist of the amide bond have important mechanistic consequences as well, and favoring concerted-type mechanism versus stepwise ones. In addition, the twist of the amide bond also provokes a higher dependence on an auxiliary water molecule for the concerted mechanism, due to the orthogonality of the lone pair of the nitrogen and the carbonyl π orbital.

5.1 Introduction

We present the comparative hydrolytic studies between **TA** and **PA** at neutral media. Experimentally, this comparison faces a twofold problem. On one hand, kinetic studies on distorted activated amides are difficult due to their fast hydrolysis. On the other hand, the mechanism for amide hydrolysis in pure water in the absence of acid or base catalysis is difficult to follow by conventional kinetic techniques because they are slow[1,18,19,200,213,214] and need to be activated in some way, which obviously affects the comparison.[2] In this respect, theoretical computational studies can be of paramount importance since they can provide with direct data on transition states and their barriers and how these barriers are changed dependent on the nature of the amide reactant. This could help in interpreting the experimental information available.

Computational studies[59,60,62–67,69,71,73,75] on the neutral hydrolysis of amides have been mainly focused on the reaction of undistorted planar amides such as formamide. In the present chapter, we extend our previous alkaline hydrolysis of twisted amide **TA** studies, to its neutral hydrolysis, or in other words, to the water-promoted hydrolysis. Both concerted and stepwise mechanism are studied and the energetic barriers are compared to ones obtained for an undistorted planar amide analogue (**PA** in Figure 3.7). We also analyze the effect of an additional explicit water molecule on the mechanism. The structures were optimized both in gas-phase and in solution by the use of SCI-PCM (for more details, see the Methodology section of page 83).

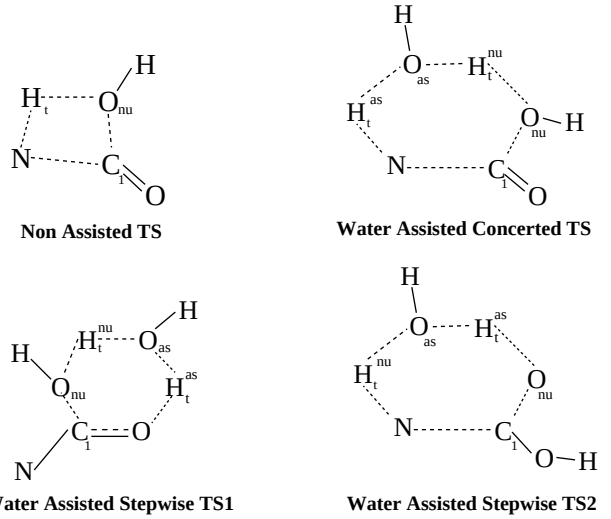

Figure 5.1: Nomenclature used along the chapter for the relevant atoms in the transition states.

5.2 Results

In this section, the main structural and energetic features of the characterized potential energy surfaces are presented. Due to the high number of structures, we will only present in detail those that corresponds to the hydrolysis reactions of the twisted amide, and we will discuss only the solution distances along the text. On the other hand, only some structures for the planar amide hydrolysis will be shown, to compare them with the analogue structures of the twisted amide reaction. The reaction mechanisms can be classified according to the number of steps involved (concerted vs. stepwise) and to the presence or not of an auxiliary water molecule. The *concerted* mechanism shows only one transition state (TS) between the reactants and the products, whereas in the *stepwise* mechanism there are two steps involved with formation of a tetrahedral amide carbon intermediate and two transition states: one that corresponds to the nucleophilic attack on the amide carbon (TS1) and another one related to the cleavage of the C-N amide bond (TS2). For both concerted and stepwise mechanisms, we also investigated the effect of an auxiliary water molecule which catalyzes the reaction by serving as a bridge in proton transfer. The combination of these different possibilities lead to four different potential energy surfaces, which have been investigated for each hydrolysis. The section is divided accordingly. It is worth noticing that the different relative energies were calculated with respect to the separate reactants: amide + water in the non-assisted reaction and amide + water + water in the water-assisted one.

In order to facilitate the identification of each transition state and intermediate of each reaction we will introduce a nomenclature to specify each stationary point. The subscripts c and s will specify whether the structure belongs to the concerted (c) or stepwise (s) mechanism. For example, $TS1_s$ will be used to name the first transition state in the stepwise mechanism and TS_c will refer to the transition state of the concerted mechanism. In addition, the superscript W will indicate the presence in the mechanism of an auxiliary water molecule which assists in the proton transfer process. Thus, TS_c will correspond to the concerted transition state with no auxiliary water, whereas TS_c^W will name the concerted mechanism transition state with one auxiliary water molecule assisting the reaction.

The nomenclature of the atoms in the various reaction mechanisms are summarized in Figure 5.1. The C_1 and O atoms correspond to the carbonyl atoms in the amide. The O_{nu^-} atom stands for the oxygen of the water molecule that makes the nucleophilic attack on the carbonyl C_1 atom. The proton that is being transfered from the nucleophile in the non water-assisted mechanism is referred as H_t^{nu}. On the other hand, when we have an additional water molecule in the hydrolysis mechanism, the oxygen atom of the water molecule that assists the hydrolysis is called O_{as}, and the H that is transfered from this water molecule to the other one is called H_t^{as}.

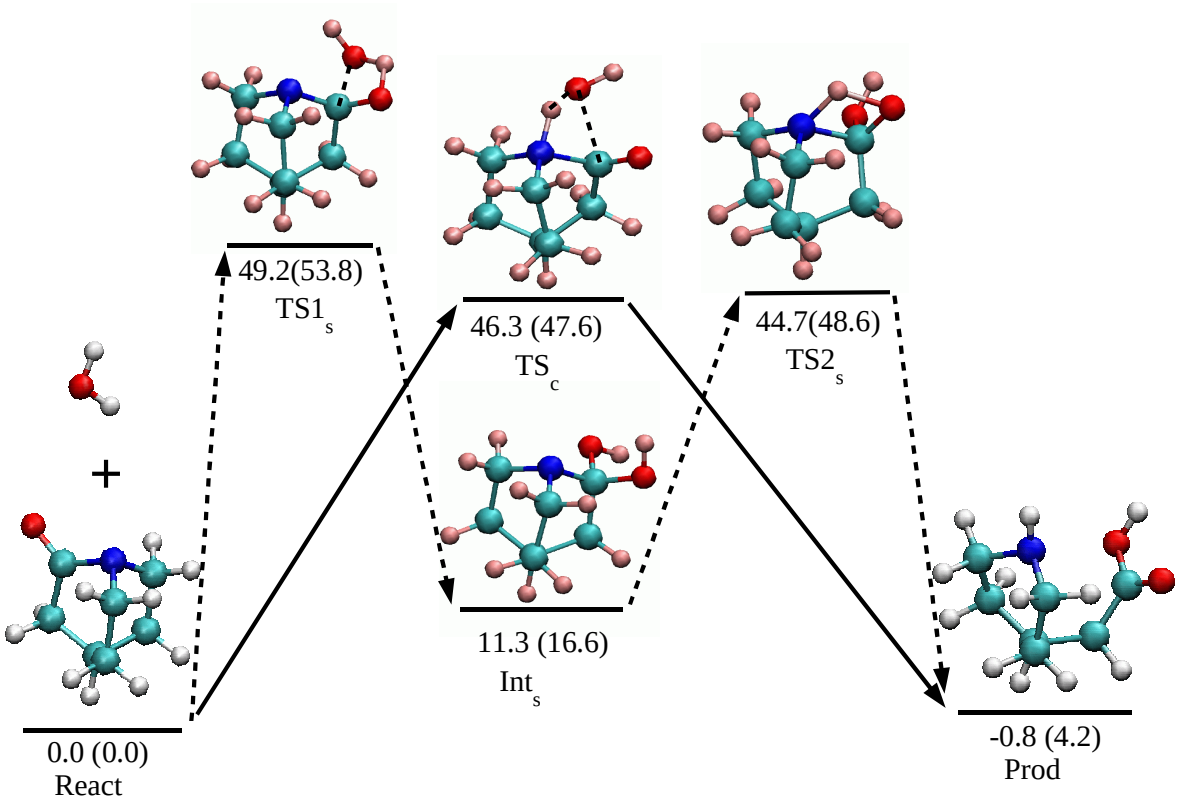

Figure 5.2: The PES for **TA** in the **Non-Assisted** hydrolysis reaction for both the concerted (regular-line) and stepwise (dashed-line) mechanism. The values correspond to the relative free energy (ΔG) in kcal/mol, in the gas phase and in solution (in brackets).

Table 5.1: B3LYP/6-31+G* Geometrical parameters for the stationary points of the PESs of the **Non-Assisted** Neutral Hydrolysis of **TA** following the Concerted and Stepwise mechanisms. The bond distances are in Å and the angles and improper dihedrals in degrees for the structures optimized in gas-phase and in solution (in bold).

	Bond distances						Angles			Improper dh.	
Concerted mechanism											
	C_1-N	C_1-O	C_1-O_{nu^-}	N-H_t	O_{nu^-}-H_t	O-H_t	τ	χ_c	χ_n	dh_C	dh_N
React	1.453	1.209	-	-	-	-	89.4	0.1	62.4	179.8	117.3
	1.448	**1.216**	**-**	**-**	**-**	**-**	**89.9**	**0.0**	**62.8**	**180.0**	**116.7**
HB	1.457	1.209	3.716	1.947	0.984	2.867	90.0	0.0	61.6	180	117.2
	1.454	**1.214**	**3.709**	**1.903**	**0.990**	**2.883**	**89.7**	**0.0**	**62.3**	**179.9**	**117.1**
TS_c	1.553	1.214	2.121	1.160	1.437	2.451	41.4	32.4	60.1	147.6	116.8
	1.524	**1.207**	**2.521**	**1.053**	**1.827**	**2.461**	**32.0**	**21.7**	**59.8**	**150.2**	**117.6**
Prod	2.974	1.215	1.359	1.017	3.823	3.753	37.2	54.5	67.5	176.5	124.9
	3.014	**1.220**	**1.353**	**1.017**	**3.889**	**3.841**	**37.7**	**54.9**	**68.1**	**175.9**	**123.4**
Stepwise mechanism											
$TS1_s$	1.446	1.316	1.751	2.673	1.209	1.286	35.3	37.6	61.8	142.4	116.0
	1.446	**1.331**	**1.709**	**2.671**	**1.196**	**1.300**	**34.2**	**38.8**	**62.0**	**141.2**	**116.3**
Int_s	1.467	1.410	1.420	2.446	2.476	0.975	24.9	60.3	60.8	119.7	119.8
	1.471	**1.413**	**1.419**	**2.475**	**2.477**	**0.974**	**26.7**	**60.6**	**61.2**	**119.3**	**119.6**
$TS2_s$	1.573	1.350	1.421	1.271	2.507	1.363	11.2	50.5	58.6	129.5	121.9
	1.558	**1.364**	**1.419**	**1.286**	**2.526**	**1.342**	**11.2**	**50.8**	**59.0**	**129.2**	**122.0**

Table 5.2: Relative Electronic Energies (ΔE_e), Zero-Point Energies (ΔE_0), Enthalpies (ΔH), Entropic Contributions (T·ΔS) and Free Energies (ΔG) for the stationary points involved in the neutral hydrolysis reaction of **TA** in gas-phase and in solution (values presented in bold). On the left-hand side the Non-Assisted reaction energetics are shown and on the right-hand side the Water-Assisted reaction for both the concerted mechanism (above) and the Stepwise mechanism (below). All the values are in kcal/mol.

	Non-Assisted					**Water-Assisted**				
	ΔE_e	ΔE_0	ΔH	**T.**ΔS	ΔG	ΔE_e	ΔE_0	ΔH	**T.**ΔS	ΔG
Concerted mechanism										
React	0.0	0.0	0.0	0.0	0.0	0.0	0.0	0.0	0.0	0.0
	0.0	**0.0**	**0.0**	**0.0**	**0.0**	**0.0**	**0.0**	**0.0**	**0.0**	**0.0**
HB	-7.9	-5.8	-6.1	-8.0	1.9	-9.2	-7.1	-7.4	-11.3	3.9
	-5.6	**-3.6**	**-3.9**	**-8.1**	**4.3**	**-**	**-**	**-**	**-**	**-**
TS_c	34.1	35.4	33.8	-12.5	46.3	17.4	17.9	15.9	-16.8	32.7
	34.2	**36.7**	**35.3**	**-12.3**	**47.6**	**20.7**	**21.3**	**19.6**	**-15.9**	**35.5**
Prod	-15.0	-11.0	-11.9	-10.5	-1.4	-19.0	-14.4	-15.6	-14.2	-1.4
	-9.1	**-5.3**	**-6.2**	**-10.3**	**4.2**	**-12.4**	**-8.0**	**-9.3**	**-14.6**	**5.4**
Stepwise mechanism										
$TS1_s$	37.1	37.6	35.9	-12.7	48.6	21.9	22.3	19.8	-17.4	37.2
	42.3	**42.7**	**41.0**	**-12.7**	**53.8**	**28.7**	**28.8**	**26.4**	**-17.4**	**43.8**
Int_s	-5.1	-0.5	-2.2	-12.9	10.7	-9.6	-4.8	-6.6	-15.8	9.2
	1.1	**5.5**	**3.9**	**-12.7**	**16.6**	**-1.2**	**3.3**	**1.6**	**-15.8**	**17.4**
$TS2_s$	30.7	32.5	30.6	-13.6	44.1	1.8	5.1	2.7	-17.1	19.8
	35.2	**37.0**	**35.0**	**-13.6**	**48.6**	**8.3**	**11.6**	**9.3**	**-17.1**	**26.4**

5.2.1 Non-assisted hydrolysis of twisted amide

The **TA** reactant has been previous presented (Figure 3.7) and it will be common to all reactions. As it can be seen in Table 5.1, this reactant presents an amide bond with a significant degree of twist (τ=89.9^o) and therefore, the $n_N \rightarrow \pi^*_{CO}$ resonance of untwisted amide bonds is broken. This leads to the loss of the partial double bond character of the C_1-N bond, which implies a pyramidalization of the nitrogen (χ_N is 62.8^o), and C_1-N bond lengthening (1.448 Å) compared to untwisted amide bonds.

We have also characterized a hydrogen-bonded complex (HB in tables) between the amide reactant and the water molecule. The hydrogen bond is established between the nitrogen atom and one of the water hydrogens. The N–H distance is 1.903 Å and the N–H-O angle is 176.1^o. On the other hand, the distance between the water O_{nu^-} and the C_1 atom is quite long, 3.709 Å. The hydrogen bond interaction with the water molecule does not introduce significant changes in the geometry of the amide bond. The nitrogen and carbonyl carbon keep their initial conformations, χ_N and χ_C are 62.3^o and 0.0^o respectively, and the amide bond is only 0.06 Å larger, namely 1.454 Å.

Concerted mechanism

Structures. The reaction pathway and the optimized stationary structures are shown in Figure 5.2. Selected geometrical parameters are given in Table 5.1. The unique transition state of this reaction mechanism corresponds to the nucleophilic attack of water on the amidic carbon, which implies the formation of the O_{nu^-}-C_1 bond, the transfer of a proton from the water to the nitrogen and the cleavage of the amide bond. All these geometrical changes occur in a concerted way but not synchronously. Based on the geometrical data at the TS and on the IRC pathway, the proton transfer is almost completed, the N-H distance is 1.053 Å and the H-O_{nu^-} distance is 1.827 Å. However, the nucleophilic attack of the O_{nu^-} to the carbonyl carbon is still in an early stage, the O_{nu^-}-C_1 distance is 2.521 Å and the C_1-N bond has elongated by only 0.1 Å, namely the C_1-N bond length is 1.524 Å. The carbonyl carbon has begun to depart from the planarity and the χ_C angle is 21.7, indicating the partial loss of double bond character of the carbonyl group.

After passing through the concerted transition state, we have the product structure, in which the amide bond is fully broken (C_1-N distance is 3.014 Å), there is a carboxyl group with a C_1-O_{nu^-} bond length of 1.353 Å, and a secondary amine with a N-H bond length of 1.017 Å. The distance between the proton transfered to the nitrogen and the original water oxygen (now bound to the carbon) is 3.889 Å. Since in this stationary point the peptide bond is absolutely broken, the τ, χ_C and χ_N parameters have lost their meaning, so now we focus on the improper dihedrals, where we can see that

the N atom keeps the pyramidal conformations ($\mathrm{dh}_N = 123.4^o$), and the C_1 atom has recovered its planarity ($\mathrm{dh}_C = 175.9^o$).

Energy profile. The relative energies with respect to the separate twisted amide and water reactants can be found in Table 5.2. The relative energies are separated in its different contributions. In general we have negative gas-phase ΔE_e for the hydrogen-bond complex HB and the product. The inclusion of ZPVE corrections slightly increases the relative energies, and entropic contributions tends to increase the relative energies with respect to the separate reactants by 8-12 kcal/mol, as corresponds to a loss of translational and rotational degrees of freedom when passing from two infinitely separate reactants to one single supramolecule. The final result after all these contributions are added is that the reaction in the gas-phase is slightly exothermic with a ΔG_{gas} of -1.4 kcal/mol, and the transition state implies a substantial barrier, 46.3 kcal/mol. Bulk solvent effects tend to stabilize the separate reactants although by an small amount. Since all the stationary points in the PES are neutral, solvation free energies are small, however, the solvation free energy of each stationary point is smaller in absolute value than the sum of the solvation free energies for the separate reactants. As a consequence the relative free energy for each stationary point is larger in solution than in the gas phase. ΔG_{aq} for HB is 4.3 kcal/mol, the TS barrier is 47.6 kcal/mol and the reaction free energy is 4.2 kcal/mol.

Stepwise mechanism

In the *stepwise mechanism*, the reaction takes place in two steps. The first step is a formation of an intermediate with a tetrahedral carbonyl carbon as a consequence of the nucleophilic attack of the water reactant into the amidic carbon. This attack is concerted with a proton transfer from the water to the oxygen atom of the carbonyl group. The second step of the reaction is the cleavage of the C_1-N bond concerted with a proton transfer from an oxygen atom to the departing nitrogen.

Structures. The reaction pathway and the optimized stationary structures are shown in Figure 5.2, whereas the geometrical parameters are given in Table 5.1. The reactant and the hydrogen-bonded complex are the same of the concerted mechanism, so we do not explain their geometrical characteristic in this section.

The first step's transition state corresponds to the nucleophilic attack of the water molecule on the carbonyl group and the transfer of the H_t atom from the water molecule to the O atom. The C_1-N distance (1.709 Å) is significantly shorter than for the concerted transition state (2.521 Å). The degree of proton transfer between the water and the carbonyl oxygen is very significant at $TS1_s$. The proton lies at an approximate intermediate distance between the two atoms, 1.196 Å from the water oxygen and 1.300 Å from the carbonyl oxygen. The degree of nucleophilic attack on the carbonyl carbon

is high as it can also be inferred from the loss of its planar conformation, being χ_C 38.8^o. The C_1-N bond is however almost unaffected at $TS1_s$.

After passing through $TS1_s$, the intermediate of the reaction is formed. The proton transfer is completed, and correspondingly, the H_t-O distance is short, 0.974 Å. The carbonyl carbon is now forming two single C-O bonds with similar distances, namely, 1.413 and 1.419 Å for C_1-O and C_1-O_{nu^-}, respectively. Now the carbon presents a tetrahedral conformation and the χ_C angle is therefore 60.6^o. This conformational change makes the C_1-N bond less twisted with a decrease of the value of τ to 26.7^o. There is also an slight elongation of the C_1-N bond to 1.471 Å.

The second step is the cleavage of the C_1-N bond concerted with a proton transfer from one of the oxygens to the nitrogen. Based on the distance values, it seems that at $TS2_s$ the proton transfer is more advanced than the C_1-N bond cleavage. The proton is slightly closer to the nitrogen, 1.342 Å, than to the oxygen, 1.286 Å. But on the other hand the C_1-N distance is 1.558 Å, less than 0.1 Å larger than in the intermediate. Finally, the product is formed, the same structure as for the concerted mechanism described in detail in the previous section.

Energy Profile. The relative energies for the stationary point of this PES are shown in Table 5.2. The energies of the reactant, the complex and the product are the same than in the concerted mechanism and the reaction is slightly exothermic in the gas phase. The inclusion of the ZPVE and entropic contributions increases the relative energies of all species and the only stationary point whose relative free energy is lower than the separate reactants is the product. It is interesting to note that the ΔE_e of the intermediate is -5.1 kcal/mol, its relative free energy ΔG increases to 10.7 kcal/mol. The free energies of $TS1_s$ and $TS2_s$ are similar but slightly larger by 4 kcal/mol for $TS1_s$, namely, ΔG_{gas} is 48.6 kcal/mol for the former and 44.1 kcal/mol for the latter. As in the concerted mechanism, the bulk solvent effects increase the relative energy of each stationary point stabilizing the separate reactants, but does not change the qualitative picture of the reaction and the first step of the reaction is still the rate-limiting step.

5.2.2 Water-Assisted hydrolysis of the twisted amide

In this section we describe the results obtained when the reactions are assisted by a catalyst water molecule. Thus, two water molecules are specifically considered in the calculations. One of the waters acts as the nucleophile that attacks on the carbonyl group, whereas a second water molecule catalyzes the reaction by serving as a bridge in the proton transfer between atoms. The transition states characterized in these reactions will correspond to a six-member ring in which several bonds are breaking and forming simultaneously.

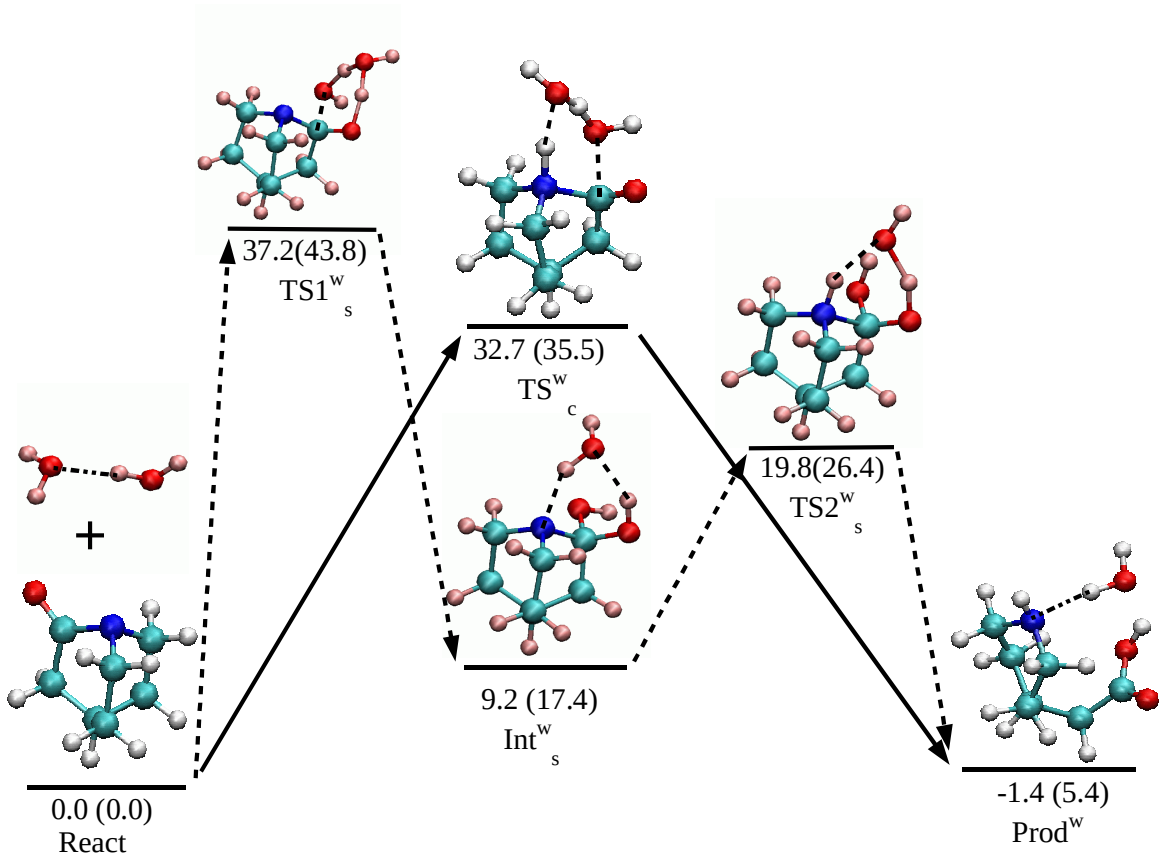

Figure 5.3: The PES for **TA** in the **Water-Assisted** hydrolysis reaction for both the concerted (regular-line) and stepwise (dashed-line) mechanism. The values correspond to the relative free energy in gas phase and in solution (in brackets).

Table 5.3: B3LYP/6-31+G* Geometrical parameters for the stationary points of the PES's of the **Water-Assisted** Neutral Hydrolysis of **TA** following the Concerted and Stepwise mechanisms. The bond distances are in Å and the angles and improper dihedrals in degrees for the structures optimized in gas-phase and in solution (in bold).

	Bond distances								Angles			Improper dh.	
Concerted mechanism													
	C_1-N	C_1-O	C_1-O_{nu^-}	N-H_t^{as}	O_{as}-H_t^{as}	O_{as}-H_t^{nu}	O_{nu^-}-H_t^{nu}	-	τ	χ_c	χ_n	dh_C	dh_N
React	1.453	1.209	-	-	-	-	-	-	89.4	0.1	62.4	180	117.2
	1.448	**1.216**	**-**	**-**	**-**	**-**	**-**	**-**	**89.9**	**0.0**	**62.8**	**180.0**	**116.7**
TS_c^W	1.553	1.210	2.139	1.121	1.474	1.257	1.189		36.0	30.8	60.3	146.0	116.5
	1.533	**1.209**	**2.348**	**1.076**	**1.641**	**1.200**	**1.247**	**-**	**30.9**	**23.8**	**60.6**	**153.2**	**116.9**
$Prod^W$	3.631	1.217	1.349	1.018	3.215	0.998	2.775		44.4	55.7	55.7	176.5	121.3
	3.512	**1.223**	**1.346**	**1.019**	**3.128**	**1.005**	**2.719**	**-**	**44.6**	**29.7**	**42.2**	**177.6**	**120.0**
Stepwise mechanism													
	C-N	$(C\text{-}O)_{carb}$	C-O_{nu^-}	N-H_t^{nu}	O_{as}-H_t^{nu}	O_{nu}--H_t^{nu}	O_{as}-H_t^{as}	O_{carb}-H_t^{as}	τ	χ_c	χ_n	dh_C	dh_N
$TS1_s^W$	1.451	1.299	1.771	2.770	1.219	1.228	1.166	1.290	35.3	43.1	61.5	136.8	117.0
	1.465	**1.312**	**1.691**	**2.792**	**1.234**	**1.210**	**1.141**	**1.324**	**35.7**	**45.7**	**62.1**	**134.3**	**116.9**
Int_s^W	1.484	1.397	1.426	1.903	0.992	2.833	1.926	0.987	26.1	59.6	60.6	120.4	119.8
	1.484	**1.406**	**1.419**	**1.878**	**0.995**	**2.875**	**1.982**	**0.985**	**25.3**	**59.9**	**61.0**	**120.1**	**119.7**
$TS2_s^W$	1.671	1.340	1.385	1.048	1.792	2.540	1.368	1.119	27.9	58.2	56.3	121.8	122.7
	1.626	**1.355**	**1.396**	**1.039**	**1.925**	**2.553**	**1.373**	**1.115**	**27.1**	**57.8**	**56.9**	**122.3**	**122.9**
$Prod^W$	3.631	1.217	1.349	1.018	3.215	4.542	0.998	3.352	44.4	55.7	55.7	176.5	121.3
	3.512	**1.223**	**1.346**	**1.019**	**3.128**	**4.455**	**1.005**	**3.352**	**44.6**	**29.7**	**42.2**	**177.6**	**120.0**

In this potential energy surface, we avoid the characterization of an hydrogen bonded complex for the approach of the two water molecules to the amide. In the previous non-assisted mechanism we showed how the relative free energy of this type of structures are positive, and therefore they will not be of interest for the overall discussion of the reaction kinetics.

The data is presented in an analogous way as in the previous section so first the concerted mechanism is discussed and then the stepwise mechanism. In each subsection, the presentation is divided in a discussion on the structures and then on the energy profile.

Concerted mechanism

Structures. Selected geometrical parameters can be found in Table 5.3. and the structures are shown in Figure 5.3. At the transition state a proton have been almost fully transfered from the assistant water molecule to the nitrogen (the N-H_t^{as} distance is 1.076 Å), the H_t^{nu} proton is almost equally shared by both water oxygens (the H_t^{nu}-O_{as} and H_t^{nu}-O_{nu^-} distance are 1.200 Å and 1.247 Å respectively), and the attacking O_{nu} is at 2.348 Å from the carbon of the carbonyl group. Comparing this transition state to the one of the non-assisted reaction we can say that the degree of proton transfer to the nitrogen is more advanced in the present case, and there is also a higher degree of nucleophilic attack indicated by a shorter O_{nu}-C_1 distance, 0.173 Å smaller than in the non-assistant water mechanism.

The product of the hydrolysis reaction is similar to the product of the non-assisted case. The only difference is that now we have a water molecule hydrogen bonded to the nitrogen. The C_1-N distance in the product is larger now, 3.512 Å whereas in the non-assisted case was 3.014 Å.

Energy Profile. The relative energies are shown in Table 5.2. In order to compare our numbers with the values for the non-assisted case, we take the values that correspond to two reactants as the reference state, amide and a water dimer. For this reference, the number of separate reactants is the same for both non-assisted and assisted reaction mechanism, and therefore, the loss of translational and rotational entropy is similar in both types of reaction mechanism, and thus, the relative free energies are more comparable. As expected, the energy barrier of this reaction is lower than the barrier of the non-assisted reaction. Gas-phase results gives a value ΔH and ΔG of 15.9 kcal/mol and 32.7 kcal/mol, respectively, whereas the gas-phase enthalpic and free energy barriers were 33.8 kcal/mol and 46.3 kcal/mol in the non-assisted case. Therefore the catalytic capacity of an auxiliary water is substantial in the gas phase, in the order of 14-19 kcal/mol depending on whether we consider the enthalpic or the free energy barrier. As in the non-assisted case, bulk solvent effects tends to increase slightly the relative energies for all the species. The resultant enthalpic and free energy barriers are 19.6 kcal/mol and 35.5 kcal/mol, respectively, which are

significantly smaller than in the non-assisted case by 15.7 and 12.1 kcal/mol, respectively. Therefore, the catalytic effect of the assisting water molecule in the concerted mechanism is very important and probably the role of this auxiliary water is essential in the hydrolysis. A number of authors has also pointed out to the importance of assisting water molecules in the hydrolysis of formamide.[61,64,65,72]

The relative free energy of the product is very similar to the one found for the non-assisted case. In the gas-phase the reaction is slightly exothermic by -1.4 kcal/mol, but is endothermic in solution by 5.4 kcal/mol. This endothermicity is much influenced by the rotational and translational loss of entropy. If we look at the enthalpic values, the reaction is exothermic in both the gas phase, -15.6 kcal/mol, and in solution, -9.3 kcal/mol.

Stepwise mechanism

As in the concerted mechanism, in the stepwise mechanism an additional water molecule decreases the reaction barriers. In both steps, a water molecule acts as a proton bridge, receiving a proton and donating one in turn. We follow the same convention as above to name this protons. H_t^{as} is the proton initially located at the assistant water, and H_t^{nu} is the proton located at the water that acts as the nucleophile in the hydrolysis. In the first step of the reaction, H_t^{nu} is transfered to the assistant water, which in turn transfers H_t^{as} to the carbonyl oxygen. In the second step, H_t^{as} returns to the assistant water and H_t^{nu} passes to the nitrogen. We will now comment on more detail each structure.

Structures. The geometrical parameters for the stationary point of this PES are shown in Table 5.3 and the geometries are depicted in Figure 5.3. $TS1_s^W$ is the transition state that corresponds to the nucleophilic attack on the amidic carbon and intermediate formation. The C_1-O_{nu^-} distance at the transition state is the shortest among the four reaction mechanism studied, namely 1.691 Å, significantly shorter than in the water-assisted concerted mechanism (TS_c^W), 2.348 Å, and moderately shorter than in the non-water assisted stepwise mechanism ($TS1_s$), 1.709 Å. The attack is concerted with a double proton transfer, one between water molecules (H_t^{nu}) and the other between the assistant water to the carbonyl oxygen (H_t^{as}). The degree of proton transfer is higher between the two water molecules than between the assistant water and the carbonyl oxygen. Thus, whereas H_t^{nu} is almost equally shared by the two water oxygens (the H_t^{nu}-O distances are 1.234 Å and 1.210 Å), H_t^{as} is still closer to the water than to the carbonyl oxygen (its distances with respect to O_{as} and O_{carb} are 1.141 Å and 1.324 Å respectively).

The intermediate structure is very similar to the non-assisted intermediate Int_s, with a water molecule hydrogen-bonded to the nitrogen atom and to one of the proton at the carboxilate group. This hydrogen bond interac-

tion elongates the C_1-N bond by 0.013 Å comparing the C_1-N distances in Int_s^W, 1.484 Å, and in Int_s, 1.471 Å.

Then, we have the second transition state $TS2_s^W$, which leads to the C_1-N bond cleavage. The C_1-N bond is quite activated at the transition state, 1.626 Å, 0.068 Å larger than in the non-assisted reaction, and almost 0.1 Å larger than in the concerted TS_c^W, 1.533 Å. The H_t^{nu} proton is completely transfered to the nitrogen (the N-H_t^{nu} bond distance is 1.039 Å), while in the non-assisted reaction this distance was 1.286 Å. On the other hand, H_t^{as} is still closer to O atom, 1.115 Å than to O_{as}, 1.373 Å. From these geometrical features, we can say than in the second step of the reaction, several changes occur in a concerted but asynchronous way. First, we have the proton transfer from the auxiliary water to the nitrogen, which then provokes the C_1-N bond cleavage and a proton transfer of the carboxilate to the assistant water molecule.

The product is the same of the concerted mechanism, where the assistant water molecule is hydrogen bonded to the nitrogen. The H_t^{as} is completely transfered to the N atom and the H_t^{nu} is completely bonded to the O_{as} atom.

Energy Profile. The relative energies of this reaction are presented in Table 5.2. As it was expected, the catalyst water molecule addition decreases the energy barrier of both steps. The relative energy of $TS1_s^W$ is 37.2 kcal/mol in the gas phase, 11.4 kcal/mol lower than in the non-assisted reaction. This difference is very similar to the addition of a second water molecule in the concerted mechanism. The catalytic factor of the assistant water molecule is even more significant in the second step, which shows an energy barrier of 19.8 kcal/mol, 24.3 kcal/mol lower than in the non-assisted case. It is important to remark that in this case the clear rate-limiting step is the first one with 37.2 kcal/mol, whereas in the non-assisted stepwise mechanism both TS1 and TS2 showed more similar reaction barriers, 48.6 and 44.1 kcal/mol respectively. The solvent effect is the same as in the other reactions, it leads to an slight increase of the relative energies, but without altering the main qualitative features. The first step of the reaction ($TS1_s^W$) is clearly the rate-limiting step of this mechanism, with a barrier in solution of 43.8 kcal/mol, much higher than the 26.4 kcal/mol barrier of $TS2_s$.

5.2.3 Hydrolysis of a planar amide analogue as reference

In order to determine the effect that the twist of the amide bond has on reaction barriers, we performed analogous calculations for the hydrolysis of a planar amide analogue to the twisted amide molecule of the previous section. The planar amide chosen is depicted in Figure 3.7, and it is the species that comes from hydrogenation and cleavage of the **TA** C_6-C_7 bond. This leads to the break of the cage structure and relieves the geometrical constraints that maintained the amide bond in a twisted conformation.

Table 5.4: Relative Electronic Energies (ΔE_e), Zero-Point Energies (ΔE_0), Enthalpies (ΔH), Entropic Contributions (T·ΔS) and Free Energies (ΔG) for the stationary point involved in the neutral hydrolysis reaction of **PA** in gas-phase and in solution (values presented in bold) are collected. On the left-hand side the Non-Assisted and on the right-hand side the Water-Assisted reaction figures are shown. The above rows correspond to the concerted mechanism and the below ones to the Stepwise mechanism.

	Non-Assisted					**Water-Assisted**				
	ΔE_e	ΔE_0	ΔH	**T.**ΔS	ΔG	ΔE_e	ΔE_0	ΔH	**T.**ΔS	ΔG
Concerted mechanism										
React	0.0	0.0	0.0	0.0	0.0	0.0	0.0	0.0	0.0	0.0
	0.0	**0.0**	**0.0**	**0.0**	**0.0**	**0.0**	**0.0**	**0.0**	**0.0**	**0.0**
HB	-3.2	-1.5	-1.6	-7.8	6.2	-5.2	-3.4	-3.5	-10.3	6.8
	-0.3	**1.1**	**1.2**	**-5.8**	**7.0**	**-**	**-**	**-**	**-**	**-**
$(TS_c)_{exo}$	42.8	43.9	42.5	-11.9	54.3	34.8	34.6	32.8	-15.6	48.3
	44.0	**45.8**	**44.3**	**-12.0**	**56.3**	**39.9**	**40.0**	**38.3**	**-15.3**	**53.6**
$(TS_c)_{endo}$	42.4	43.1	41.6	-11.8	53.5	35.2	35.2	33.3	-16.1	49.3
	45.5	**46.4**	**45.0**	**-11.7**	**56.7**	**40.7**	**40.7**	**39.0**	**-15.5**	**54.5**
Prod	6.5	9.8	8.9	-9.8	18.7	2.8	6.5	5.3	-13.8	19.1
	12.7	**15.7**	**14.9**	**-9.6**	**24.5**	**10.3**	**13.8**	**12.6**	**-13.6**	**26.2**
Stepwise mechanism										
$(TS1_s)_{exo}$	40.4	40.9	39.6	-11.3	50.9	27.9	28.6	26.9	-14.8	41.6
	44.3	**45.2**	**44.0**	**-11.2**	**55.1**	**34.8**	**36.3**	**34.6**	**-15.2**	**49.8**
$(TS1_s)_{endo}$	37.8	38.2	36.8	-11.6	48.4	25.5	25.8	23.9	-15.9	39.8
	41.8	**42.7**	**41.3**	**-11.5**	**52.9**	**33.1**	**34.2**	**32.4**	**-15.6**	**48.0**
Int_s	14.9	18.4	16.8	-12.3	29.1	12.1	15.7	14.1	-15.3	29.5
	20.8	**24.2**	**22.6**	**-12.4**	**35.0**	**20.4**	**23.8**	**22.3**	**-15.2**	**37.5**
$(TS2_s)_{exo}$	48.5	49.4	47.6	-12.6	60.2	25.5	26.9	24.4	-17.5	41.9
	52.5	**53.4**	**51.6**	**-12.7**	**64.3**	**31.1**	**33.4**	**30.8**	**-17.7**	**48.5**
$(TS2_s)_{endo}$	45.9	46.9	45.1	-12.6	57.7	22.8	25.6	23.0	-17.6	40.7
	50.5	**51.3**	**49.6**	**-12.6**	**62.1**	**30.4**	**32.8**	**30.4**	**-17.4**	**47.8**

As can be seen in Figure 3.7, the reactant now shows an untwisted amide bond with a corresponding low value of τ, 3.1^o, and a nitrogen atom in a quasi-planar conformation ($\chi_N = 11.6^o$). This is the standard situation for an amide bond for which there is a resonance between the lone pair of the nitrogen and carbonyl π bond, which leads to a partial double C_1-N bond character, and therefore, the C_1-N bond length is shorter than the amide bond for the twisted amide reactant.

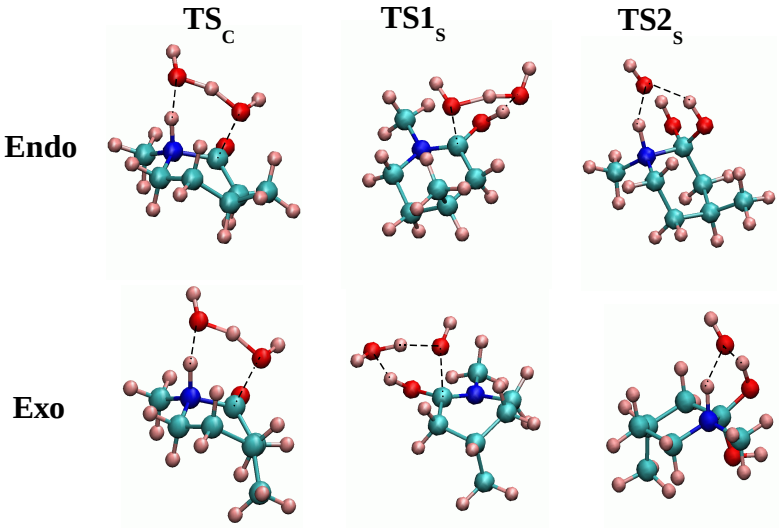

Figure 5.4: The different optimized Transition State structures for **PA**.

Due to the methyl group presence at the C_3 position, there will be two possibilities for TS1 and TS2 transition states, those that corresponds to attacks and proton transfers in an *exo* or an *endo* position with respect to this methyl group. In Figure 5.4, both possibilities are depicted for the case of the non-assisted concerted and stepwise mechanisms.

The barriers for exo and endo TS's are very similar, although there is a consistent stabilization of endo TS's. In general, both exo and endo reaction pathways give the same qualitative picture. Our energetic barriers are in reasonable qualitative agreement with previous calculations on the hydrolysis of formamides by other groups. Oie et al.[60] studied the neutral hydrolysis of the formamide using Moller-Plesset perturbation theory, for both concerted and stepwise mechanisms. They found that the energy barrier in the gas phase for the concerted mechanism at MP2/6-31G**//3-21G level of theory was 42.0 kcal/mol, whereas when they considered the stepwise mechanism, the water molecule approximation required the same energy. The second step of the hydrolysis, that is, the peptide bond cleavage had a relative energy of 39 kcal/mol with respect to the reactants. Krug et al.[62] studied the neutral, acid and alkaline hydrolysis of the formamide

at MP2(FULL)/6-31G**//4-31G level of theory. They found that the energy barrier for the concerted neutral hydrolysis was 44 kcal/mol. They also calculated the energy barrier for the stepwise mechanism, where the energy barrier for the first step was 42 kcal/mol and 35 kcal/mol for the second step. All these values compare reasonably well with our ΔE values in the non-assisted mechanism. Thus, we obtain values of ΔE_e in the gas phase of 42.0-43.0 kcal/mol for the concerted non-assisted mechanism, values of 38.0-40.4 kcal/mol for the first step of the stepwise non-assisted mechanism. However, our values for the $TS2_s$ are somewhat larger, around 45 kcal/mol. This latter transition state is significantly stabilized in the water-assisted mechanism, obtaining similar gas phase free energy barriers (39.8 kcal/mol for $TS1_s^W$ and 40.7 kcal/mol for $TS2_s^W$). Interestingly the concerted transition state is only moderately stabilized by the additional water molecule, and we obtain free energy barriers of 48-49 kcal/mol in the gas phase and 53-54 kcal/mol in solution. Antonczak et al.[64,65] also determined the importance of an auxiliary water molecule for the neutral hydrolysis of formamide in the concerted mechanism. Using Moller-Plesset perturbation theory at Hartree-Fock geometries, they also determined that the effect of an auxiliary water molecule provides a moderate stabilization of the neutral transition state. Their MP3 values for the free energy barriers in solution were 59.3 kcal/mol for the non-assisted case and 56.7 kcal/mol for the water-assisted case, in good agreement with our values, 56-57 kcal/mol and 53.6 54.5 kcal/mol, respectively. In a more recent paper, Ruiz-López and co-workers[75] studied the amide bond formation in aqueous solution, the reverse reaction to the neutral hydrolysis of formamide, including static and dynamic solvent effects using a continuum dielectric method for the former and a QM/MM method for the latter. They investigated the non-assisted mechanism and they found that stepwise and concerted processes had similar activation free energies, 45.12 kcal/mol in the gas phase for the the concerted mechanism and 45.75 kcal/mol for the stepwise mechanism, being the breakdown of the intermediate through a TS2 type transition state rate limiting, as it is our case for the non-assisted mechanism. From their results, we can say that both reaction mechanism, concerted and stepwise may compete in the case of the neutral hydrolysis of formamide.

Consequently, planar amides, opposite to highly twisted amides, hydrolyze under neutral pH conditions either through a stepwise or a concerted mechanism, depending on the specific chemical environment of the amide bond. For instance our calculations show that in the case of **PA**, there is a preference for stepwise mechanism by 4-5 kcal/mol. However, in the case of formamide a competitive situation between both reaction mechanisms has been reported.[75] Therefore, it seems difficult that in the case of undistorted amides, there is a generic reaction mechanism that can be applied to all cases, and the preference for a concerted or a stepwise mechanism depends on the particular amide reactant.

Table 5.5: The relative ΔG's (in kcal/mol) of the different Transition States between **TA** and **PA** involved in the non-assisted and water assisted reactions, both in gas-phase and in solution (in bold)

	ΔG_{twist}	ΔG^{endo}_{planar}	$\Delta\Delta G^{endo}$	ΔG^{exo}_{planar}	$\Delta\Delta G^{exo}$
			Non-Assisted		
TS_c	46.3	53.5	7.2	54.3	8.0
	47.6	**56.7**	**9.1**	**56.3**	**8.7**
$TS1_s$	48.6	48.4	-0.2	50.9	2.3
	53.8	**52.9**	**-0.9**	**55.1**	**1.3**
$TS2_s$	44.1	57.7	13.6	60.2	16.1
	48.6	**62.1**	**13.5**	**64.3**	**15.7**
			Water-Assisted		
TS_c	32.7	49.3	16.6	48.3	15.6
	35.5	**54.5**	**19.0**	**53.6**	**18.1**
$TS1_s$	37.2	39.8	2.6	41.6	4.4
	43.8	**48.0**	**4.2**	**49.8**	**6.0**
$TS2_s$	19.8	40.7	20.9	41.9	22.1
	26.4	**47.8**	**21.4**	**48.5**	**22.1**

5.3 Discussion

The neutral hydrolysis of amides studied in the present chapter show a rich mechanistic picture with several pathways (concerted/stepwise water assisted/non-water assisted) and possible transition states involved. To ease the comparison between the hydrolysis reaction of **TA** and **PA**, in Table 5.5 the energetic barriers of all the transition states are shown. We also give the differential energy barrier, $\Delta\Delta G$, between the planar and twisted amide hydrolysis:

$$\Delta\Delta G^{endo} = \Delta G^{endo}_{planar} - \Delta G_{twisted} \quad (5.1)$$

$$\Delta\Delta G^{exo} = \Delta G^{exo}_{planar} - \Delta G_{twisted} \quad (5.2)$$

In general, $\Delta\Delta G$'s are positive indicating that there is a substantial acceleration of the hydrolysis caused by the amide bond twist. However, there are also substantial differences among the various $\Delta\Delta G$'s, which ranges from -0.9 to +22.1 kcal/mol. The largest values are found for $TS2^W_s$ transition states in the water-assisting mechanisms, and the lowest values are found for the $TS1_s$'s of the non water-assisted case. In this latter case and for endo transition states, slightly negative $\Delta\Delta G$ values are found, -0.9 kcal/mol in solution. Thus, in general there is a substantial reaction acceleration caused by the twist of the amide bond, but with an interesting dependence on the reaction mechanism and specific transition state considered.

The nucleophilic attack on the carbon in both concerted and stepwise process is coupled with proton transfer, to the nitrogen in the concerted case and to an oxygen in the stepwise $TS1_s$ transition state. Therefore, the differential barriers are reflecting the effect that the loss of $n_N \rightarrow \pi^*_{CO}$ resonance in **TA** has on the destabilization of the reactant, but also on the N and O basicities. These changes in basicity were characterized in Chapter 3 by estimates of the pKa values for a series of twisted and planar amides. The calculations revealed that the loss of $n_N \rightarrow \pi^*_{CO}$ resonance in twisted amides increases the basicity of N and decreases the one of the oxygen. In fact, twisted amides prefer to be protonated at the nitrogen, whereas in planar amides the O-protonated tautomer is more stable, as previously remarked by Greenberg *et al.*[17,77] in the context of gas-phase ab initio calculations. The mechanistic implications that can be expected from these changes in basicities are that transition states that imply a protonation on the oxygen will be favored in planar amides, while transition states with proton transfer to the nitrogen will be favored for twisted amides. In summary, there are various electronic and structural features affected by the twist of the C-N bond in amides that can be relevant to understand the differential barriers between the hydrolysis of **TA** and **PA**, but they can be concisely stated as: i) loss of $n_N \rightarrow \pi^*_{CO}$ resonance and destabilization of the reactant, ii) higher basicity of the N and iii) lower basicity of the O in the amidic unit.

Based on these qualitative arguments, we expect that the rate acceleration in twisted amides to be maximum when there are process which required a proton transfer to the nitrogen, and minimum when the carbonyl oxygen receive a proton from a water molecule. In fact this is the case, the largest $\Delta\Delta G$ in both non-assisted and water-assisted mechanism is found for $TS2_s$, 13.5 kcal/mol for $\Delta\Delta G^{endo}$ and 15.7 kcal/mol for $\Delta\Delta G^{exo}$ in the non-assisted mechanism, and 22.1 kcal/mol in the water-assisted mechanism. On the contrary, the first transition state of the stepwise mechanism $TS1_s$ shows very low values of $\Delta\Delta G$, -0.9 and 1.4 kcal/mol for endo and exo $\Delta\Delta G$. In these cases, the destabilization of the reactant in **TA** and lower reaction barrier is balanced by the fact that the nucleophilic attack is concerted with a proton transfer to the oxygen, which is less favorable in **TA** than in **PA**. The two effects almost cancel each other and we have transition states of similar energetic barriers.

Finally, $\Delta\Delta G$ values for the concerted transition states show a remarkable dependence on whether the reaction is catalyzed by an assisting water molecule. In the non-assisted case, one find intermediate values for $\Delta\Delta G$, 9.1 kcal/mol for $\Delta\Delta G^{endo}$ and 8.7 kcal/mol for $\Delta\Delta G^{exo}$. These values are much lower than what one could expect looking at $TS2_s$ and from the 15-20 kcal/mol destabilizant effect expected from the rotational barriers of undistorted amides. However, in the water-assisted mechanism, the rate acceleration is more pronounced and the differential barriers show a remarkable increase, 19.0 kcal/mol for $\Delta\Delta G^{endo}$ and 22.1 kcal/mol for $\Delta\Delta G^{exo}$. This

indicates that the hydrolysis of twisted amide through concerted mechanism is more sensitive to the presence of an assistant water molecule than the hydrolysis of the planar amide. The origin of this higher sensitivity is the orthogonality between the nitrogen lone pair (n_N) and the carbonyl π bond (π_{CO}). In planar amides, both orbitals are coplanar, n_N defines the plane of proton transfer and π_{CO} the plane of nucleophilic attack. A single water molecule participating in the concerted reaction shows a relatively correct orientation for both proton transfer and nucleophilic attack, and correspondingly, the transition state is an almost planar four-member ring (the dihedral defined by N-C_1-O_{nu}-H_t is only 6-8^o). In the case of a twisted amide, and due to the orthogonality between n_N and π_{CO}, a single water molecule will have more problems to adopt an optimal conformation for the proton transfer and nucleophilic attack. This strain in orientation is reflected by a transition state with a high departure from the four-member ring planarity formed by N-C_1-O_{nu}-H_t, the associated dihedral angle being 24^o. As a consequence, the transition state of the twisted amide will be favored to a higher extent than the transition state of the planar amide by the presence of an additional water molecule in the mechanism and the formation of a more flexible six-member ring in the water-assisted mechanism. The additional water molecule will introduce a necessary extra flexibility to orient optimally a proton for the transfer to n_N and a nucleophilic attack in the π_{CO} plane.

In summary, our calculations reveal important rate accelerations for the water promoted hydrolysis of twisted amides with respect to its untwisted analogue. These rate accelerations are maximum for transition states TS_c and $TS2_s$, on the order of 20 kcal/mol, and much more reduced for $TS1_s$ due to the required O-protonation. The experimentally observed rate acceleration will depend on the preferred reaction mechanism for each reaction, which according to our calculations also shows an interesting dependence on the amide bond twist.

In Figure 5.5, we depict the reaction free energy profiles for the four reaction mechanism investigated for each hydrolysis. In the case of **PA**, there is a slight preference for the concerted pathway in the non-assisted mechanism and for stepwise mechanism in the water-assisted reaction. In addition, both transition states in the water-assisted reaction, $TS1_s^W$ and $TS2_s^W$, have similar free energy barriers. Chalmet *et al.*[75] also found similar barriers for the hydrolysis of formamide. Their conclusion based on the non-assisted mechanism is that both reactions mechanism may compete depending on the specific type of amide and conditions involved. Note however, that experimental hydrolytic studies of neutral hydrolysis are scarce due to its slowness. Isotope effects in the alkaline hydrolysis of formamide[196] support the idea of an stepwise mechanism with two transition states of similar energy, but it is doubtful how this data can be transfered to neutral hydrolysis. Nevertheless, in the case of twisted amides, there is a clear pref-

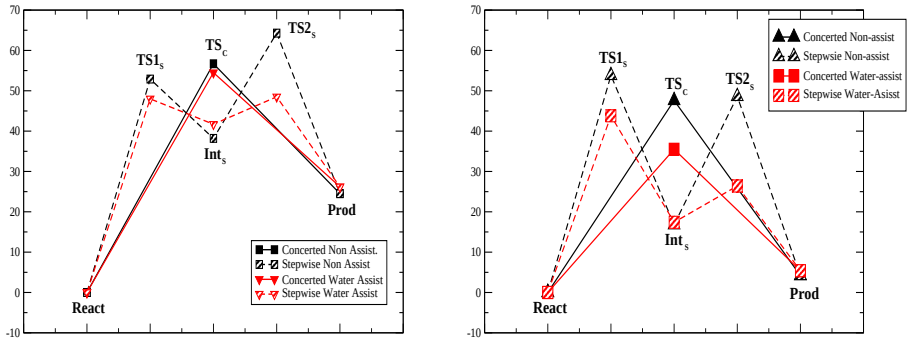

Figure 5.5: Aqueous Free Energy reaction profiles for the hydrolysis of **PA** (left) and **TA** (right) for the concerted /stepwise and non-assisted/water-assisted reaction mechanims.

erence for concerted mechanisms (see Figure 5.5). The free energy barrier in the water-assisted case is 35.5 kcal/mol versus the 43.8 kcal/mol stepwise mechanism barrier. In addition, in this latter case the $TS1_s^W$ is clearly the reaction rate-limiting step, with a barrier height almost 18 kcal/mol higher than the second step $TS2_s^W$. Thus our calculations reveal that the twist of the amide bond not only has an effect on the relaxation of barriers in the neutral hydrolysis of amides, but also has a deep mechanistic influence, favoring concerted mechanisms. This is so because of the requirement of O-protonation in the stepwise mechanism, which is a very unfavorable situation for twisted amides, as reported by the work of Greenberg*et al.*,[17,77] and by our own pK_a estimates in aqueous solvent.[80] Taking together the results for the hydrolysis of both **TA** and **PA**, and comparing the energetic barriers for the rate-limiting transition states of the lowest-energy mechanism in each case (TS_c^W for **TA**, and $TS1_s^W$ for **PA**), we predict a rate-acceleration corresponding to a $\Delta\Delta G$ of 12-13 kcal/mol, sensibly larger than the 7-9 kcal/mol characterized in the case of the alkaline hydrolysis of these amides by quantum chemical calculations.[79] This would suggest that the degree of rate-acceleration of the hydrolysis of amides upon twisting is pH dependent, in line with the experiments of Brown *et al.*[2,55] which observed a different rate acceleration of twisted amides in basic and acid pH's, a factor of 10^7 under basic conditions and a factor of a factor of 10^{11} under acid-catalyzed conditions. Interestingly, Kirby *et al.*[56,57] have found that a twisted amide with a similar degree of twist as in **TA** hydrolyzes much faster and suggested that a different mechanism than in the alkaline hydrolysis could be at hand for neutral and slightly acid pH's. In this line, the calculations presented

in this chapter show a higher acceleration of the twisted amide hydrolysis with respect to the planar one than at alkaline pH's, and substantial mechanistic differences between the hydrolysis of **TA** and **PA**. Besides, the fact that Kirby *et al.* were unable to trap an intermediate in the hydrolysis of a twisted amide similar to **TA**, at intermediate range of pH, could be reconcile with the fact that we observe a tendency for concerted mechanism at neutral pH's.

5.4 Concluding Remarks

The neutral hydrolysis of **TA** has been presented and the results compared to those of **PA**. Concerted and stepwise mechanism were considered, along with the possibility of an auxiliary water molecule as a catalyst. Our calculations suggest significant differences between the hydrolysis of both amides which can be summarized as follows,

- Significant activation of the twisted amide towards hydrolysis by factors that goes from few kcal/mol to around 20 kcal/mol depending on the transition state and mechanism compared.
- A clear preferential for concerted mechanism in the case of twisted amides, for which the nucleophilic attack on the carbonyl are coupled with proton transfer to the nitrogen, in agreement with proton affinities evaluation in the gas phase and pKa estimations in solution.
- A destabilization of transition states that imply O-protonation, i.e., first transition state of the stepwise mechanism.
- The twisted amide concerted hydrolysis mechanism has a higher dependence on the assistant water molecule, due to orthogonality between the nitrogen lone pair and the carbonyl π bond.

In general, we predict that the rate acceleration caused by the twist of the amide bond in neutral pH should be higher than the one in alkaline pH, although its experimental kinetic determination is difficult due to the slow hydrolysis of unactivated amides.

Chapter 6

Acidic Hydrolysis

Abstract

We present an ab-initio study of the acid hydrolysis of a highly twisted amide and of a planar amide analogue. The aim of these studies is to investigate the effect that nitrogen pyramidalization has on the reaction barriers and mechanism of the acid hydrolysis of amides. Concerted and stepwise mechanism were investigated using Density Functional Theory and Polarizable Continuum Model (PCM) calculations to take into account bulk solvent effects. Remarkable differences were observed between the mechanism of both twisted and planar amide, motivated mainly because of the preference for N-protonation of the former and O-protonation of the latter at acidic pH's. In addition, we were also able to determine that the hydrolytic mechanism of a highly twisted amide will be pH dependent. Thus, there is a preference for a stepwise mechanism with formation of an intermediate for the acid-hydrolysis, whereas the neutral hydrolysis undergoes through a concerted-type mechanism. There is a nice agreement between the characterized intermediate and available X-ray data and a good agreement between our data and the kinetically estimated rate-acceleration of hydrolysis with respect to analogous undistorted amide compounds. This work, along with previous ab-initio calculations, describes a complex and rich chemistry for the hydrolysis of highly twisted amides and its dependence on the pH's range. The theoretical data provided allows for a better understanding of the available kinetic data of the rate-acceleration of amides upon twisting, and the relation of the observed rate acceleration with pH-dependent mechanism and intrinsic differential reactivity with loss of amide resonance.

6.1 Introduction

In the present chapter we continue with this series of calculations, analyzing the acidic hydrolysis regime of the highly twisted amide (**TA**) and its analogous planar amide (**PA**) (see Figure 3.7). As in the neutral hydrolysis, both the concerted and stepwise mechanism are considered, and the reaction is evaluated for the non-assisted and water-assisted mechanism following the same methodological protocol (for more details, see the Methodology in page 83).

As we have explained in Chapter 3, Greenberg *et al.*[17,77] found that in the gas phase and contrary to behavior of undistorted amides, twisted amides are protonated at the nitrogen instead of at the oxygen, which suggested important mechanistic differences for the hydrolysis of twisted amides in acidic and neutral medium. However, most of the acidic hydrolysis studied theoretically[62,64,65] and experimentally[59,196,200,215,216] involve undistorted amides. For example, Krug *et al.* calculated the acidic hydrolysis reaction taking into account both the N- and O- protonated site for the undistorted formamide. Moreover, Brown *et al.* reported[2,55] significant accelerations for the hydrolysis of distorted amides, where the degree of acceleration seems to depend on the pH conditions, ranging from 7 orders of magnitude for the alkaline hydrolysis to 11 orders of magnitude for acid-catalyzed hydrolysis. More recently, Kirby et al.[56–58] also reported the rapid hydrolysis in water (under slight acidic conditions) of a highly twisted amide bond in 1-aza-2-adamantanone, suggesting an even higher acceleration of the hydrolysis rate.

Therefore, taking into account all these experimental evidences and our theoretical calculations determining a pKa value of 6-7 for the most twisted amides (Chapter 3), we characterize the acidic hydrolysis reaction for *TA* and *PA*. This study complement our previous work in this field and allow us to characterize the similarities and differences in the hydrolysis of highly twisted amides at three different pH ranges: acid, neutral and alkaline.

6.2 Results

In this section we present the main structural and energetic features of the acidic hydrolysis of the twisted amide (**TA**). The structures were optimized both in gas-phase and in solution (for more details see the Methodology section in page 83) although in the current section we only refer to the geometries optimized in solution. The reaction is studied following two different mechanisms: i) The concerted mechanism shows only one transition state (TS) between the reactants and the product, and ii) the stepwise mechanism with a carbon tetrahedral intermediate and two transition states: the first one corresponds to a nucleophile attack of the water molecule at the

carbonyl C_1 atom (TS1) of the protonated amide, and the second one to the cleavage of the amide bond (TS2). For both concerted and stepwise mechanisms, we also present the effect of an auxiliary water molecule which catalyzes the reaction by serving as a bridge in proton transfer. The gas phase and solution energies were employed to calculate the relative energies with respect to the separate reactants: amide + H_3O^+ in the non-assisted reaction and amide + H_3O^+ + water in the water-assisted reaction.

In order to facilitate the identification of each transition state and intermediate of each reaction, we will introduce a nomenclature analogous to the one used in the neutral hydrolysis to specify each stationary point. Thus, the subscripts c and s will specify whether the structure belongs to the concerted (c) or stepwise (s) mechanism, while the superscript W will indicate the presence in the mechanism of an auxiliary water molecule which assists in the proton transfer process. Moreover, in Figure 6.1, we schematically show the atom nomenclature for some types of transition states. The C_1 and O atoms correspond to the carbonyl atoms in the amide. The O_{nu^-} atom stands for the oxygen of the water molecule that makes the nucleophilic attack on the carbonyl C_1 atom. The proton that is being transfered from the nucleophile in the non water-assisted mechanism is referred as H^1_{nu}. On the other hand, when we have an additional water molecule in the hydrolysis mechanism, the oxygen atom of the water molecule that assists the hydrolysis is called O_{as}, and the H that is transfered from this water molecule to the other one is called H^1_{as}.

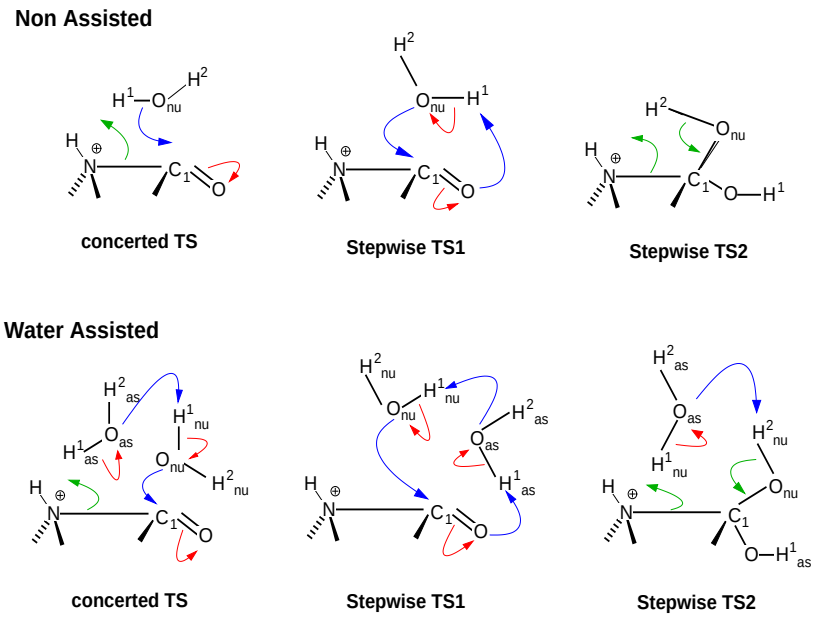

Figure 6.1: Nomenclature used along the chapter for the relevant atoms in the transition states.

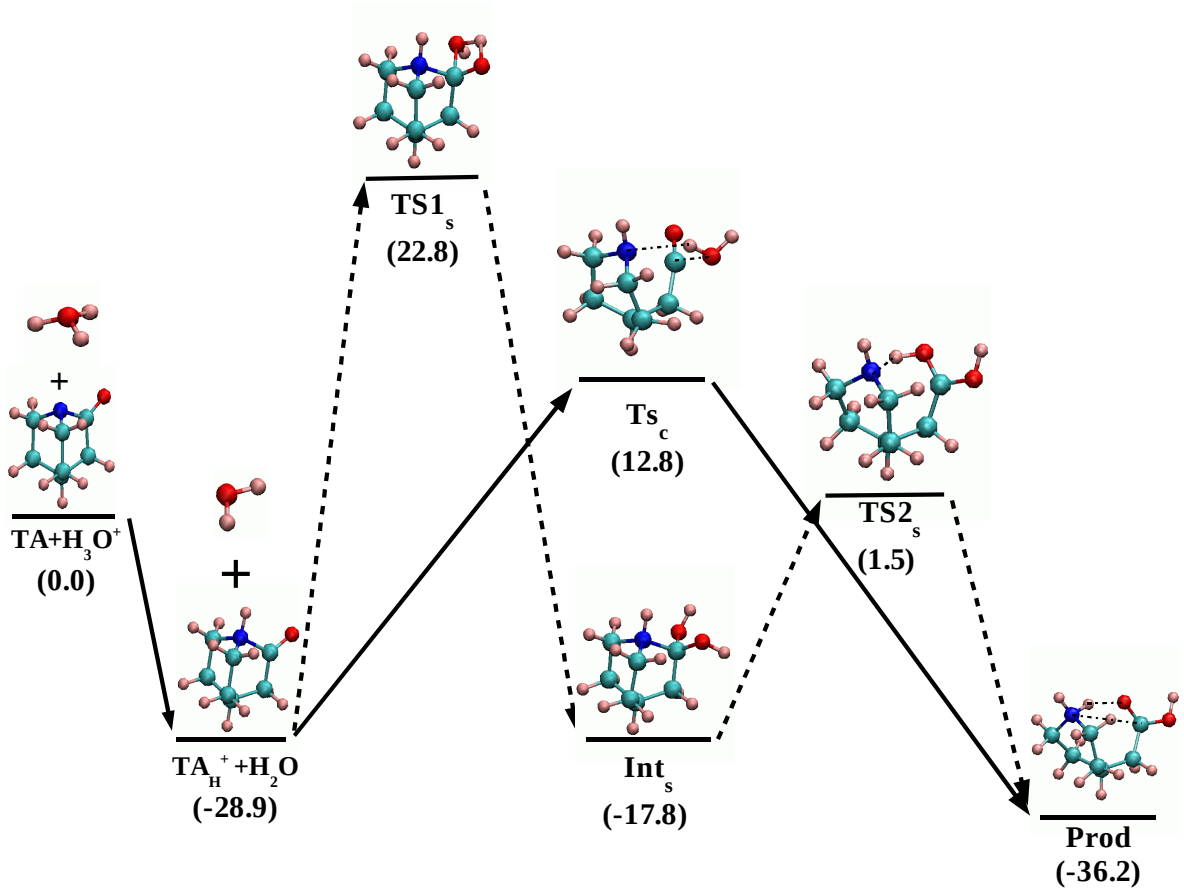

Figure 6.2: The PES for **TA** in the **Non-Assisted** hydrolysis reaction for both the concerted (regular-line) and stepwise (dashed-line) mechanism. The values correspond to Free Energy (ΔG) in kcal/mol for structures optimized in solution.

Table 6.1: B3LYP/6-31+G* geometrical parameters for the stationary points of the PES's of the **Non-Assisted** acidic hydrolysis of **TA** following the concerted and stepwise mechanisms. The bond distances are in Å and the angles and improper dihedrals in degrees for the structures optimized in gas-phase and in solution (in bold).

	Bond Distances							**Angles**			**Improper dh.**	
	Concerted mechanism											
	C_1-**N**	C_1-**O**	$C_1-O_{nu^-}$	H^1-O_{nu^-}	H^1-**N**	-	-	τ	χ_c	χ_n	**dh**$_C$	**dh**$_N$
TA	1.453	1.209	-	-	-	-	-	89.4	0.1	62.4	180.0	117.2
	1.448	**1.216**	**-**	**-**	**-**	**-**	**-**	**89.9**	**0.0**	**62.8**	**180.0**	**116.7**
TA_H	1.553	1.189	-	-	-	-	-	90.0	0.0	58.0	180	120.9
	1.529	**1.189**	**-**	**-**	**-**	**-**	**-**	**90.0**	**0.1**	**59.1**	**179.9**	**120.1**
HB	1.532	1.193	3.568	0.970	3.569	-	-	90.0	0.0	58.5	180	120.4
	1.516	**1.198**	**3.647**	**0.971**	**3.445**	**-**	**-**	**89.3**	**0.1**	**59.1**	**179.9**	**120.2**
TS$_c$	2.648	1.146	2.020	0.981	2.137	-	-	56.6	27.1	69.1	152.9	115.4
	2.603	**1.172**	**1.638**	**0.989**	**2.250**	**-**	**-**	**57.0**	**44.0**	**63.0**	**135.9**	**116.6**
Prod	3.455	1.229	1.332	3.888	1.044	-	-	87.4	9.0	67.7	179.2	116.1
	3.532	**1.224**	**1.341**	**4.056**	**1.033**	**-**	**-**	**86.5**	**11.3**	**67.8**	**178.9**	**117.5**
	Stepwise mechanism											
	C_1-**N**	C_1-**O**	$C_1-O_{nu^-}$	H^1-O_{nu^-}	H^1-**O**	H^2-O_{nu^-}	H^2-**N**	τ	χ_c	χ_n	**dh**$_C$	**dh**$_N$
$TS1_s$	1.564	1.291	1.633	1.193	1.348	0.980	3.247	28.1	40.4	57.3	139.7	120.3
	1.559	**1.309**	**1.568**	**1.184**	**1.365**	**0.984**	**3.224**	**18.8**	**42.5**	**58.5**	**137.4**	**120.2**
Int_s	1.561	1.392	1.383	2.671	0.974	0.975	2.775	23.5	56.7	57.3	126.3	123.3
	1.557	**1.390**	**1.384**	**2.635**	**0.975**	**0.977**	**2.725**	**28.1**	**57.9**	**57.4**	**122.3**	**123.3**
$TS2_s$	2.914	1.290	1.292	2.242	0.983	0.980	2.560	49.2	60.5	68.3	171.0	121.6
	3.019	**1.286**	**1.286**	**2.264**	**0.987**	**0.981**	**2.793**	**51.1**	**60.2**	**68.0**	**173.2**	**123.7**

Table 6.2: Relative Electronic Energies (ΔE_e), Zero-Point Energies (ΔE_o), Enthalpies (ΔH), Entropic Contributions ($T.\Delta S$) and Free Energies (ΔG) for the Stationary Points involved in the **Non-Assisted** Acidic Hydrolysis Reaction of **TA** in gas-phase and in solution (values presented in bold).

	ΔE_e	ΔE_0	ΔH	**T.**ΔS	ΔG
Concerted mechanism					
TA + H_3O^+	0.0	0.0	0.0	0.0	0.0
	0.0	**0.0**	**0.0**	**0.0**	**0.0**
$TA_H^+ + H_2O$	-64.4	-63.4	-63.4	-1.3	-62.1
	-31.2	**-30.2**	**-30.2**	**-1.3**	**-28.9**
HB	-80.4	-78.0	-77.9	-8.7	-69.2
	-38.0	**-36.3**	**-36.5**	**-8.6**	**-27.9**
TS_c	-43.0	-41.1	-41.9	-11.6	-30.3
	0.2	**2.1**	**1.3**	**-11.5**	**12.8**
Prod	-92.2	-86.6	-87.6	-11.7	-75.9
	-52.0	**-46.6**	**-47.6**	**-11.4**	**-36.2**
Stepwise mechanism					
$TS1_s$	-28.4	-26.8	-28.4	-13.0	-15.3
	9.2	**10.9**	**9.3**	**-13.6**	**22.8**
Int_s	-74.1	-68.6	-70.1	-13.1	-57.0
	-34.2	**-29.0**	**-30.5**	**-12.7**	**-17.8**
$TS2_s$	-52.2	-48.6	-49.9	-12.5	-37.4
	-12.3	**-9.5**	**-10.7**	**-12.3**	**1.5**

6.2.1 Non-assisted hydrolysis

We consider the unprotonated amide and the hydronium ion as the reactants of the reaction. This will facilitate the comparison with our previous work for the alkaline and neutral hydrolysis, in which obviously the reference amide was in its unprotonated form. The geometry of the unprotonated twisted amide is the one characterized in the previous reaction pathways, so their geometrical parameters have been previously explained (see page 82).

It is well established that the initial protonation of the amide by the hydronium ion lead to the N-protonated tautomer.[17,77,80] In fact, highly twisted amides can show very high pK_a values(5-7),[80] which indicates that the possibility that the hydrolysis of highly twisted amides goes through an acid-type reaction is available at significant higher pH's than for undistorted amides. In the protonated twisted amide (TA_H), the amide bond is highly activated and the C_1-N bond distance is 1.529 Å, 0.1 Å larger than in the unprotonated TA amide. Concomitantly, the C_1-O distance is 1.189 Å, 0.3 Å shorter. As expected, the protonation does not change the maximum degree of the twisting (τ is 90.0^o), the planarity of the C_1 atom (χ_C is 0.0^o) and the pyramidalization of the N atom (χ_N is 59.1^o).

The protonated amide TA_H and the attacking water molecule can form a hydrogen bonded complex when the water approaches the amide reactant. However, although the relative energy of this complex is lower than the TA_H plus water molecule in gas-phase, when the effect of the solvent is introduced its relative energy is higher and therefore this complex will not be relevant for the discussion of reactivity in the present chapter.

Concerted mechanism

Structures. The reaction pathway is depicted in Figure 6.2 and the geometrical parameters are presented in Table 6.1. The unique transition state of this reaction pathway corresponds to the nucleophilic attack of the O_{nu^-} at the carbonyl C_1 atom, concerted with a proton transfer from the water molecule to the nitrogen atom and the cleavage of the peptide bond. All these changes do not occur simultaneously. If we look at the geometry of the TS_c and based on the IRC pathway, we see that the nucleophilic attack is advanced (the O_{nu^-}-C_1 distance is 1.638 Å), and the C_1-N bond is almost broken (2.603 Å), although the proton is not transfered yet since this atom is much closer to O_{nu^-} than to the N atom (0.989 Å and 2.250 Å respectively). The early formation of the C_1-O_{nu^-} bond is also reflected in the conformation of the C_1 atom that has lost it planarity (the χ_C value is 44.0^o).

In the characterized product of the reaction the amide bond is completely broken (the C_1-N distance is 3.532 Å) and a carboxyl group is formed with a C_1-O_{nu^-} distance of 1.341 Å. Notice that the proton is fully transfered to the nitrogen (the N-H^1 and O_{nu^-}-H^1 distances are 1.033 Å and 4.056 Å respectively). Besides, one of the protons bound to nitrogen is hydrogen bonded to the unprotonated oxygen of the carboxylic group. Because of the cleavage of the amide bond, τ, χ_C and χ_N angles have lost their meaning and in order to get useful information on the conformation of atoms around the nitrogen and carbon atoms, it is more appropriate to analyze the values of the improper dihedrals. In this sense, it can be observed that the C_1 atom has recovered its planarity (dh_C is 178.9^o) and the nitrogen has adopted a pyramidal conformation (dh_N is 117.5^o).

Energy profile. The relative energies for the different stationary points of this reaction pathway are presented in Table 6.2 for the geometries optimized in gas-phase and in solution. The relative energies are separated in their different contributions. In gas-phase, all the electronic energies are negative due to high stabilization caused by the proton transfer from hydronium to the amide (-64.4 kcal/mol). Inclusion of ZPVE corrections increases the relative energies between 1 to 5 kcal/mol. Entropic contributions also increase the relative energy of the species with respect to reactants because of the loss of translational and rotational degrees of freedom when rearranging from two infinitely separated reactants into one single molecular structure.

Accordingly, in gas-phase the reaction is exothermic with a ΔH_{gas} of -87.6 kcal/mol and a free energy barrier of -30.3 kcal/mol.

Bulk solvent effects favor the separated reactants and specially the reactants that combine charge with small volume, i.e., the hydronium ion. As a consequence, there is a substantial increase of relative energies of all the species with respect to the unprotonated amide plus hydronium molecule, although the energy profile is analogous to the gas-phase. The reaction is still very exothermic with a reaction enthalpy of -47.6 kcal/mol, and a free energy barrier of 12.8 kcal/mol.

Stepwise mechanism

In the stepwise mechanism the hydrolysis reaction takes place in two steps (apart from the initial amide protonation step): i) the nucleophilic attack of the water molecule at the carbonyl C_1 atom concerted with a proton transfer from the water molecule to the oxygen atom forming a tetrahedral intermediate and ii) the cleavage of the C_1-N peptide bond concerted with a proton transfer from one of the oxygens to the nitrogen atom. The reaction pathway is depicted in Figure 6.2.

Structures. Selected geometrical parameters are shown in Table 6.1. The reactant and the product are the same than in the concerted mechanism. The first transition state ($TS1_s$) corresponds to the nucleophilic attack of the O_{nu^-} water oxygen atom on the carbonyl group concerted with a proton transfer from the water molecule to the carbonyl oxygen. The C_1-O_{nu^-} bond distance is 1.568 Å, slightly shorter than in the concerted mechanism (1.638 Å). The nucleophilic attack changes the conformation of the C_1 atom adopting a non-planar conformation (χ_C is 42.5^o). The H^1 is transfered from the water molecule to the carbonyl oxygen and at $TS1_s$ the proton is shared by both atoms, although is slightly closer to O_{nu^-} (1.184 Å) than to the carbonyl O atom (1.365 Å). The C_1-N amide bond is only slightly elongated by 0.03 Å at $TS1_s$ with respect to the amide bond in protonated amide.

At intermediate Int_s, the proton transfer is completed (O-H^1 is 0.975 Å) and the C_1 atom is bound to two oxygen atoms with similar distances (1.390 and 1.384 Å) and in a tetrahedral conformation. The amide bond distance is still very similar, 1.557 Å, to the one shown by the protonated amide, 1.529 Å. Kirby *et al.* characterized[57] by X-ray diffraction the tetrahedral intermediate in the hydrolysis reaction of a highly twisted amide similar to our TA (illustrated in Figure 6.3). There is a very nice agreement of our structure with the X-ray structure for the intermediate of Kirby: they determined a peptide bond distance of 1.552(4) Å and in our optimized structure is 1.557 Å, in addition, the two C-O bond distances for their structure were 1.382(4) Å, while in our tetrahedral intermediate are 1.384 and 1.390 Å. This suggests that the intermediate trapped by Kirby *et al.* corresponded

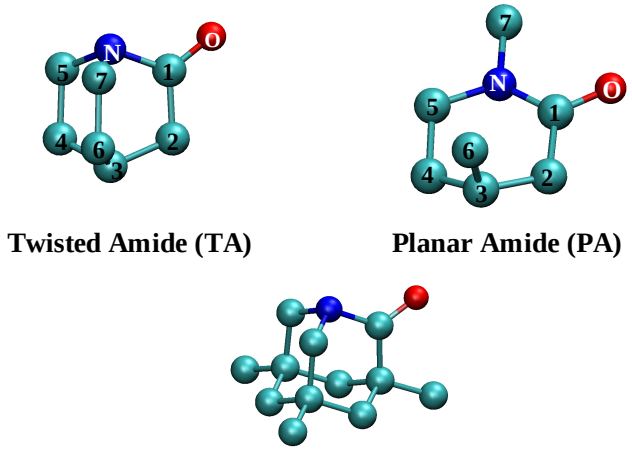

Figure 6.3: Above the two amide reactants used along the present study: on the left-hand side **TA** and on the right-hand side **PA**. Below, the highly twisted amide characterized by Kirby *et al.*[57] For clarity, the hydrogen atoms are not depicted.

to the intermediate of the acid-hydrolysis reaction (see Discussion, Section 6.3).

The second step of the reaction is the cleavage of the amide bond concerted with a proton transfer from one of the oxygens to the nitrogen atom. The transfered proton is the one bound to the O_{nu^-} atom (H^2). The bond breaking/forming process are not synchronous. At the $TS2_s$ transition state, the proton transfer is at a very early stage (the H^2-O_{nu^-} distance is 0.981 Å) while the amide cleavage is quite advanced (the C_1-N distance is broken 3.019 Å).

Energy profile. The relative energies for this reaction are presented in Table 6.2. The reactant and the product are the same of the concerted mechanism so the reaction is exothermic both in gas phase and in solution. The relative free energies in the gas phase of $TS1_s$ and $TS2_s$ are -15.3 and -37.4 kcal/mol respectively, so the first step is clearly rate-limiting. When solvent effects are considered both barriers increased to 22.8 kcal/mol ($TS1_s$) and 1.5 kcal/mol ($TS2_s$), but still the first step is the clear rate-limiting step. The relative free energy of the intermediate is -57.0 kcal/mol in the gas phase and -17.8 in solution. Thus, the barrier for intermediate cleavage is around 19.3 kcal/mol in solution, a sufficient high barrier to have a significant lifetime to be detected.

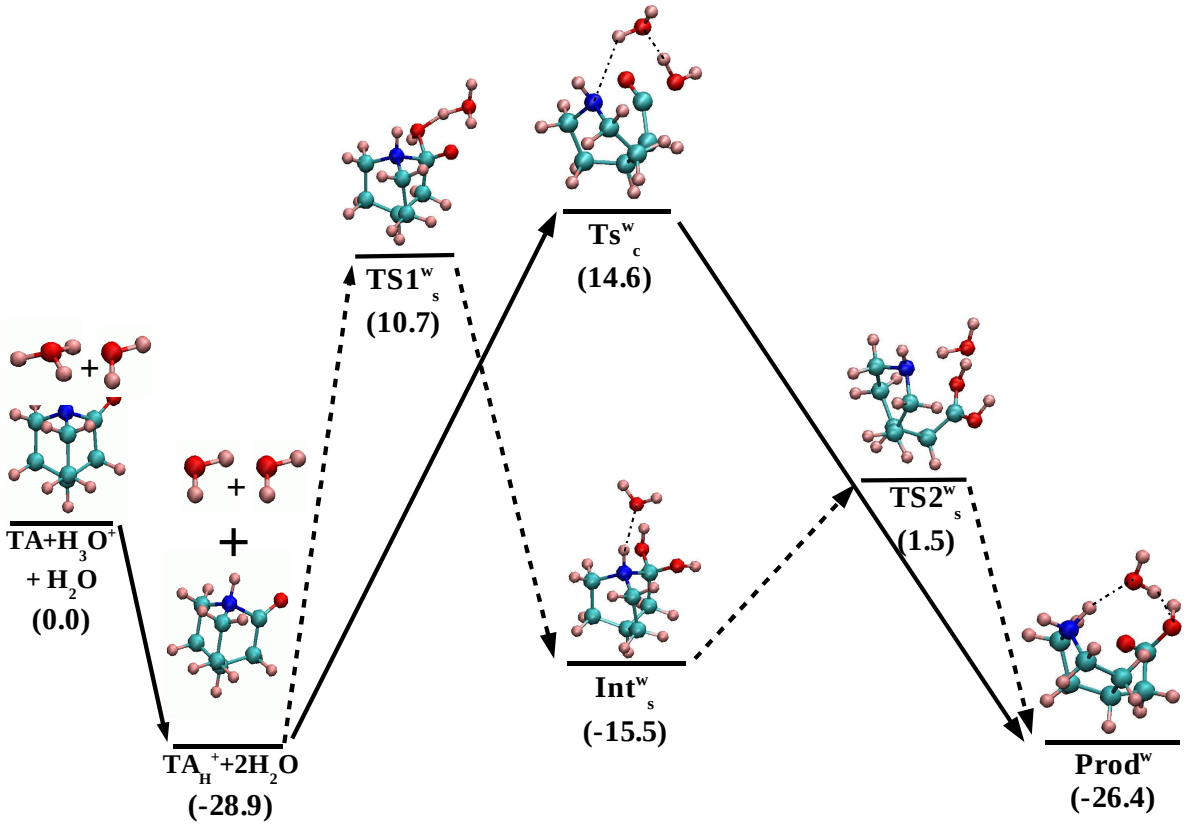

Figure 6.4: The B3LYP/6-31+G(d) structures for **TA** in the **Water-Assisted** hydrolysis reaction for both the concerted (regular-line) and stepwise (dashed-line) mechanism. The values correspond to the relative free energy (ΔG) in kcal/mol for structures optimized in solution.

Table 6.3: B3LYP/6-31+G* geometrical parameters for the stationary points of the PES's of the **Water-Assisted** acidic hydrolysis of **TA** following the concerted and stepwise mechanisms. The bond distances are in Å and the angles and improper dihedrals in degrees for the structures optimized in gas-phase and in solution (in bold).

	Bond Distances										**Angles**			**Improper dh.**	
	Concerted mechanism														
	C_1-**N**	C_1-**O**	$C_1-O_{nu^-}$	H^1_{nu}-O_{nu^-}	H^1_{nu}-O_{as}	$H^1_{as}-O_{as}$	H^1_{as}-**N**	-	-	-	τ	χ_c	χ_n	**dh**$_C$	**dh**$_N$
TA	1.453	1.209	-	-	-	-	-	-	-	-	89.4	0.1	62.4	180.0	117.2
	1.448	**1.216**	**-**	**-**	**-**	**-**	**-**	**-**	**-**	**-**	**89.9**	**0.0**	**62.8**	**180.0**	**116.7**
TA_H	1.553	1.189	-	-	-	-	-	-	-	-	90.0	0.0	58.0	180	120.9
	1.529	**1.189**	**-**	**-**	**-**	**-**	**-**	**-**	**-**	**-**	**90.0**	**0.1**	**59.1**	**179.9**	**120.1**
TS_c^W	2.905	1.161	1.731	1.039	1.513	0.973	2.554	-	-	-	32.4	39.1	69.3	174.2	117.7
$Prod^W$	4.046	1.375	1.210	3.735	0.976	1.785	1.042	-	-	-	86.9	65.5	58.7	180.0	119.3
	Stepwise mechanism														
	C_1-**N**	C_1-**O**	$C_1-O_{nu^-}$	H^1_{nu}-O_{nu^-}	H^1_{nu}-O_{as}	H^1_{nu}-**N**	$H^2_{nu}-O_{nu^-}$	$H^2_{nu}-O_{as}$	$H^1_{as}-O_{as}$	H^1_{as}-**O**	τ	χ_c	χ_n	**dh**$_C$	**dh**$_N$
$TS1_s^W$	1.619	1.260	1.626	1.310	1.143	3.382	0.974	2.959	1.021	1.640	35.4	47.4	57.6	132.6	120.4
	1.631	**1.267**	**1.583**	**1.280**	**1.166**	**2.971**	**0.978**	**2.912**	**1.013**	**1.713**	**36.8**	**48.7**	**59.1**	**131.2**	**120.0**
Int_s^W	1.557	1.402	1.375	3.408	0.973	3.463	0.982	2.013	3.762	0.973	33.2	58.3	42.3	121.7	123.4
	1.555	**1.397**	**1.380**	**3.414**	**0.973**	**3.516**	**0.987**	**1.886**	**3.830**	**0.975**	**33.0**	**58.6**	**58.0**	**121.4**	**123.3**
$TS2_s^W$	3.381	1.305	1.274	2.656	1.051	1.646	1.072	1.436	2.213	0.984	40.8	62.5	68.8	173.7	116.9
	3.040	**1.290**	**1.286**	**2.764**	**0.984**	**2.184**	**1.010**	**1.697**	**1.823**	**0.999**	**34.2**	**61.4**	**69.4**	**178.5**	**116.6**
$Prod^W$	4.046	1.375	1.210	4.313	1.785	1.042	3.735	0.976	3.228	0.980	86.9	65.5	58.7	180.0	119.3

Table 6.4: Relative Electronic Energies (ΔE_e), Zero-Point Energies (ΔE_o), Enthalpies (ΔH), Entropic Contributions ($T.\Delta S$) and Free Energies (ΔG) for the Stationary Points involved in the **Water-Assisted** Acidic Hydrolysis Reaction of **TA** in gas-phase and in solution (values presented in bold). The reference was chosen as TA + H_3O^+ + H_2O

	ΔE_e	ΔE_0	ΔH	**T.**ΔS	ΔG
Concerted mechanism					
TA + $H_3O^+ + H_2O$	0.0	0.0	0.0	0.0	0.0
	0.0	**0.0**	**0.0**	**0.0**	**0.0**
$TA_H^+ + 2(H_2O)$	-64.4	-63.4	-63.4	-1.3	-62.1
	-31.2	**-30.2**	**-30.2**	**-1.3**	**-28.9**
HB	-88.0	-82.9	-83.6	-18.5	-65.0
	-41.1	**-37.2**	**-38.5**	**-19.8**	**-18.7**
TS_c^W	-53.1	-49.1	-50.4	-20.5	-29.9
			-5.9*		**14.6***
Prod	-96.4	-88.6	-90.0	-20.2	-69.8
			-47.0*		**-26.8***
Stepwise mechanism					
$TS1_s^W$	-60.7	-55.5	-58.3	-24.0	-34.3
	-15.3	**-10.6**	**-13.5**	**-24.2**	**10.7**
Int_s^W	-90.5	-82.4	-84.5	-22.7	-61.8
	-42.3	**-35.2**	**-37.1**	**-21.6**	**-15.5**
$TS2_s^W$	-74.0	-68.4	-71.0	-23.9	-47.1
	-24.8	**-19.1**	**-21.3**	**-22.8**	**1.5**

(*) Geometries optimized in gas-phase

6.2.2 Water-assisted hydrolysis

In this type of mechanisms, the reaction is catalyzed by an extra water molecule which assists in the proton transfer processes along the reaction. The reference reactants for this reaction are the unprotonated amide, an hydronium ion and a water molecule. After the protonation of the amide TA_H, we have two independent water molecules, one of them acts as the nucleophile whereas the other is the assistant water molecule serving as a bridge in proton transfers. Along the reaction pathway there are two different protons that are transfered (H^1_{nu} and H^1_{as}) which are defined in Figure 6.1. This section is subdivided analogously to the previous section, first we discuss the concerted mechanism, and then, the stepwise mechanism. Besides, in each case we first present the structures and then the energies. A diagram showing the final free energies for each stationary point of both pathways can be found in Figure 6.4.

Concerted mechanism

Structures. Selected geometrical parameters can be found in Table 6.3. The reactant structures are the same than in the non-assisted reaction, so we do not describe them in this section. Several attempts to optimize the geometries of TS_c^W and $Prod^W$ with SCI-PCM method failed, so their geometries correspond to gas-phase optimizations. Bulk solvent effects for these structures were determined by single-point calculations at the gas-phase geometries. The error due to this fact is expected to be small because gas-phase and solution geometries are in general very similar for the rest of mechanisms characterized in this chapter.

The transition state of the water-assisted concerted mechanism TS_c^W shows a quite advanced nucleophilic attack with a C_1-O_{nu^-} distance of 1.731 Å, the cleavage of the C_1-N bond is also quite accomplished at the transition state (C_1-N distance is 2.905 Å), but the protons are not transfered yet. The H^1_{nu} atom is closer to the O_{nu^-} atom (1.039 Å) than to the O_{as} atom (1.513 Å) and the H^1_{as} atom is still bound to the O_{as} (0.973 Å). The C_1-N distance is 0.3 Å longer than in the non-assisted TS_c and the C_1-O_{nu^-} distance is longer as well but by only 0.1 Å.

The product of the reaction is analogous to the one of the non-assisted reaction, the main difference being that the C_1-N distance is 0.5 Å longer than in the non-assisted case, i.e., 4.046 Å. This is due to the presence of the additional water molecule, which forms two hydrogen bonds, one with the amine and the other with the carboxylic group.

Energy profile. Relative energies for the different structures of the water -assisted mechanism can be found in Table 6.4. The reference reactants for the calculation of relative energies are the twisted amide, the hydronium ion and a water molecule. The fact that as reference state we have three infinitely separated reactants make the entropic contributions to increase significantly the relative energies of the transition state and product with respect to the reactants, by around 20 kcal/mol. This is due to the lose of the rotational and translational entropy. As a consequence, when looking at the gas-phase enthalpic barrier we can state a significant catalytic effect of the assistant water molecule. Thus the relative energy of TS_c^W is -50.4 kcal/mol, lower than the energy of the non-assisted TS_c, -41.9 kcal/mol. However, if we look at the relative free energies now the numbers are more similar, -29.9 kcal/mol for TS_c^W and -30.3 kcal/mol for TS_c.

The inclusion of the bulk solvent effect again favors the separated reactants, and hence, higher relative energies are obtained. We emphasized however, that in this case these bulk solvent effects have been evaluated at the gas-phase geometries, and therefore they are less reliable. The final aqueous free energy barrier for the reaction is 14.6 kcal/mol and the reaction free energy is -26.8 kcal/mol.

Stepwise mechanism

In the stepwise mechanism, the auxiliary water molecule acts as a bridge in proton transfer in both steps of the reaction. An scheme with the nomenclature for the transfered protons can be found in Figure 6.1. There are two protons that are transfered along the reaction pathway: i) H^1_{nu} is initially located at the nucleophilic water molecule, in the first step this proton goes to the assistant water molecule whereas in the second step it goes to the nitrogen ii) H^1_{as} initially is located at the assistant water molecule, in the intermediate is bound to the carbonyl oxygen and in the second step it returns back to the assistant water molecule.

Structures. The structures optimized in solution with the SCI-PCM method are shown in Figure 6.4 and selected geometrical parameters can be found in Table 6.3. For this pathway, we were able to optimize all the structures with the SCI-PCM method, and we will comment only these geometries throughout the text below. The first step corresponds to the nucleophilic attack of O_{nu^-} on the carbonyl group and a proton transfer to the oxygen atom of the carbonyl group. $TS1^W_s$ is the transition state for this first step, which shows a O_{nu^-}-C_1 distance of 1.583 Å, very similar to the one in the non-assisted $TS1_s$ (1.568 Å), and 0.2 Å shorter than in the concerted TS^W_c transition state. Therefore, at the transition state the nucleophilic attack is more advanced than in the concerted mechanism with little influence of the assistant water molecule in this behavior. H^1_{nu} proton is located at very similar distances from O_{nu^-} (1.280 Å) and O_{as} (1.166 Å), however, the H^1_{as} proton transfer is still at an early stage, being H^1_{as}-O_{as} distance 1.013 Å. Finally the amide C_1-N bond distance is 1.631 Å, 0.072 Å longer than in the non-assisted case.

The structure of the intermediate in the water-assisted mechanism Int^W_s is very similar to the intermediate Int_s of the non-assisted case. The difference between both structures is that in Int^W_s, there is a water molecule hydrogen bound to the proton of the nitrogen. The bond distances of the near-by atoms to the carbon and to the nitrogen are very similar in both cases. The C_1 atom presents the typical tetrahedral conformation (χ_C is 58.6^o) for the intermediate of the reaction, and the C_1-N bond distance is 1.555 Å, only slightly elongated (by around 0.02 Å) with respect to the protonated amide reactant. As in the non-assisted reaction, we remark the coincidence between the geometrical parameters for our optimized intermediate and the characterized geometrical data by X-ray diffraction (amide bond distance of 1.552(4) Å and C-O bond distances were 1.382(4) Å).

The transition state for the second step of the reaction, $TS2^W_s$, shows a quite long C_1-N distance, namely 3.040 Å, slightly longer than in the non-assisted $TS2_s$, 3.019 Å, and around 0.1 Å larger than in the concerted TS^W_c. However, the degree of proton transfer is low, since H^1_{nu} and H^1_{as} protons are still bound to O_{as} and O respectively. The H^1_{nu} proton is at 0.984 and 2.184

Å with respect to O_{as} and N, respectively, whereas H^2_{nu} is at 1.010 and 1.697 Å with respect to O_{nu^-} and O_{as}. Therefore, there is a high asynchrony in the second step of the reaction between amide bond cleavage and proton transfer, the former occurring first than the latter.

Energy profile. Relative energies are summarized in Table 6.4. As in the non-assisted case, the first step of the reaction, $TS1^W_s$ is the rate-limiting step, however, the effect of the assistant water molecule in relaxing the corresponding barriers is more important than for the concerted mechanism. In the gas-phase, the ΔH of $TS1^W_s$ is -58.3 kcal/mol, 29.9 kcal/mol lower than in the non-assisted reaction, whereas ΔG is -34.3 kcal/mol, 19.0 kcal/mol lower than in the non-assisted reaction. On the other hand, the ΔG of TS2 is -47.1 kcal/mol, almost 10 kcal/mol lower than the non-assisted TS2.

Bulk solvent effects again favor the separated reactants although the effect is not the same at both transition states. The solvation free energy for $TS1^W_s$ is higher (in absolute value) than for $TS2^W_s$. Nevertheless, the first step of the reaction is still rate limiting with a free energy barrier of 10.7 kcal/mol versus the 1.5 kcal/mol relative free energy displayed by $TS2^W_s$. Also, comparing these numbers with the values obtained for the concerted mechanism, we can conclude that the relative free energies and enthalpies for the transition states of the stepwise mechanism are lower than the barrier obtained for the transition state of the concerted mechanism (ΔG of TS^W_c was 14.6 kcal/mol), therefore, we can say that the water-assisted stepwise mechanism is the preferred pathway for the acidic hydrolysis of the highly twisted amide **TA**. This implies the formation of an intermediate structure with a sufficient long lifetime to be detected, since the difference in free energy between this intermediate and $TS2^W_s$ is 17.0 kcal/mol.

6.2.3 Planar amide as reference

In order to determine the rate acceleration of the acidic hydrolysis caused by the twist of the amide bond, the same methods as in the previous section were employed to characterize barriers for the acidic hydrolysis of an undistorted planar amide **PA** (see Figure 6.3) closely related to the highly twisted amide **TA**, which comes from the hydrogenation and cleavage of the **TA** C_6-C_7 bond. This leads to the breaking of the cage structure relaxing the geometrical constraints that maintained the amide bond in a twisted conformation. The **PA** reactant now shows a planar untwisted amide bond with a corresponding low value of τ, 1.8^o, and a nitrogen atom in a quasi-planar conformation ($\chi_N = 8.4^o$). This is the standard situation for an undistorted amide bond with some degree of delocalization between the lone pair of the nitrogen and carbonyl π bond, leading to a partial double C_1-N bond character. In fact, the C_1-N bond length is shorter, 1.363 Å, than for the twisted amide reactant, 1.448 Å. An important difference in the acid hydrolysis of planar and twisted amides, is that the protonation of

the planar amide reactant occurs at the oxygen, and therefore, we have a different mechanism for the acid hydrolysis compared to the one previously described for the twisted amide. In addition, the O-protonation makes the concerted mechanism to be very unlikely, since it would require a double proton transfer to the nitrogen atom in an unique step. Therefore, only a stepwise mechanism was considered in this case.

Table 6.5: Relative Electronic Energies (ΔE_e), Zero-Point Energies (ΔE_o), Enthalpies (ΔH), Entropic Contributions ($T.\Delta S$) and Free Energies (ΔG) for the stationary points involved in the Acidic Hydrolysis Reaction of **PA** in gas-phase and in solution (values presented in bold), for both **Non-Assisted** and **Water-Assisted** reaction pathways.

	ΔE_e	ΔE_0	ΔH	**T.**ΔS	ΔG
Non Assisted					
PA + H_3O^+	0.0	0.0	0.0	0.0	0.0
	0.0	**0.0**	**0.0**	**0.0**	**0.0**
$PA_H^+ + H_2O$	-57.8	-57.7	-57.6	-0.7	-56.9
	-21.0	**-21.1**	**-21.0**	**-0.8**	**-20.2**
HB	-77.1	-75.2	-75.4	-9.1	-66.3
TS1	-13.6	-13.1	-14.7	-13.1	-1.6
	26.7	**26.9**	**25.3**	**-13.0**	**38.3**
Int	-48.2	-43.9	-45.3	-12.5	-32.8
	-7.7	**-3.4**	**-4.8**	**-12.4**	**7.7**
TS2	-27.0	-24.3	-25.6	-12.0	-13.6
	10.6	**12.9**	**11.7**	**-11.4**	**23.1**
Prod	-64.9	-60.4	-61.3	-10.8	-50.5
	-26.9	**-22.3**	**-23.3**	**-11.1**	**-12.2**
Water Assisted					
PA + H_3O^+ + H_2O	0.0	0.0	0.0	0.0	0.0
	0.0	**0.0**	**0.0**	**0.0**	**0.0**
$PA_H^+ + 2(H_2O)$	-57.8	-57.7	-57.6	-0.7	-56.9
	-21.0	**-21.1**	**-21.0**	**-0.8**	**-20.2**
TS1^w	-34.7	-31.2	-34.0	-23.8	-10.2
	10.2	**14.0**	**11.2**	**-24.0**	**35.2**
Int^w	-61.3	-55.0	-56.6	-20.9	-35.7
	-13.9	**-8.0**	**-9.6**	**-21.1**	**11.5**
TS2^w	-52.2	-48.0	-50.5	-23.1	-27.5
			-1.4(*)		**21.7(*)**
Prod^w	-77.5	-70.9	-72.2	-19.6	-52.6
			-24.9(*)		**-5.3(*)**

(*) Geometries optimized in gas-phase

The energetic values are presented in Table 6.5. Due to presence of the methyl group at the C_3 position there are two possibilities for the reaction, which correspond to attacks and proton transfers in an exo or an endo posi-

tion with respect to this methyl group. However, as it was shown definitely in the neutral hydrolysis,[81] the endo attack is more stable pathway. Hence, we discuss only this reaction pathway.

The energetic barriers are higher than the barriers of the twisted amide. In the gas-phase all the relative energies (electronic, enthalpic, free energy) are negative with respect to the unprotonated amide and water reactants due to the high energy relaxation upon amide protonation. The inclusion of solvent effects lead to higher relative energies, and now the transition states and intermediate show positive relative free energies. The first step of the reaction is the rate-limiting step with a free energy barrier of 38.3 kcal/mol in the non-assisted mechanism and 35.2 in the water-assisted mechanism.

Comparison with the available experimental data and theoretical calculations on acidic hydrolysis are not free of difficulties due to the different amide reactants and reference states used in theoretical calculations when evaluating relative energies. Experimentally, Guthrie *et al.*[59] reported an activation free energy for DMF of 26.3 kcal/mol at 25 ^{0}C, while Langlois and Broche[217] determined an activation energy of 18.4 kcal/mol for the same undistorted amide. Besides, Bolton and co-workers[218,219] measured the acidic hydrolysis for a large set of primary amides. They found that the activation energy was in the range of 18.8-21.5 kcal/mol. More recently, the group of Brown[200] reported the study of the formamide hydrolysis and they estimated a ΔH of 17.0 $\pm$ 0.4 kcal/mol for the acidic hydrolysis. These values for enthalpic and free energy barriers are significantly smaller than the ones characterized in the present work for planar amide **PA**, which shows an enthalpic barrier of 32.2 kcal/mol and free energy barrier of 55.4 kcal/mol with respect to the protonated amide plus two water molecules infinitely separated.

On the other hand, most of the theoretical studies for the acid hydrolysis of amides are based in formamide as amide reactant. Krug *et al.*[62] determined the acidic hydrolysis for the formamide in gas-phase taken into account both the N- and O- protonation state at the MP2/6-31G**//4-31G level of theory, where they obtained an electronic energy barrier of 24.0 kcal/mol for the O-protonated case, the analogous pathway to our planar amide, choosing the protonated amide and separately water molecules as reference. On the other hand, Antonczak *et al.*[64,65] used as reference the hydrogen-bonded structure between formamide and a water molecule plus another water molecules infinitely separated that acted as the nucleophile of the reaction. They obtained an electronic energy barrier of 27.6 and -6.9 kcal/mol for the non-assisted and water-assisted reaction respectively, at MP2/6-31G**//B3LYP/6-31G** level of theory in gas-phase. Manojkumar *et al.*[220] calculated an electronic barrier of 24.5 kcal/mol using the same reference for the acidic hydrolysis of formamide at MP2/6-311++G**//B3LYP/6-311++G**. Since, these values were lower than the barrier characterized for **PA**, we calculated the energy barriers for TS1 of

both formamide and N,N dimethyl-acetamide (DMA) using the same protocol described in Methodology (page 83), considering both the non-assisted and water-assisted pathway. The departing structure for the optimization was "equivalent" to the TS1 of PA, where we kept the same geometrical disposition for the water molecule(s) and the amide bond, changing in each case the side chain for the formamide and N,N dimethyl acetamide. In the case of the formamide, we obtained an electronic barrier of 29.2 kcal/mol for the non-assisted reaction and -4.6 kcal/mol for the water-assisted reaction, in good agreement with the results presented by Antonczak *et al.*[64,65] On the other hand, the electronic barrier of DMA was found to be 40.3 kcal/mol in the non-assisted reaction and 15.3 kcal/mol in the water-assisted one, clearly closer to the barrier of **PA** (44.2 and 23.1 kcal/mol respectively) than to the formamide's. Based on these results, we can conclude that our methodology is appropriate and that is coherent with previous ab-initio calculations. The higher barrier for the hydrolysis of the **PA** compound could be due to the fact that tertiary amides show higher barriers than formamide, and also, the ring structure of **PA** could be contributing with some stheric effect to a higher barriers than in N,N dimethyl acetamide. However, as the main purpose of this study is the rate-acceleration due to the amide bond twist, it is important to keep analogous geometries for both twisted and planar amide as it is the case for **TA** and **PA**, with the aim of isolating the effect of the amide bond.

6.3 Discussion

The general picture that comes from our calculations (see Figure 6.5) is that the first step of the reaction in the water-assisted stepwise mechanism, nucleophilic attack on the amide carbon, is the rate-limiting step for the acid hydrolysis of both twisted and planar amides. In the case of the twisted amide, the concerted pathway implies a higher enthalpic and free energy barrier, both in the gas phase and in solution. That is, the final aqueous free energy barriers are 10.7 kcal/mol for $TS1_s$ and 14.6 kcal/mol for TS_c, measured with respect to the unprotonated amide and hydronium molecule. In addition, the aqueous enthalpic barriers also favor $TS1_s$ (-13.5 kcal/mol) over TS_c (-10.8 kcal/mol). Besides, gas-phase free energies and enthalpies favor the stepwise mechanism over the concerted one. In summary, the acid hydrolysis of our highly twisted amide goes through a stepwise mechanism with formation of an intermediate and first step as rate-limiting, contrary to the behavior previously described for the neutral hydrolysis of this same species,[81] for which a concerted pathway is preferred.

Evidences for a stepwise mechanism comes from the experiments of Kirby *et al.*,[56–58] who conducted hydrolysis of a twisted amide with a similar degree of twisting as TA. At slightly acidic pH, an intermediate could be trapped,

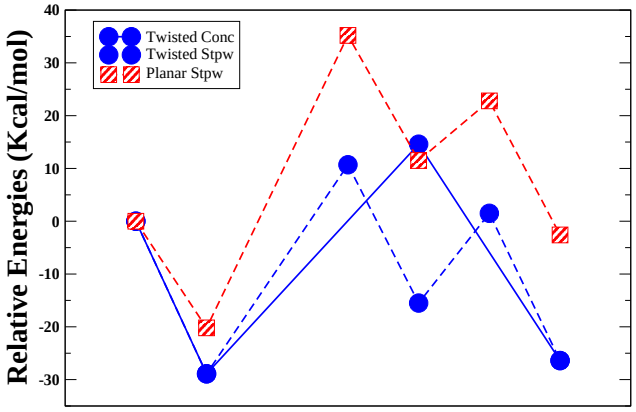

Figure 6.5: Aqueous free energy reaction profiles comparing the **Water-Assisted** hydrolysis reaction through a concerted and a stepwise mechanism between **TA** and **PA**.

which shows a very nice agreement in its geometrical properties as the one characterized with the present work (see Results, Section 6.2). These intermediate was very rapidly cleavaged upon pH neutralization, a fact that can be explained by the low barriers for intermediate cleavage $TS2_s$ in the neutral hydrolysis,[81] 9.0 kcal/mol, and the higher barrier for intermediate cleavage found at the acid hydrolysis in the present work, 17.0 kcal/mol, allowing a significant lifetime for the acid-hydrolysis intermediate. It should be also emphasized that pK_a estimations for these types of twisted amides[80] points to values between 5-7 units, indicating that the acid-hydrolysis regime for highly twisted amides is accessible at only slightly acidic pH's.

On the other hand, Wang *et al.*[55] have determined the enthalpic and free energy barriers for the hydrolysis of a highly twisted amide. The values are 10.3 kcal/mol for $\Delta H^{\neq}$ and there is a quite high entropy induced barrier of 5-6 kcal/mol, as expected for highly ordered transition states with various protons in flight. These experimental barriers are reflecting the water attack requirements on the already protonated amide[55] and are therefore to be compared to our values with $TAH^+ + 2(H_2O)$ as reference. Taking into account $TS1_s$, we obtain an enthalpic barrier of 5.1 kcal/mol in the gas-phase and 16.7 kcal/mol in solution, whereas the free energy barriers are 27.8 kcal/mol and 39.6 kcal/mol in gas-phase and aqueous phase, respectively. Thus, our calculated barriers in the aqueous-phase are significantly larger than the experimental ones, specially after entropic contributions are considered. This behavior have also been observed in the comparison of previous

Table 6.6: Relative ΔH's and ΔG's of the different transition states between **PA** and **TA** in kcal/mol for the structures optimized in gas-phase and in solution (in bold), for both the **Non-Assisted** and **Water-Assisted** reactions.

	ΔH_{twist}	ΔH_{planar}	$\Delta\Delta H$	ΔG_{twist}	ΔG_{planar}	$\Delta\Delta G$
Non Assisted						
$TS1_s$	-28.4	-14.7	13.7	-15.3	-1.6	13.7
	9.3	**25.3**	**16.0**	**22.8**	**38.3**	**15.5**
$TS2_s$	-49.9	-25.6	24.3	-37.4	-13.6	23.8
	-10.7	**11.7**	**22.4**	**1.5**	**23.1**	**21.6**
Water Assisted						
$TS1_s$	-58.3	-34.0	24.3	-34.3	-10.2	24.1
	-13.5	**11.2**	**24.7**	**10.7**	**35.2**	**24.5**
$TS2_s$	-71.0	-50.5	20.5	-47.1	-27.5	19.6
	-21.3	**-0.3**	**21.0**	**1.5**	**22.8**	**21.3**

theoretical calculations and experimental values.[200] There could be several reasons for the observed differences. First, the exact values of the aqueous barriers are highly sensitive to bulk solvent effects, and small variations in the specific solvation free energies for each of the charged species can lead to substantial differences in the actual values of the barriers. Besides, the high entropic penalties for the reaction observed in the calculations are partially due to the highly order nature of our transition states, but also they are due to the big loss of translational and rotational degrees of freedom when going from the three infinitely separated isolated reactants (protonated amide plus two water molecules) to the supramolecular transition state structure. Our calculations describe the separated reactants as isolated entities with non-constrained translational and rotational motions, i.e., leading to a very high entropy. However, the solute reactants and water molecules in a real system will not have such a degree of freedom due to interactions with nearby solvent molecules. In this sense, a more realistic reference state for the calculations could then be some type of hydrogen bonded supracomplex, which could be characterized with simulations with a significant amount of specific solvent molecules around the amide solute.[75,221]

Nevertheless, our main interest is to describe the rate-acceleration of the hydrolysis of the twisted amide versus the planar amide, i.e., determine relative barriers ($\Delta\Delta G$) between closely related reactions. One then can expect a suitable cancellation of methodological errors, specially, if approximations of the same kind are made when choosing the reference states for both reactions. Kinetic studies have revealed that the acid hydrolysis of highly twisted amides measured for a series of highly twisted anilides are 11 orders of magnitude faster than the reactions with planar N-methyl acetanilide,[2] which corresponds to differences in k_1/K_a values (that is, both

the protonation (K_a) and hydrolytic (k_1) steps are involved). This implies a differential in free energy barrier ($\Delta\Delta G^{\neq}$) of 25.3 kcal/mol (ln 10^{11}) with unprotonated amide as reference. In Table 6.6, the theoretical data for the $\Delta\Delta H$ and $\Delta\Delta G$ in the assisted and non-assisted mechanism are collected. Our calculated value for the $\Delta\Delta G$ in aqueous phase when the rate limiting transition state $TS1_s$ is considered is 24.5 kcal/mol, in excellent agreement with the experimental estimates. Thus it seems that our model systems for the hydrolysis of a highly twisted amide are capturing the essential features of the distinct reactivity of twisted amides versus planar amides, although to reach quantitative agreement for the absolute barriers for each reaction probably better models are required, including a higher number of explicit water molecules and more accurate solvation models. It is remarkable that the values of $\Delta\Delta H$ and $\Delta\Delta G$ are similar for each reaction type, indicating that differential entropic effects between planar and twisted amide reactions are small. In addition, gas-phase and aqueous-phase $\Delta\Delta H$ and $\Delta\Delta G$ values for each reaction type are also very similar. For example, the gas-phase $\Delta\Delta G$ for the water-assisted $TS1_s$ is 24.1 kcal/mol versus 24.5 kcal/mol in solution. Notice that this small bulk solvent effects in the evaluation of $\Delta\Delta G$ make our numbers less sensible to errors in evaluating the bulk solvation free energies. Finally, there is a high sensitivity of $\Delta\Delta H$ and $\Delta\Delta G$ values on the presence of the assistant-water molecule. Thus, the value of the rate-acceleration for non-assisted mechanism ($\Delta\Delta G_{aq} = 15.5$ kcal/mol) is substantially lower than for the water-assisted mechanism ($\Delta\Delta G_{aq} = 24.5$ kcal/mol). This indicates that hydrolysis of the twisted amide is more stabilized by an extra explicit water molecule than the hydrolysis of the planar amide.

6.4 Concluding Remarks

In summary, our calculations reveal that the acid hydrolysis of highly twisted amides are subject to a stepwise mechanism with formation of an intermediate. The main difference between this mechanism and the one displayed by undistorted amides is that the initial N-protonation of the former leads to a very activated amide bond. Therefore, high values for the corresponding $\Delta\Delta H^{\neq}$ and $\Delta\Delta G^{\neq}$ were determined. There is also an intricate dependence of the preferred mechanism as a function of pH: *stepwise mechanism is predicted for acid and alkaline hydrolysis and concerted for neutral hydrolysis.* We remark that the acid hydrolysis regime for highly twisted amide can be reached at very high pH values, since the pKa's of these twisted compounds can be close to 6-7 pKa units.[80] The results shown in this chapter and in previous work[79–81] lead to the description of an intriguing chemistry and complex mechanistic picture for the hydrolytic mechanism of highly twisted amides as compared to undistorted analogues, allowing for a better under-

standing of the substantial rate-accelerations found experimentally for this set of compounds, not only as a results of lower rate-limiting barriers, but also as a consequence of important effect of the twist of the amide bond in the nature of the mechanisms involved in the hydrolysis.

Part III

Conclusions

The purpose of this thesis was the characterization of the electronic properties and reactivity towards hydrolysis of highly twisted amides. The interest of these amides steams from the substantial different properties that they show with respect to undistorted planar amides. First, we have analyzed the origin of the high stability of planar amides and how the traditional resonance model can be a valid explanation when first-principles quantum indexes are used. Thus, delocalization indexes based on the analysis of the second order electronic density in the framework of Atoms in Molecules theory were calculated for a series of amides with different degree of twist. Delocalization indexes can be taken as a bridge that reconciles orbital based methods with a description of the electronic structure based on non-arbitrary partitions of electron densities. The results demonstrated that the electronic origin of amide stability can be associated to high electron delocalizations along the N-C-O skeleton, in line with the traditional resonance model in amides. We found that delocalization index between nitrogen and oxygen atoms (δ_{ON}) is better correlated to the stability of the amide bond than geometrical parameters such as the torsional angle τ. In this sense, we found a linear relationship between the degree of electron delocalization measured by δ_{ON} and the stability of amide bond with respect to torsional distortions of the geometry. Once analyzed the origin of the high stability of planar amides in terms of delocalization indexes, we determined the chemical (basicity and reactivity) consequences of the lost of the electron resonance stabilization by inducing a twist on the amide, and determining a series of properties.

Basicity. The breakdown of the $n_N \rightarrow \pi^*_{CO}$ resonance in twisted amides will lead to a higher basicity of the nitrogen. In fact, while protonated planar amides show the O-tautomer as the most stable one, twisted amides show a preference for nitrogen protonation. Another important aspect, is that highly twisted amides can show very high pK_a values in the order of 5-7 pKa units. This leads to an important population of N-protonated forms of twisted amides at neutral or only slightly acidic pH's.

Reactivity. The work was completed by the study of the hydrolysis mechanism and rate-acceleration for twisted amides in various pH regimes: alkaline, neutral and acidic. In each case, we have compared the hydrolysis of a highly twisted amide **TA** with its planar analogue **PA**. As inferred from geometrical and electronic properties based on delocalization indexes, there is a full loss of $n_N \rightarrow \pi^*_{CO}$ in the **TA** amide, whereas **PA** shows an amide bond with the standard degree of electron resonance for undistorted amides. The different electronic features of both amides are reflected in their hydrolysis reactions. Based on our calculations, we have observed a rich and complex chemistry for the hydrolysis of our model highly twisted amide as a function of pH. At alkaline medium, an stepwise mechanism is observed for the hydrolysis of **TA** with both steps of the reaction showing similar barriers after the inclusion of the assistant water molecule.[79] Taking the first step of

Table 6.7: $\Delta\Delta G$ along the entire pH range for the water-assisted hydrolysis reaction. The mechanisms and rate-limiting steps are referred to **TA**.

	Acidic	**Neutral**[a]	**Alkaline**[b,c]
Mechanism	Stepwise	Concerted	Stepwise
Rate-limiting	TS1	TS_c	TS1
$\Delta\Delta H_{gas}$	24.3	8.0	-
$\Delta\Delta G_{gas}$	24.1	7.1	4.9
$\Delta\Delta H_{aq}$	24.7	12.8	-
$\Delta\Delta G_{aq}$	24.5	12.5	7.0

[a] taken from ref.[81] [b] taken from ref.[79] [c] We did not calculate the enthalpic contribution separately.

the reaction as the rate-limiting one, a moderate rate-acceleration ($\Delta\Delta G\approx$ 7 kcal/mol) with respect to analogous planar amides was observed. At neutral pH, however, a concerted pathway is the lowest-energy mechanism which leads to higher rate-acceleration with respect to planar amides than in alkaline pH ($\Delta\Delta G\approx$ 12 kcal/mol). Finally, at acidic medium, an stepwise mechanism is again the favored mechanism, in this case it is clearly the first-step of the reaction the rate-limiting step. In addition, the acid-hydrolysis shows the highest rate-acceleration ($\Delta\Delta G\approx$ 24 kcal/mol, measured with the unprotonated amide as reference reactant), due both to the $n_N \rightarrow \pi^*_{CO}$ resonance and to a higher basicity of the twisted amides. These results are consistent with the structures that Kirby *et al.* had synthesized for the similar twisted amide 1-aza-2-adamantanone[57](depicted in Figure 6.3). They found that when the **TA** was dissolved in water, it rapidly hydrolyzed to give the cleavage of the C-N bond but at acidic conditions they were able to characterize a structure equivalent to Int_s. That is consistent with our theoretical picture in which the hydrolysis takes place in one concerted step (without forming an intermediate) at neutral pH's, but at acidic pH´s a stepwise mechanism is involved with intermediate formation.

The degree of rate-acceleration due to the torsional catalysis is also highly influenced by the media (see Table 6.7). The highest acceleration is observed for the acid medium, and the lowest for alkaline one. This is so, since in the acidic medium the inherent higher reactivity of the amide in twisted species is combined with the higher basicity of the amide nitrogen upon twisting and therefore a more favored protonation. In fact, our estimations for the pK_a of highly twisted amides[80] points to values between 5-7 pK_a units. Thus, the acid hydrolysis of twisted amides is accessible to even relatively high pH values, almost in the neutral or slightly acidic pH range.

In summary, although the kinetic of an undistorted amide shows a picture where the highest rates are obtained at alkaline or acidic media and much lower rates at neutral media,[1] the rate-acceleration due to the twist of

the amide bond increases as the the pH decreases, because of a combination of increased reactivity amide carbon and higher basicity of the amide nitrogen. In fact, the change in the basicity properties in amides upon twisting is key to understand the differential mechanistic picture along the different pH ranges. The torsion of the amide bond and loss of $n_N \rightarrow \pi^*_{CO}$ resonance leads to profound changes in the protonation properties of amides, favoring N-protonation and showing pK_a values between 5-7 for the highly twisted amides. This makes a concerted pathway to be favored in the neutral hydrolysis[81] since it implies a protonation at the nitrogen in the corresponding transition state. Regarding acid-hydrolysis, the change in basicity of nitrogen coupled with the loss of $n_N \rightarrow \pi^*_{CO}$ resonance lead to the highest rate-accelerations of the twisted amides with respect to undistorted amides (taking the unprotonated amide as reference), and lead to a different pathway with an initial N-protonation of the twisted amide, instead of the O-protonation as in undistorted amides. All these data together give a coherent account and lies the theoretical basis for the important rate-accelerations observed upon torsion of the amide bond. We also emphasize that in certain cases (acid hydrolysis stepwise mechanism, and neutral hydrolysis concerted mechanism) the resultant mechanism is more sensible than the hydrolysis of undistorted amides towards the presence of an auxiliary water acting as a bridge in the proton transfer process, indicating that torsion of the amide bond is not sufficient by itself in leading to an efficient cleavage of the amide bond, but its effect should be accompanied by acid/base catalyst which helps reducing barriers for the in flight protons at the transition states. This clearly sets up a limit to the potential of torsional catalysis *per se* like in catalytic antibodies if it is not accompanied by a proper acid/base catalytic mechanism in turn. In summary, one should bear in mind that the torsionally induced higher reactivity of the amide can lead to a higher dependence of the hydrolytic mechanism on a properly located acid catalyst for N-protonation.

Part IV

Further Work

In this thesis work, we have studied the electronic and chemical consequences that the twist of the amide bond have on the rate-acceleration of the hydrolysis reaction of amides. In general, distortion of the amide bond leads to lower free energy barriers for the hydrolysis and we were able to determine interesting mechanistic differences for the hydrolysis of twisted and undistorted planar amides. An extension of the present work of considerable interest could therefore be the analysis of enzymatic or proteic systems for which this type of ground-state destabilization is at the center of the catalytic activity. To name two examples of this type of activity, one could cite catalytic antibodies or protein splicing mechanism. In the case of catalytic antibodies[41–43] the catalysis is thought to be induced by the recognition of the antibody of a geometry that resemble the transition state of the reaction, which in the case of peptide cleavage would imply a breakdown of the planarity of this group and a distortion of the peptide bond. In the case of protein splicing, a similar "ground-state" destabilization has been proposed to be responsible for the relaxation of the reaction barrier.[37–40] In protein splicing, a non-active protein becomes biologically activated after the release of an inner segment of the protein, called Intein.[39,222] The peptide bond cleavage takes place with neither the aid of any enzyme nor external source of energy, only by the combination of several amino acids located in the Intein.[223,224] It is thought that the breakdown of the peptide bond is facilitated by the twist of the amide bond and the mechanistic studies developed in the present thesis could be relevant for a full understanding of the molecular details of this type of catalysis.

In fact, during this Ph.D, preliminary studies have been carried out on the protein splicing process, approaching the problem from two different perspectives: i) study of small model systems using pure quantum methods and ii) studies with the full intein using more approximate methodologies such as mixed Quantum Mechanics/Molecular Mechanics Hamiltonians (QM/MM methods).[225] The purpose of these studies was to determine the influence of the environment on the reaction. The proteic environment could favor or disfavor a reaction pathway by steric, electrostatic or another type of interaction. Among these effects, one possibility is that the residue located at the vicinity of the scissile peptide bond could distort the peptide bond, and as demonstrated along this thesis, could in this way break the $n_N \rightarrow \pi^*_{CO}$ electron resonance, and facilitate the cleavage of the peptide bond. Unfortunately, we felt that these studies were still in a preliminar stage and that further work is needed to reach reliable conclusions.

Bibliography

[1] Smith, R. M.; Hansen, D. E. *J. Am. Chem. Soc.*, **1998**, *120*, 8910.

[2] Brown, R. S. In *The Amide Linkage: Selected Structural Aspects in Chemistry, Biochemistry and Materials Science*; Greenberg, A., Breneman, C. M., Liebman, J. F., Eds.; John Wiley Sons, Inc., 2000.

[3] Lehninger, A. L.; Nelson, D. L.; Cox, M. M. *Principles of Biochemistry.* Worth, New York, 1993.

[4] Hirota, E.; Sugisaki, R.; Nielsen, C. J.; Sorensen, G. O. *J. Mol. Spectrosc.*, **1974**, *49*, 251.

[5] Chakrabarti, P.; Dunitz, J. D. *Helv. Chim. Acta*, **1982**, *65*, 1555.

[6] Vankatesan, K.; Ramakumar, S. In *Structural Studies of Molecular Biological Interest*; Dodson, G., Glusker, J. P., Sayre, D., Eds.. pp 137–153. Oxford University Press, New York. 1981.

[7] Costain, C. C.; Dowling, J. M. *J.Chem. Phys.*, **1960**, *32*, 158.

[8] Kurland, R. J.; Wilson, E. B. *J.Chem. Phys.*, **1957**, *27*, 585.

[9] Robin, M. B.; Bovey, F. A.; Basch, H. *The Chemistry of Amides.* Wiley-Interscience, London, 1970.

[10] Stewart, W. E.; Siddall, T. H. *Chem. Rev.*, **1970**, *70*, 517.

[11] Toriumi, Y.; Kasuya, A.; Itai, A. *J. Org. Chem.*, **1990**, *55*, 259.

[12] Wiberg, K. B.; Laidig, K. E. *J. Am. Chem. Soc.*, **1987**, *109*, 5935.

[13] Wiberg, K. B.; Breneman, C. M. *J. Am. Chem. Soc.*, **1992**, *114*, 831.

[14] Glendening, E. D.; Hrabal(II), J. A. *J. Am. Chem. Soc.*, **1997**, *119*, 12940.

[15] Eglinton, G. *An Introduction to Spectroscopic Methods for the Identification of Organic Compounds*, volume 1. F. Scheinmann, Pergamon Press, Oxford, 1970.

[16] Lambert, J. B.; Shurvell, H. F.; Verbit, L.; Cooks, R. G. *Organic Structural Analysis*. Macmillan Publishing Co., Inc., New York, 1976.

[17] Greenberg, A.; Venanzi, C. A. *J. Am. Chem. Soc.*, **1993**, *115*, 6951.

[18] Hine, J.; King, R. S. M.; Midden, W. R.; Sinha, A. *J. Org. Chem.*, **1981**, *46*, 3186.

[19] Radzicka, A.; Wolfenden, R. *J. Am. Chem. Soc.*, **1996**, *118*, 6105.

[20] Pauling, L. *The nature of the chemical bond, 3rd ed.* Cornell University Press, Ithaca, 1960.

[21] Pauling, L.; Wheland, G. W. *J. Chem. Phys.*, **1933**, *1*, 362.

[22] Wheland, G. W.; Pauling, L. *J. Am. Chem. Soc.*, **1935**, *57*, 2086.

[23] Wheland, G. W. *The Theory of Resonance and its Applications to Organic Chemistry*. Wiley, New York, 1955.

[24] Foster, J. P.; Weinhold, F. *J. Am. Chem. Soc.*, **1980**, *102*, 7211.

[25] Reed, A. E.; Curtiss, L. A.; Weinhold, F. *Chem. Rev.*, **1988**, *88*, 899.

[26] Glendening, E. D.; Weinhold, F. *J. Comp. Chem.*, **1998**, *19*, 593.

[27] Sunner, B.; Piette, L. H.; Schneider, W. G. *Can. J. Chem.*, **1960**, *38*, 681.

[28] Kamei, H. *Bull. Chem. Soc. Jpn.*, **1968**, *41*, 2269.

[29] Drakenberg, T.; Forsen, S. *J. Phys. Chem.*, **1970**, *74*, 1.

[30] Drakenberg, T. *Tetrahedron Lett.*, **1972**, *18*, 1743.

[31] Chan, B.; Shukla, J. P.; Walker, S. *J. Mol. Struct.*, **1983**, *102*, 165.

[32] Olson, L. F.; Li, Y.; Houk, K. N.; Kresge, A. J.; Schaad, L. J. *J. Am. Chem. Soc.*, **1995**, *117*, 2992.

[33] Nalewajski, R. F. *J. Am. Chem. Soc.*, **1978**, *100*, 41.

[34] Williams, J. O.; Alsenoy, C. V.; Schafer, L. *J. Mol. Struct. (THEOCHEM)*, **1981**, *76*, 171.

[35] Jasien, P. G.; Stevens, W. J.; Krauss, M. *J. Mol. Struct. (THEOCHEM)*, **1986**, *139*, 197.

[36] Tsuzuki, S.; Tanabe, K. *J. Chem. Soc., Perkin Trans. 2*, **1991**, *8*, 1255.

[37] Romanelli, A.; Shekhtman, A.; Cowburn, D.; Muir, T. W. *Proc. Natl. Acad. Sci. USA*, **2004**, *101*, 6397.

[38] Poland, B. W.; Xu, M. Q.; Quiocho, F. A. *J. Biol. Chem.*, **2000**, *275*, 16408.

[39] Paulus, H. *Annu. Rev. Biochem.*, **2000**, *69*, 447.

[40] Xu, M. Q.; Perler, F. B. *EMBO*, **1996**, *15*, 5146.

[41] Schumann, M.; Lopez, X.; Karplus, M.; Gouverneur, V. *Tetrahedron*, **2001**, *57*, 10299.

[42] Houk, K. N.; Hilvert, D. *J. Am. Chem. Soc.*, **1996**, *118*, 6462.

[43] Tantillo, D. J.; Houk, K. N. *J. Org. Chem.*, **1999**, *64*, 3066.

[44] Harrison, R. K.; Stein, R. L. *J. Am. Chem. Soc.*, **1992**, *114*, 3464.

[45] Cox, C.; Young, V. G.; Lectka, T. *J. Am. Chem. Soc.*, **1997**, *119*, 2307.

[46] Cox, C.; Lectka, T. *J. Am. Chem. Soc.*, **1998**, *120*, 10660.

[47] Mannfors, B. E.; Mirkin, N. G.; Palmo, K.; Krimm, S. *J. Phys. Chem. A*, **2003**, *107*, 1825.

[48] Gilli, G.; Bertolasi, V.; Belluccu, F.; Ferretti, V. *J. Am. Chem. Soc.*, **1986**, *108*, 2420.

[49] Wiberg, K. B.; Hadad, C. M.; Rablen, P. R.; Cioslowski, J. *J. Am. Chem. Soc.*, **1992**, *114*, 8644.

[50] Wiberg, K. B.; Rablen, P. R. *J. Am. Chem. Soc.*, **1993**, *115*, 9234.

[51] Wiberg, K. B.; Rablen, P. R. *J. Am. Chem. Soc.*, **1995**, *117*, 2201.

[52] Wiberg, K. B.; Rush, D. J. *J. Am. Chem. Soc.*, **2001**, *123*, 2038.

[53] Blackburn, G. M.; Plackett, J. D. *J. Chem. Soc., Perkin Trans. 2*, **1972**, *9*, 1366.

[54] Blackburn, G. M.; Skaife, C. J.; Kay, I. T. *J. Chem. Research*, **1980**, *10*, 294.

[55] Wang, Q. P.; Bennet, A. J.; Brown, R. S.; Santarsiero, B. D. *J. Am. Chem. Soc.*, **1991**, *113*, 5757.

[56] Kirby, A. J.; Komarov, I. V.; Wothers, P. D.; Feeder, N. *Angew. Chem. Intl. Ed. Engl.*, **1998**, *37*, 785.

[57] Kirby, A. J.; Komarov, I. V.; Feeder, N. *J. Am. Chem. Soc.*, **1998**, *120*, 7101.

[58] Kirby, A. J.; Komarov, I. V.; Feeder, N. *J. Chem. Soc., Perkin Trans. 2*, **2001**, *4*, 522.

[59] Guthrie, J. P. *J. Am. Chem. Soc.*, **1974**, *96*, 3608.

[60] Oie, T.; Loew, G. H.; Burt, S. K.; Binkley, J. S.; MacElroy, R. D. *J. Am. Chem. Soc.*, **1982**, *104*, 6169.

[61] Weiner, S. J.; Singh, U. C.; Kollman, P. *J. Am. Chem. Soc.*, **1985**, *107*, 2219.

[62] Krug, J.; Popelier, P.; Bader, R. F. W. *J. Phys. Chem.*, **1992**, *96*, 7604.

[63] Jensen, J. H.; Baldridge, K. K.; Gordon, M. S. *J. Phys. Chem.*, **1992**, *96*, 8340.

[64] Antonczak, S.; Ruiz-López, M. F.; Rivail, J. L. *J. Am. Chem. Soc.*, **1994**, *116*, 3912.

[65] Antonczak, S.; Ruiz-López, M. F.; Rivail, J. L. *J. Mol. Mod.*, **1997**, *3*, 434.

[66] Dobbs, K. D.; Dixon, D. A. *J. Phys. Chem.*, **1996**, *100*, 3965.

[67] Rauk, A.; Glover, S. A. *J. Org. Chem.*, **1996**, *61*, 2337.

[68] Hori, K.; Kamimura, A.; Ando, K.; Mizumura, M.; Ihara, Y. *Tetrahedron*, **1997**, *53*, 4317.

[69] Kallies, B.; Mitzner, R. *J. Mol. Mod.*, **1998**, *4*, 183.

[70] Zheng, Y.-J.; Ornstein, R. L. *J. Mol. Struct.*, **1998**, *429*, 41.

[71] Stanton, R. V.; Perakyla, M.; Bakowies, D.; Kollman, P. A. *J. Am. Chem. Soc.*, **1998**, *120*, 3448.

[72] Bakowies, D.; Kollman, P. A. *J. Am. Chem. Soc.*, **1999**, *121*, 5712.

[73] Glover, S. A.; Rauk, A. *J. Org. Chem.*, **1999**, *64*, 2340.

[74] Strajbl, M.; Florián, J.; Warshel, A. *J. Am. Chem. Soc.*, **2000**, *122*, 5354.

[75] Chalmet, S.; Harb, W.; Ruiz-López, M. F. *J. Phys. Chem. A*, **2001**, *105*, 11574.

[76] Somayaji, V.; Brown, R. S. *J. Org. Chem.*, **1986**, *51*, 2676.

[77] Greenberg, A.; Moore, D. T.; DuBois, T. D. *J. Am. Chem. Soc.*, **1996**, *118*, 8658.

[78] Slebocka-Tilk, H.; Brown, R. S. *J. Org. Chem.*, **1987**, *52*, 805.

[79] Lopez, X.; Mujika, J. I.; Blackburn, G. M.; Karplus, M. *J. Phys. Chem. A*, **2003**, *107*, 2304.

[80] Mujika, J. I.; Mercero, J. M.; Lopez, X. *J. Phys. Chem. A*, **2003**, *107*, 6099.

[81] Mujika, J. I.; Mercero, J. M.; Lopez, X. *J. Am. Chem. Soc.*, **2005**, *127*, 4445.

[82] Mujika, J. I.; Mercero, J. M.; Lopez, X. *submitted*, **2005**.

[83] Mujika, J. I.; Matxain, J. M.; Eriksson, L. A.; Lopez, X. *submitted*, **2005**.

[84] Mercero, J. M.; Matxain, J. M.; Lopez, X.; York, D. M.; Largo, A.; Eriksson, L. A.; Ugalde, J. M. *Int. J. of Mass Spectr.*, **2005**, *240*, 37.

[85] Schrödinger, E. *Ann. Physik*, **1926**, *79*, 361.

[86] Heisenberg, W. *Z. Physik*, **1925**, *33*, 879.

[87] Dirac, P. A. M. *R. Soc. Lond. A*, **1926**, *113*, 621.

[88] Schrödinger, E. *Ann. Physik*, **1926**, *79*, 734.

[89] Born, M.; Oppenheimer, J. R. *Ann. Physik*, **1927**, *44*, 455.

[90] Levine, N. I. *Quantum Chemistry*. Prentice Hall Inc., New Jersey, 1991.

[91] Szabo, A.; Ostlund, N. S. *Modern Quantum Chemistry*. McGraw-Hill, New York, 1992.

[92] Parr, R. G.; Yang, W. *Density-Functional Theory of Atoms and Molecules*. Oxford Univeersity Press, New York, 1989.

[93] Kryachko, E. S.; Na, E. V. L. *Energy Density Functional Theory of Many-electron Systems*. Kluwer Academic Publishers, London, 1990.

[94] Foulkes, W. M. C.; Mitas, L.; Needs, R. J.; Rajagopal, G. *Rev. Mod. Phys.*, **2001**, *73*, 33.

[95] Heitler, W.; London, F. *Z. Physik*, **1927**, *44*, 455.

[96] Hund, F. *Z. Physik*, **1931**, *73*, 1.

[97] Mulliken, R. S. *Phys. Rev.*, **1932**, *40*, 55.

[98] Hartree, D. R. *Proc. Cambridge Philos. Soc.*, **1928**, *24*, 89.

[99] Fock, V. *Z. Physik*, **1930**, *61*, 126.

[100] Moller, C.; Plesset, M. S. *Phys. Rev.*, **1934**, *46*, 618.

[101] Shavitt, I. *Mol. Phys.*, **1998**, *94*, 3.

[102] Sherrill, C. D.; Schaefer, H. F. *Adv. Quantum Chem.*, **1999**, *34*, 143.

[103] Pople, J. A.; Krishnan, R.; Schlegel, H. B.; Binkley, J. S. *Int. J. Quant. Chem.*, **1978**, *14*, 545.

[104] Bartlett, R. J.; Purvis, G. D. *Int. J. Quant. Chem.*, **1978**, *14*, 516.

[105] Bartlett, R. J. *Modern electronic structure theory.* World Scientific, London, 1995.

[106] Andersson, K.; Malmqvist, P. A.; Roos, B. O.; Sadlej, A. J.; Wolinski, K. *J. Phys. Chem.*, **1990**, *94*, 5483.

[107] Andersson, K.; Malmqvist, P. A.; Roos, B. O. *J. Phys. Chem.*, **1992**, *96*, 1218.

[108] Hohenberg, P.; Kohn, W. *Phys. Rev.*, **1964**, *136*, B864.

[109] Kohn, W.; Sham, L. J. *Phys. Rev. A*, **1965**, *140*, 1133.

[110] Stowaser, R.; Hoffmann, R. *J. Am. Chem. Soc.*, **1999**, *121*, 3414.

[111] Gunnarsson, O.; Lundqvist, B. I.; Wilkens, J. W. *Phys. Rev. Lett.*, **1974**, *10*, 1319.

[112] Kar, T.; Angyan, J. G.; Shannigrahi, A. B. *J. Phys. Chem. A*, **2000**, *104*, 9953.

[113] Vosko, S. H.; Wilk, L.; Nusair, M. *Can. J. Phys*, **1980**, *58*, 1299.

[114] Slater, J. C. *Quantum Theory of Molecules and Solids. Vol. 4. The Self-Consistent Field for Molecules and Solids.* McGraw-Hill, New York, 1974.

[115] Labanowski, J.; Andelzelm, J. *Density Functional Methods in Chemistry.* Springer-Verlag, New York, 1991.

[116] Tschinke, V.; Ziegler, T. *Theor. Chim. Acta*, **1991**, *81*, 651.

[117] Johnson, B. G.; Gill, P. M. W.; Pople, J. A. *J. Chem. Phys.*, **1993**, *98*, 5612.

[118] Becke, A. D. *J. Chem. Phys.*, **1993**, *98*, 5648.

[119] Lee, C.; Yang, W.; Parr, R. G. *Phys. Rev. B*, **1988**, *37*, 785.

[120] Becke, A. D. *Phys. Rev. A*, **1988**, *38*, 3098.

[121] Ziegler, T. *Chem. Rev.*, **1991**, *91*, 651.

[122] Schlegel, H. B. *J. Comp. Chem.*, **1982**, *3*, 214.

[123] Schlick, T. In *Reviews in Computational Chemistry, vol. 3*, Lipkowith, K. B.; Boyd, D. B., Eds. VCH Publishers, Inc., New York. 1992.

[124] McKee, M. L.; Page, M. *Reviews in Computational Chemistry, Vol. 4*. VCH Publishers, Inc., New-York, 1993.

[125] Stewart, J. J. P. *J. Comp. Chem.*, **1986**, *13*, 157.

[126] Head, J. D.; Zerner, M. C. *Chem. Phys. Lett.*, **1985**, *122*, 264.

[127] Baker, J. *J. Comp. Chem.*, **1986**, *7*, 385.

[128] Taylor, H.; Simons, J. *J. Phys. Chem.*, **1985**, *89*, 684.

[129] Nichols, J.; Taylor, H.; Schmidt, P.; Simons, J. *J. Chem. Phys.*, **1990**, *92*, 340.

[130] Hehre, W. J.; Radom, L.; v. R. Schleyer, P.; Pople, J. A. *Ab-Initio Molecular Orbital Theory*. Wiley Interscience, New-York, 1986.

[131] Cramer, C. J. *Essentials of Computational Chemistry: Theories and Models*. John Wiley & Sons, Chichester, England, 2$^{\text{nd}}$ edition, 2002.

[132] Lopez, X.; Dejaegere, A.; Karplus, M. *J. Am. Chem. Soc.*, **1999**, *121*, 5548.

[133] Lopez, X.; Dejaegere, A.; Karplus, M. *J. Am. Chem. Soc.*, **2001**, *123*, 11755.

[134] Tomassi, J.; Persico, J. *Chem. Rev.*, **1994**, *94*, 2027.

[135] Cramer, J. C.; Truhlar, D. G. *Chem. Rev.*, **1999**, *99*, 2161.

[136] Orozco, M.; Luque, F. J. *Chem. Rev.*, **2000**, *100*, 4187.

[137] Miertus, S.; Tomasi, J. *Chem. Phys.*, **1982**, *65*, 239.

[138] Scrocco, S. M. E.; Tomasi, J. *J. Chem. Phys.*, **1981**, *55*, 117.

[139] Barone, V.; Cossi, M.; Tomasi, J. *J. Chem. Phys.*, **1997**, *107*, 3210.

[140] Cossi, M.; Barone, V.; Cammi, R.; Tomasi, J. *Chem. Phys. Lett.*, **1996**, *255*, 327.

[141] Pierotti, R. A. *Chem. Rev.*, **1976**, *76*, 717.

[142] Floris, F. M.; Tomasi, J.; Pascual-Ahuir, J. L. *J. Comput. Chem.*, **1991**, *12*, 784.

[143] Barone, V.; Cossi, M. *J. Phys. Chem. A*, **1998**, *102*, 1995.

[144] Cammi, R.; Tomasi, J. *J. Comput. Chem.*, **1995**, *16*, 1449.

[145] Chipman, D. M. *J. Chem. Phys.*, **1997**, *106*, 10194.

[146] Frisch, Æ.; Frisch, M. J. *Gaussian 98 User's Reference*. Gaussian, Inc., Pittsburgh, PA, 2nd edition, 1999.

[147] Fogarasi, C.; Szalay, P. *J. Phys. Chem. A*, **1997**, *101*, 1400.

[148] Lauvergnat, D.; Hiberty, P. *J. Am. Chem. Soc.*, **1997**, *119*, 9478.

[149] Mo, Y.; Schleyer, P. V. R.; Wu, W.; Lin, M.; Zhang, Q.; Gao, J. *J. Phys. Chem. A*, **2003**, *107*, 10011.

[150] Laidig, K. E.; Cameron, L. M. *J. Am. Chem. Soc.*, **1996**, *118*, 1737.

[151] Bader, R. F. W. *Atoms in Molecules: A Quantum Theory*. Oxford University Press, Oxford, U. K., 1990.

[152] Yamada, S. *J. Org. Chem.*, **1996**, *61*, 941.

[153] Greenberg, A.; Thomas, T. D.; Bevilacqua, C. R.; Coville, M.; Ji, D.; Tsai, J. C.; Wu, G. *J. Org. Chem.*, **1992**, *57*, 7093.

[154] Perrin, C. L. *J. Am. Chem. Soc.*, **1991**, *113*, 2865.

[155] Laidig, K. E. *J. Am. Chem. Soc.*, **1992**, *114*, 7912.

[156] Gatti, C.; Fantucci, P. *J. Phys. Chem.*, **1993**, *97*, 11677.

[157] Fradera, X.; Austen, M. A.; Bader, F. W. *J. Phys. Chem. A*, **1999**, *103*, 304.

[158] Poater, J.; Sola, M.; Duran, M.; Fradera, X. *J. Phys. Chem. A*, **2001**, *105*, 2052.

[159] Frisch, M. J.; Trucks, G. W.; Schlegel, H. B.; Scuseria, G. E.; Robb, M. A.; Cheeseman, J. R.; Zakrzewski, V. G.; Montgomery, J. A.; Stratmann, R. E.; Burant, J. C.; Dapprich, S.; Millam, J. M.; Daniels, A. D.; Kudin, K. N.; Strain, M. C.; O. Farkas, J. T.; Barone, V.; Cossi,

M.; Cammi, R.; Mennucci, B.; Pomelli, C.; Adamo, C.; Clifford, S.; Ochterski, J.; Petersson, G. A.; Ayala, P. Y.; Cui, Q.; Morokuma, K.; Malick, D. K.; Rabuck, A. D.; Raghavachari, K.; Foresman, J. B.; Cioslowski, J.; Ortiz, J. V.; Stefanov, B. B.; Liu, G.; Liashenko, A.; Piskorz, P.; Komaromi, I.; Gomperts, R.; Martin, R. L.; Fox, D. J.; Keith, T.; Al-Laham, M. A.; Peng, C. Y.; Nanayakkara, A.; Gonzalez, C.; Challacombe, M.; Gill, P. M. W.; Johnson, B. G.; Chen, W.; Wong, M. W.; Andres, J. L.; Head-Gordon, M.; Replogle, E. S.; Pople, J. A. *Gaussian 98 (Revision A.2)*. Gaussian, Inc., Pittsburgh PA, 1998.

[160] Vosko, S. H.; Wilk, L.; Nusair, M. *Can. J. Phys.*, **1980**, *58*, 1200.

[161] Lee, C.; Yang, W.; Parr, R. G. *Phys. Rev. B*, **1988**, *37*, 785.

[162] Ferretti, V.; Bertolasi, V.; Gilli, P.; Gilli, G. *J. Phys. Chem.*, **1993**, *97*, 13568.

[163] Biegler-König, F. W.; Bader, R. F. W.; Tang, T. H. *J. Comput. Chem.*, **1982**, *3*, 317.

[164] Poater, J.; Sola, M.; Duran, M.; Fradera, X. *Theor. Chem. Acc.*, **2002**, *107*, 362.

[165] Krygowski, T. M.; Ejsmont, K.; Stepien, B. T.; Cyranski, M. K.; Poater, J.; Sola, M. *J. Org. Chem.*, **2004**, *69*, 6634.

[166] Wiberg, K. B.; Rablen, P. R.; Rush, D. J.; Keith, T. A. *J. Am. Chem. Soc.*, **1995**, *117*, 4261.

[167] Silva, C.; Nieto, O.; Cossio, F.; York, D.; de Lera, A. *Chem. Eur. J.*, **2005**, *11*, 1734.

[168] Jean, Y.; Demachy, I.; Lledos, A.; Maseras, F. *Theochem*, **2003**, *632*, 131.

[169] Otani, Y.; Nagae, O.; Naruse, Y.; Inagaki, S.; Ohno, M.; Yamaguchi, K.; Yamamoto, G.; Uchiyama, M.; Ohwada, T. *J. Am. Chem. Soc.*, **2003**, *125*, 15191.

[170] Bennet, A. J.; Somayaji, V.; Brown, R. S.; Santarsiero, B. D. *J. Am. Chem. Soc.*, **1991**, *113*, 7563.

[171] *Dictionary of Organic Compounds, 5 ed.* Chapman and Hall, New York, 1982.

[172] Pranata, J.; Davis, G. D. *J. Phys. Chem.*, **1995**, *99*, 14340.

[173] Chipman, D. M. *J. Phys. Chem. A*, **2002**, *106*, 7413.

[174] Pliego, J. R.; Riveros, J. M. *J. Phys. Chem. A*, **2001**, *105*, 7241.

[175] Pliego, J. R.; Riveros, J. M. *J. Phys. Chem. A*, **2002**, *106*, 7434.

[176] Lopez, X.; Schaefer, M.; Dejaegere, A.; Karplus, M. *J. Am. Chem. Soc.*, **2002**, *124*, 5010.

[177] Perdew, J. P.; Chevary, J. A.; Vosko, S. H.; Jackson, K. A.; Pederson, M. R.; Singh, D. J.; Fiolhais, C. *Phys. Rev. B*, **1992**, *46*, 6671.

[178] Perdew, J.; Burke, K.; Wang, Y. *Phys. Rev. B*, **1996**, *54*, 16533.

[179] McQuarrie, D. A. *Statistical Mechanics*. University Science Books, 2000.

[180] Cossi, M.; Barone, V.; Cammi, R.; Tomasi, J. *Chem. Phys. Lett.*, **1996**, *225*, 327.

[181] Cancès, E.; Mennucci, B.; Tomasi, J. *J. Chem. Phys.*, **1997**, *107*, 3032.

[182] Barone, V.; Cossi, M.; Tomasi, J. *J. Comput. Chem.*, **1998**, *19*, 404.

[183] Davies, J.; Doltsinis, N. L.; Kirby, A.; Roussev, C.; Sprik, M. *J. Am. Chem. Soc.*, **2002**, *124*, 6594.

[184] Hall, H. J. *J. Am. Chem. Soc.*, **1957**, *79*, 5441.

[185] Reed, A. E.; Weinstock, R. B.; Weinhold, F. *J. Chem. Phys.*, **1985**, *83*, 735.

[186] Glendening, E. D.; Badenhoop, J. K.; Weinhold, F. *J. Comput. Chem.*, **1998**, *19*, 628.

[187] Howard, A.; Kollman, P. *J. Am. Chem. Soc.*, **1988**, *110*, 7195.

[188] Pracejus, H. *Chem. Ber.*, **1959**, *92*, 988.

[189] Schrodinger, Inc., Portland OR. *Jaguar, 3.5 ed.*, 1998.

[190] York, D. M.; Karplus, M. *J. Phys. Chem. A*, **1999**, *103*, 11060.

[191] Tomassi, J.; Persico, J. *Chem. Rev.*, **1994**, *94*, 2027.

[192] Foresman, J. B.; Keith, T. A.; Wiberg, K. B.; Snoonian, J.; Frisch, M. J. *J. Phys. Chem.*, **1996**, *100*, 16098.

[193] Wiberg, K. B.; Castejon, H. *J. Comput. Chem.*, **1996**, *17*, 185.

[194] Bunton, C. A.; Nayak, B.; O'Connor, C. *J. Org. Chem.*, **1968**, *33*, 572.

[195] Robinson, B. A.; Tester, J. W. *Int. J. Chem. Kinet.*, **1990**, *22*, 431.

[196] Brown, R. S.; Bennet, A. J.; Slebocka-Tilk, H. *Accounts of Chemical Research*, **1992**, *25*, 481.

[197] Brown, R. S.; Bennet, A. J.; Slebocka-Tilk, H.; Jodhan, A. *J. Am. Chem. Soc.*, **1992**, *114*, 3092.

[198] Slebocka-Tilk, H.; Bennet, A. J.; Keillor, J. W.; Brown, R. S.; Guthrie, J. P.; Jodhan, A. *J. Am. Chem. Soc.*, **1990**, *112*, 8507.

[199] Slebocka-Tilk, H.; Bennet, A. J.; ; Hogg, H. J.; Brown, R. S. *J. Am. Chem. Soc.*, **1991**, *113*, 1288.

[200] Slebocka-Tilk, H.; Sauriol, F.; Monette, M.; Brown, R. S. *Can. J. Chem.*, **2002**, *80*, 1343.

[201] Slebocka-Tilk, H.; Neverov, A. A.; Brown, R. S. *J. Am. Chem. Soc.*, **2003**, *125*, 1851.

[202] Alagona, G.; Scrocco, E.; Tomas, J. *J. Am. Chem. Soc.*, **1975**, *97*, 6976.

[203] Pliego, J. R. *Chem. Phys.*, **2004**, *306*, 273.

[204] O'Brien, J. F.; Pranata, J. *J. Phys. Chem.*, **1995**, *99*, 12759.

[205] Pearson, R. G. *J. Am. Chem. Soc.*, **1986**, *108*, 6109.

[206] Ford, G. P.; Wang, B. *J. Am. Chem. Soc.*, **1992**, *114*, 10563.

[207] Chandrasekhar, J.; Smith, S.; Jorgensen, W. *J. Am. Chem. Soc.*, **1985**, *107*, 154.

[208] Bertran, J.; Ruiz-Lopez, M. F.; Rinaldi, D.; Rivail, J. L. *Theor. Chim. Acta*, **1992**, *84*, 181.

[209] Gonzalez, C.; Schlegel, B. *J. Chem. Phys.*, **1989**, *90*, 2154.

[210] Gonzalez, C.; Schlegel, B. *J. Phys. Chem.*, **1990**, *94*, 5523.

[211] Marlier, J. F. *J. Am. Chem. Soc.*, **1999**, *121*, 4356.

[212] Marlier, J. F. *Acc. Chem. Res.*, **2001**, *34*, 283.

[213] Kahne, D.; Still, W. C. *J. Am. Chem. Soc.*, **1988**, *110*, 7529.

[214] Bryant, R. A. R.; Hansen, D. E. *J. Am. Chem. Soc.*, **1996**, *118*, 5498.

[215] Bennet, A. J.; Slebocka-Tilk, H.; Brown, R. S.; Guthrie, J. P.; Jodhan, A. *J. Am. Chem. Soc.*, **1990**, *112*, 8497.

[216] Bennet, A. J.; Slebocka-Tilk, H.; Brown, R. S. *J. Am. Chem. Soc.*, **1992**, *114*, 3088.

[217] Langlois, S.; Broche, A. *Bull. Soc. Chim. Fr.*, **1964**, *4*, 812.

[218] Bolton, P. D. *Aust. J. Chem.*, **1966**, *19*, 1013.

[219] Bolton, P. D.; Jackson, G. L. *Aust. J. Chem.*, **1971**, *24*, 969.

[220] Manojkumar, T. K.; Suh, S. B.; Oh, K. S.; Cho, S. J.; Cui, C.; Zhang, X.; Kim, K. S. *J. Org. Chem.*, **2005**, *70*, 2651.

[221] Zahn, D. *Chem. Phys.*, **2004**, *300*, 79.

[222] Liu, X. Q. *Annu. Rev. Biochem.*, **2000**, *34*, 61.

[223] Perler, F. B.; Comb, D. G.; Jack, W. E.; Moran, L. S.; Quiang, B. *Proc. Natl. Acad. Sci. USA.*, **1992**, *89*, 5577.

[224] Kawasaki, M.; Satow, Y.; Ohya, Y.; Anraku, Y. *FEBS Lett.*, **1997**, *412*, 518.

[225] Field, M. J.; Bash, P. A.; Karplus, M. *J. Comp. Chem.*, **1990**, *11*, 700.